

PROJECT COMPLETION
REPORT NO. 527X

The Turbulent Transport and Biological Structure of Eutrophication Models

Volume I

Preserving the Statistical Structure
in Lake Transport Calculations

K. W. Bedford,
Associate Professor

R. W. Sykes,
Associate Professor

C. Babajimopolous,
Research Assistant

Department of Civil Engineering
The Ohio State University

United States Department
of the Interior

CONTRACT NO.
A-039-OHIO
B-063-OHIO



THE TURBULENT TRANSPORT AND BIOLOGICAL STRUCTURE
OF EUTROPHICATION MODELS

Volume I

Preserving the Statistical Structure
in Lake Transport Calculations

by

K. W. Bedford, Ph.D.
Associate Professor of Civil Engineering,

R. W. Sykes, Ph.D.
Associate Professor of Civil Engineering, and

C. Babajimopolous, Ph.D.
Research Assistant

The Department of Civil Engineering
The Ohio State University

* * * *

Project Completion Report, Volume I
Office of Water Resources Research and Technology
Matching Grant B-036-OHIO

* * * *

May 31, 1978

* * * *

PREFACE

The analysis of eutrophication processes and pollutant transport has been aided by an overwhelming number of numerical models, each purporting some advantage over existing formulations. Difficulties with these models exist and their utility is often called into question, particularly with regard to verification. The following research report is a two-volume report which attempts to review, and clarify, the basic assumptions in these models and to suggest extensions or improvements in the structure which will reduce the amount of artificial empiricism. The first volume suggests improvements in the turbulent transport structure and the second volume describes the primary productivity formulation available and identifies optimal representation.

ACKNOWLEDGMENTS

This volume is the first volume of the project completion report for OWRT Matching Grant Contract B-036-OHIO. The principal investigators, Drs. K. W Bedford and R. M. Sykes, were extremely fortunate to have been able to support and associate with an excellent group of graduate students. As a result, this volume is, in substantial part, the doctoral thesis of Christos Babajimopolous, whose diligence, patience, and thorough work are sincerely appreciated and acknowledged. He and his fellow doctoral candidate, Kenneth Smarkel, provided excellent examples of proper science and research to the other students on this project, Michael Trimeloni and Bipin Shah. The authors wish to thank the staff of the Water Resources Center for their help in the smooth administration of this project in the face of ever-increasing paperwork. Last, but certainly most importantly, the authors very much thank the Office of Water Resources Research and Technology for their support of this research.

TABLE OF CONTENTS

| | <u>Page</u> |
|--|-------------|
| PREFACE | ii |
| ACKNOWLEDGMENTS | iii |
| LIST OF TABLES | viii |
| LIST OF FIGURES | ix |
| LIST OF SYMBOLS | xiii |
| Chapter | |
| I. INTRODUCTION AND OBJECTIVE | 1 |
| II. REVIEW OF TURBULENT TRANSPORT MODELS | 5 |
| III. TURBULENCE | 10 |
| A. General Characteristics of Turbulence | 11 |
| 1. Definitions | 11 |
| 2. Scales of Turbulent Motion | 13 |
| 3. Frequency Spectra | 15 |
| 4. Wave-Number Spectra | 17 |
| 5. Taylor's Frozen Turbulence Hypothesis | 21 |
| 6. Energy Cascade-Kolmogorov Theory | 25 |
| 7. Observations of Five-Thirds Law | 28 |
| 8. Energy Subranges in 2-D Turbulence | 31 |
| B. Classical Analytic Approaches to Turbulence Computations | 33 |
| 1. Averaging Procedures | 33 |
| 2. Reynolds Axioms | 37 |
| 3. Reynolds Stresses and the Closure Problem | 38 |
| 4. Computational Approaches to the Closure Problem | 41 |
| a) First Order Theory | 41 |
| b) Second Order Theory | 42 |
| IV. FILTRATION | 44 |
| A. Filter Methodology | 45 |

TABLE OF CONTENTS (continued)

| | <u>Page</u> |
|---|-------------|
| 1. Filter Methodology | 44 |
| 2. The Use of the Convolution Integral in the Construction of a Filter | 45 |
| B. Filter Performance Criteria | 53 |
| C. A Review of Filters Used in Turbulence | 54 |
| 1. Top-Hat Filter | 54 |
| 2. Gaussian Filter | 56 |
| 3. Sub-Grid Scale Filter | 57 |
| D. A Filter for Distorted Grid Cells | 57 |
| V. DERIVATION OF FILTERED TRANSPORT EQUATIONS | 61 |
| A. Statement of the Navier-Stokes and Transport Equations | 63 |
| B. Assumptions Used in Circulation Calculations | 65 |
| C. Derivation of the Filtered Equations | 67 |
| D. Residual Field Model | 72 |
| E. Equations for the Biological Model | 75 |
| F. Summary of the Filtered Equations. | 77 |
| G. Non-Dimensionalization | 79 |
| H. Boundary Conditions | 84 |
| 1. Momentum Equations | 84 |
| 2. Transport Equation | 84 |
| VI. NUMERICAL SOLUTION | 85 |
| A. Grid Layout | 85 |
| B. Spatial Differencing Procedures | 86 |
| C. Time Marching Procedure | 101 |
| D. Pressure Field Technique | 103 |
| E. Computational Sequence | 112 |
| VII. MODEL IMPLEMENTATION | 114 |
| A. Basin Selection and Input Parameters | 115 |
| B. Surface Wind Shear Specification | 117 |
| C. Statistical Preparation of the Results | 119 |
| D. Summary of Runs | 121 |
| VIII. RESULTS | 124 |
| A. Optimization of the Residual Field Coefficient, c | 124 |
| B. Program Performance Results | 127 |
| C. Predicted Results - Averaged Quantities | 127 |

TABLE OF CONTENTS (continued)

| | <u>Page</u> |
|--|-------------|
| D. Predicted Results - Trubulence Spectra | 136 |
| 1. Velocity Spectra | 136 |
| (a) Spectra at Different Depths | 136 |
| (b) Spectra with Different Basins | 136 |
| (c) Spectra with Different Shears | 136 |
| (d) Spectra with Different Time Step | 136 |
| (e) Spectra with No Deterministic Structure in the Surface Boundary Condition | 155 |
| (f) Spectra with No Filtration | 155 |
| 2. Passive Contaminant Spectra | 155 |
| (a) Spectra at Different Depths | 155 |
| (b) Spectra with Different Prandtl Numbers | 155 |
| 3. Biochemically Active Contaminant Spectra | 170 |
| E. Preliminary Observation of the Results | 170 |
| 1. Velocity Spectra | 170 |
| 2. Concentration Spectra | 175 |
| IX. INTERPRETATION AND DISCUSSION | 177 |
| A. Interpretation | 177 |
| B. Discussion | 189 |
| X. CONCLUSIONS | 193 |
| APPENDIX | |
| A. Fourier Transforms | 195 |
| B. Autocorrelation Coefficient | 199 |
| C. Definition of Stationarity and Ergodicity | 203 |
| D. Computer Programs | 206 |
| REFERENCES | 207 |

LIST OF TABLES

| | <u>Page</u> |
|--|-------------|
| 2.1 Lake Transport Models | 7 |
| 6.1 Equations Used in the Numerical Model | 102 |
| 7.1 Basins and Input Parameters | 116 |
| 7.2 Summary of Computer Runs | 123 |
| 8.1 Maximum Length Scales (m) where a -3 Slope is Observed. Concentration Runs Include also the Maximum Scale where the Tail End Changes Slope | 174 |

LIST OF FIGURES

| | <u>Page</u> |
|-----|--|
| 3.1 | Frequency Spectrum (after Reynolds, 1974) 16 |
| 3.2 | Aliasing in a One-Dimensional Spectrum (after Tennekes and Lumley, 1972) 20 |
| 3.3 | Comparison of Measured Values of the Velocity Correlation Function with Calculations Based on Taylor's Hypothesis (after Monin and Yaglom, 1975) 24 |
| 3.4 | Comparison between Time and Spatial Correlations According to Taylor's Hypothesis (after Hinze, 1975) 24 |
| 3.5 | Characteristic Ranges of a Turbulent Motion (after Reynolds, 1974) 28 |
| 3.6 | Measured One-Dimensional Spectra of the Horizontal (u) and Vertical (w) Wind Velocity Components at a Height of 300 m. (after Monin and Yaglom, 1975) 29 |
| 4.1 | The Finite Ramp 45 |
| 4.2 | Derivative of the Finite Ramp 46 |
| 4.3 | a) Unit Impulse, b) Shifted Impulse of Area, A. 47 |
| 4.4 | Convolution of Two Rectangular Pulses 48 |
| 4.5 | Convolution of a Rectangular and an Exponential Pulse 48 |
| 4.6 | Convolution of a Triangular and a Rectangular Pulse 49 |
| 4.7 | Classification of Filters 51 |
| 6.1 | Arrangements of Variables in Grid Sections (after Paul and Lick, 1976) 87 |
| 6.2 | Typical Nodal Cells for Grid System (after Paul and Lick, 1976) 88 |

| | | |
|------|---|-----|
| 6.3 | Horizontal Plane at Nodal Section-Indexing | 89 |
| 6.4 | Vertical Plane at Half Nodal Section-Indexing | 90 |
| 6.5 | Comparison of Modified Wave Numbers (after Kwak, et al., 1975) | 94 |
| 7.1 | 1-Lag Markov Model | 120 |
| 8.1 | Optimization of Subgrid Coefficient "c" | 126 |
| 8.2 | Velocity Field at Depth=0.0 | 128 |
| 8.3 | Velocity Field at Depth=0.125 | 129 |
| 8.4 | Velocity Field at Depth=0.250 | 130 |
| 8.5 | Velocity Field at Depth=0.500 | 131 |
| 8.6 | Velocity Field at Depth=0.875 | 132 |
| 8.7 | Non-Dimensional u-Velocity Profile | 133 |
| 8.8 | Non-Dimensional v-Velocity Profile | 134 |
| 8.9 | Vertical Velocities at Basin Center for Basin 1, Run 1 and Time Step=45 | 135 |
| 8.10 | Energy Spectrum; Depth=0.125; Run 1 | 137 |
| 8.11 | Energy Spectrum; Depth=0.25; Run 1 | 138 |
| 8.12 | Energy Spectrum; Depth=0.5; Run 1 | 139 |
| 8.13 | Energy Spectrum; Depth=0.125; Run 2 | 140 |
| 8.14 | Energy Spectrum; Depth=0.250; Run 2 | 141 |
| 8.15 | Energy Spectrum; Depth=0.500; Run 2 | 142 |
| 8.16 | Energy Spectrum; Depth=0.125; Run 3 | 143 |
| 8.17 | Energy Spectrum; Depth=0.250; Run 3 | 144 |

| | | |
|------|---|-----|
| 8.18 | Energy Spectrum; Depth=0.500; Run 3 | 145 |
| 8.19 | Energy Spectrum; Depth=0.125; Run 5 | 146 |
| 8.20 | Energy Spectrum; Depth=0.250; Run 5 | 147 |
| 8.21 | Energy Spectrum; Depth=0.500; Run 5 | 148 |
| 8.22 | Energy Spectrum; Depth=0.125; Run 7 | 149 |
| 8.23 | Energy Spectrum; Depth=0.250; Run 7 | 150 |
| 8.24 | Energy Spectrum; Depth=0.500; Run 7 | 151 |
| 8.25 | Energy Spectrum; Depth=0.125; Run 6 | 152 |
| 8.26 | Energy Spectrum; Depth=0.250; Run 6 | 153 |
| 8.27 | Energy Spectrum; Depth=0.500; Run 6 | 154 |
| 8.28 | Energy Spectrum; Depth=0.125; Run 12 | 156 |
| 8.29 | Energy Spectrum; Depth=0.250; Run 12 | 157 |
| 8.30 | Energy Spectrum; Depth=0.500; Run 12 | 158 |
| 8.31 | Energy Spectrum; Depth=0.0; Run 4 | 159 |
| 8.32 | Energy Spectrum; Depth=0.5; Run 4 | 160 |
| 8.33 | Concentration Spectrum; Depth=0.125; Run 8 | 161 |
| 8.34 | Concentration Spectrum; Depth=0.250; Run 8 | 162 |
| 8.35 | Concentration Spectrum; Depth=0.500; Run 8 | 163 |
| 8.36 | Concentration Spectrum; Depth=0.125; Run 9 | 164 |
| 8.37 | Concentration Spectrum; Depth=0.250; Run 9 | 165 |
| 8.38 | Concentration Spectrum; Depth=0.500; Run 9 | 166 |
| 8.39 | Concentration Spectrum; Depth=0.125; Run 10 | 167 |

| | | |
|------|---|-----|
| 8.40 | Concentration Spectrum; Depth=0.25; Run 10 | 168 |
| 8.41 | Concentration Spectrum; Depth=0.50; Run 10 | 169 |
| 8.42 | Concentration Spectrum; Biochemically Active Contaminant; Depth=0.125; Run 11 | 171 |
| 8.43 | Concentration Spectrum; Biochemically Active Contaminant; Depth=0.250; Run 11 | 172 |
| 8.44 | Concentration Spectrum; Biochemically Active Contaminant; Depth=0.500; Run 11 | 173 |
| 9.1 | Kinetic Energy Spectrum Indicating Two-Dimensional Turbulence (after Palmer, 1973) | 178 |
| 9.2 | Kinetic Energy Spectra Indicating Two-Dimensional Atmospheric Turbulence (after Julian, et al., 1970) | 180 |
| 9.3 | Energy Spectra Subject to an Increasing and Subsiding Wind Field (after Lemmin, et al., 1974) | 181 |
| 9.4 | Energy Spectra Subject to a Diminishing Wind Field (after Lemmin, et al., 1974) | 181 |
| 9.5 | Chlorophyll Spectra (after Leigh-Abbott, et al., 1978) | 184 |
| 9.6 | Chlorophyll Spectrum (after Leigh-Abbot, et al., 1978) | 185 |
| 9.7 | Temperature and Chlorophyll a Spectra (after Fasham and Pugh, 1976) | 186 |
| 9.8 | Energy and Chlorophyll a Spectra (after Powell, et al., 1975) | 186 |
| 9.9 | Theoretical Chlorophyll Spectrum (after Denman, et al., 1977) | 186 |
| 9.10 | Chlorophyll a Spectrum (after Fasham and Pugh, 1976) | 188 |
| 9.11 | Schematic Space of the Velocity and Temperature Spectra for $Pr \geq 1$ (after Monin and Yaglom, 1975) | 188 |
| B.1 | Autocorrelation Function Plots (Autocorrelograms) (after Bendat and Piersol, 1966) | 202 |

LIST OF SYMBOLS

| <u>SYMBOL</u> | <u>DEFINITION</u> |
|-------------------------------|--|
| A_H | Characteristic Eddy Viscosity |
| B | Benthos |
| b_o | Horizontal Reference Length |
| C | Concentration |
| C_M | Reference Concentration |
| Cov | Covariance |
| C_1, C_2, C' | Constants |
| D | Vertical Scale |
| $E(\omega)$ | Frequency Spectrum |
| $E(\underline{k})$ | Three-Dimensional Wave Number Spectrum |
| $E(k_1), E(k_2),$ $E(k_3)$ | One-Dimensional Wave Number Spectra |
| f | Coriolis Parameter (Chapter V) |
| Fr | Froude Number |
| F2 | Light Function |
| G | Filter Function |
| g | Acceleration of Gravity |

| | |
|-----------------|--|
| G_1, G_2, G_3 | Filter Lengths in x, y, z direction respectively |
| $h(\epsilon)$ | Response Function |
| h_0 | Vertical Reference Length |
| k | Wave Number |
| K_{bd} | Specific Anaerobic Benthic Decay Rate |
| K_{br} | Specific Aerobic Benthic Decay Rate |
| K_c | Monod Half Velocity for Algal Growth |
| k_c | Cutoff Wave Number |
| K_d | Specific Zooplankton Decay Rate to Nutrients |
| K_n | Monod Half Velocity for Orthophosphate Uptake |
| K_o | Monod Half Velocity for Aerobic Activity |
| K_{pr} | Specific Algal Decay Rate to Nutrients |
| K_z | Monod Half Velocity for Zooplankton Growth |
| k_1, k_2, k_3 | Wave Number in x, y, z Direction Respectively |
| L | Horizontal Scale |
| l_1, l_2, l_3 | Length Scales in x, y, z Direction Respectively |
| N_u | Nutrients |
| O | Oxygen |
| P | Pressure |
| P | Phytoplankton (Chapter V, Section E) |
| Pr | Prandtl Number |
| $R(\tau)$ | Autocorrelation Function |

| | |
|--------------------------------|---|
| Re | Reynolds Number |
| Ro | Rosby Number |
| S_{ij} | Strain-Rate Tensor |
| t | Time |
| U | Mean Speed by which Disturbances are Transported |
| u, v, w | Velocity Components |
| u', v', w' | Turbulent Velocity Components |
| u_1, u_2, u_3 | Velocity Components (Chapter III) |
| U_0 | Reference Velocity |
| v_1 | Kolmogorov Velocity Microscale |
| $W(\underline{\xi}, \tau)$ | Weighting Function |
| w_s | Sinking Velocity |
| x, y, z | Cartesian Coordinate Directions |
| x_1, x_2, x_3 | Cartesian Coordinate Directions (Chapter III) |
| Z | Zooplankton |
| γ | Filter Constant |
| δ | Dirac Delta Function |
| δ_{ij} | Kronecker Delta |
| $\Delta_1, \Delta_2, \Delta_3$ | Non-Symmetrical Filter Lengths in x, y, z Direction Respectively |
| Δ_A | Symmetrical Filter Length |
| Δt | Time Step |
| $\bar{\epsilon}$ | Dissipation Rate |
| η | Kolmogorov Length Microscale |

| | |
|------------------------|--|
| θ | Period or Wavelength |
| λ | Wave Length |
| μ | Molecular Viscosity |
| $\mu(\bar{t})$ | Arithmetic Mean |
| $\hat{\mu}_x$ | Maximum Specific Algal Growth Rate |
| $\hat{\mu}_z$ | Maximum Specific Zooplankton Growth Rate |
| ν | Kinematic Viscosity |
| ξ | Enstrophy Dissipation Rate |
| ρ | Density |
| σ^2 | Variance |
| σ_i | Reynolds Stresses |
| τ | Separation Distance (Space or Time) |
| τ_{ij} | Reynolds Stresses |
| τ_{wx}, τ_{wy} | Wind Shear Stress in x or y Direction Respectively |
| τ_1 | Kolmogorov Time Microscale |
| ω | Frequency |

CHAPTER I

INTRODUCTION AND OBJECTIVE

One of the drawbacks of modern industrialization and population growth is the large amount of contaminants entering lakes and seas. These contaminants can be chemical or biological substances (nutrients) or heat. Eutrophication refers to the degradation processes occurring in an aquatic system resulting from excessive nutrients being available to the aquatic system from external sources. As nutrients are added to the aquatic system, more phytoplankton and zooplankton life is supported. When these organisms die, the decomposition consumes dissolved oxygen. Excessive accumulation of decaying organic matter in the hypolimnion is augmented by the lack of wind induced mixing with oxygenated water during stratification, and often leads to an anoxic hypolimnion condition. In addition, the eutrophication process results in algal blooms. These algal blooms and contaminants adversely affect municipal water supplies, aquatic life and the recreational value of affected areas. There are increasing numbers of lakes where deterioration is so great that federally funded restoration measures are being implemented. Since rehabilitation requires great expense, mathematical transport models that are able to simulate and predict contaminant transport and eutrophication

processes are necessary to help identify the optimal management and restoration policy.

It is utopian to expect these transport models to predict the correct velocity field and contaminant concentration at each point in the lake. The reason is that water mass and contaminant movements are dominated by very complex random turbulent motions. Therefore, the best a transport model can do is predict the gross or averaged features of the turbulent flows. Model accuracy will therefore be a function of how well the turbulent processes, at the length scales realized in these models, are delineated within the model.

The traditional modelling approach to the numerical pollutant transport problem is the finite difference or finite element solution of governing equations prepared by Reynolds averaging. According to the Reynolds procedure the equations are averaged over time or space, yielding equations in averaged variables. The most important requirements or manifestations of this modeling method are: (1) An eddy viscosity concept be used to cope with the Reynolds stress closure problem; (2) A very coarse grid, on the order of kilometers, be employed to effectively reduce the computer cost; and (3) A second order numerical differentiation scheme is used for the representation of spatial derivatives. The models resulting from the Reynolds averaging procedure achieve very reasonable solution times but predictions for verification have failed. As an example, Allender (1976) statistically compared the predicted values of existing transport models against field data for Lake Michigan and the null hypothesis of zero velocity being the best prediction. He came to the

conclusion that the zero velocity was the best prediction! There are three general reasons for this failure: (1) The model structure is faulty, i. e. inconsistent averaging, improper eddy viscosity representation, and incorrect input data preparation; (2) Too much time is spent in improving the biological structure of these models, the "adding a new trophic level mentality" (Indeed Smarke (1978) has shown that a dramatically simple biological structure is satisfactory if the turbulence is represented properly); and (3) the accepted technique of verification is wrong.

The astonishing failure of the existing transport models to predict the field data raises a question of what constitutes a model validation. The current procedure is to erect a monitoring network, usually without advice from the numerical analyst, and to compare the collected field data with the predicted model values of the averaged variables. However, this procedure is faulty. The primary reason is that turbulent flows are stochastic in nature (Monin and Yaglom, 1975) indicating that at best the only verification possible is that of the statistics of the turbulent flow field. If the statistical details of the turbulent structure can be numerically calculated and verified then much more confidence can be placed in the calculated output of the average quantities.

None of the available transport models preserve those statistics, therefore failures of the existing models can be reduced and a significant step towards proper verification made by being more exact in the capability of numerically calculating the statistics of the turbulent eddy structure. The ideal situation is to numerically resolve all the scales present in the turbulent

field. However, this requires a number of nodal points on the order of $Re^{9/4}$ (Kwak, et al. 1975, Leonard, 1974). For a typical basin (surface area of 1.53 km^2), which is used in this thesis this means over 18×10^6 nodal points. This exceeds the capability of the largest available computers. Therefore, not only should the turbulent details be calculable but the solution domain must also have a relatively coarse network of cells. The solution of this problem is the overall objective of this report.

CHAPTER II

REVIEW OF TURBULENT TRANSPORT MODELS

As mentioned in the introduction, the classical approach to the formulation of the numerical transport problem is by averaging the governing equations over space or time. As a result of this averaging, new double correlation terms arise called Reynolds fluxes or Reynolds stresses. In this chapter a classification of the lake transport models based on the treatment of the Reynolds terms will be presented. The most well known lake models will be classified according to the particular averaging technique and briefly reviewed. At the chapter's end some advanced numerical turbulence models employing newly developed averaging techniques will be presented.

For a long time the evolution of transport models coincided with the added sophistication in the description of the Reynolds stresses and Reynolds fluxes. These Reynolds terms represent the activity of a large number of turbulent scales and therefore, their mathematical representation is very difficult. There are basically three methods of approximating the Reynolds terms in lake transport models: (a) the constant eddy viscosity method; (b) the variable eddy viscosity method; and (c) the inertial subrange method. In the constant eddy viscosity method, the Reynolds fluxes are approximated by

a constant coefficient (eddy diffusivity) multiplied by a concentration gradient, while the Reynolds stresses are approximated by the product of a constant coefficient (eddy viscosity) and the angular deformation. In the variable viscosity method the constant coefficient of the first method is replaced by a variable coefficient. The form of this coefficient is determined empirically often as a function of position (a mixing length) or temperature. The third method is a variable viscosity method but based on the theoretical calculations of the energy transfer required by the grid size of the numerical model. In this method the grid size is small enough to be included in the inertial subrange (Chapter III, Section A.6) and the eddy viscosity and eddy diffusivity are computed by considering the well known form of energy transfer in the inertial subrange.

The lake transport models which use these methods have one of the following forms: (a) circulation models; (b) pollutant transport models and (c) eutrophication models. Table 2.1 presents some of the most well known lake transport models. All of these models use second order finite differencing and constant eddy viscosity or variable eddy viscosity for the approximation of the Reynolds terms. It should be noted that Table 2.1 is not a complete list of lake transport models. For additional publications the reader is referred to review papers by Cheng (1976) and Lick (1976) for lake circulation models and to Smarke (1978) for eutrophication models.

The inertial subrange method has been proposed by Deardorff (1970) who used a 3-D model to study channel flow turbulence at large Reynolds

Table 2.1 Lake Transport Models

| CIRCULATION | POLLUTANT TRANSPORT | EUTROPHICATION |
|----------------------|----------------------|-------------------------|
| Liggett (1969) | Cheng (1975) | Di Toro, et al. (1971) |
| Liggett (1970) | Lick (1976) | Canale, et al. (1973) |
| Paul and Lick (1973) | Paul and Lick (1976) | Baca, et al. (1976) |
| Cheng (1975) | | Bierman (1976) |
| Lick (1976) | | <u>Ecosystem Models</u> |
| Paul and Lick (1976) | | Chen, et al. (1975) |
| | | Scavia (1976) |

numbers. The eddy viscosities were formulated from Smagorinsky, et al. (1965) and are parameterized by the size of the numerical cell. It has been shown by Lilly (1967) that Smagorinsky's method is compatible with the existence of an inertial subrange that encompasses the grid interval. Deardorff's method, modified by Schumann (1973) to account for distorted grids, was used by Spraggs and Street (1975) to predict the temperature regime and energy transfer in reservoirs and cooling ponds subjected to thermal loading. Finally Bedford and Shah (1977) used Spraggs and Street's method to implement a 3-D sediment transport model of Maumee Bay.

By virtue of the fact that the grid size is incorporated directly in the eddy viscosity the inertial subrange method is a better approximation of the Reynolds terms than the constant eddy viscosity and the variable eddy viscosity methods. However, as Leonard (1974) indicates it has not been very satisfactory in preserving the correct cascade characteristics (Chapter III) in a turbulent flow field. In the last four years there has been an effort at Stanford University and at Kings College, England aimed at structuring models which preserve the correct spectral form of the cascade process. In these works the energy cascade is not viewed solely as an energy loss of the large scales due to an eddy viscosity as in the previous methods. The advection terms are modified, by using a Taylor series expansion to allow for a more complete presentation of the energy cascade process. The first paper to appear was that of Leonard (1974) followed by Kwak, et al. (1975), Shaanan, et al. (1975), Mansour, et al. (1977) and Ferziger, et al. (1977). For details on the above method the

reader is referred to the review papers by Reynolds and Cebeci (1974), Reynolds (1976), Love (1976) and to the Symposium on Turbulent Shear Flows (1977).

The models developed in these references have the common characteristic that: (1) they are limited to unconfined geometries; (2) they use periodic boundary conditions; (3) they do not include any external source of energy; (4) they are limited to cubical cells; and (5) they are applicable to three-dimensional homogeneous turbulence. In this report the method developed in these references are applied to the problem of shallow basin, wind driven, lake transport of momentum and pollution. In so doing these efforts must be extended to permit the prediction of mass transport with ongoing biochemical interaction.

The introductory information for the development of this model is presented in Chapters III and IV. The equations for this model and their numerical approximation are presented in Chapters V and VI.

CHAPTER III

TURBULENCE

According to Hinze (1975, p.2): "Turbulent fluid flow is an irregular condition of flow in which the various quantities show a random variation with time and space coordinates, so that statistically distinct average values can be discerned". In addition to the irregularity condition that makes a deterministic approach to turbulence impossible, turbulence also has the following characteristics:

- a) it is characterized by large Reynolds numbers;
- b) it is diffusive i.e., spreads velocity fluctuations, and causes rapid mixing of mass, heat and momentum;
- c) it is dissipative; viscous effects convert all available kinetic energy into heat.

Consequently turbulent flow lasts as long as energy is supplied. Without this energy turbulence decays very fast. The main source of energy for the maintenance of turbulence is shear in the mean flow. Bouyancy or magnetic fields can also supply energy.

In the remainder of this chapter some of the general characteristics of turbulence, aspects of the statistical description of turbulence and classical analytical approaches to turbulence will be presented.

A. General Characteristics of Turbulence:

1) Definitions

In this section two terms, which are required for the development of the remainder of this chapter are defined. These terms are: homogeneous turbulence and isotropic turbulence.

Homogeneous turbulence is that form of turbulence where the statistical properties of the field (spectrum, velocity correlations, probability distributions of velocity and pressure, etc.) do not depend on the position in the flow field. Therefore, if u is the x -direction velocity in the positions x_1 and x_2 , the correlation function is defined as

$$R_{uu} = \overline{u(x_1) u(x_2)} \quad ; \quad (3.1)$$

where the overbar denotes an averaged quantity. It depends only on the vector difference of x_1 and x_2 ; i.e.

$$R_{uu} = R_{uu}(x_2 - x_1) \quad (3.2)$$

Also the N -dimensional probability density function of $u(x_1), u(x_2), \dots, u(x_N)$, for any number of points, depends only on the distances $x_2 - x_1, \dots, x_N - x_1$ and does not change if the same vector y is added to all x_1, x_2, \dots, x_N ;

$$\begin{aligned}
P_{x_1, x_2, \dots, x_N} (u_1, u_2, \dots, u_N) &= \\
&= P_{x_1+y, x_2+y, \dots, x_N+y} (u_1, u_2, \dots, u_N) \\
&= P_{x_2-x_1, \dots, x_N-x_1} (u_1, u_2, \dots, u_N) . \quad (3.3)
\end{aligned}$$

It must be noted that in homogeneous turbulence the statistical properties of the field are independent of the particular position in the flow field but they do depend on the direction. An extension of homogeneous turbulence is isotropic turbulence.

Isotropic turbulence is homogeneous turbulence in which all the statistical properties of the field are independent of direction. Therefore, the correlation function R_{uu} is unaltered by any rotation of the vector $x_1 x_2$. In particular in a homogeneous isotropic field the mean square value of the three velocity components u_1, u_2, u_3 are equal;

$$\overline{u_1^2} = \overline{u_2^2} = \overline{u_3^2} . \quad (3.4)$$

The concept of homogeneous and also of isotropic turbulence is basically a mathematical idealization. For a flow to be homogeneous it is required that all the mean values of the flow (mean velocity, pressure, temperature) be

constant throughout the whole space. This can be true only in some finite region of space which is very far from all the boundaries. Therefore, homogeneity exists only in some specific region and not throughout the whole space.

Nevertheless the concept of homogeneous and isotropic turbulence is used very extensively. The reasons are that: a) it is relatively simple and constitutes an approximation to the highly nonhomogeneous and anisotropic real turbulence over small spatial regions; and b) the mathematical concept of homogeneous turbulence is very valuable in describing the small-scale components of real turbulence (for definition of scales see next section). The statistical regime of these components, as will be explained later, is taken to be locally homogeneous and isotropic. Therefore, any real turbulence may be considered as locally homogeneous and locally isotropic, which simplifies, very much, the mathematical investigation.

Whenever shear and therefore a velocity gradient exists, the turbulence is nonhomogeneous and therefore anisotropic. Since shear is necessary for its existence this form of turbulence is usually called "shear flow turbulence"

2) Scales of Turbulent Motion

In order to describe a certain turbulent motion it is necessary to introduce the notion of scales of turbulence i.e. a time scale and a space scale. The magnitude of these scales depends on the dimensions of the flow field and the velocities present. For example, for lake turbulence a length scale is expected to be of the order of a characteristic length of the basin and a time scale of the order of the ratio between characteristic length of the basin

and a mean velocity. These two scales are the maximum scales present in the flow field. A study of pictures of turbulent flows and of oscillograms of velocity fluctuations shows that there are a very large number of scales. These scales are bounded from above by the maximum scales and from below by the action of the molecular viscosity. Actually there is a cascade process (see Section A.6 of this chapter) by which the large scales generate ever-smaller sizes until molecular viscosity becomes important and dissipation of energy into heat occurs. Associated with these scales are certain quasi periodicities and frequencies. The adjective "quasi" is used because the irregularity and disorderliness of turbulence involves the impermanence of the various frequencies and periodicities. Therefore, it can be said that turbulence consists of the superposition of ever-smaller periodic motions. A periodicity in the velocity distribution involves a velocity gradient. Since a certain vortex is associated with a velocity gradient it is considered that turbulence consists of the superposition of a large number of eddies each one characterized by a characteristic length and time scale. Basically there are three characteristic ranges of eddies (scales); the largest, the smallest and the intermediate ones. The largest eddy sizes are the ones that do most of the momentum and contaminant transport. Therefore, in the development of the theory of turbulence attention was first given to the study of the largest scale eddies. G. Taylor (1915, 1932), L. Prandtl (1925) and T. Von Karman (1930) formulated "semi-empirical theories of turbulence". These theories were based on an extensive amount of experimental work on the large-scale components of turbulence in pipe flows, channels, free turbulent flows (jets, wakes) and boundary layers.

The smallest scales were studied first by A.M. Obukhov (1941) and the intermediate scales by A.N. Kolmogorov (1941) who proposed the universal equilibrium theory. According to this theory, at high Reynolds numbers the smallest scales have a universal structure which is independent of the larger scales and the mean flow. In the smallest scales the energy which is supplied from the larger scales dissipates into heat. It is always assumed that the rate of energy supply equals the rate of dissipation. Therefore, the viscosity, $\nu(L^2/T)$, and the rate of dissipation of turbulent kinetic energy per unit mass of fluid, $\bar{\epsilon}(L^2 T^{-3})$ govern the kinematic features of this range of scales.

The intermediate scales are the ones that constitute the so called inertial subrange. In these scales viscosity is not important but presents non-the-less a universal character defined by the rate of energy dissipation (see Section A.6 of this chapter).

A detailed description of the small and the intermediate scales with their most important characteristics is given below.

3) Frequency Spectra

Frequency spectra are very important in statistically analyzing any turbulent flow. The reason is that measuring instruments are usually capable of recording flow variables as a function of time. All the recorded time histories include the contributions of a large range of frequencies. By passing the complete signal through a spectral analysis these frequencies are determined. Consider for example, the x-direction fluctuating component, u_1' , of the velocity field recorded at one point. Assuming that the field is quasi-steady,

there exist a function, $E(\omega)$ which when integrated over the whole range of frequencies gives an average value of $u_1'^2$:

$$\int_0^{\infty} E(\omega) d\omega = \overline{u_1'^2} \quad (3.5)$$

The function $E(\omega)$ is called the spectral density or power spectral density of the signal. A typical power spectrum is given in Figure 3.1. The dashed curve indicates that complete power spectrum where ω_L and ω_U denote the lower and upper limit to which the frequency scanning is extended. The solid line indicates the spectrum when a band-pass filter is used. ω_1 and ω_2 are the lower and the upper frequencies passed through the filter and $\Delta\omega = \omega_2 - \omega_1$.

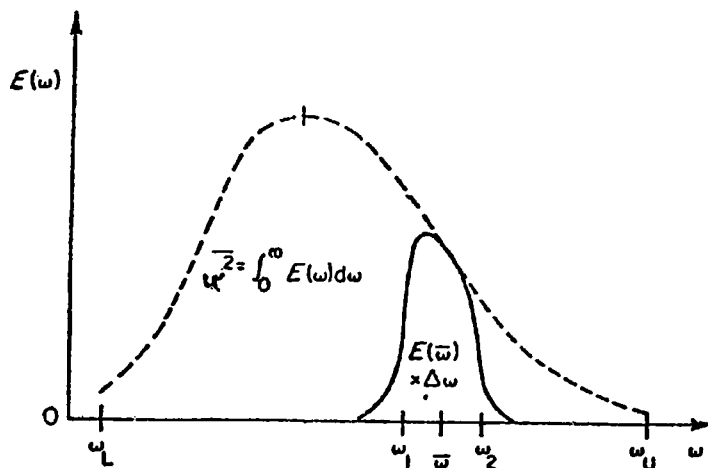


Figure 3.1 Frequency Spectrum. Solid Curve-Contribution for Filters with Nominal Limits ω_1 and ω_2 ; Dashed Curve-Complete Power Spectrum. (after Reynolds, 1974).

Expressing $u_1'(t)$ as a Fourier integral it can be shown by some algebra (Hinze 1975, p. 61) that the spectral density $E(\omega)$ and the autocorrelation coefficient

$$R(\tau) = \frac{\overline{u_1'(t) u_1'(\tau - t)}}{u_1'^2} \quad (3.6)$$

are Fourier cosine transforms:

$$R(\tau) = \frac{1}{u_1'^2} \int_0^{\infty} E(\omega) \cos 2\pi\omega\tau \, d\omega \quad (3.7)$$

$$E(\omega) = \frac{1}{4u_1'^2} \int_0^{\infty} R(\tau) \cos 2\pi\omega\tau \, d\tau \quad (3.8)$$

The relationships (3.7) and (3.8) were first pointed out by Taylor therefore $E(\omega)$ is very commonly called Taylor's one-dimensional energy spectrum.

Since $R(\tau)$ and $E(\omega)$ are Fourier transforms they give the same information in different ways. If only small eddies are present the autocorrelation drops very fast to zero and $E(\omega)$ exists mainly in the range of the high frequencies. When only large eddies are present the autocorrelation approaches zero more slowly and $E(\omega)$ exists mainly in the range of small frequencies.

4) Wave-Number Spectra

Many times the spatial structure of a turbulent field is desired. In this

case the frequency, ω , has to be replaced by its analogous wave number, $k = 2\pi/\lambda$, where λ is the wavelength of an harmonic element. The relationships (3.7) and (3.8) are written as:

$$R(r) = \frac{1}{\overline{u_1'^2}} \int_0^{\infty} E(k_1) \cos k_1 r \, dk_1 \quad (3.9)$$

$$E(k_1) = 4 \overline{u_1'^2} \int_0^{\infty} R(r) \cos k_1 r \, dr \quad (3.10)$$

where $R(r)$ is the spatial correlation, r is the distance between the points where the velocity fluctuation is observed, k_1 is the wave number in x-direction and $E(k_1)$ is the one-dimensional wave number spectrum.

Equations (3.9) and (3.10) do not take into account the three-dimensional nature of turbulence. To include this the three-dimensional spectrum has to be considered. This is done in a similar way to the one-dimensional case by transforming with respect to each of the three space coordinates (Hinze, 1975, p.204), Reynolds (1974, p.88):

$$R(\underline{x}, \underline{r}) = \iiint_{-\infty}^{\infty} E(k_1, k_2, k_3) \exp \left[i(k_1 r_1 + k_2 r_2 + k_3 r_3) \right] dk_1 dk_2 dk_3 \quad (3.11)$$

$$E(k_1, k_2, k_3) = \frac{1}{8\pi^3} \iiint_{-\infty}^{\infty} R(\underline{x}, \underline{r}) \exp \left[-i (k_1 r_1 + k_2 r_2 + k_3 r_3) \right] dr_1 dr_2 dr_3 \quad (3.12)$$

Equations (3.11) and (3.12) are expressed in vector notation as:

$$R(\underline{x}, \underline{r}) = \int_{-\infty}^{\infty} E(\underline{k}) \exp (i \underline{k} \cdot \underline{r}) d\underline{k} \quad (3.13)$$

$$E(\underline{k}) = \frac{1}{8\pi^3} \int_{-\infty}^{\infty} R(\underline{x}, \underline{r}) \exp (-i \underline{k} \cdot \underline{r}) d\underline{r} \quad (3.14)$$

The relationship between the one-dimensional spectrum $E(k_1)$ and three-dimensional spectrum $E(\underline{k})$ is given as: (Reynolds, 1974, p.89)

$$E(k_1) = \int_{-\infty}^{\infty} \int_{-\infty}^{\infty} E(\underline{k}) dk_2 dk_3 \quad (3.15)$$

which indicates disadvantage of the one-dimensional spectrum: in addition to the energy associated with a particular scale of disturbances \underline{k} it includes also the effect of larger k disturbances. This effect is called aliasing and can be seen more easily in Figure 3.2.

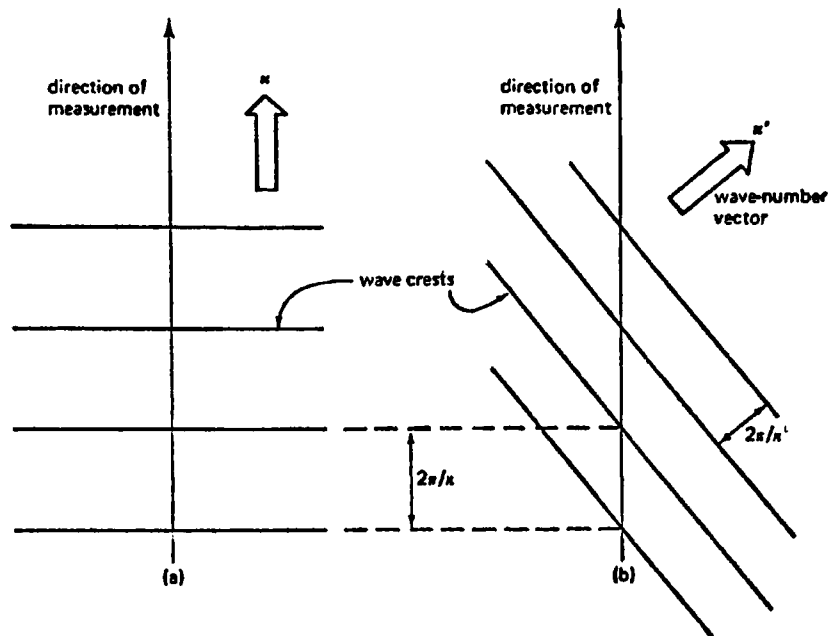


Figure 3.2 Aliasing in a one-dimensional spectrum: (a) a wave of true wave number k , aligned with the line of measurement, (b) a wave of wave number $k' > k$, with wave-number vector oblique to the line of measurement.

(after Tennekes and Lumley, 1972)

Suppose that measurements of wave number, k , are taken along a straight line. Then disturbances of wave number, k' , greater than k , occurring in a direction oblique to the direction of measurement is not distinguishable from the disturbances of wave-number, k . To avoid the aliasing problem the three-dimensional spectrum is used. However this introduces the directional information which makes physical reasoning difficult. This problem is eliminated by integrating $E(\underline{k})$ over spherical shells in \underline{k} - space. The three-dimensional spectrum derived in this way is a function of the magnitude of the wave number, \underline{k} , but not of its direction. Also it does not have the disadvantage of aliasing.

Often in practice the one-dimensional spectra of u_1, u_2, u_3 are known separately. To obtain the spectrum that represents the kinetic energy at a given wave number, the three one-dimensional spectra are added together. (Tennekes and Lumley, 1972, p.250). The resultant spectrum is referred to as the three-dimensional spectrum.

5) Taylor's Frozen Turbulence Hypothesis

Wave number spectra are many times more desirable than frequency spectra. As in Reynolds (1974, p.91) two specific advantages of the wave number spectra are:

- "(1) Wave number spectra are much less strongly influenced by mean convection than are frequency spectra, and thus provide more direct insight into the time and length scales of the turbulence; and
- (2) three-dimensional spectra are more clearly related to disturbances of a particular size."

However, the spatial structure of turbulence is very difficult to determine. This requires simultaneous recording of oscillations at a relatively large number of points in the flow field which is very impractical. Therefore, the existence of a way to convert the one-dimensional frequency spectra into one-dimensional wave number spectra is very important. This is done by means of Taylor's frozen turbulence hypothesis. Taylor (1938) formulated his hypothesis for grid-generated turbulence in a wind tunnel. According to this hypothesis the turbulent fluctuations are much smaller than a typical mean

flow. Consequently it is assumed that the instantaneous velocity at one point, \underline{x}_0 , is replaced by the mean velocity at that point. Taylor next assumed that for small time intervals the turbulent fluctuations are transported past this point with the mean velocity without any distortion. Therefore, the transport of turbulence past this point is equivalent to the movement of an unchanging pattern past this point. Of course, the assumption of non-distortion of turbulence is not completely true because there is always a change in pattern even in small time intervals. However, in many cases the changing process is very slow and the assumption of unchanged pattern does not introduce a large error. This assumption is called the frozen turbulence hypothesis since turbulence is assumed to be "frozen" in a reference frame moving past the point, \underline{x}_0 , with the mean velocity. The frozen turbulence hypothesis is very valuable since according to this, the spectral contribution at frequency ω is generated by a sinusoidal wave with wave number, $k = 2\pi/\lambda$, given by $k = \omega/U$. (λ is the wave-length of the sinusoidal wave and U is the mean speed with which the disturbances are transported past the measuring point). Also the time delay, τ , is equivalent to a separation distance $r = U\tau$ in the direction of convection. Using the above relationships the correlation function and the frequency spectrum of Equations (3.7) and (3.8) are written as:

$$R\left(\frac{r}{U}\right) = \frac{U}{u_1'^2} \int_0^{\infty} E(kU) \cos kr \, dk \quad ; \quad (3.16)$$

$$E(kU) = \frac{4 u_1'^2}{U} \int_0^{\infty} R\left(\frac{r}{U}\right) \cos kr \, dr \quad (3.17)$$

Comparison of Equations (3.16) and (3.17) with (3.9) and (3.10) shows that the one-dimensional wave number spectrum is estimated as:

$$E(k_1) = U E(\omega) \quad (3.18)$$

where:

$$k_1 = \frac{\omega}{U} \quad (3.19)$$

implying the ω and k_1 have consistent units i.e. cycles or radians. When ω is measured in cycles and k_1 in radians, Equations (3.18) and (3.19) are written as:

$$E(k_1) = \frac{U}{2\pi} E(\omega) ; \text{ and} \quad (3.20)$$

$$k_1 = \frac{2\pi\omega}{U} \quad (3.21)$$

The validity of Taylor's hypothesis is shown in Figures 3.3 and 3.4. Figure 3.3 is from the original paper by Taylor (1938) presented in Monin and Yaglom (1975) and Figure 3.4 is from Favre, et al. (1938) as presented in Hinze (1975). Both compare time and spatial correlations for grid generated turbulence and the agreement is completely satisfactory. Taylor's frozen turbulence hypothesis applies not only for nearly homogeneous and isotropic grid generated turbulence but also through large parts of non-homogeneous turbulent flows when the ratio u'/U is less than 0.1 (Reynolds, 1974, p.91). Therefore, it is applicable in most turbulent flows but not too near a wall.

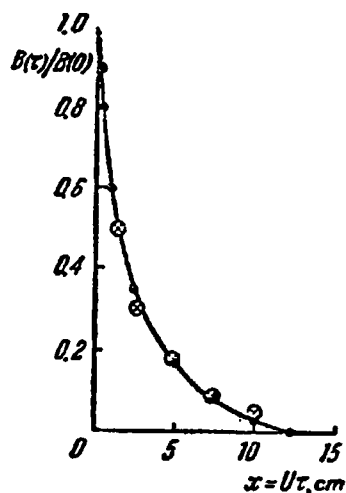


Figure 3.3 Comparison of Measured Values of the Velocity Correlation Function (Solid Points) with Calculations Based on Taylor's Hypothesis (After Monin and Yaglom, 1975)

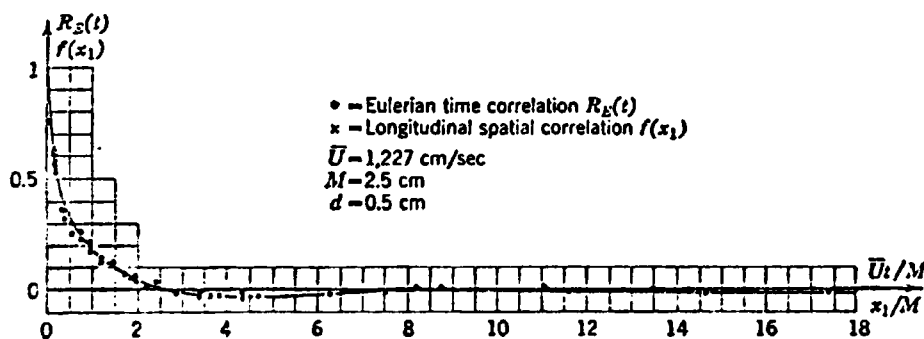


Figure 3.4 Comparison between Time and Spatial Correlations According to Taylor's Hypothesis. (Favre, A., et al., Recherche Aeronaut., Paris, No. 32, p.21, 1953) (After Hinze, 1975)

6) Energy Cascade - Kolmogorov Theory

Energy enters the flow field at the large length scales. At these scales eddies are generally non-homogeneous and anisotropic and the Reynolds number is very large. Therefore, viscosity is not important and energy dissipation does not occur. However, these scales produce through inertial interactions a large hierarchy of smaller scales until a level is reached where the Reynolds number is very small (Re_{cr}). As a consequence viscosity becomes very important and conversion of kinetic energy into heat occurs. Viscosity does not control the rate of energy dissipation. The small scales adjust themselves so that all the energy transferred to them dissipates. The smaller the viscosity, the smaller the scales that survive. This process of continuous energy transfer to the dissipation scales is called "the energy cascade" and it is very neatly described in Monin and Yaglom (1975, Chapter 8). According to them the largest disturbances in a turbulent flow have a length scale, l_1 , which is of the same order of magnitude of the length scale, L , of the flow as a whole. In addition, the velocity scale, v_1 , is of the same order of magnitude as the changes Δv in the mean flow velocity over distances of the order of L . The Reynolds number $Re_1 = v_1 l_1 / \nu$ is very large and these first order disturbances break down into smaller scales l_2 with velocity scale v_2 . The Reynolds number $Re_2 = v_2 l_2 / \nu$ is smaller than Re_1 but still much larger than Re_{cr} . Therefore, the secondary disturbances are still unstable and break down to smaller length scales l_3 and so on until a length scale $l_n = \eta$ is reached where Re_n is of the order of magnitude of Re_{cr} . These scales are

hydrodynamically stable and do not break down any more. Their energy is spent in overcoming frictional forces and is therefore, dissipated into heat.

Kolmogorov (1941) in his famous equilibrium theory was the first one to recognize that despite the fact that the small eddies obtain all their energy from the non-homogeneous and anisotropic large eddies are in fact homogeneous and isotropic and independent of the properties of the large components of the motion. Since the time scales of the small eddies are much smaller than the time scale of the mean flow they are also regarded as quasi-stationary, i.e., not depending explicitly on time but changing only because of its dependence on the slowly changing characteristics of the mean flow. The fact that the small eddies are independent of the mean flow does not mean that the statistical state of small-scale fluctuations is the same in all flows. The mean motion affects the small scale fluctuations through the energy flux, which is transferred throughout all the range of scales to the dissipation scales. Assuming that there is no energy dissipation in the intermediate scales the mean amount of energy converted into heat per unit mass of the fluid per unit time (dissipation rate, $\bar{\epsilon}$) equals the mean amount of energy transferred to the largest scale eddies per unit mass of fluid per unit time. The dissipation rate, $\bar{\epsilon}$, is given

$$\bar{\epsilon} = \frac{1}{2} \nu \sum_{i,j} \overline{\left(\frac{\partial u'_i}{\partial x_j} + \frac{\partial u'_j}{\partial x_i} \right)^2} \quad (3.22)$$

Kolmogorov, in his first similarity hypothesis, assumed that the statistical regime of the smallest scale disturbances, where energy dissipation

occurs, depends on ϵ and ν . Using these two parameters, Kolmogorov formed the following length, time and velocity scales

$$\eta = \left(\frac{\nu^3}{\bar{\epsilon}}\right)^{1/4}, \quad \tau_1 = \left(\frac{\nu}{\bar{\epsilon}}\right)^{1/2}, \quad v_1 = (\nu \bar{\epsilon})^{1/4} \quad (3.23)$$

These scales are called the Kolmogorov microscales. Based on these scales the Reynolds number is derived to be $Re_{cr} = \eta v_1 / \nu = 1$. The length scale, η , is the maximum scale where viscosity is important. In his second similarity hypothesis Kolmogorov assumed that for scales much greater than η but much smaller than L the statistical regime of the turbulent fluctuation depends only on $\bar{\epsilon}$ and is independent of ν . In these scales the inertial transfer of energy to smaller eddies dominates and therefore they constitute the so called inertial subrange.

Figure 3.5 borrowed from Reynolds (1974) shows the above ideas.

Kolmogorov formulated a very important law for the inertial subrange. This law is the "two-thirds" law according to which the mean square of the difference of the velocities at two points in the inertial subrange is given by $c_1 (\bar{\epsilon} r)^{2/3}$ where c_1 is a numerical constant and r is the distance between the two points. A law equivalent to "two-thirds" law in wave space is the "five-thirds" law according to which the spectral density of the kinetic energy of turbulence is given by:

$$E(k) = c_2 \bar{\epsilon}^{2/3} k^{-5/3} \quad (3.24)$$

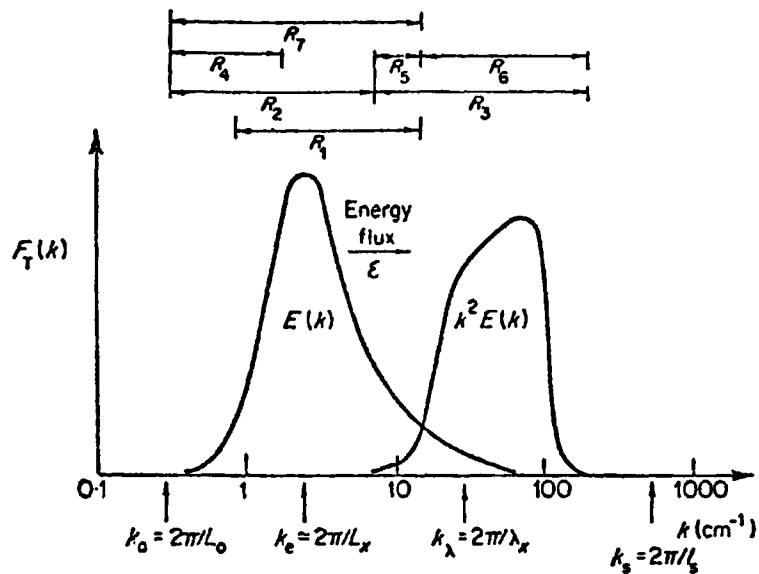


Figure 3.5 Characteristic ranges of a turbulent motion, illustrated by three-dimensional wave-number spectra of energy $E(k)$ and dissipation $k^2 E(k)$. The Reynolds number for the case considered, $Re_0 = 10^5$, is about the lowest at which an inertial subrange exists. The wave-numbers correspond roughly to $L_0 = 20$ cm.

- R_1 range of energy-containing motions
- R_2 range peculiar to the particular flow
- R_3 universal equilibrium range
- R_4 range of energy extraction
- R_5 inertial subrange
- R_6 dissipative range
- R_7 range of inertial scaling

(after Reynolds, 1974)

where c_2 is another constant and k is the wave number. Formula (3.24) was first obtained by Obukhov (1949 a, b) and has been verified by several investigators (see next section). It is very important in the computation of any turbulent flow because the parameterization of the non-resolvable scales depends on knowing the wave length of this range.

7) Observation of Five-Thirds Law

The validity of the five-thirds law has been confirmed by many investigators for atmospheric and aquatic turbulence. Monin and Yaglom (1975, p.467) present a very good summary of the verification of this law in atmospheric

turbulence. Figure 3.6 borrowed from this section shows that there is an appreciable region of wave number where the five-thirds law is satisfied.

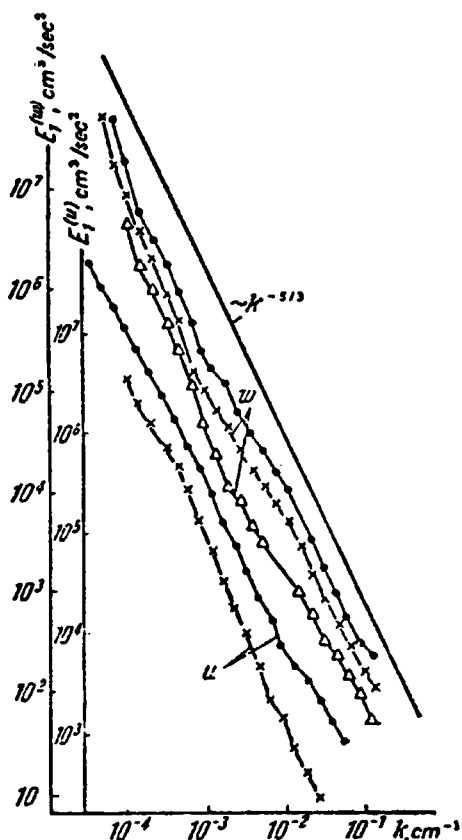


Fig. 3:6 Measured one-dimensional spectra of the horizontal (u) and vertical (w) wind-velocity components at a height of 300 m. (after Monin and Yaglom, 1975)

An extensive amount of work exists in verification of the five-thirds law in aquatic turbulence. Cannon (1971) observed the motion in a coastal plain estuary. Even though an inertial subrange does not exist, he found that most of the spectra follow the five-thirds law in periods less than 4 minutes and greater than 8 minutes. He also found that some spectra follow a -1 slope.

Dillon et al. (1976) measured low-frequency turbulence in the epilimnion of Lake Tahoe by using Savonius rotor current meter positioned at three depths. They used Taylor's frozen turbulence hypothesis to convert frequency spectra to wave-number spectra and they found that the five-thirds law is generally satisfied at wavelengths ranging generally between 10 and 110 m. They note that turbulence cannot be assumed isotropic and therefore a true inertial subrange does not exist.

Grant et al. (1962) used a hot film anemometer to compute the turbulence spectra in a tidal channel. They found that in wavelengths 6.28cm-628cm the data followed closely the five-thirds law.

Palmer (1973) used a current meter and a hot-film anemometer to develop the kinetic energy spectra in Lake Ontario. Measurements were taken at two stations at a depth of 5.8m. The first station was 1km offshore in 9m of unstratified water and the second well offshore in 22m of water with a well established thermocline. He found that the nearshore spectra from both the hot film and the current meter are characterized by a general slope of -3.0. The offshore spectra followed the five-thirds law at wavelengths of 0.6-20m.

Webster (1969) used the Taylor's hypothesis to convert measured oceanic frequency spectra to wave number spectra. He found that the five thirds law was observed at length scales ranging from 500m-5000m. These scales are the largest ones where this law was found to be satisfied in aquatic turbulence.

The verification of the five-thirds law in large scales is very encouraging for those deriving the numerical representation of geophysical flows. As

will be shown this law allows the easy formulation of transport models which use relatively coarse grids. All turbulent activity not resolved by this coarse grid will be parameterized by existing techniques (Chapter V, Section D).

8) Energy Subranges in 2-D Turbulence

Two-dimensionality is typical of the large scale motion of the atmosphere and of the large scale motion of the oceans. Also two-dimensionality prevails in shallow regions of lakes and ocean. Therefore, an extended portion of literature is devoted to the study of 2-D flows and the energy transfer in them.

In 2-D flows in addition to energy another quantity has to be conserved. This is one-half the squared vorticity called enstrophy. Therefore, two kinds of dissipation may occur, namely energy, $\bar{\epsilon}$, and enstrophy, ξ . Correspondingly, two kinds of inertial ranges can be defined: that of Kolmogorov (inertial subrange) and that of enstrophy (enstrophy subrange). Fjørtoft (1953) was the first one to report that when energy enters the system at a wave number, k_1 , only one fraction transfers into greater wave numbers while the rest of it transfers to the smaller wave numbers. Kraichnan (1967) and Leith (1968) formulated Fjørtoft's (1953) theory. According to these studies and unlike the 3-D flows where energy flows one way to smaller scales as $k^{-5/3}$ (Equation 3.24), a reverse situation occurs in 2-D flows. Suppose that a fluid is excited by a force confined at $k \sim k_1$ and it supplies energy at steady rate, $\bar{\epsilon}$ and enstrophy at steady rate $\xi \sim 2k_1^2 \bar{\epsilon}$. Then on the one hand energy transfers to smaller scales as:

$$E(k) = c' \xi^{2/3} k^{-3} \quad (3.25)$$

and dissipates in the viscous range. On the other hand, however, it transfers to larger scales towards zero wave number as Equation 3.24. If sufficient energy exists it saturates all the larger scales and piles up at the lowest possible wave number when reaches the outer boundaries of the physical system.

Kraichnan (1971) corrected Equation (3.25) to:

$$E(k) = c' \xi^{2/3} k^{-3} \left(\ln \frac{k}{k_i} \right)^{-1/3} \quad (3.26)$$

Also he points out that the energy and enstrophy ranges are mutually exclusive. That is there is zero enstrophy transfer in the energy subrange and zero energy transfer in the enstrophy subrange.

Lilly (1969) tested the above models by numerically integrating the 2-D Navier-Stokes equations and using a random forcing disturbance in the neighborhood of a wave number, k_e . His results verified the $k^{-5/3}$ range at wave numbers smaller than k_e . However, the k^{-3} range was less clearly verified due to numerical problems.

Spectral analysis of large-scale meteorological data has shown that the k^{-3} spectrum is very common in atmospheric turbulence. The works by Benton, et al. (1958), Julian, et al. (1970), Winn-Nielsen (1967) are representative of the k^{-3} spectrum in the atmosphere.

Lemmin, et al. (1974) used a current meter to estimate the energy spectra in Lake Ontario. The spectra were computed during the passage of a storm. At the beginning of the storm the spectra showed a -3 slope indicating a 2-D turbulence. Eventually a peak appeared in the spectrum and after the end of the storm the slope changed to -5/3. They interpreted the peak as an energy input from breaking of surface waves. The -5/3 slope indicated that after the energy source was exhausted the structure of turbulence changed from two-dimensional to three dimensional.

B. Classical Analytic Approaches to Turbulence Computations

1) Averaging Procedures

A study of a turbulence oscillogram shows that the turbulent flow consists of a variety of oscillations with no obvious regularity. The effect of this is that the instantaneous value of all the dynamic fields behaves in a very disordered way. The existence of all these oscillations and also the fact that the same turbulence pattern cannot be obtained even if the same conditions are repeatedly applied, makes the use of averaging a necessary tool in any turbulence computation. This averaging allows the transition of the instantaneous field from a disordered to a smooth nature.

The standard procedure in averaging is the decomposition of the instantaneous field $f(x_1, x_2, x_3, t) = f(\underline{x}, t)$ into a mean and a fluctuating component as:

$$f = \bar{f} + f' \quad (3.27)$$

where f is the instantaneous value of the variable being averaged, \bar{f} is the average value and f' is a fluctuating component such that $\overline{f'} = 0$. The average value is determined by a) time averaging, b) space averaging, or c) ensemble averaging.

As in Monin-Yaglom (1965, Chapter 2) a general space-time averaging is given by:

$$\overline{f(x_1, x_2, x_3, t)} = \iiint_{-\infty}^{-\infty} f(x_1 - \xi_1, x_2 - \xi_2, x_3 - \xi_3, t - \tau) \omega(\xi_1, \xi_2, \xi_3, \tau) d\xi_1 d\xi_2 d\xi_3 d\tau \quad (3.28)$$

where $\omega(\underline{\xi}, \tau)$ is some weighting function satisfying the normalization condition

$$\iiint_{-\infty}^{\infty} \omega(\xi_1, \xi_2, \xi_3, \tau) d\xi_1 d\xi_2 d\xi_3 d\tau = 1 \quad (3.29)$$

Depending on $\omega(\underline{\xi}, \tau)$ Equation (3.28) takes the form of a time or space averaging. If $\omega(\underline{\xi})$ and $\omega(\tau)$ have a constant value over a parallelepiped and are equal to zero outside it and if δ is a Dirac delta function, then Equation (3.27) converts to a time averaging if $\omega(\underline{\xi}, \tau) = \omega(\tau) \delta(\underline{\xi})$. The same equation converts to a space averaging if $\omega(\underline{\xi}, \tau) = \omega(\underline{\xi}) \delta(\tau)$. Time and space averaging are not very convenient because they generally depend on the time interval or space volume chosen for averaging. Therefore, they give many different mean values. To avoid this problem an ensemble averaging is used which is simpler and has more universal properties. To obtain this an

experiment has to be performed under identical conditions a large number of times and the value $f(\underline{x}, t)$ has to be obtained in each one of them. The arithmetic mean of all these values give the ensemble mean. When the number of experiments becomes very large the ensemble mean approaches the probability mean (see Appendix C for definitions). The ensemble mean is not convenient to be used in practice because usually only one experiment exists. Therefore, there is a necessity of taking the averages over some time or space interval and to examine under what conditions these averages approach the probability mean. It is obvious that ensemble averaging does not eliminate the problem of ordinary space or time averaging but just alters the formulation of the problem.

In order for the mean (time or space) obtained over one single experiment approach the probability mean the averaging interval (time or space) has to be very large and ergodicity necessitates that the turbulent field has to be stationary or homogeneous relating to time or space averaging respectively. This is explained below. Consider first the time averaging. In this case the dependence of $f(\underline{x}, t)$ on \underline{x} is insignificant and the mean is written as:

$$\bar{f}(t) = \frac{1}{T} \int_{t-T/2}^{t+T/2} f(t + \tau) d\tau \quad (3.30)$$

In order that (3.30) approaches the probability mean as $T \rightarrow \infty$ it is shown in Monin and Yaglom (1965, p.244) that:

$$\overline{f(t)} = f = \text{constant} \quad (3.31)$$

Equation (3.31) indicates that the process has to be time independent, i.e., stationary. Stationarity is difficult to be assumed in the case of natural turbulent flows. Here short time intervals are considered so that the process can be assumed stationary. In these cases the probability mean is found by time-averaging. For this to be possible it is necessary that the time means as $T \rightarrow \infty$ converge to the probability mean and that the means taken over time, T , in the course of which the process may be assumed stationary, will already be fairly close to the limits corresponding to $T \rightarrow \infty$ (Monin and Yaglom, 1965, p.246).

In the case of space averaging the situation is similar. Here the dependence of $f(\underline{x}, t)$ on t is insignificant and the mean is written as:

$$f(\underline{x}) = \frac{1}{ABC} \int_{-A/2}^{A/2} \int_{-B/2}^{B/2} \int_{-C/2}^{C/2} f(x_1 + \xi_1, x_2 + \xi_2, x_3 + \xi_3) d\xi_1 d\xi_2 d\xi_3 \quad (3.32)$$

As in the case of time averaging in order that (3.32) approaches the probability mean for $A \rightarrow \infty$, $B \rightarrow \infty$, $C \rightarrow \infty$ (or at least one of them being true) a similar expression to Equation (3.31) must exist:

$$f(\underline{x}) = f = \text{constant} \quad (3.33)$$

Equation (3.33) indicates that the mean has to be independent of the position in the flow field, i.e., homogeneity. Therefore, in space averaging the flow field has to be homogeneous. As in the case of time averaging homogeneity is

difficult to be assumed under natural conditions except in small space regions. The assumption of an inertial subrange provides a very good way of defining these regions.

Summarizing this section, it is concluded that when the turbulent flow can be considered as being stationary, averaging with respect to time should be used. When the turbulent flow is homogeneous space averaging should be considered.

2) Reynolds Axioms

In the previous section it was shown that in the computation of turbulent flows the instantaneous values of the flow variables are decomposed into a mean and a fluctuating component (Equation 3.27). Then an averaging procedure was used (Equations 3.30 and 3.32) to determine the mean value. If Equations (3.30) and (3.32) are used in the differential equations of fluid dynamics an unworkable set of equations will be derived. Therefore, rules which obey (3.30) and (3.32) and which allow sufficiently simple equations to be derived must be used. These rules are the so called Reynolds axioms because they were first derived by Reynolds (1894). If g and h are two variables and c is a constant then the Reynolds axioms are the following:

$$\overline{g + h} = \bar{g} + \bar{h} \quad (3.34)$$

$$\overline{c g} = c \bar{g} \quad (3.35)$$

$$\overline{\frac{\partial g}{\partial t}} = \frac{\partial}{\partial t} \bar{g} \quad (3.36)$$

$$\overline{\overline{g h}} = \overline{\overline{g h}} = \overline{g h} \quad (3.37)$$

It can be shown (Okubo, 1964) that Equations (3.34) through (3.37) satisfy Equations (3.30) and (3.32)

3) Reynolds Stresses and the Closure Problem

In the previous two sections the existing techniques for the transition of the fluid dynamic variables from a complex and irregular character, associated with turbulence, to a smooth and gradually varying one were discussed. In this section the application of these techniques to the equations of motion will be presented.

The Navier-Stokes equations and the continuity equation for incompressible flow are written as:

(Schlichting, 1968)

$$\rho \left(\frac{\partial u}{\partial t} + \frac{\partial}{\partial x}(u^2) + \frac{\partial}{\partial y}(uv) + \frac{\partial}{\partial z}(uw) \right) = - \frac{\partial P}{\partial x} + \mu \nabla^2 u \quad (3.41 a)$$

$$\rho \left(\frac{\partial v}{\partial t} + \frac{\partial}{\partial x}(vu) + \frac{\partial}{\partial y}(v^2) + \frac{\partial}{\partial z}(vw) \right) = - \frac{\partial P}{\partial y} + \mu \nabla^2 v \quad (3.41 b)$$

$$\rho \left(\frac{\partial w}{\partial t} + \frac{\partial}{\partial x}(wu) + \frac{\partial}{\partial y}(wv) + \frac{\partial}{\partial z}(w^2) \right) = - \frac{\partial P}{\partial z} + \mu \nabla^2 w \quad (3.41 c)$$

$$\frac{\partial u}{\partial x} + \frac{\partial v}{\partial y} + \frac{\partial w}{\partial z} = 0 \quad (3.41 d)$$

The flow variables are expressed as in Equation (3.27)

$$u = \bar{u} + u' \quad , \quad v = \bar{v} + v' \quad , \quad w = \bar{w} + w' \quad , \quad P = \bar{P} + P' \quad (3.42)$$

Substitution of Equation (3.42) into (3.41) and averaging results in the following equations:

$$\rho \left(\frac{\partial \bar{u}}{\partial t} + \frac{\partial}{\partial x} (\bar{u}\bar{u}) + \frac{\partial}{\partial y} (\bar{u}\bar{v}) + \frac{\partial}{\partial z} (\bar{u}\bar{w}) \right) = - \frac{\partial \bar{P}}{\partial x} + \mu \nabla^2 \bar{u} - \rho \left[\frac{\partial}{\partial x} \overline{u'^2} + \frac{\partial}{\partial y} \overline{u'v'} + \frac{\partial}{\partial z} \overline{u'w'} \right] \quad (3.43 \text{ a})$$

$$\rho \left(\frac{\partial \bar{v}}{\partial t} + \frac{\partial}{\partial x} (\bar{v}\bar{u}) + \frac{\partial}{\partial y} (\bar{v}\bar{v}) + \frac{\partial}{\partial z} (\bar{v}\bar{w}) \right) = - \frac{\partial \bar{P}}{\partial y} + \mu \nabla^2 \bar{v} - \rho \left[\frac{\partial}{\partial x} \overline{u'v'} + \frac{\partial}{\partial y} \overline{v'^2} + \frac{\partial}{\partial z} \overline{v'w'} \right] \quad (3.43 \text{ b})$$

$$\rho \left(\frac{\partial \bar{w}}{\partial t} + \frac{\partial}{\partial x} (\bar{w}\bar{u}) + \frac{\partial}{\partial y} (\bar{w}\bar{v}) + \frac{\partial}{\partial z} (\bar{w}\bar{w}) \right) = - \frac{\partial \bar{P}}{\partial z} + \mu \nabla^2 \bar{w} - \rho \left[\frac{\partial}{\partial x} \overline{w'u'} + \frac{\partial}{\partial y} \overline{w'v'} + \frac{\partial}{\partial z} \overline{w'^2} \right] \quad (3.43 \text{ c})$$

Equations (3.43), called the Reynolds equations, contain the terms relating to the mean motion and additional terms on the right hand side due to the turbulent motion. These terms are often interpreted as stresses on an

element of the fluid in addition to the viscous stresses. They are called apparent, virtual stresses of turbulent flow, or Reynolds stresses. The components of the stress tensor due to the turbulent velocity components of the flow are:

$$\begin{pmatrix} \sigma'_x & \tau'_{xy} & \tau'_{xz} \\ \tau'_{xy} & \sigma'_y & \tau'_{yz} \\ \tau'_{xz} & \tau'_{yz} & \sigma'_z \end{pmatrix} = - \begin{pmatrix} \overline{\rho u'^2} & \overline{\rho u'v'} & \overline{\rho u'w'} \\ \overline{\rho u'v'} & \overline{\rho v'^2} & \overline{\rho v'w'} \\ \overline{\rho u'w'} & \overline{\rho v'w'} & \overline{\rho w'^2} \end{pmatrix}$$

Equations (3.44) are written as:

$$\begin{aligned} \rho \left(\frac{\partial \bar{u}}{\partial t} + \frac{\partial \bar{u}\bar{u}}{\partial x} + \frac{\partial}{\partial y} (\bar{u}\bar{v}) + \frac{\partial}{\partial z} (\bar{u}\bar{w}) \right) &= - \frac{\partial \bar{P}}{\partial x} + \mu \nabla^2 \bar{u} \\ &+ \left(\frac{\partial}{\partial x} \sigma'_x + \frac{\partial}{\partial y} \tau'_{xy} + \frac{\partial}{\partial z} \tau'_{xz} \right) \end{aligned} \quad (3.46a)$$

$$\begin{aligned} \rho \left(\frac{\partial \bar{v}}{\partial t} + \frac{\partial \bar{v}\bar{u}}{\partial x} + \frac{\partial}{\partial y} (\bar{v}\bar{v}) + \frac{\partial}{\partial z} (\bar{v}\bar{w}) \right) &= - \frac{\partial \bar{P}}{\partial y} + \mu \nabla^2 \bar{v} \\ &+ \left(\frac{\partial}{\partial x} \tau'_{xy} + \frac{\partial}{\partial y} \sigma'_y + \frac{\partial}{\partial z} \tau'_{yz} \right) \end{aligned} \quad (3.46b)$$

$$\begin{aligned} \rho \left(\frac{\partial \bar{w}}{\partial t} + \frac{\partial \bar{w}\bar{u}}{\partial x} + \frac{\partial}{\partial y} (\bar{w}\bar{v}) + \frac{\partial}{\partial z} (\bar{w}\bar{w}) \right) &= - \frac{\partial \bar{P}}{\partial z} + \mu \nabla^2 \bar{w} \\ &+ \left(\frac{\partial}{\partial x} \tau'_{xz} + \frac{\partial}{\partial y} \tau'_{yz} + \frac{\partial}{\partial z} \sigma'_z \right) \end{aligned} \quad (3.46c)$$

$$\frac{\partial \bar{u}}{\partial x} + \frac{\partial \bar{v}}{\partial y} + \frac{\partial \bar{w}}{\partial z} = 0 \quad (3.46d)$$

The difficulty in solving Equations (3.46) arises from the presence of the new unknowns (Reynolds stresses). The system is indeterminate because it contains more unknowns than equations. The problem of solving Equations (3.46) is referred to as the closure problem. Most of the theoretical work in turbulence is associated with the difficulties arising from this problem. In the next section the most standard methods of closing the system of Equations (3.46) by approximating the Reynolds stresses will be discussed.

4) Computational Approaches to the Closure Problem

a) First Order Theory

The first order models are the simplest existing models in closing the Equations (3.46). To reduce the number of unknowns in (3.46) the Reynolds stresses are computed in terms of other unknowns. Therefore, the number of unknowns is reduced down to the number of equations.

The equation used is the following:

$$\tau_{ij} = -K \left(\frac{\partial \bar{u}_i}{\partial x_j} + \frac{\partial \bar{u}_j}{\partial x_i} \right) = -K S_{ij} \quad (3.47)$$

where K is the eddy viscosity which is assumed to be a function of the averaged flow variables and S_{ij} is the strain-rate tensor. The eddy viscosity K is computed by a form suggested by Smagorinsky (1965) as:

$$K = (ch)^2 \left[\frac{\partial \bar{u}_i}{\partial x_j} \left(\frac{\partial \bar{u}_i}{\partial x_j} + \frac{\partial \bar{u}_j}{\partial x_i} \right) \right]^{1/2} \quad (3.48)$$

where c is a constant and h is the mesh separation distance. If an inertial subrange exists it can be shown that (3.48) is consistent with the Kolmogorov energy spectrum (3.24). A special case of the first order theory is the constant eddy viscosity and the variable eddy viscosity methods very commonly used in lake transport models. In these methods K is considered arbitrarily constant or variable depending on position or temperature (Chapter II).

For more details on first order models, see Chapter V, Section D.

b) Second Order Theory

The second order theory involves equations for the Reynolds stresses which have to be solved in addition to the Navier-Stokes equations.

These equations are the following (Harlow, et al., 1967):

$$\begin{aligned} & \frac{\partial \overline{u'_i u'_j}}{\partial t} + \bar{u}_k \frac{\partial \overline{u'_i u'_j}}{\partial x_k} + \overline{u'_i u'_k} \frac{\partial \bar{u}_j}{\partial x_k} + \overline{u'_j u'_k} \frac{\partial \bar{u}_i}{\partial x_k} + \frac{\partial \overline{u'_i u'_j u'_k}}{\partial x_k} \\ & = - \left(\overline{u'_i \frac{\partial \phi'}{\partial x_j}} + \overline{u'_j \frac{\partial \phi'}{\partial x_i}} \right) + \nu \left(\overline{u'_i \frac{\partial^2 u'_j}{\partial x_k^2}} + \overline{u'_j \frac{\partial^2 u'_i}{\partial x_k^2}} \right) \end{aligned} \quad (3.49)$$

where ϕ is the ratio of pressure to density.

To make (3.49) determinate a flux approximation for the Reynolds stress is used:

$$\overline{u'_j u'_k} = \frac{2}{3} q \delta_{jk} - K S_{jk} \quad (3.50)$$

where q is the kinetic energy of the turbulent fluctuations and δ_{jk} is the kronecker delta. An equation now for q is needed. This is given by:

$$\begin{aligned} \frac{\partial \bar{q}}{\partial t} + \bar{u}_k \frac{\partial \bar{q}}{\partial x_k} = & K \bar{S}_{jk} \frac{\partial \bar{u}_j}{\partial x_k} - \frac{\partial}{\partial x_k} \overline{(u'_k q')} - \frac{\partial}{\partial x_k} \overline{(u'_k \phi')} \\ & + \nu \frac{\partial^2 \bar{q}}{\partial x_k^2} - \overline{\nu \left(\frac{\partial u'_j}{\partial x_k} \right)^2} \end{aligned} \quad (3.51)$$

For more information on the second order theory the reader is referred to Lilly (1967), Daly, et al. (1970), Harlow, et al. (1967) and Deardorff (1973).

CHAPTER IV

FILTRATION

One of the very important tools in signal processing is signal filtration.. By filtration it is meant that some undesired information of the signal is removed by the use of a mathematical device or a physical process. For example, if a signal or process is composed of oscillatory activity with a finite number of frequencies, a filter can remove specified frequencies such as 60 Hertz Notch filters for line noise, or all frequencies which are larger or smaller than some cutoff frequency. Therefore, only the relevant frequencies are kept for further processing.

Filters are in use in many engineering applications. The mathematical modelling of turbulence is one of them. Here the necessary discretization of time and space is in fact a process of filtration which requires that the governing equations be properly filtered and therefore consistent with the act of discretization.

In this chapter some of the most important characteristics of filters and their application to turbulent flow computations will be discussed. Since the most applicable definition of a filter is through the convolution integral the first section of this chapter is devoted to the description of this integral.

A. Filter Methodology

1) The Convolution Integral

The best way of defining the convolution integral is by following the method applied in systems analysis where the response of a linear system to certain signals is desired. Here the input signal is decomposed into a set of elementary signals and the response of the system to each one of those is determined. By assuming that the system is linear and the principle of superposition applies the total response of the system is determined by the superposition of all these separate responses. The expression which states the total response of the system in terms of these separate elementary responses is called the convolution integral. To express the convolution integral mathematically the elementary signal (impulse or delta function) and the elementary response of the system (impulse response) have to be defined.

Consider the finite ramp function (Figure 4.1), where θ is the time or space variable.

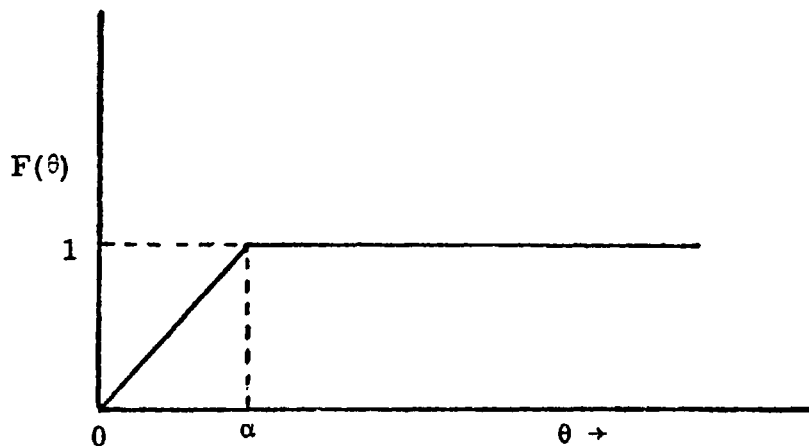


Figure 4.1 The Finite Ramp

Next consider the derivative of the finite ramp, $\frac{dF(\theta)}{d\theta}$

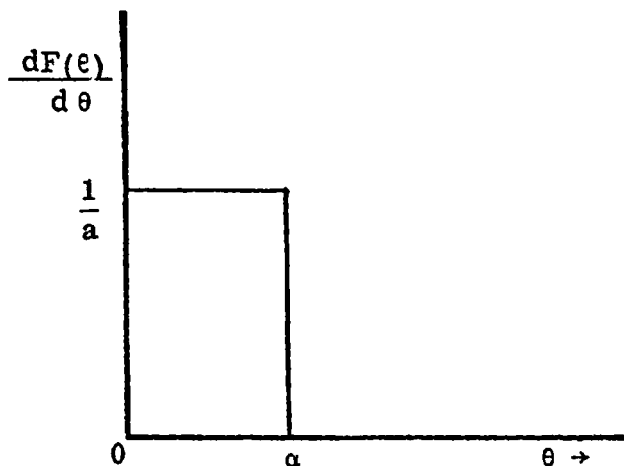


Figure 4.2 Derivative of the finite ramp

It is seen that the derivative of the finite ramp is a rectangular pulse of length α , magnitude $1/\alpha$ and area unity. No matter how small α is the area remains constant at unity. An impulse or delta function is the first derivative of the finite ramp as α approaches zero:

$$\delta(\theta) = \lim_{\alpha \rightarrow 0} \frac{dF(\theta)}{d\theta} \quad (4.1)$$

The graphical representation of $\delta(\theta)$ at $\theta = 0$ and $\theta = \beta$ is shown in Figure 4.3. The factor multiplying the unit impulse in Figure 4.3b indicates that the area (strength) of the impulse is not unity but A .

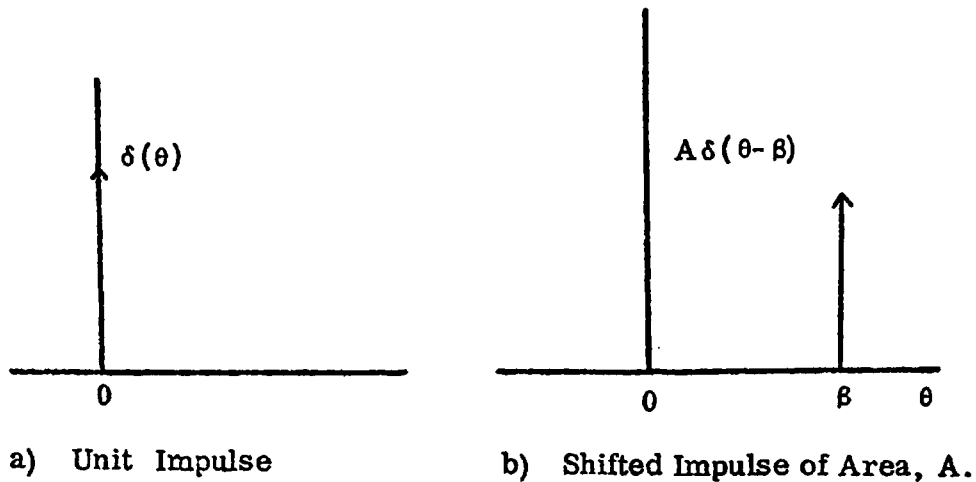


Figure 4.3

Therefore the impulse or delta function is a very narrow pulse with a total area of unity. The response of a system to the impulse or delta function is called the impulse response. The usefulness of the impulse response and therefore of the delta function, is that it can be used to obtain the response of the system to any input signal. For this the input signal $x(\theta)$ is decomposed into a continuum of impulses of strength $x(\theta) d\theta$. The form of these impulses is $x(\lambda) \delta(\theta - \lambda) d\lambda$. The complete input signal is written as:

$$x(\theta) = \int_{-\infty}^{\infty} x(\lambda) \delta(\theta - \lambda) d\lambda \quad (4.2)$$

The response to each elementary impulse is $h(\theta)$ multiplied by the strength of the impulse and it is positioned so that it coincides with the point in time or space of application of the impulse: $x(\lambda) h(\theta - \lambda) d\lambda$. The total response of the system $y(\theta)$ is written as:

$$y(\theta) = \int_{-\infty}^{\infty} x(\lambda) h(\theta - \lambda) d\lambda \quad (4.3)$$

The integral (4.3) is called the convolution of $x(\theta)$ and $h(\theta)$ and is denoted as $x(\theta) * h(\theta)$. Generally the convolution of the functions $g_1(\theta)$ and $g_2(\theta)$ is written as:

$$g_1(\theta) * g_2(\theta) = \int_{-\infty}^{\infty} g_1(\lambda) g_2(\theta - \lambda) d\lambda \quad (4.4)$$

Some examples of convolution borrowed from Cooper, et al (1967) are shown in Figures 4.4 through 4.6.

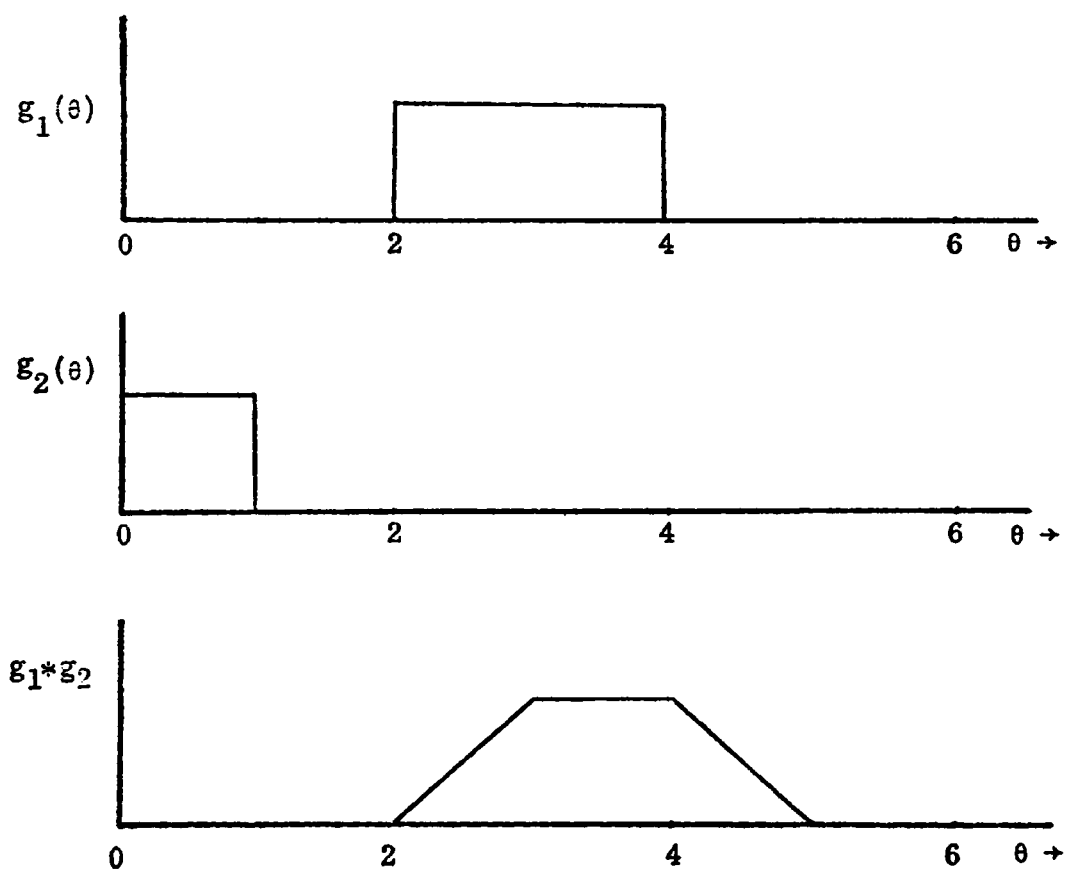


Figure 4.4 Convolution of Two Rectangular Pulses

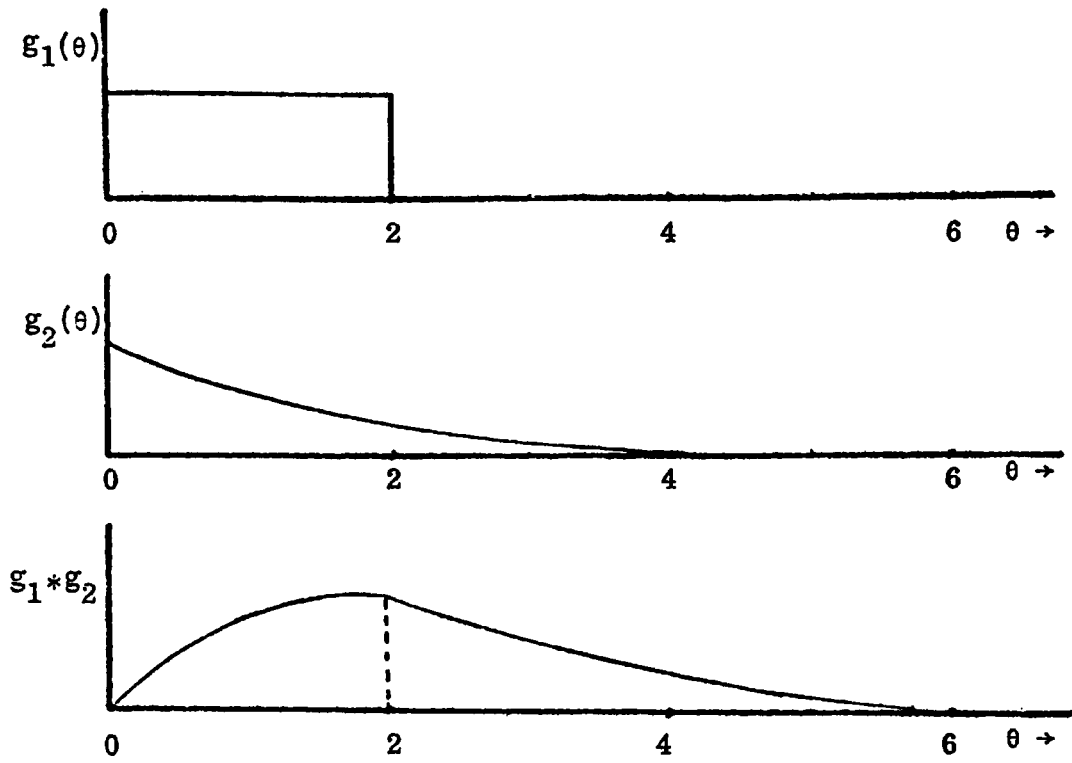


Figure 4.5 Convolution of a Rectangular and an Exponential Pulse

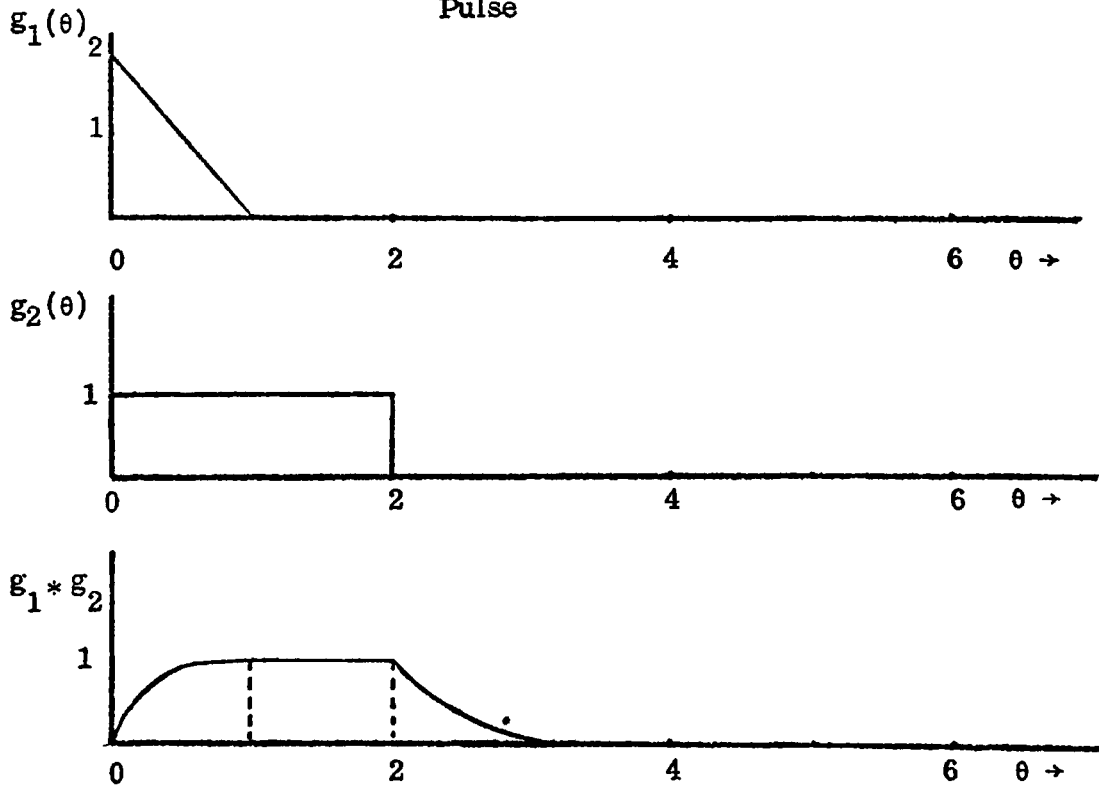


Figure 4.6 Convolution of a Triangular and a Rectangular Pulse

Figures 4.4 through 4.6 show that the convolution integral can be thought as an averaging, smoothing or weighting operation. This property of the convolution integral is very useful in the construction of a filter by which some undesired property of a function is removed.

2) The Use of the Convolution Integral in the Construction of a Filter

The filtering operation is defined as:

$$y(\theta) = \int_{-\infty}^{\infty} G(\theta - \lambda) x(\lambda) d\lambda \quad (4.5)$$

where $x(\lambda)$ is the input signal which consists of a desired and an undesired component, $G(\theta - \lambda)$ is a filter which removes the undesired component of $x(\lambda)$ and $y(\theta)$ is the output of the filtering operation. The discrete representation of (4.5) is given by

$$y_i = \sum_{k=-\infty}^{\infty} G_{i-k} x_k. \quad (4.6)$$

In this case, the filter G can be thought of as consisting of a set of weights, which, when applied to the input signal x_k , produce y_i . Depending on its transmission ability a filter is classified as high pass filter, low pass filter band pass and band rejection. A high pass filter transmits the high frequency components and rejects those lower than a specified cutoff frequency. A low pass filter transmits the low frequency components and rejects those above the cutoff frequency. A band pass filter allows a certain range of frequencies to pass and rejects the rest of them. A band rejection filter rejects a certain

range of frequencies and allows the rest of them (Figure 4.7).

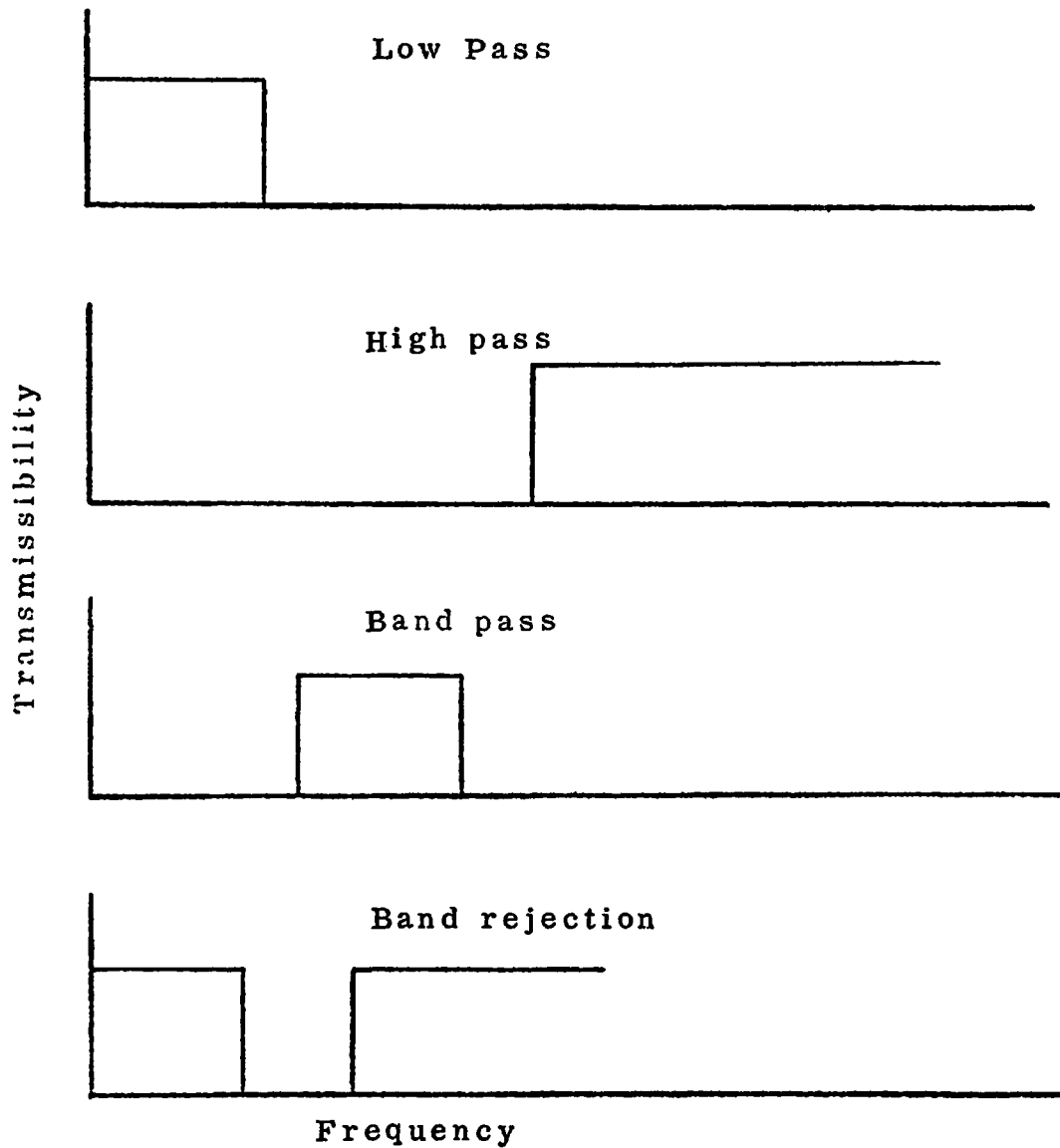


Figure 4.7 Classification of Filters

A filter also is classified as recursive and nonrecursive. A recursive filter recirculates the output back into the input while in a nonrecursive filter the output is a function of the input terms only. The reader can find an extensive

description of filters in Otnes and Enochson(1972), Stanley (1975), and Hamming (1977).

To show the ability of a filter to reject a certain portion of frequencies consider Equation (4.6) after a simple change of variables is performed.

$$y_i = \sum_{k=-\infty}^{\infty} G_k x_{i-k} \quad (4.7)$$

Let $G_k = 1/3$, $k = -1, 0, 1$ and $x_t = R \cos(\omega t + \psi)$. In this case Equation (4.7) is a three point simple moving averaging. This is written as:

$$y_i = \frac{1}{3} (x_{i-1} + x_i + x_{i+1}) \quad (4.8)$$

which after some algebra (Bloomfield, 1976) yields:

$$y_i = \frac{1}{3} R \cos(\omega t + \psi) (1 + 2\cos \omega) \quad (4.9)$$

Therefore the output y_i is obtained by multiplying the input by $\frac{1}{3}(1 + 2\cos \omega)$. This function is zero for $\omega = 2\pi/3$ and obtains the maximum value for $\omega = 0$. Therefore if the input signal consists of a number of cosine terms, the frequencies near zero will pass relatively undiminished while the frequencies equal to $2\pi/3$ will be removed completely. Since any set of data can be written as a sum of cosine terms the frequency presentation of the filtering procedure becomes obvious.

In the first two sections of this chapter the filter characteristics were presented in general terms. In the remaining sections the filtering technique in relation to turbulence computations will be presented.

B. Filter Performance Criteria

The numerical computation of turbulent flows requires that the flow field must be divided into rectangular cells and the velocity field (and contaminant concentration) be computed at the nodal points. This velocity field is a gross solution over the whole cell. The numerical model cannot consider oscillations of scales smaller than twice the cell size. However these smaller scales have to be accounted for in some way because otherwise the solution does not conserve energy and is therefore erroneous. This necessitates the filtering of the equations so that they are written only in terms of large scale components and which when solved yield the correct spectral structure of the energy cascade. The terms which are based on the small scales and which arise from the filtration are then modelled.

The filtration formula used in turbulence computations has, in accordance to Equation (4.5), the following form:

$$\bar{f}(\underline{x}) = \int G(\underline{x} - \underline{x}') f(\underline{x}') d\underline{x}' \quad ; \quad (4.10)$$

where the integration is over the entire flow volume. Here $f(\underline{x})$ is a variable that contains all the scales, $\bar{f}(\underline{x})$ represents the large scales or resolvable scales of $f(\underline{x})$ (filtered field) and $G(\underline{x})$ is a filter function. $f(\underline{x})$ now can be

decomposed into its resolvable and residual components as:

$$f = \bar{f} + f' \quad (4.11)$$

where, it should be noted that, \bar{f} is not the mean used in classical turbulence.

The filter function $G(\underline{x})$ has to satisfy the following two requirements:

$$\int G(\underline{x}) d\underline{x} = 1 \quad (4.12)$$

and the first and the second moment of $G(\underline{x})$ must exist.

If these two requirements are not satisfied the filter is not suitable for grid-based turbulence computations.

The filters which are used most frequently in turbulence computations are described in the next section.

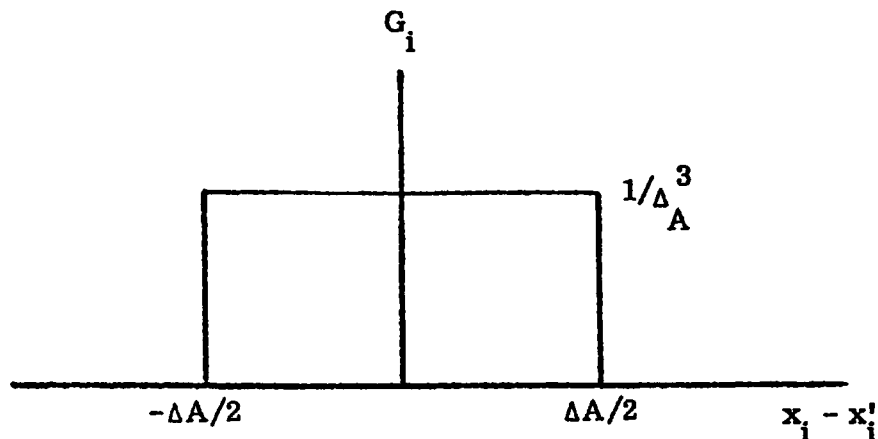
C. A Review of Filters used in Turbulence

1. Top-hat Filter

The top-hat filter is the most commonly used filter in turbulence computations. It is usually stated as volume averaging of the N.S. equations.

The form of this filter is:

$$G(\underline{x} - \underline{x}') = \begin{cases} 1/\Delta_A^3 & \left| x_i - x'_i \right| < \Delta_A/2 \quad i=1,2,3 \\ 0 & \text{otherwise} \end{cases} \quad (4.13)$$



The deficiency of this filter is that it does not remove the small scale oscillations from the filtered field sufficiently. This is shown from the Fourier transform of the velocity field (Kwak et al., 1975, p. 8)

$$\bar{\underline{u}}(\underline{k}) = \left[\prod_{i=1}^3 \frac{\sin(k_i \Delta A/2)}{k_i \Delta A/2} \right] \underline{u}(\underline{k}), \quad (4.14)$$

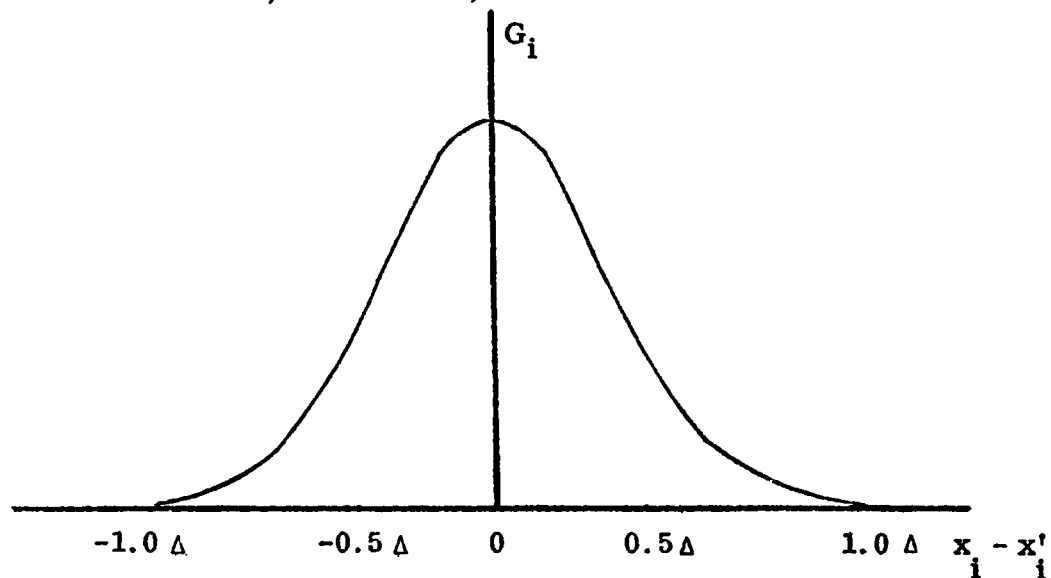
where the velocity field is expressed as a function of the wave number, \underline{k} .

Equation (4.14) indicates that the filtered field contains oscillatory components at all wave numbers, instead of removing the large wave number components.

This filter has been used by several meteorologists as Smagorinsky, et al. (1965), Leith (1965) to predict the general atmospheric circulation. Lilly (1967) also used this filter to study numerically simulated small-scale turbulence. Deardorff (1970, 1971 and 1973) carried extensive research on turbulent channel flows and atmospheric turbulence. Spraggs and Street (1975) used the top-hat filter to study thermally influenced hydrodynamic flows. Lick (1976) and Paul and Lick (1976), used this filter in Lake Erie circulation models.

This filter has been proposed by Leonard (1974) and has been used extensively at Stanford University by Kwak, et al. (1975), Shaanan, et al. (1975), Mansour, et al. (1977) and Ferziger, et al. (1977) in large-eddy simulations of turbulence. The Gaussian filter has the following form:

$$G(\underline{x} - \underline{x}') = \left\{ \sqrt{\frac{\gamma}{\pi}} \frac{1}{\Delta} \right\}^3 \exp \left[-\gamma (\underline{x} - \underline{x}')^2 / \Delta^2 \right] \quad (4.15)$$



where γ is a constant and Δ is the filter length. Filter length twice the grid size has been used by all the investigators reported at the beginning of this paragraph.

The Fourier transform of the velocity field is given by (Kwak, et al. 1975):

$$\hat{\underline{u}}(\underline{k}) = \underline{\hat{u}}(\underline{k}) \exp \left(-\frac{\Delta^2}{4\gamma} k^2 \right), \quad (4.16)$$

where a Fourier transform is denoted by the symbol, $\hat{\cdot}$.

which shows that the filtered field becomes very small for large values of the wave number, k . The requirements (4.12) also are satisfied and therefore this filter has the desired properties and can be used with no major difficulty. Its only disadvantage is that it is symmetrical and therefore it can be used only in the computation of turbulent flows by using cubical cells.

3. Sub-Grid Scale Filter

A generally good filter that cannot be used because it does not fulfil the second of the requirements (4.12) is the following (Kwak, et al. 1975):

$$G(\underline{x} - \underline{x}') = \prod_{i=1}^3 \frac{\sin(\underline{x}_i - \underline{x}'_i)/\Delta A}{\pi(\underline{x}_i - \underline{x}'_i)} \quad (4.17)$$

where $\Delta A = \pi/k_c$ and k_c is the cut-off wave number. This filter has the desired property that by defining k_c properly, the residual field can be sub-grid scale. However it cannot be used because its second moment involves integrals of the form

$$\int_{-\infty}^{\infty} \frac{x^2 \sin(\pi x / \Delta A)}{\pi x} dx \quad (4.18)$$

which do not exist.

D. A Filter for Distorted Grid Cells

Lake turbulence is characterized by horizontal scales which are many orders of magnitude larger than the vertical cells. Here cubical cells are

impractical and therefore the filter (4.15) cannot be used. In this section a Gaussian filter which can be used in highly distorted cells is proposed. This filter has the following form:

$$G_i(x_i - x_i') = \sqrt{\frac{\gamma}{\pi}} \frac{1}{\Delta_i} \exp \left[-\gamma (x_i - x_i')^2 / \Delta_i^2 \right] \quad (4.19)$$

(i=1,2,3 (no summation))

where Δ_i is the filter length in the three directions. To identify this filter it is compared with a normally distributed variable y having mean μ equal to zero, variance equal to σ^2 , $N(0, \sigma^2)$, and density function given by:

$$G(y) = \frac{1}{\sqrt{2\pi}\sigma} \exp \left(-\frac{1}{2} \frac{y^2}{\sigma^2} \right) \quad (4.20)$$

Comparison of (4.19) and (4.20) shows that (4.19) is a Gaussian function with mean and variance given by

$$\mu = 0 \quad ; \quad \text{and} \quad \sigma^2 = \frac{\Delta_i^2}{2\gamma} \quad (4.21)$$

The first and the second moment of (4.20) are given by (Dudewicz, 1976, pp. 118-119):

$$E(y) = \int_{-\infty}^{\infty} y G(y) dy = \mu = 0 \quad (4.22)$$

$$E(y^2) = \int_{-\infty}^{\infty} y^2 G(y) dy = \sigma^2 + \mu^2 = \sigma^2 \quad (4.23)$$

To show the properties of the filter (4.19) it is applied to the velocity $u(x_1, x_2, x_3)$. The filtered field will be:

$$\bar{u}(x_i) = \sqrt{\frac{\gamma}{\pi}} \frac{1}{\Delta_i} \int_{-\infty}^{\infty} u(x_i') e^{-\gamma(x_i - x_i')^2 / \Delta_i^2} dx_i' \quad (4.24)$$

(i=1, 2, 3 (no summation))

Letting $x_i - x_i' = -\xi_i$ Equation (4.24) becomes:

$$\bar{u}(x_i) = \sqrt{\frac{\gamma}{\pi}} \frac{1}{\Delta_i} \int_{-\infty}^{\infty} u(x_i + \xi_i) e^{-\gamma\xi_i^2 / \Delta_i^2} d\xi_i \quad (4.25)$$

The Fourier transform of Equation (4.25) is given by:

$$\hat{\bar{u}}(k_i) = \sqrt{\frac{\gamma}{\pi}} \frac{1}{\Delta_i} \iint_{-\infty}^{\infty} u(x_i + \xi_i) e^{-\gamma\xi_i^2 / \Delta_i^2} e^{-jk_i x_i} dx_i d\xi_i$$

which is written as:

$$\hat{\bar{u}}(k_i) = \sqrt{\frac{\gamma}{\pi}} \frac{1}{\Delta_i} \int_{-\infty}^{\infty} \left[\int_{-\infty}^{\infty} u(x_i + \xi_i) e^{-jk_i x_i} dx_i \right] e^{-\gamma\xi_i^2 / \Delta_i^2} d\xi_i \quad (4.26)$$

The bracketed quantity is the Fourier transform of $u(x_i + \xi_i)$. Therefore,

Equation (4.26) is written as:

$$\hat{\bar{u}}(k_i) = \sqrt{\frac{\gamma}{\pi}} \frac{1}{\Delta_i} \int_{-\infty}^{\infty} \hat{u}(x_i + \xi_i) e^{-\gamma\xi_i^2 / \Delta_i^2} d\xi_i \quad (4.27)$$

Now (Miller p.160):

$$\hat{u}(x_i + \xi_i) = \hat{u}(x_i) e^{-jk_i \xi_i}, \text{ and}$$

therefore Equation (4.27) becomes:

$$\bar{u}(k_i) = \sqrt{\frac{\gamma}{\pi}} \frac{1}{\Delta_i} \hat{u}(x_i) \int_{-\infty}^{\infty} e^{-(\gamma \xi_i^2 / \Delta_i^2 - jk_i \xi_i)} d\xi_i. \quad (4.28)$$

After evaluation of the integral (Spiegel, p.98), Equation (4.28) becomes:

$$\bar{u}(k_i) = \sqrt{\frac{\gamma}{\pi}} \frac{1}{\Delta_i} \hat{u}(x_i) \sqrt{\frac{\pi}{\gamma}} \Delta_i e^{-k_i^2 \Delta_i^2 / 4\gamma}$$

and finally

$$\bar{u}(k_i) = u(k_i) \exp\left(-\frac{\Delta_i^2}{4\gamma} k_i^2\right) \quad (4.29)$$

Equation (4.29) is equivalent to Equation (4.16). As in (4.16) the filtered field approaches zero as the wave number becomes larger. Here, however, the direction is also considered. As in Equation (4.16) the filter length is obtained as $\Delta_i = 2 \Delta x_i$, where Δx_i is the mesh size.

CHAPTER V

DERIVATION OF FILTERED TRANSPORT EQUATIONS

Complete 3-D computations of turbulent flows require resolution of scales down to the Kolmogorov microscale, $\eta = (\nu^3/\epsilon)^{1/4}$. The number of mesh points required is $Re^{9/4}$, where Re is the Reynolds number (Kwak, et al. 1975, Leonard 1974) and exceeds the capability of the largest available computers. The solution to this problem is to compute the large scales present which contain most of the turbulent energy and are responsible for most of the momentum transport. The small scales, which play a very important role in the energy dissipation of the large scales are then empirically modeled. As in Chapter III, one common method of defining the large scales is by averaging over the volume of a cell and accounting for the subgrid scale motions by an eddy viscosity model. The nonlinear terms in the Navier Stokes equations are left unmodified. In this case the rate of energy transfer from the large scales through to the small scales (energy cascade) to dissipation is conducted by an artificial eddy viscosity. Lilly (1967) used the above method to study the distortion of homogeneous and isotropic turbulence by a strain rate. Deardorff (1970, 1971) used the same method to compute a 3-D channel flow at large Reynolds numbers, however, he had to decrease the eddy coefficients

for the subgrid scale motion used by Lilly. That was an indication that too much weight was given to the extraction of energy from the large scales due to the eddy viscosity. Deardorff (1973) used a more sophisticated 2nd order model for the subgrid scale Reynolds stresses. He derived subgrid transport equations to study the turbulence in an atmospheric boundary layer. Spraggs and Street (1975), also used this method to predict "the temperature regime and energy transfer in reservoir and cooling ponds subjected to thermal loading". The averaging of their equations was slightly different. Instead of grid volume averaging, Schumann's (1973) method, of averaging over the surface of grid boxes was used.

All of the above research was accomplished by the use of classical finite difference methods. An alternative way of solving the same problem is by the use of spectral methods described by Orszag and Israeli (1975). The solution is decomposed by means of Fourier analysis into its spectral components and the solution of each of these components is found. The method is still in the stage of development but presents some attractive characteristics. Boundary conditions can be considered exactly while in finite differences they usually lead to loss of accuracy. Also the decomposition of the solution into spectral components can be very convenient for turbulence computations.

The disadvantages of the spectral methods are that they require more storage and computer time than the finite difference methods and they can be applied only to square geometries. Moreover, they have to date ignored the residual stresses resulting from the averaging of the equations.

In this chapter the filter derived in Chapter IV, Section D is used in the derivation of the filtered equations necessary to study the large scale lacustine velocity and concentration fluctuations. Also the assumptions used in lake circulation calculations, the residual field model, the equations for the bio-chemically active source/sink term which is included in the contaminant transport model, and the boundary conditions used are presented.

A. Statement of the Navier-Stokes and Transport Equations:

The equations used in this work are the conservation of momentum equations (Navier Stokes equations) and the transport equation. The complete equations are given by (Schlichting 1968, Hinze 1975):

x - Momentum:

$$\frac{\partial u}{\partial t} + \frac{\partial}{\partial x} (uu) + \frac{\partial}{\partial y} (uv) + \frac{\partial}{\partial z} (uw) - fv = -\frac{1}{\rho} \frac{\partial P}{\partial x} + \nu \left(\frac{\partial^2 u}{\partial x^2} + \frac{\partial^2 u}{\partial y^2} + \frac{\partial^2 u}{\partial z^2} \right) \quad (5.1)$$

y - Momentum:

$$\frac{\partial v}{\partial t} + \frac{\partial}{\partial x} (vu) + \frac{\partial}{\partial y} (vv) + \frac{\partial}{\partial z} (vw) + fu = -\frac{1}{\rho} \frac{\partial P}{\partial y} + \nu \left(\frac{\partial^2 v}{\partial x^2} + \frac{\partial^2 v}{\partial y^2} + \frac{\partial^2 v}{\partial z^2} \right) \quad (5.2)$$

z - Momentum:

$$\frac{\partial w}{\partial t} + \frac{\partial}{\partial x} (wu) + \frac{\partial}{\partial y} (wv) + \frac{\partial}{\partial z} (ww) = -\frac{1}{\rho} \frac{\partial P}{\partial z} +$$

$$v \left(\frac{\partial^2 w}{\partial x^2} + \frac{\partial^2 w}{\partial y^2} + \frac{\partial^2 w}{\partial z^2} \right) + g \quad (5.3)$$

Continuity:

$$\frac{\partial u}{\partial x} + \frac{\partial v}{\partial y} + \frac{\partial w}{\partial z} = 0$$

Transport:

$$\frac{\partial c}{\partial t} + \frac{\partial}{\partial x} (cu) + \frac{\partial}{\partial y} (cv) + \frac{\partial}{\partial z} (cw) = \frac{\partial}{\partial x} \left(\mu \frac{\partial c}{\partial x} \right) +$$

$$\frac{\partial}{\partial y} \left(\mu \frac{\partial c}{\partial y} \right) + \frac{\partial}{\partial z} \left(\mu \frac{\partial c}{\partial z} \right) \quad (5.4)$$

where:

$u(x, y, z, t)$ = velocity in x-direction;

$v(x, y, z, t)$ = velocity in y-direction;

$w(x, y, z, t)$ = velocity in z-direction;

$P(x, y, z, t)$ = pressure;

ρ = density;

f = Coriolis parameter;

g = acceleration of gravity;

μ = molecular viscosity

$c(x,y,z,t)$ = concentration; and

t = time.

B. Assumptions Used in Circulation Calculations:

Equations (5.1) to (5.4) are solved using the following assumptions:

(1) Shallow water; according to this assumption the vertical scale is negligible in comparison to the horizontal scale ($D/L \ll 1$). As a result variations in the vertical velocity are small compared to the gravity term and the vertical momentum equation reduces to a hydrostatic pressure change. In this work $D/L = 0.009$ and therefore it is reasonable to make this assumption. The shallow water assumption has been used extensively in lake and ocean modeling (Liggett 1970, Haq and Lick 1975, Crowley 1968, Bryan 1967, Gedney and Lick 1972, Simons 1971, 1972, Paskausky 1971, Leendertse 1970, Sheng and Lick 1975, Paul and Lick 1976). The advantage of this assumption is that the order of the system of Equations (5.1) to (5.4) is reduced and thus the computer time required for its solution decreases appreciably.

(2) Rigid lid assumption; according to this assumption used by Bryan (1969), Liggett (1969, 1970), Bennett (1974), Haq and Lick (1975), Lick (1976), Paul and Lick (1976), Sheng and Lick (1975) a slippery rigid lid, allowing horizontal motions but no vertical motions, is put at the surface of the water. The free surface displacement is estimated by computing the pressure under the rigid lid and relating it hydrostatically to the free surface. This assump-

tion can be used when the ratio

$$\epsilon = \frac{L^2 f^2}{g D}$$

is very small (Ball 1965, Bennett 1974). Here, L is a horizontal characteristic length, f is the Coriolis parameter, g is acceleration of gravity and D is a vertical characteristic length. This ratio is the square of the ratio of the fundamental seiche period to the inertial period. In this work, using $f = 10^{-4} \text{ sec}^{-1}$ (Great Lakes region), implies $\epsilon = 0.0002$, and therefore a rigid lid can reasonably be assumed. The advantage of this assumption is that the surface gravity waves and the numerical instabilities associated with them are eliminated. Therefore, larger time steps are permitted in the numerical computation of hydrodynamic flows. A thorough analysis of the rigid lid assumption is given by Lick (1976) and Haq and Lick (1975).

(3) Coriolis effects are neglected. As in Boyce (1974), when the inertial period $\tau_i = 2\pi/f$ is larger than a characteristic time scale the Coriolis force is considered unimportant in the dynamics of the phenomenon in question. A typical inertial period is $\tau_i \approx 17.5$ hours while the total time over which computations were made in this work is no more than 6 hours. Thus it is assumed that the Coriolis force can be omitted.

(4) The flow field is considered homogeneous in temperature. Stratification complicates the analysis, therefore, at this time no temperature effects are included.

(5) The molecular viscous terms are very small in comparison with the turbulent stresses and therefore are omitted.

(6) The transport model includes a source/sink term which accounts for biological growth or decay. A sinking velocity (w_s) is added to the vertical fluid velocity to account for gravitational particle settling.

C. Derivation of the Filtered Equations:

Using the assumptions described in the previous section the equations for the filtered field are the following (x-direction is positive northward, y-direction is positive eastward and z-direction is positive downward):

x - Momentum:

$$\frac{\partial \bar{u}}{\partial t} + \frac{\partial}{\partial x}(\bar{u}\bar{u}) + \frac{\partial}{\partial y}(\bar{u}\bar{v}) + \frac{\partial}{\partial z}(\bar{u}\bar{w}) = -\frac{1}{\rho} \frac{\partial \bar{P}}{\partial x} \quad (5.5)$$

y - Momentum:

$$\frac{\partial \bar{v}}{\partial t} + \frac{\partial}{\partial x}(\bar{v}\bar{u}) + \frac{\partial}{\partial y}(\bar{v}\bar{v}) + \frac{\partial}{\partial z}(\bar{v}\bar{w}) = -\frac{1}{\rho} \frac{\partial \bar{P}}{\partial y} \quad (5.6)$$

z - Momentum:

$$\frac{\partial \bar{P}}{\partial z} = \rho g \quad (5.7)$$

Continuity:

$$\frac{\partial \bar{u}}{\partial x} + \frac{\partial \bar{v}}{\partial y} + \frac{\partial \bar{w}}{\partial z} = 0 \quad (5.8)$$

Transport:

$$\frac{\partial \bar{c}}{\partial t} + \frac{\partial}{\partial x} (\bar{c}\bar{u}) + \frac{\partial}{\partial y} (\bar{c}\bar{v}) + \frac{\partial}{\partial z} \overline{c(w + w_s)} = \bar{S} \quad (5.9)$$

where overbars denote filtered quantities. In the previous equations the following relationships have been used (Kwak, et al. 1975):

$$\frac{\partial \bar{f}}{\partial \underline{x}} = \frac{\partial \bar{f}}{\partial \underline{x}}$$

and

$$\frac{\partial \bar{f}}{\partial t} = \frac{\partial \bar{f}}{\partial t}$$

The terms which need special attention are the double correlations \overline{uu} , \overline{uv} , \overline{uw} , \overline{vu} , \overline{vv} , \overline{vw} , \overline{cu} , \overline{cv} and $\overline{c(w + w_s)}$. Considering that each variable consists of a filtered and a residual component (Chapter IV) then two typical terms \overline{uv} and \overline{uc} are written as:

$$\overline{uv} = \overline{(\bar{u} + u')(\bar{v} + v')} = \overline{\bar{u}\bar{v}} + \overline{\bar{u}v'} + \overline{u'\bar{v}} + \overline{u'v'} = \overline{\bar{u}\bar{v}} + R_{uv}; \text{ and} \quad (5.10)$$

$$\overline{cu} = \overline{\bar{c}\bar{u}} + \overline{\bar{c}u'} + \overline{c'\bar{u}} + \overline{c'u'} = \overline{\bar{c}\bar{u}} + T_u \quad (5.11)$$

In the above equations

$$R_{uv} = \overline{\bar{u}v'} + \overline{u'\bar{v}} + \overline{u'v'} \quad , \quad \text{and}$$

$$T_u = \overline{c'u'} + \overline{c'u} + \overline{c'u'}$$

represent the residual field contribution to the advection term. The term $-\rho R_{uv}$ is called the residual or Reynolds stress. The treatment of R_{uv} and T_u will be discussed in Section E of this chapter. The terms which need further clarification are; \overline{uv} and \overline{cu} . First \overline{uv} is considered:

$$\overline{uv}(\underline{x}_0, t) = \int_{-\infty}^{\infty} G(\underline{x}_0 - \underline{x}) \overline{uv}(\underline{x}) d\underline{x} \quad (5.12)$$

$\overline{uv}(\underline{x})$ is localized by using a Taylor series expansion (Leonard 1974, Kwak, et al. 1975). Equation (5.12) is then written as:

$$\begin{aligned} \overline{uv}(\underline{x}_0, t) = & \int_{-\infty}^{\infty} \overline{uv}(x_0, y_0, z_0, t) G(\underline{x}_0 - \underline{x}) d\underline{x} + \int_{-\infty}^{\infty} \frac{\partial}{\partial x} \overline{uv}(x - x_0) G_1(x_0 - x) dx \\ & + \int_{-\infty}^{\infty} \frac{\partial}{\partial y} \overline{uv}(y - y_0) G_2(y_0 - y) dy \\ & + \int_{-\infty}^{\infty} \frac{\partial}{\partial z} \overline{uv}(z - z_0) G_3(z_0 - z) dz \\ & + \frac{1}{2} \int_{-\infty}^{\infty} \frac{\partial^2}{\partial x^2} \overline{uv}(x - x_0)^2 G_1(x_0 - x) dx \\ & + \frac{1}{2} \int_{-\infty}^{\infty} \frac{\partial^2}{\partial y^2} \overline{uv}(y - y_0)^2 G_2(y_0 - y) dy \\ & + \frac{1}{2} \int_{-\infty}^{\infty} \frac{\partial^2}{\partial z^2} \overline{uv}(z - z_0)^2 G_3(z_0 - z) dz + \text{higher order terms} \end{aligned} \quad (5.13)$$

where $G(\underline{x}_0 - \underline{x})$ is the 3-D filter and G_1, G_2, G_3 are the filter components in x, y, z direction respectively.

Using Equations (4.12), (4.22) and (4.23), Equation (5.13) becomes

$$\overline{\overline{uv}} = \overline{uv} + \frac{\Delta_1^2}{4\gamma} \frac{\partial^2}{\partial x^2} (\overline{uv}) + \frac{\Delta_2^2}{4\gamma} \frac{\partial^2}{\partial y^2} (\overline{uv}) + \frac{\Delta_3^2}{4\gamma} \frac{\partial^2}{\partial z^2} (\overline{uv}) \quad (5.14a)$$

If a symmetrical filter was used, Equation (5.13) would be written as:

$$\overline{\overline{uv}} = \overline{uv} + \frac{\Delta_A^2}{4\gamma} \nabla^2 (\overline{uv}); \quad (5.14b)$$

where Δ_A is the filter length.

The second order terms in (5.14b) are called the Leonard terms while $-\rho \Delta_A^2 / 4\gamma \frac{\partial^2}{\partial x_i^2} (\overline{uv})$ are called the Leonard stresses. These terms are very important in extracting energy from the large scales (Leonard 1974) and are included when the large scale motions vary in a non-negligible way over an averaging volume. The residual field terms play a reduced role in the dissipation of large scales energy.

Similarly as Equation (5.14) was derived $\overline{\overline{cu}}$ is written as:

$$\overline{\overline{cu}} = \overline{cu} + \frac{\Delta_1^2}{4\gamma} \frac{\partial^2}{\partial x^2} (\overline{cu}) + \frac{\Delta_2^2}{4\gamma} \frac{\partial^2}{\partial y^2} (\overline{cu}) + \frac{\Delta_3^2}{4\gamma} \frac{\partial^2}{\partial z^2} (\overline{cu}) \quad (5.15)$$

Equations (5.5) through (5.9) can now be written as:

x - Momentum:

$$\begin{aligned}
& \frac{\partial \bar{u}}{\partial t} + \frac{\partial}{\partial x} \left(\bar{u}\bar{u} + \frac{\Delta_1^2}{4\gamma} \frac{\partial^2}{\partial x^2} (\bar{u}\bar{u}) + \frac{\Delta_2^2}{4\gamma} \frac{\partial^2}{\partial y^2} (\bar{u}\bar{u}) + \frac{\Delta_3^2}{4\gamma} \frac{\partial^2}{\partial z^2} (\bar{u}\bar{u}) \right) \\
& + \frac{\partial}{\partial y} \left(\bar{u}\bar{v} + \frac{\Delta_1^2}{4\gamma} \frac{\partial^2}{\partial x^2} (\bar{u}\bar{v}) + \frac{\Delta_2^2}{4\gamma} \frac{\partial^2}{\partial y^2} (\bar{u}\bar{v}) + \frac{\Delta_3^2}{4\gamma} \frac{\partial^2}{\partial z^2} (\bar{u}\bar{v}) \right) \\
& + \frac{\partial}{\partial z} \left(\bar{u}\bar{w} + \frac{\Delta_1^2}{4\gamma} \frac{\partial^2}{\partial x^2} (\bar{u}\bar{w}) + \frac{\Delta_2^2}{4\gamma} \frac{\partial^2}{\partial y^2} (\bar{u}\bar{w}) + \frac{\Delta_3^2}{4\gamma} \frac{\partial^2}{\partial z^2} (\bar{u}\bar{w}) \right) \\
& = - \frac{1}{\rho} \frac{\partial \bar{P}}{\partial x} - \frac{\partial}{\partial x} R_{uu} - \frac{\partial}{\partial y} R_{uv} - \frac{\partial}{\partial z} R_{uw} \quad (5.16)
\end{aligned}$$

y - Momentum:

$$\begin{aligned}
& \frac{\partial \bar{v}}{\partial t} + \frac{\partial}{\partial x} \left(\bar{u}\bar{v} + \frac{\Delta_1^2}{4\gamma} \frac{\partial^2}{\partial x^2} (\bar{u}\bar{v}) + \frac{\Delta_2^2}{4\gamma} \frac{\partial^2}{\partial y^2} (\bar{u}\bar{v}) + \frac{\Delta_3^2}{4\gamma} \frac{\partial^2}{\partial z^2} (\bar{u}\bar{v}) \right) \\
& + \frac{\partial}{\partial y} \left(\bar{v}\bar{v} + \frac{\Delta_1^2}{4\gamma} \frac{\partial^2}{\partial x^2} (\bar{v}\bar{v}) + \frac{\Delta_2^2}{4\gamma} \frac{\partial^2}{\partial y^2} (\bar{v}\bar{v}) + \frac{\Delta_3^2}{4\gamma} \frac{\partial^2}{\partial z^2} (\bar{v}\bar{v}) \right) \\
& + \frac{\partial}{\partial z} \left(\bar{v}\bar{w} + \frac{\Delta_1^2}{4\gamma} \frac{\partial^2}{\partial x^2} (\bar{v}\bar{w}) + \frac{\Delta_2^2}{4\gamma} \frac{\partial^2}{\partial y^2} (\bar{v}\bar{w}) + \frac{\Delta_3^2}{4\gamma} \frac{\partial^2}{\partial z^2} (\bar{v}\bar{w}) \right) \\
& = - \frac{1}{\rho} \frac{\partial \bar{P}}{\partial y} - \frac{\partial}{\partial x} R_{vu} - \frac{\partial}{\partial y} R_{vv} - \frac{\partial}{\partial z} R_{vw} \quad (5.17)
\end{aligned}$$

Hydrostatic Pressure:

$$\frac{\partial \bar{P}}{\partial z} = \rho g \quad (5.18)$$

Continuity:

$$\frac{\partial \bar{u}}{\partial x} + \frac{\partial \bar{v}}{\partial y} + \frac{\partial \bar{w}}{\partial z} = 0 \quad (5.19)$$

Transport:

$$\begin{aligned} & \frac{\partial \bar{c}}{\partial x} + \frac{\partial}{\partial x} \bar{c}\bar{u} + \frac{\Delta_1^2}{4\gamma} \frac{\partial^2}{\partial x^2} (\bar{c}\bar{u}) + \frac{\Delta_2^2}{4\gamma} \frac{\partial^2}{\partial y^2} (\bar{c}\bar{u}) + \frac{\Delta_3^2}{4\gamma} \frac{\partial^2}{\partial z^2} (\bar{c}\bar{u}) \\ & + \frac{\partial}{\partial y} \bar{c}\bar{v} + \frac{\Delta_1^2}{4\gamma} \frac{\partial^2}{\partial x^2} (\bar{c}\bar{v}) + \frac{\Delta_2^2}{4\gamma} \frac{\partial^2}{\partial y^2} (\bar{c}\bar{v}) + \frac{\Delta_3^2}{4\gamma} \frac{\partial^2}{\partial z^2} (\bar{c}\bar{v}) \\ & + \frac{\partial}{\partial z} \bar{c} \overline{(w + w_s)} + \frac{\Delta_1^2}{4\gamma} \frac{\partial^2}{\partial x^2} (\bar{c} \overline{(w + w_s)}) + \frac{\Delta_2^2}{4\gamma} \frac{\partial^2}{\partial y^2} (\bar{c} \overline{(w + w_s)}) \\ & \quad \quad \quad + \frac{\Delta_3^2}{4\gamma} \frac{\partial^2}{\partial z^2} (\bar{c} \overline{(w + w_s)}) \\ & = \frac{\partial}{\partial x} T_u + \frac{\partial}{\partial y} T_v + \frac{\partial}{\partial z} T_w + S \end{aligned} \quad (5.20)$$

D. Residual Field Model:

Most of the energy cascade process occurs through the Leonard's terms while the residual stresses play a secondary role. They can be

modelled as in Lilly (1967), Deardorff (1970, 1971), Spraggs and Street (1975) or Kwak, et al. (1975). By partial analogy to the molecular case

$$R_{ij} - \frac{1}{3} R_{kk} \delta_{ij} = -K \overline{S}_{ij} ; \quad (5.21)$$

where:

$$\overline{S}_{ij} = \left(\frac{\partial \overline{u}_i}{\partial x_j} + \frac{\partial \overline{u}_j}{\partial x_i} \right) . \quad (5.22)$$

\overline{S}_{ij} is called the strain-rate tensor, K is an effective viscosity (eddy viscosity) associated with the residual field and

$\frac{1}{3} R_{kk} \delta_{ij}$ is carried to allow the left hand side of Equation (5.21) to become zero when the indices are contracted (Hinze 1959, p.21).

The residual fluxes $T_i = \overline{c'u'_i} + \overline{c'u} + \overline{c'u'_i}$ are modelled by

$$T_i = \frac{K}{Pr} \frac{\partial c}{\partial x_i} ; \quad (5.23)$$

where the eddy diffusivity is related to the eddy viscosity by a turbulent prandtl number (Pr).

The eddy viscosity is computed as in Smagorinsky, et al. (1965). The fundamental assumption is that an inertial subrange exists which encompasses the grid interval. As it is discussed in Chapter III, Section A.7, the largest scales where an inertial subrange exists were found to be 500 to 5000 m. Therefore by using a relatively small grid 100 m the assumption of the existence of an inertial subrange is not bad.

A dimensional analysis is now applied for the determination of K .

Expressing K as a function of the rate of energy dissipation, $\bar{\epsilon}$ and a representative filter length Δ , here taken to be as in Deardorff (1970, 1971)

$$\Delta = (\Delta_1 \Delta_2 \Delta_3)^{\frac{1}{3}}$$

the eddy viscosity K is expressed as:

$$K = c^{4/3} \bar{\epsilon}^{-1/3} \Delta^{4/3} \quad (5.24)$$

As in Deardorff (1970), in homogeneous and isotropic turbulence, which is the case in the inertial subrange

$$\bar{\epsilon} = K \frac{\partial u_i}{\partial x_j} \left(\frac{\partial u_i}{\partial x_j} + \frac{\partial u_j}{\partial x_i} \right) \quad (5.25)$$

By setting (5.25) to (5.24) one obtains:

$$K = (c \Delta)^2 \left[\frac{\partial u_i}{\partial x_j} \left(\frac{\partial u_i}{\partial x_j} + \frac{\partial u_j}{\partial x_i} \right) \right]^{1/2} \quad (5.26)$$

and therefore K is expressed in terms of filtered quantities. The constant c has to be determined (Chapter VIII, Section A).

The right hand side of (5.26) is rewritten in averaged quantities as:

$$\begin{aligned}
 K &= (c \Delta)^2 \left[\frac{\partial u}{\partial x} \left(\frac{\partial u}{\partial x} + \frac{\partial u}{\partial x} \right) + \frac{\partial u}{\partial y} \left(\frac{\partial u}{\partial y} + \frac{\partial v}{\partial x} \right) + \frac{\partial u}{\partial z} \left(\frac{\partial u}{\partial z} + \frac{\partial w}{\partial x} \right) \right. \\
 &\quad + \frac{\partial v}{\partial x} \left(\frac{\partial v}{\partial x} + \frac{\partial u}{\partial y} \right) + \frac{\partial v}{\partial y} \left(\frac{\partial v}{\partial y} + \frac{\partial v}{\partial y} \right) + \frac{\partial v}{\partial z} \left(\frac{\partial v}{\partial z} + \frac{\partial w}{\partial y} \right) \\
 &\quad \left. + \frac{\partial w}{\partial x} \left(\frac{\partial w}{\partial x} + \frac{\partial u}{\partial z} \right) + \frac{\partial w}{\partial y} \left(\frac{\partial w}{\partial y} + \frac{\partial v}{\partial z} \right) + \frac{\partial w}{\partial z} \left(\frac{\partial w}{\partial z} + \frac{\partial w}{\partial z} \right) \right]^{1/2} \\
 &= (c \Delta)^2 \left[2 \left(\left(\frac{\partial u}{\partial x} \right)^2 + \left(\frac{\partial v}{\partial y} \right)^2 + \left(\frac{\partial w}{\partial z} \right)^2 \right) + \left(\frac{\partial v}{\partial x} + \frac{\partial u}{\partial y} \right)^2 + \left(\frac{\partial w}{\partial y} + \frac{\partial v}{\partial z} \right)^2 \right. \\
 &\quad \left. \left(\frac{\partial u}{\partial z} + \frac{\partial w}{\partial x} \right)^2 \right]^{1/2} \quad (5.27)
 \end{aligned}$$

E. Equations for the Biological Model:

The contaminant transport model also includes a biochemically active source/sink term (S). The model includes four species (phytoplankton, zooplankton, oxygen and nutrients) and benthos. The equations used are given in Smarke (1978) and are as follows:

$$S = \frac{O}{O + K_O} \left[\mu_x F_2 \frac{N}{N + K_N} P - K_{pr} P - \frac{\hat{\mu}_z}{Y} \frac{P}{P + K_z} Z \right] \quad (5.28).$$

Zooplankton:

$$S = \frac{O}{O + K_O} \left[\hat{\mu}_z \frac{P}{P + K_z} Z - K_d Z \right] \quad (5.29)$$

Oxygen:

$$S = \frac{O}{O + K_o} \left[Y_{pd} \hat{u}_x F2 \frac{N}{K_n + N} P - Y_{pd} K_{pr} P - Y_{zd} K_d Z \right. \\ \left. - Y_{pd} \left(\frac{1}{Y} - 1 \right) \hat{u}_z \frac{P}{K_z + P} Z - \frac{1}{\Delta z} Y_{bd} K_{br} B \right] \quad (5.30)$$

Nutrients:

$$S = \frac{O}{O + K_o} \left[C_{pd} \hat{u}_x F2 \frac{N}{N + K_n} P + C_{pd} K_{pr} P + C_{zd} K_d Z \right. \\ \left. + C_{pd} \left(\frac{1}{Y} - 1 \right) \hat{u}_z \frac{P}{P + K_z} Z + \frac{1}{\Delta z} C_{bd} K_{br} B \right] \\ + \frac{K_o}{O + K_o} \frac{1}{\Delta z} C_{bd} K_{bd} B \quad (5.31)$$

Benthos:

$$\frac{\partial B}{\partial t} = W_s P - \frac{O}{K_o + O} K_{br} B - \frac{K_o}{K_o + O} K_{bd} B \quad (5.32)$$

where:

P = Phytoplankton concentration ;

Z = Zooplankton concentration ;

O = Oxygen concentration ;

N = Nutrient concentration ; and

B = Benthos concentration .

The rest of the symbols are rate coefficients and are defined in the list of symbols .

F. Summary of the Filtered Equations:

Using the relationships (5.21) and (5.23) for the residual stresses and fluxes and dropping overbars the equations for the filtered field are the following:

Continuity:

$$\frac{\partial u}{\partial x} + \frac{\partial v}{\partial y} + \frac{\partial w}{\partial z} = 0 \quad (5.33)$$

x - Momentum:

$$\begin{aligned}
& \frac{\partial u}{\partial t} + \frac{\partial}{\partial x} \left(uu + \frac{\Delta_1^2}{4\gamma} \frac{\partial^2}{\partial x^2} (uu) + \frac{\Delta_2^2}{4\gamma} \frac{\partial^2}{\partial y^2} (uu) + \frac{\Delta_3^2}{4\gamma} \frac{\partial^2}{\partial z^2} (uu) \right) \\
& + \frac{\partial}{\partial y} \left(uv + \frac{\Delta_1^2}{4\gamma} \frac{\partial^2}{\partial x^2} (uv) + \frac{\Delta_2^2}{4\gamma} \frac{\partial^2}{\partial y^2} (uv) + \frac{\Delta_3^2}{4\gamma} \frac{\partial^2}{\partial z^2} (uv) \right) \\
& + \frac{\partial}{\partial z} \left(uw + \frac{\Delta_1^2}{4\gamma} \frac{\partial^2}{\partial x^2} (uw) + \frac{\Delta_2^2}{4\gamma} \frac{\partial^2}{\partial y^2} (uw) + \frac{\Delta_3^2}{4\gamma} \frac{\partial^2}{\partial z^2} (uw) \right) \\
& = -\frac{1}{\rho} \frac{\partial P}{\partial x} + \frac{\partial}{\partial x} \left(K \left(\frac{\partial u}{\partial x} + \frac{\partial u}{\partial x} \right) \right) + \frac{\partial}{\partial y} \left(K \left(\frac{\partial u}{\partial y} + \frac{\partial v}{\partial x} \right) \right) \\
& \qquad \qquad \qquad + \frac{\partial}{\partial z} \left(K \left(\frac{\partial u}{\partial z} + \frac{\partial w}{\partial x} \right) \right)
\end{aligned} \tag{5.34}$$

y - Momentum:

$$\begin{aligned}
& \frac{\partial v}{\partial t} + \frac{\partial}{\partial x} \left(uv + \frac{\Delta_1^2}{4\gamma} \frac{\partial^2}{\partial x^2} (uv) + \frac{\Delta_2^2}{4\gamma} \frac{\partial^2}{\partial y^2} (uv) + \frac{\Delta_3^2}{4\gamma} \frac{\partial^2}{\partial z^2} (uv) \right) \\
& + \frac{\partial}{\partial y} \left(vv + \frac{\Delta_1^2}{4\gamma} \frac{\partial^2}{\partial x^2} (vv) + \frac{\Delta_2^2}{4\gamma} \frac{\partial^2}{\partial y^2} (vv) + \frac{\Delta_3^2}{4\gamma} \frac{\partial^2}{\partial z^2} (vv) \right) \\
& + \frac{\partial}{\partial z} \left(vw + \frac{\Delta_1^2}{4\gamma} \frac{\partial^2}{\partial x^2} (vw) + \frac{\Delta_2^2}{4\gamma} \frac{\partial^2}{\partial y^2} (vw) + \frac{\Delta_3^2}{4\gamma} \frac{\partial^2}{\partial z^2} (vw) \right) \\
& = -\frac{1}{\rho} \frac{\partial P}{\partial y} + \frac{\partial}{\partial x} \left(K \left(\frac{\partial v}{\partial x} + \frac{\partial u}{\partial y} \right) \right) + \frac{\partial}{\partial y} \left(K \left(\frac{\partial v}{\partial y} + \frac{\partial v}{\partial y} \right) \right) + \frac{\partial}{\partial z} \left(K \left(\frac{\partial v}{\partial z} + \frac{\partial w}{\partial y} \right) \right)
\end{aligned} \tag{5.35}$$

Hydrostatic Pressure:

$$\frac{\partial P}{\partial z} = \rho g \quad (5.36)$$

Transport:

$$\begin{aligned} \text{Pr} \left[\frac{\partial c}{\partial t} + \frac{\partial}{\partial x} \left(cu + \frac{\Delta_1^2}{4\gamma} \frac{\partial^2}{\partial x^2} (cu) + \frac{\Delta_2^2}{4\gamma} \frac{\partial^2}{\partial y^2} (cu) + \frac{\Delta_3^2}{4\gamma} \frac{\partial^2}{\partial z^2} (cu) \right) \right. \\ \left. + \frac{\partial}{\partial y} \left(cv + \frac{\Delta_1^2}{4\gamma} \frac{\partial^2}{\partial x^2} (cv) + \frac{\Delta_2^2}{4\gamma} \frac{\partial^2}{\partial y^2} (cv) + \frac{\Delta_3^2}{4\gamma} \frac{\partial^2}{\partial z^2} (cv) \right) \right. \\ \left. + \frac{\partial}{\partial z} \left(c(w + w_s) + \frac{\Delta_1^2}{4\gamma} \frac{\partial^2}{\partial x^2} (c(w + w_s)) + \frac{\Delta_2^2}{4\gamma} \frac{\partial^2}{\partial y^2} (c(w + w_s)) \right. \right. \\ \left. \left. + \frac{\Delta_3^2}{4\gamma} \frac{\partial^2}{\partial z^2} (c(w + w_s)) \right) \right] = \frac{\partial}{\partial x} \left(K \frac{\partial c}{\partial x} \right) + \frac{\partial}{\partial y} \left(K \frac{\partial c}{\partial y} \right) \\ + \frac{\partial}{\partial z} \left(K \frac{\partial c}{\partial z} \right) + S \quad (5.37) \end{aligned}$$

where K is given by Equation (5.27).

G. Non Dimensionalization:

As in Paul and Lick (1976) the following variables are used to non-dimensionalize Equations (5.33) through (5.37).

$$u^* = \frac{u}{U_0} ; \quad v^* = \frac{v}{U_0} ;$$

$$w^* = \frac{b_0}{U_0 h_0} w ; \quad x^* = \frac{x}{b_0} ;$$

$$y^* = \frac{y}{b_0} ; \quad z^* = \frac{z}{h_0} ;$$

$$P^* = \frac{R_e P}{\rho_0 g h_0 Fr^2} ; \quad t^* = \frac{A_H}{b_0^2} t ;$$

$$\Delta_1^* = \frac{\Delta_1}{b_0} ; \quad \Delta_2^* = \frac{\Delta_2}{b_0} ;$$

$$\Delta_3^* = \frac{\Delta_3}{h_0} ; \quad \Delta^* = \frac{\Delta}{b_0} ;$$

$$c^* = \frac{c}{c_M}$$

where:

U_0 = reference velocity;

b_0 = horizontal reference length;

h_0 = vertical reference length;

A_H = characteristic eddy viscosity;

c_M = reference concentration;

$R_e = \frac{U_0 b_0}{A_H} = \text{Reynolds number}; \text{ and}$

$Fr = \frac{U_0}{\sqrt{gh_0}} = \text{Froude number.}$

Using the above variables and dropping asterisks, Equations (5.33) through (5.37) become:

Continuity:

$$\frac{\partial u}{\partial x} + \frac{\partial v}{\partial y} + \frac{\partial w}{\partial z} = 0 \quad (5.38)$$

x - Momentum:

$$\begin{aligned} \frac{\partial u}{\partial t} + \text{Re} \left[\frac{\partial}{\partial x} \left(uu + \frac{\Delta_1^2}{4\gamma} \frac{\partial^2}{\partial x^2} (uu) + \frac{\Delta_2^2}{4\gamma} \frac{\partial^2}{\partial y^2} (uu) + \frac{\Delta_3^2}{4\gamma} \frac{\partial^2}{\partial z^2} (uu) \right) \right. \\ + \frac{\partial}{\partial y} \left(uv + \frac{\Delta_1^2}{4\gamma} \frac{\partial^2}{\partial x^2} (uv) + \frac{\Delta_2^2}{4\gamma} \frac{\partial^2}{\partial y^2} (uv) + \frac{\Delta_3^2}{4\gamma} \frac{\partial^2}{\partial z^2} (uv) \right) \\ \left. + \frac{\partial}{\partial z} \left(uw + \frac{\Delta_1^2}{4\gamma} \frac{\partial^2}{\partial x^2} (uw) + \frac{\Delta_2^2}{4\gamma} \frac{\partial^2}{\partial y^2} (uw) + \frac{\Delta_3^2}{4\gamma} \frac{\partial^2}{\partial z^2} (uw) \right) \right] \\ = - \frac{\partial P}{\partial x} + \text{Re} \left[\frac{\partial}{\partial x} \left(K \left(\frac{\partial u}{\partial x} + \frac{\partial u}{\partial x} \right) \right) + \frac{\partial}{\partial y} \left(K \left(\frac{\partial u}{\partial y} + \frac{\partial v}{\partial y} \right) \right) \right. \\ \left. + \left(\frac{b_0}{h_0} \right)^2 \frac{\partial}{\partial z} \left(K \frac{\partial u}{\partial z} \right) \right] \quad (5.39) \end{aligned}$$

y - Momentum:

$$\begin{aligned}
\frac{\partial v}{\partial t} + R_e \left[\frac{\partial}{\partial x} \left(uv + \frac{\Delta_1^2}{4\gamma} \frac{\partial^2}{\partial x^2} (uv) + \frac{\Delta_2^2}{4\gamma} \frac{\partial^2}{\partial y^2} (uv) + \frac{\Delta_3^2}{4\gamma} \frac{\partial^2}{\partial z^2} (uv) \right) \right. \\
+ \frac{\partial}{\partial y} \left(vv + \frac{\Delta_1^2}{4\gamma} \frac{\partial^2}{\partial x^2} (vv) + \frac{\Delta_2^2}{4\gamma} \frac{\partial^2}{\partial y^2} (vv) + \frac{\Delta_3^2}{4\gamma} \frac{\partial^2}{\partial z^2} (vv) \right) \\
\left. + \frac{\partial}{\partial z} \left(wv + \frac{\Delta_1^2}{4\gamma} \frac{\partial^2}{\partial x^2} (wv) + \frac{\Delta_2^2}{4\gamma} \frac{\partial^2}{\partial y^2} (wv) + \frac{\Delta_3^2}{4\gamma} \frac{\partial^2}{\partial z^2} (wv) \right) \right] \\
= - \frac{\partial P}{\partial y} + R_e \left[\frac{\partial}{\partial x} \left(K \left(\frac{\partial v}{\partial x} + \frac{\partial u}{\partial y} \right) \right) + \frac{\partial}{\partial y} \left(K \left(\frac{\partial v}{\partial y} + \frac{\partial v}{\partial y} \right) \right) \right. \\
\left. + \left(\frac{b_0}{h_0} \right)^2 \frac{\partial}{\partial z} \left(K \frac{\partial v}{\partial z} \right) \right] \quad (5.40)
\end{aligned}$$

Hydrostatic Pressure:

$$\frac{\partial P}{\partial z} = \frac{R_e}{F^2 r} \quad (5.41)$$

Transport:

$$\begin{aligned}
 \text{Pr} \left[\frac{\partial c}{\partial t} + \text{Re} \left[\frac{\partial}{\partial x} \left((cu) + \frac{\Delta_1^2}{4\gamma} \frac{\partial^2}{\partial x^2} (cu) + \frac{\Delta_2^2}{4\gamma} \frac{\partial^2}{\partial y^2} (cu) + \frac{\Delta_3^2}{4\gamma} \frac{\partial^2}{\partial z^2} (cu) \right) \right. \right. \\
 + \frac{\partial}{\partial y} \left((cv) + \frac{\Delta_1^2}{4\gamma} \frac{\partial^2}{\partial x^2} (cv) + \frac{\Delta_2^2}{4\gamma} \frac{\partial^2}{\partial y^2} (cv) + \frac{\Delta_3^2}{4\gamma} \frac{\partial^2}{\partial z^2} (cv) \right) \\
 + \frac{\partial}{\partial z} \left((c(w+w')) + \frac{\Delta_1^2}{4\gamma} \frac{\partial^2}{\partial x^2} (c(w+w')) + \frac{\Delta_2^2}{4\gamma} \frac{\partial^2}{\partial y^2} (c(w+w')) \right. \\
 \left. \left. + \frac{\Delta_3^2}{4\gamma} \frac{\partial^2}{\partial z^2} (c(w+w')) \right) \right] \right] = \\
 = \text{Re} \left[\frac{\partial}{\partial x} \left(K \frac{\partial c}{\partial x} \right) + \frac{\partial}{\partial y} \left(K \frac{\partial c}{\partial y} \right) + \left(\frac{b_0}{h_0} \right)^2 \frac{\partial}{\partial z} \left(K \frac{\partial c}{\partial z} \right) \right] + \frac{b_0^2}{A_H C_M} S
 \end{aligned} \tag{5.42}$$

In the momentum equations the terms $\left(\frac{h_0}{b_0}\right)^2 \frac{\partial w}{\partial x}$ and $\left(\frac{h_0}{b_0}\right)^2 \frac{\partial w}{\partial y}$ are dropped because they are small comparing to the terms $\frac{\partial u}{\partial z}$ and $\frac{\partial v}{\partial z}$ respectively

In the above equations the eddy coefficient, K, is written as:

$$\begin{aligned}
 K = (c_\Delta)^2 \left[2 \left(\left(\frac{\partial u}{\partial x} \right)^2 + \left(\frac{\partial v}{\partial y} \right)^2 + \left(\frac{\partial w}{\partial z} \right)^2 \right) + \left(\frac{\partial v}{\partial x} + \frac{\partial u}{\partial y} \right)^2 \right. \\
 \left. + \left(\frac{h_0}{b_0} \frac{\partial w}{\partial y} + \frac{b_0}{h_0} \frac{\partial v}{\partial z} \right)^2 + \left(\frac{b_0}{h_0} \frac{\partial u}{\partial z} + \frac{h_0}{b_0} \frac{\partial w}{\partial x} \right)^2 \right]^{1/2} \tag{5.43}
 \end{aligned}$$

H. Boundary Conditions

The following boundary conditions are used for the momentum and transport equations.

1) Momentum Equations

Surface:

Wind dependent stresses, τ_{wx} , τ_{wy} are imposed as:

$$\tau_{wx} = \left. \frac{\partial u}{\partial z} \right|_{z=0}$$

$$\tau_{wy} = \left. \frac{\partial v}{\partial z} \right|_{z=0}$$

Solid boundaries:

$$u = 0$$

$$v = 0$$

$$w = 0$$

2) Transport Equation

Boundaries:

No flux through boundaries is allowed.

Bottom:

No diffusive flux is allowed.

CHAPTER VI

NUMERICAL SOLUTION

Equations (5.33) to (5.37) are solved numerically by a new version of the time splitting procedure originally developed by Paul and Lick (1973, 1976). Here the second order corrective terms which result in the equations by the filtering procedure require a fourth order overall spatial accuracy. Therefore Paul and Lick's model was rederived to incorporate this high spatial accuracy. The solution of equations (5.33) to (5.36) requires that a new equation for the pressure, P , be derived from continuity and solved. For increased accuracy, this equation is formulated numerically.

In this chapter the spatial differencing, the time marching procedure and the pressure field solution technique are discussed.

A. Grid Layout

The staggered grid mesh developed in Los Alamos Laboratories (Welch, et al. 1966) was used in this work. According to this the horizontal velocities are defined at nodal points, the vertical velocities are defined at half nodal points in the vertical and half nodal points in the horizontal except for the surface where the vertical velocities are defined at nodal points in the vertical and half nodal points in the horizontal. The concentration is defined at half nodal

points in the horizontal and nodal points in the vertical and the surface pressure is defined at half nodal points in the horizontal. The advantage of this scheme is that, when written in this fashion, mass and momentum are conserved over a cell. Typical horizontal and vertical arrangements are shown in Figure 6.1, also typical nodal cells are shown in Figure 6.2. The indices used are k, m, n in x, y, z direction respectively. Horizontal and vertical planes indicating the numbering of the cells are shown in Figures 6.3 and 6.4.

In the numerical solution of the equations, variables are sometimes needed at points where they are not defined. In this case they are computed as simple averages of the neighboring values.

B. Spatial Differencing Procedures

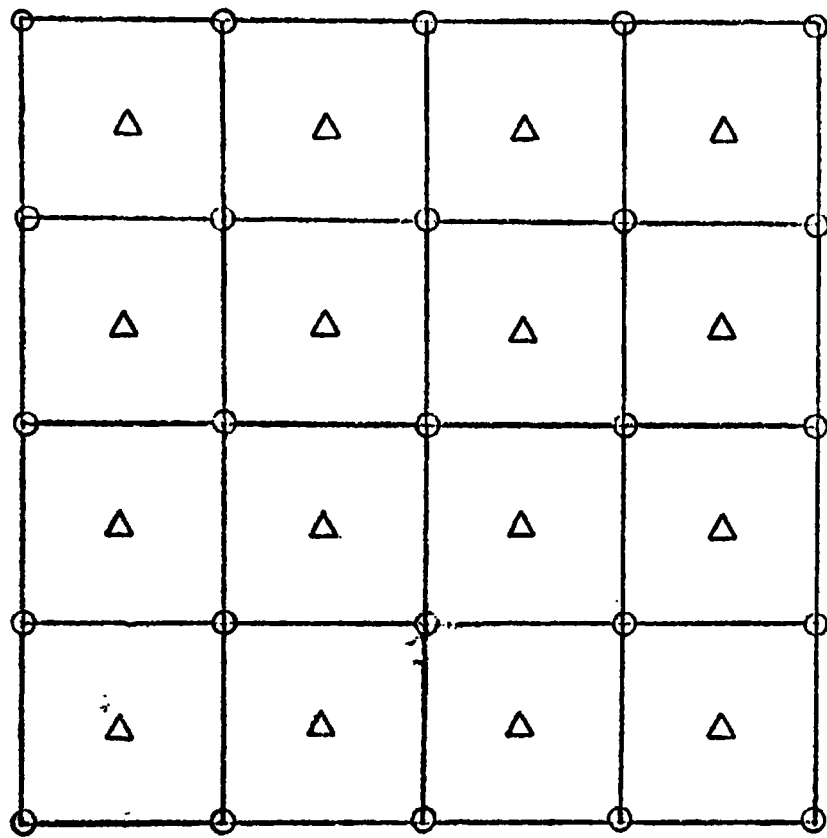
The inertial terms in Equations (5.33) to (5.37) contain terms of the form $u_i u_j$ and second order differential Leonard terms of the form

$$\frac{\Delta^2}{4\gamma} \frac{\partial^2}{\partial x_k^2} u_i u_j .$$

As mentioned in Chapter V these terms are very

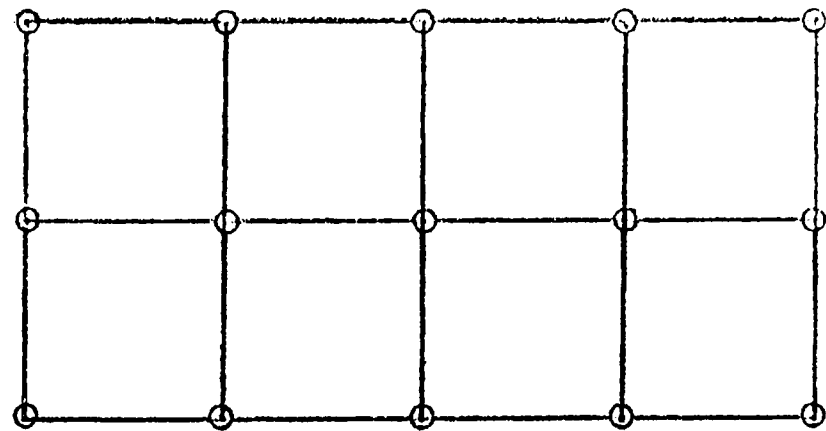
important and they always have to be included in the mathematical modeling of any turbulent flow. Their presence, however, necessitates the use of a high accuracy differencing scheme for the first order differential terms of the form $\frac{\partial}{\partial x_j} u_i u_j$. A conventional second order differencing scheme

includes Leonard-like second order terms as its truncation error, and therefore it is not sufficient when the Leonard terms are included. Another

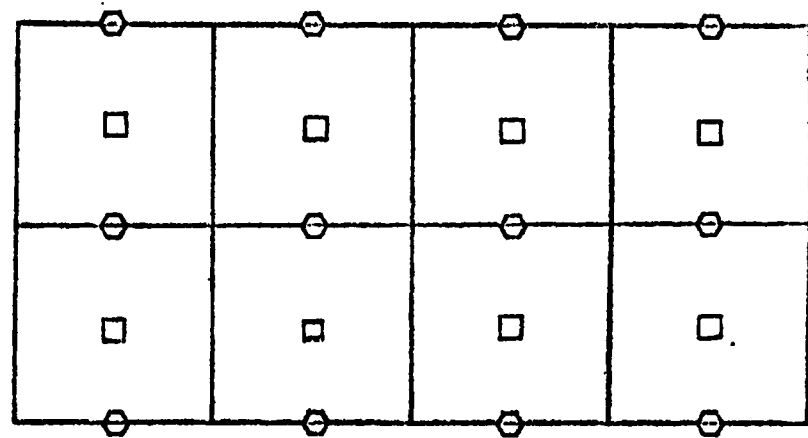


Horizontal Plane

- - u, v
- △ - c, w
- - c
- - w



Vertical Plane at Nodal Section



Vertical Plane at Half Nodal Section

Figure 6.1 Arrangements of Variables in Grid Sections (After Paul and Lick, 1976)

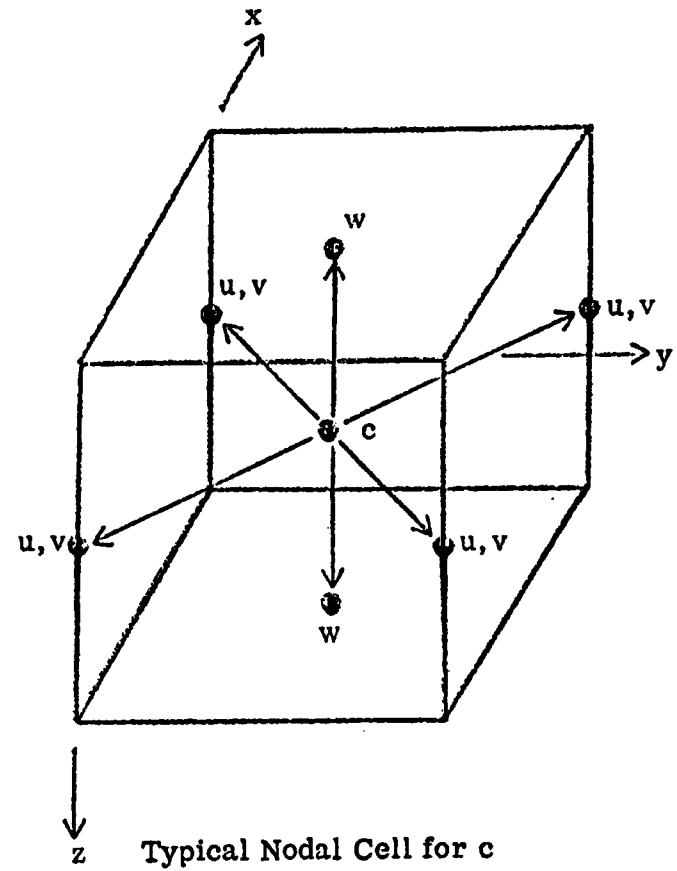
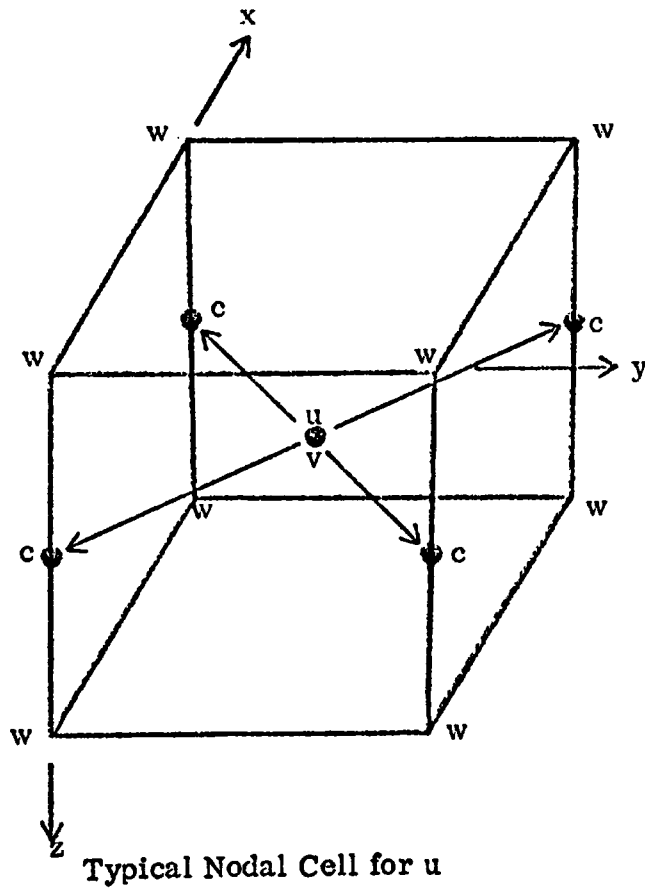


Figure 6.2 Typical Nodal Cells for Grid System (After Paul and Lick, 1976)

| | | | | |
|--|--|--|--|--|
| | | $k, m + \frac{1}{2}, n + \frac{5}{2}$ ● | | |
| | | $k, m + \frac{1}{2}, n + \frac{3}{2}$ ● | | |
| $k, m - \frac{3}{2}, n + \frac{1}{2}$ ● | $k, m - \frac{1}{2}, n + \frac{1}{2}$ ● | $k, m + \frac{1}{2}, n + \frac{1}{2}$ ● | $k, m + \frac{3}{2}, n + \frac{1}{2}$ ● | $k, m + \frac{5}{2}, n + \frac{1}{2}$ ● |
| | | $k, m + \frac{1}{2}, n - \frac{1}{2}$ ● | | |
| | | $k, m + \frac{1}{2}, n - \frac{3}{2}$ ● | | |

Figure 6.3 Horizontal Plane at Nodal Section. -Indexing

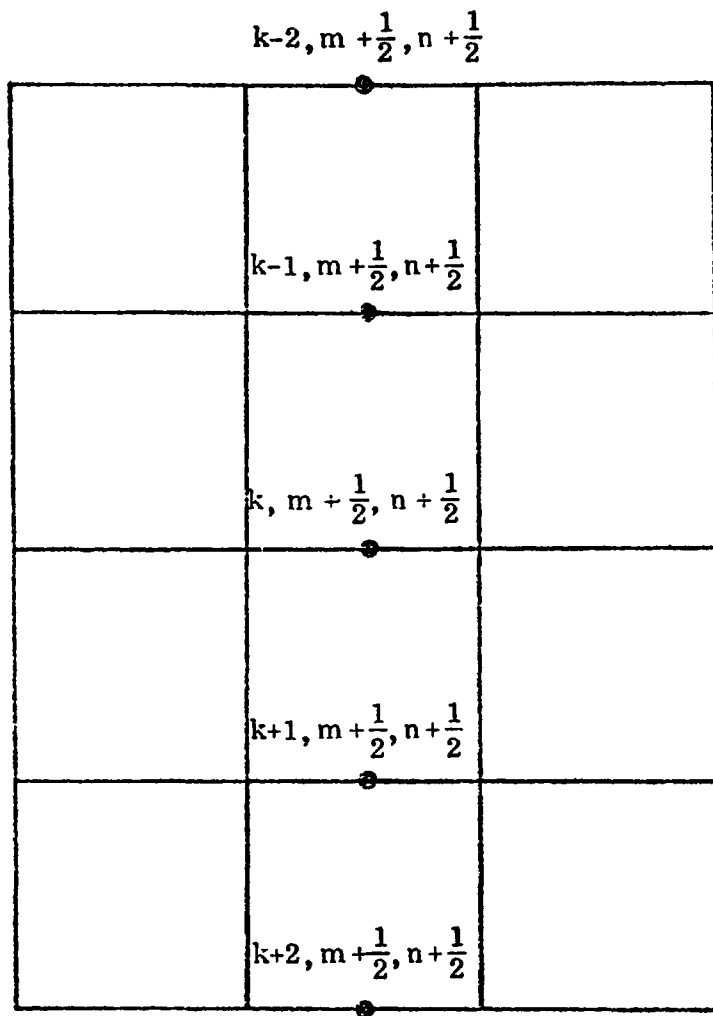


Figure 6.4 Vertical Plane at Half Nodal Section. -Indexing

reason for the use of a high order differencing scheme is the need for resolving wave numbers up to the Nyquist frequency, π/Δ . π/Δ is the maximum wave number that can be represented in a grid of size, Δ . (Bloomfield 1976, p.29).

A fourth order accurate scheme (Collatz 1961, p. 538, Kwak, et al. 1975) is used for the first order differential terms. Since the Leonard and the residual stress terms are second order differentials they can be approximated by second order differencing scheme to give fourth order accuracy. Therefore, a fourth order accuracy for the first order differentials and a second order accuracy for the second order differentials derives fourth order overall accuracy.

The fourth order accurate scheme used here is derived from the second order operator applied over one and two mesh spaces as follows:

$$\frac{\partial u}{\partial x} = \frac{4}{3} \frac{u_{n+1} - u_{n-1}}{2\Delta x} - \frac{1}{3} \frac{u_{n+2} - u_{n-2}}{4\Delta x}$$

or

$$\frac{\partial u}{\partial x} = \frac{1}{12\Delta x} (u_{n-2} - 8u_{n-1} + 8u_{n+1} - u_{n+2}) \quad (6.1)$$

The ability of Equation (6.1) to resolve high wave number components is presented by Kwak, et al. (1975) and Mansour, et al. (1977). This is as follows: suppose $u(x)$ is represented by a discrete Fourier expansion as:

$$u(x) = \sum_{n_1} \hat{u}(k_1) e^{ik_1 x} \quad (6.2)$$

where:

$$n_1 = -N/2, \dots, 0, 1, \dots, N/2 - 1$$

N = number of nodal points in x direction and the wave number in x direction, k_1 is given by:

$$k_1 = \frac{2\pi}{N\Delta} n_1 \quad (6.3)$$

Consider now that $u(x)$ is given by a single Fourier component as:

$$u(x) = \hat{u}(k_1) e^{ik_1 x} \quad (6.4)$$

Substituting Equation (6.4) into Equation (6.1), the Fourier transform of $\partial u / \partial x$ is the following:

$$\frac{\partial \hat{u}}{\partial x} = \frac{1}{12\Delta x} (e^{-2ik_1 \Delta x} - 8e^{-ik_1 \Delta x} + 8e^{ik_1 \Delta x} - e^{2ik_1 \Delta x}) \hat{u}(k_1)$$

or

$$\frac{\partial \hat{u}}{\partial x} = ik_1' \hat{u}(k_1) \quad (6.5)$$

where:

$$k'_1 = \frac{1}{6\Delta} (8 \sin k_1 \Delta x - \sin 2k_1 \Delta x). \quad (6.6)$$

k'_1 is a modified wave number.

If a second order differencing scheme is used:

$$\frac{\partial u}{\partial x} = \frac{1}{2\Delta x} (u_{i+1} - u_{i-1}) \quad (6.7)$$

and the modified wave number is:

$$k''_1 = \frac{1}{\Delta x} \sin(k_1 \Delta x) \quad (6.8)$$

The exact Fourier transform of $\partial u / \partial x$ is given by:

$$\frac{\partial \hat{u}}{\partial x} = i k_1 \hat{u}(k_1) \quad (6.9)$$

where k_1 is given by Equation (6.3). Comparison of k_1 , k'_1 and k''_1 is shown in Figure 6.5. The improvement of fourth order over the second order differencing scheme is obvious.

Equation (6.1) cannot be used directly in this model because the first order terms contain double velocity correlations of the form $u_i u_j$. An equivalent to Equation (6.1) numerical scheme that is also energy and momentum conservative (Kwak, et al. 1975) is used in this work. For a typical term $\partial / \partial x (uv)$ this scheme is derived as follows:

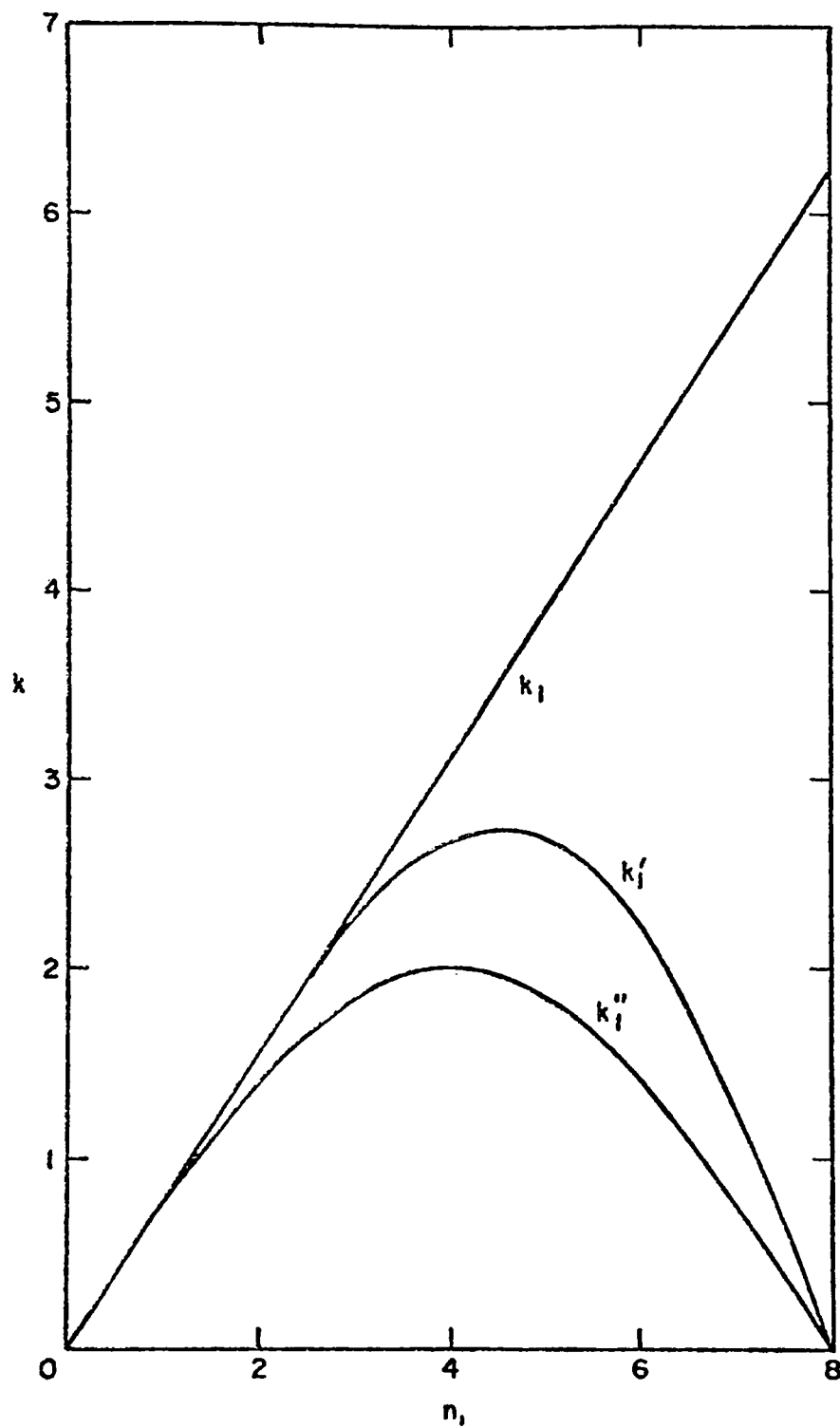


Figure 6.5 Comparison of Modified Wave Numbers (After Kwak, et al., 1975)

$$\frac{\partial uv}{\partial x} = \frac{4}{3} \left. \frac{\partial uv}{\partial x} \right|_{\Delta x} - \frac{1}{3} \left. \frac{\partial uv}{\partial x} \right|_{2\Delta x} \quad (6.10)$$

where $\left. \frac{\partial uv}{\partial x} \right|_{\Delta x}$ and $\left. \frac{\partial uv}{\partial x} \right|_{2\Delta x}$ denote central differencing over one and two mesh spaces.

$\left. \frac{\partial uv}{\partial x} \right|_{\Delta x}$ is written as:

$$\left. \frac{\partial uv}{\partial x} \right|_{\Delta x} = \frac{1}{2} \left[\frac{(uv)_{n+1} - (uv)_{n-1}}{2\Delta x} + u_n \frac{v_{n+1} - v_{n-1}}{2\Delta x} + v_n \frac{u_{n+1} - u_{n-1}}{2\Delta x} \right] \text{ or}$$

$$\left. \frac{\partial uv}{\partial x} \right|_{\Delta x} = \frac{1}{4\Delta x} \left[(uv)_{n+1} - (uv)_{n-1} + u_n(v_{n+1} - v_{n-1}) + v_n(u_{n+1} - u_{n-1}) \right] \quad (6.11)$$

Similarly $\left. \frac{\partial uv}{\partial x} \right|_{2\Delta x}$ is written as:

$$\left. \frac{\partial uv}{\partial x} \right|_{2\Delta x} = \frac{1}{2} \left[\frac{(uv)_{n+2} - (uv)_{n-2}}{4\Delta x} + u_n \frac{v_{n+2} - v_{n-2}}{4\Delta x} + v_n \frac{u_{n+2} - u_{n-2}}{4\Delta x} \right] \text{ or}$$

$$\left. \frac{\partial uv}{\partial x} \right|_{2\Delta x} = \frac{1}{8\Delta x} \left[(uv)_{n+2} - (uv)_{n-2} + u_n(v_{n+2} - v_{n-2}) + v_n(u_{n+2} - u_{n-2}) \right] \quad (6.12)$$

Substitution of Equations (6.11) and (6.12) into Equation (6.10) gives:

$$\begin{aligned} \frac{\partial uv}{\partial x} &= \frac{1}{3 \Delta x} \left[(uv)_{n+1} - (uv)_{n-1} + u_n(v_{n+1} - v_{n-1}) + v_n(u_{n+1} - u_{n-1}) \right] \\ &\quad - \frac{1}{24 \Delta x} \left[(uv)_{n+2} - (uv)_{n-2} + u_n(v_{n+2} - v_{n-2}) + v_n(u_{n+2} - u_{n-2}) \right] \end{aligned} \quad (6.13)$$

Equation (6.13) is a five-node scheme and cannot be used for the nodal points which are located one cell behind or one cell ahead of a wall. For these nodes an unsymmetric fourth order scheme is used (Kollatz 1961, p. 538).

This scheme is as follows:

Wall 1 cell behind:

$$\frac{\partial u}{\partial x} = \frac{1}{12 \Delta x} (-3 u_{n-1} - 10 u_n + 18 u_{n+1} - 6 u_{n+2} + u_{n+3}) \quad (6.14)$$

Wall 1 cell ahead:

$$\frac{\partial u}{\partial x} = \frac{1}{12 \Delta x} (3 u_{n+1} + 10 u_n - 18 u_{n-1} + 6 u_{n-2} - u_{n-3}) \quad (6.15)$$

For a typical term $\frac{\partial uv}{\partial x}$ this scheme is written in an equivalent to Equation (6.13) form as follows:

Wall 1 cell behind:

$$\begin{aligned} \frac{\partial uv}{\partial x} &= \frac{1}{24 \Delta x} \left[-3 (uv)_{n-1} - 10 (uv)_n + 18 (uv)_{n+1} - 6 (uv)_{n+2} \right. \\ &\quad + (uv)_{n+3} + u_n (-3v_{n-1} - 10v_n + 18v_{n+1} - 6v_{n+2} + v_{n+3}) \\ &\quad \left. + v_n (-3u_{n-1} - 10u_n + 18u_{n+1} - 6u_{n+2} + u_{n+3}) \right] \end{aligned} \quad (6.16)$$

Wall 1 cell ahead:

$$\begin{aligned} \frac{\partial uv}{\partial x} = \frac{1}{24 \Delta x} & \left[3 (uv)_{n+1} + 10 (uv)_n - 18 (uv)_{n-1} + 6 (uv)_{n-2} \right. \\ & - (uv)_{n-3} + u_n (3v_{n+1} + 10v_n - 18v_{n-1} + 6v_{n-2} - v_{n-3}) \\ & \left. + v_n (3u_{n+1} + 10u_n - 18u_{n-1} + 6u_{n-2} - u_{n-3}) \right] \quad (6.17) \end{aligned}$$

Equations (6.16) and (6.17) cannot be applied for nodes lying on the boundaries because they extend one node beyond the boundary. This does not create a problem in the horizontal direction and also in the bottom boundary of the vertical direction since velocities are zero on the solid boundaries. Therefore, the solution domain extends only to one node before a solid boundary. However, in the surface where the terms $\frac{\partial}{\partial z}(wu)$ and $\frac{\partial}{\partial z}(wv)$ need to be evaluated (6.16) cannot be applied. Instead a second order unsymmetric scheme is used (Kollatz 1961, p 538). For one variable, w , this is written as:

Boundary behind:

$$\frac{\partial w}{\partial z} = \frac{1}{2 \Delta z} (-3 w_k + 4 w_{k+1} - w_{k+2}) \quad (6.18)$$

Boundary ahead:

$$\frac{\partial w}{\partial z} = \frac{1}{2 \Delta z} (3 w_k - 4 w_{k-1} + w_{k-2}) \quad (6.19)$$

An equivalent to Equation (6.16) scheme is written as:

Surface boundary:

$$\frac{\partial wu}{\partial z} = \frac{1}{4\Delta z} \left[4(wu)_{k+1} - (wu)_{k+2} + w_k(-3u_k + 4u_{k+1} - u_{k+2}) + u_k(4w_{k+1} - w_{k+2}) \right] \quad (6.20)$$

where w_{surface} is set to zero because of the rigid lid assumption. For the Leonard term the second order central differencing scheme (6.3) is used.

A typical Leonard term is written as:

$$\frac{\Delta_1^2}{4\gamma} \frac{\partial}{\partial x} \frac{\partial^2 uv}{\partial x^2} = \frac{\Delta_1^2}{4\gamma} \frac{1}{2\Delta x} \left[\frac{\partial^2 uv}{\partial x^2} \Big|_{n+1} - \frac{\partial^2 uv}{\partial x^2} \Big|_{n-1} \right]$$

where $\frac{\partial^2 uv}{\partial x^2}$ is written as;

$$\frac{\partial^2 uv}{\partial x^2} = 2 \frac{\partial u}{\partial x} \frac{\partial v}{\partial x} + u \frac{\partial^2 v}{\partial x^2} + v \frac{\partial^2 u}{\partial x^2} \quad (6.21)$$

The familiar second order scheme is used for the last two terms in (6.21),

$$\frac{\partial^2 v}{\partial x^2} = \frac{1}{\Delta x^2} (v_{n+1} - 2v_n + v_{n-1}) \quad (6.22)$$

When the term (6.21) needs to be evaluated on the wall unsymmetric second order differencing schemes are used (Kollatz 1961, p. 538).

Wall behind:

$$\frac{\partial v}{\partial x} = \frac{1}{2 \Delta x} (-3v_n + 4v_{n+1} - v_{n+2}) \quad (6.23)$$

$$\frac{\partial^2 v}{\partial x^2} = \frac{1}{\Delta x^2} (2v_n - 5v_{n+1} + 4v_{n+2} - v_{n+3}) \quad (6.24)$$

Wall ahead:

$$\frac{\partial v}{\partial x} = \frac{1}{2 \Delta x} (3v_n - 4v_{n-1} + 4v_{n-2}) \quad (6.25)$$

$$\frac{\partial^2 v}{\partial x^2} = \frac{1}{\Delta x^2} (-2v_n + 5v_{n-1} - 4v_{n-2} + v_{n-3}) \quad (6.26)$$

For the residual field terms (6.3) and (6.22) are used. A typical term is

written as;

$$\begin{aligned} \frac{\partial}{\partial x} K \left(\frac{\partial v}{\partial x} + \frac{\partial u}{\partial y} \right) &= \frac{\partial K}{\partial x} \left(\frac{\partial v}{\partial x} + \frac{\partial u}{\partial y} \right) + K \frac{\partial}{\partial x} \left(\frac{\partial v}{\partial x} + \frac{\partial u}{\partial y} \right) \\ &= \frac{K_{m,n+1} - K_{m,n-1}}{2 \Delta x} \left(\frac{v_{m,n+1} - v_{m,n-1}}{2 \Delta x} + \frac{u_{m+1,n} - u_{m-1,n}}{2 \Delta y} \right) \\ &\quad + \frac{K_{m,n}}{\Delta x} \left[\frac{v_{m,n+1} - 2v_{m,n} + v_{m,n-1}}{\Delta x} + \frac{u_{m+1,n+\frac{1}{2}} - u_{m-1,n+\frac{1}{2}}}{2 \Delta y} \right. \\ &\quad \left. - \frac{u_{m+1,n-\frac{1}{2}} - u_{m-1,n-\frac{1}{2}}}{2 \Delta y} \right] \\ &= \frac{K_{m,n+1} - K_{m,n-1}}{2 \Delta x} \left(\frac{v_{m,n+1} - v_{m,n-1}}{2 \Delta x} + \frac{u_{m+1,n} - u_{m-1,n}}{2 \Delta y} \right) \end{aligned}$$

$$+ \frac{K_{m,n}}{\Delta x} \left[\frac{v_{m,n+1} - 2v_{m,n} + v_{m,n-1}}{\Delta x} + \frac{u_{m+1,n+1} - u_{m-1,n+1} - u_{m+1,n-1} + u_{m-1,n-1}}{4\Delta y} \right] \quad (6.27)$$

As mentioned in the Grid Layout section, the concentration is defined at half nodal points in the horizontal and nodal points in the vertical. This necessitates a special treatment of the boundary points and also of the points which are one node away from a boundary. The latter will be considered first.

The fourth order accurate symmetric differencing scheme (6.13) extends two nodes in each direction beyond the point where a term needs to be evaluated. Therefore, it cannot be used to evaluate the term $\frac{\partial}{\partial x_i} (u_i c)$ in the first node away from the boundary node. For these nodes the unsymmetric fourth order schemes (6.16), (6.17) are used. Because of the special arrangement of the concentration nodes the solution domain extends over all the nodal points. (In contrast the momentum equations solution domain starts from the second node and ends at the node before the last one in each horizontal direction). Therefore, in order to incorporate the correct boundary conditions it is better to look upon fluxes at the boundary points instead of considering strict mathematical approximation of each term. Consider, for example, the flux in x-direction:

$$F = K \frac{\partial c}{\partial x} - \left(cu + \frac{\Delta^2}{4\gamma} \frac{\partial^2}{\partial x^2} cu + \frac{\Delta^2}{4\gamma} \frac{\partial^2}{\partial y^2} cu + \frac{\Delta^2}{4\gamma} \frac{\partial^2}{\partial z^2} cu \right) \quad (6.28)$$

In the first nodal point the following equation is considered:

$$\begin{aligned}
 \left. \frac{\partial F}{\partial x} \right|_{m+\frac{1}{2}, n+\frac{1}{2}} &= \frac{1}{\Delta x} \left[F_{m+\frac{1}{2}, n+1} - F_{m+\frac{1}{2}, n}^0 \right] \\
 &= \frac{1}{\Delta x} \left[K \left. \frac{\partial c}{\partial x} \right|_{m+\frac{1}{2}, n+1} - \left((cu)_{m+\frac{1}{2}, n+1} + \frac{\Delta_1^2}{4\gamma} \left. \frac{\partial^2 cu}{\partial x^2} \right|_{m+\frac{1}{2}, n+1} \right. \right. \\
 &\quad \left. \left. + \frac{\Delta_1^2}{4\gamma} \left. \frac{\partial^2 cu}{\partial y^2} \right|_{m+\frac{1}{2}, n+1} + \frac{\Delta_1^2}{4\gamma} \left. \frac{\partial^2 cu}{\partial z^2} \right|_{m+\frac{1}{2}, n+1} \right) \right] \quad (6.29)
 \end{aligned}$$

Similar Equations apply to all the boundaries. The equations used are summarized as in Table 6.1.

C. Time Marching Procedure

A first order accurate time marching scheme is used:

$$\frac{\partial u}{\partial t} = \frac{u^{L+1} - u^L}{\Delta t} \quad (6.30)$$

Even though Equation (6.30) is not compatible with the 4th order overall spatial accuracy, it is used because of its stability especially in long time computations.

In shallow water basins the size of the time step is very much limited by the small vertical scale. To overcome this problem an implicit vertical diffusion scheme is used in this work. According to this scheme Equations (5.35) to (5.36) are formulated and solved as follows:

Table 6.1 Equations Used in the Numerical Model

| Term | Interior | Surface | Node before the boundary node | boundary node |
|---|-----------|-----------|-------------------------------------|--------------------------|
| $\frac{\partial}{\partial x_j} u_i u_j$ | 6.13 | | 6.16, 6.17 | velocity=0 |
| i=1,2 - j=1,2 | | | | |
| $\frac{\partial}{\partial x_j} c u_j$ | 6.13 | | 6.16, 6.17 | 6.29 |
| j = 1,2 | | | | |
| $\frac{\partial}{\partial x_j} u_i u_j$ | 6.13 | 6.20 | 6.17 | velocity=0 |
| i=1,2 - j =3 | | | | |
| $\frac{\partial}{\partial x_j} c u_j$ | 6.13 | 6.29 | 6.16, 6.17 | 6.29 |
| j = 3 | | | | |
| Leonard terms | 6.3 | | | 6.23, 6.24 6.25, 6.26 |
| Residual field | 6.3, 6.22 | 6.3, 6.22 | | |

$$\frac{\partial u}{\partial t} - Re \left(\frac{b_0}{h_0} \right)^2 \frac{\partial}{\partial z} \left(K \frac{\partial u}{\partial z} \right) = G(u) - \frac{\partial P_s}{\partial x} \quad (6.31)$$

$$\frac{\partial v}{\partial t} - Re \left(\frac{b_0}{h_0} \right)^2 \frac{\partial}{\partial z} \left(K \frac{\partial v}{\partial z} \right) = F(v) - \frac{\partial P_s}{\partial y} \quad (6.32)$$

P_s is the surface pressure and $G(u)$ and $F(v)$ contain the rest of the terms for the x-momentum and y-momentum equations respectively. When discretized the left hand sides of (6.31) and (6.32) are solved implicitly for new values at time $L+1$ while the right hand side are formulated from information at time L . The formulation of (6.31) and (6.32) requires that:

(1) the horizontal velocities be split into two components, the first to be solved implicitly and the second explicitly; and (2) consistent with number 1, an equation for pressure be formulated from (6.31) and (6.32). The velocity split and the pressure equation formulation are presented in the next section.

D. Pressure Field Solution Technique

The solution of Equations (5.33) to (5.36) requires one more equation for the pressure, P . Because of the shallow water assumption and the resulting hydrostatic pressure relation, this pressure equation must be based on vertically averaged velocities. The normal procedure, as described in Liggett (1970), is to vertically average Equations (5.34) and (5.35) and to differentiate the resulting two equations with respect to x and y respectively. These two resulting equations are added together and the result is required to satisfy the vertically integrated continuity equation. The resulting equation is a Poisson

type pressure equation. In this work the same procedure is used in the splitting procedure but for higher accuracy, instead of using (5.34) and (5.35), the finite differenced form of them is used. The divergence is obtained numerically and the final equation is in finite difference form instead of differential form. This concept was first used in lake models by Dr. J. F. Paul at the EPA Great Lakes Research Laboratory, Grosse Ile, Michigan and is extended to the fourth order problem herein as follows:

Equations (6.31) and (6.32) are written with vertical diffusion solved implicitly in time as:

Surface;

$$\frac{u_k^{L+1} - u_k^L}{\Delta t} - R_e \left(\frac{b_o}{h_o} \right)^2 \frac{2}{\Delta z} \left[K_{k+1/2} \frac{u_{k+1}^{L+1} - u_k^{L+1}}{\Delta z} - K_k \tau_{wx}^{L+1} \right] = G_k^L(u) - \frac{\partial P_s}{\partial x}, \quad (6.33)$$

and

$$\frac{v_k^{L+1} - v_k^L}{\Delta t} - R_e \left(\frac{b_o}{h_o} \right)^2 \frac{2}{\Delta z} \left[K_{k+1/2} \frac{v_{k+1}^{L+1} - v_k^{L+1}}{\Delta z} - K_k \tau_{wy}^{L+1} \right] = F_k^L(v) - \frac{\partial P_s}{\partial y} \quad (6.34)$$

where;

$$\tau_{wx}^{L+1} = \frac{\partial u}{\partial z} \Big|_{z=0}^{L+1}, \quad \tau_{wy}^{L+1} = \frac{\partial v}{\partial z} \Big|_{z=0}^{L+1}, \text{ and}$$

L indicates the time step.

For the Interior:

$$\begin{aligned} \frac{u_k^{L+1} - u_k^L}{\Delta t} - R_e \left(\frac{b_o}{h_o} \right)^2 \frac{1}{\Delta z^2} \left[K_{k+1/2} (u_{k+1}^{L+1} - u_k^{L+1}) \right. \\ \left. - K_{k-1/2} (u_k^{L+1} - u_{k-1}^{L+1}) \right] = G_k^L(u) - \frac{\partial P_s}{\partial x} \end{aligned} \quad (6.35)$$

and

$$\begin{aligned} \frac{v_k^{L+1} - v_k^L}{\Delta t} - R_e \left(\frac{b_o}{h_o} \right)^2 \frac{1}{\Delta z^2} \left[K_{k+1/2} (v_{k+1}^{L+1} - v_k^{L+1}) \right. \\ \left. - K_{k-1/2} (v_k^{L+1} - v_{k-1}^{L+1}) \right] = F_k^L(v) - \frac{\partial P_s}{\partial y} \end{aligned} \quad (6.36)$$

Equations (6.33) to (6.36) are rewritten at the surface as:

$$\begin{aligned} \left(\frac{1}{\Delta t} + R_e \left(\frac{b_o}{h_o} \right)^2 \frac{2}{\Delta z^2} K_{k+1/2} \right) \begin{Bmatrix} u_k^{L+1} \\ v_k^{L+1} \end{Bmatrix} - R_e \left(\frac{b_o}{h_o} \right)^2 \frac{2}{\Delta z^2} K_{k+1/2} \begin{Bmatrix} u_{k+1}^{L+1} \\ v_{k+1}^{L+1} \end{Bmatrix} \\ = \begin{Bmatrix} G_k^L(u) \\ F_k^L(v) \end{Bmatrix} + \frac{1}{\Delta t} \begin{Bmatrix} u_k^L \\ v_k^L \end{Bmatrix} - \begin{Bmatrix} g^{L+1} \\ q^{L+1} \end{Bmatrix} - \begin{Bmatrix} \partial P_s / \partial x \\ \partial P_s / \partial y \end{Bmatrix}; \end{aligned} \quad (6.37)$$

where;

$$g^{L+1} = R_e \left(\frac{b_o}{h_o} \right)^2 \frac{2}{\Delta z} K_k \tau_{wx}^{L+1}, \quad \text{and}$$

$$q^{L+1} = R_e \left(\frac{b_o}{h_o} \right)^2 \frac{2}{\Delta z} K_k \tau_{wx}^{L+1}.$$

For the Interior ($1 < k < KLM$):

$$-R_e \left(\frac{b_o}{h_o} \right)^2 \frac{1}{\Delta z^2} K_{k-1/2} \begin{pmatrix} u_{k-1}^{L+1} \\ v_{k-1}^{L+1} \end{pmatrix} + \left(\frac{1}{\Delta t} + R_e \left(\frac{b_o}{h_o} \right)^2 \frac{1}{\Delta z^2} (K_{k+1/2} + K_{k-1/2}) \right) \begin{pmatrix} u_k^{L+1} \\ v_k^{L+1} \end{pmatrix}; \quad \text{and}$$

$$-R_e \left(\frac{b_o}{h_o} \right)^2 \frac{1}{\Delta z^2} K_{k+1/2} \begin{pmatrix} u_{k+1}^{L+1} \\ v_{k+1}^{L+1} \end{pmatrix} = \begin{pmatrix} G_k^L(u) \\ F_k^L(v) \end{pmatrix} + \frac{1}{\Delta t} \begin{pmatrix} u_k^L \\ v_k^L \end{pmatrix}$$

$$- \begin{pmatrix} \partial P_s / \partial x \\ \partial P_s / \partial y \end{pmatrix} \quad (6.38)$$

where; KLM indicates the node before the last one.

For $k = \text{KLM}$:

$$\begin{aligned}
 & -\text{Re} \left(\frac{b_0}{h_0} \right)^2 \frac{1}{\Delta z^2} K_{k-1/2} \begin{pmatrix} u_{k-1}^{L+1} \\ v_{k-1}^{L+1} \end{pmatrix} + \left(\frac{1}{\Delta t} + \text{Re} \left(\frac{b_0}{h_0} \right)^2 \frac{1}{\Delta z^2} (K_{k+1/2} \right. \\
 & \left. + K_{k+1/2}) \right) \begin{pmatrix} u_k^{L+1} \\ v_k^{L+1} \end{pmatrix} \\
 & = \begin{pmatrix} G_k^L(u) \\ F_k^L(v) \end{pmatrix} + \frac{1}{\Delta t} \begin{pmatrix} u_k^L \\ v_k^L \end{pmatrix} - \begin{pmatrix} \partial P_s / \partial x \\ \partial P_s / \partial y \end{pmatrix}. \tag{6.39}
 \end{aligned}$$

Equations (6.37) to (6.39) are written as:

$$A \underline{u}^{L+1} = \underline{G} + \underline{U} - \frac{\partial P_s}{\partial x} \underline{I} \tag{6.40}$$

$$A \underline{v}^{L+1} = \underline{F} + \underline{V} - \frac{\partial P_s}{\partial y} \underline{I} ; \tag{6.41}$$

where A is a tridiagonal array, \underline{G} , \underline{U} , \underline{F} , \underline{V} are vectors and \underline{I} is a unit vector. Since the equations for u_k^{L+1} and v_k^{L+1} are linear, u_k^{L+1} and v_k^{L+1} are written as:

$$u_k^{L+1} = u_k^Q + u_k^P \tag{6.42}$$

$$v_k^{L+1} = v_k^Q + v_k^P ; \quad (6.43)$$

Such that:

$$A u_k^Q = \underline{G} + \underline{U} ; \quad (6.44)$$

$$A u_k^P = - \frac{\partial P_s}{\partial x} \underline{I} ; \quad (6.45)$$

$$A v_k^Q = \underline{F} + \underline{V} ; \quad \text{and} \quad (6.46)$$

$$A v_k^P = - \frac{\partial P_s}{\partial x} \underline{I} . \quad (6.47)$$

The solution for u_k^P and v_k^P is obtained as:

$$u_k^P = - \lambda_k \frac{\partial P_s}{\partial x} ; \quad \text{and} \quad (6.48)$$

$$v_k^P = - \lambda_k \frac{\partial P_s}{\partial y} ; \quad (6.49)$$

where λ_k satisfies

$$A \underline{\lambda} = \underline{I} . \quad (6.50)$$

To obtain the equation for the pressure, Equations (6.40) and (6.41) are

integrated over the vertical coordinate using the following summation scheme

$$\sum_{k=1}^{KLM} \psi_k B_k \quad (6.51)$$

where B_k is (6.40) or (6.41) and

$$\psi_k = \begin{cases} \Delta z/2 & : & k = 1 \\ \Delta z & : & 1 < k < KLM. \end{cases}$$

After cancelling the terms of opposite sign, the following equations are obtained:

$$\frac{1}{\Delta t} \sum_k \psi_k (u_k^{L+1} - u_k^L) + R u_{KLM}^{L+1} = -S \frac{\partial P_s}{\partial x} + \sum_k \psi_k G_k^L, \text{ and} \quad (6.52)$$

$$\frac{1}{\Delta t} \sum_k \psi_k (v_k^{L+1} - v_k^L) + R v_{KLM}^{L+1} = -S \frac{\partial P_s}{\partial y} + \sum_k \psi_k G_k^L; \quad (6.53)$$

where :

$$S = \Delta z * (KLM - 1/2), \text{ and}$$

$$R = \left(\frac{b_0}{h_0}\right)^2 \frac{1}{\Delta z} K_{KLM+1/2}$$

The numerical divergence of Equations (6.52) and (6.53) is now obtained considering that Equations (6.52) and (6.53) are evaluated at points (m,n)

while the pressure is evaluated at points $(m+1/2, n+1/2)$. The resulting two equations are added together as follows:

$$\frac{(6.52)_{m+1,n+1} + (6.52)_{m,n+1} - (6.52)_{m+1,n} - (6.52)_{m,n}}{\Delta x}$$

$$+ \frac{(6.53)_{m+1,n+1} + (6.53)_{m+1,n} - (6.53)_{m,n+1} - (6.53)_{m,n}}{\Delta y}$$

Considering now the summed continuity equation:

$$w_{k_1, m+1/2, n+1/2} = \sum_k \psi_k \frac{u_{k, m, n+1} - u_{k, m, n} + u_{k, m+1, n+1}}{2\Delta x}$$

$$\frac{- u_{k, m+1, n}}{2\Delta x}$$

$$+ \sum_k \psi_k \frac{v_{k, m+1, n} - v_{m, m, n} + v_{k, m+1, n+1}}{2\Delta y}$$

$$\frac{- v_{k, m, n+1}}{2\Delta y}$$

(6.54)

and using Equations (6.42), (6.43), (6.48) and (6.49) the following equation is obtained for the pressure:

$$\begin{aligned}
\frac{2}{\Delta t} w_{k1, m+1/2, n+1/2}^Q &= \left[(S - R\lambda_{KLM}) \frac{\partial P_s}{\partial x} \Big|_{m+1, n+1} \right. \\
&+ (S - R\lambda_{KLM}) \frac{\partial P_s}{\partial x} \Big|_{m, n+1} - (S - R\lambda_{KLM}) \frac{\partial P_s}{\partial x} \Big|_{m+1, n} \\
&- (S - R\lambda_{KLM}) \frac{\partial P_s}{\partial x} \Big|_{m, n} \left. \right] \frac{1}{\Delta x} + \left[(S - R\lambda_{KLM}) \frac{\partial P_s}{\partial y} \Big|_{m+1, n+1} \right. \\
&+ (S - R\lambda_{KLM}) \frac{\partial P_s}{\partial y} \Big|_{m+1, n} - (S - R\lambda_{KLM}) \frac{\partial P_s}{\partial y} \Big|_{m, n+1} \\
&- (S - R\lambda_{KLM}) \frac{\partial P_s}{\partial y} \Big|_{m, n} \left. \right] \frac{1}{\Delta y}. \tag{6.55}
\end{aligned}$$

In deriving (6.55) the corrective procedure of Hirt and Harlow (1967) has been used for the term $\frac{\partial}{\partial t} (w(z=0))$. According to this procedure this term is written as a simple backward time difference with the present time level set to zero. This is necessitated by the fact that some non zero value for the vertical velocity is computed at the surface. This contradicts the rigid lid assumption and has to be accounted for in order to prevent it from growing in time.

Equation (6.55) gives the pressure field in the interior. Near boundaries the appropriate $\partial P_s / \partial x$ or $\partial P_s / \partial y$ are replaced by the appropriate

summed equation for u^P or v^P . Therefore, the momentum equations are used to derive boundary conditions for the pressure equation. The summed equation for u^P is written as:

$$\begin{aligned}
 - (S - R \lambda_{KLM}) \frac{\partial P_s}{\partial x} &= \frac{1}{\Delta t} \sum_k \psi_k u_k^P = \frac{1}{\Delta t} \sum_k \psi_k u^{L+1} \\
 &\quad - \frac{1}{\Delta t} \sum_k \psi_k u^Q \quad (6.56)
 \end{aligned}$$

while the summed equation for v^P is written as:

$$\begin{aligned}
 - (S - R \lambda_{KLM}) \frac{\partial P_s}{\partial y} &= \frac{1}{\Delta t} \sum_k \psi_k v_k^P = \frac{1}{\Delta t} \sum_k \psi_k v^{L+1} \\
 &\quad - \frac{1}{\Delta t} \sum_k \psi_k v^Q \quad (6.57)
 \end{aligned}$$

Thus whenever near a wall, (6.56) or (6.57) evaluated along the wall is substituted in (6.55).

E. Computational Sequence

1. It is assumed that initial conditions are known.
2. Concentrations are computed by solving Equation (5.37) by implicit vertical diffusion scheme.
3. The convective and horizontal viscous terms are calculated.
4. The u_k^Q and v_k^Q velocities (Equations (6.44) and (6.46)) are calculated at each nodal point.

5. The pressure field is solved (Equation (6.55)).
6. The u_k^P and v_k^P velocities (Equations (6.45) and (6.47)) are computed and hence the horizontal velocities u_k^{L+1} and v_k^{L+1} (Equations (6.42) and (6.43)).
7. The vertical velocities are calculated by vertically integrating the continuity equation.
8. The present step is complete.

CHAPTER VII

MODEL IMPLEMENTATION

As mentioned in the introduction, existing lake transport models generally fail to predict the correct velocity field (Allender, 1976). The basic reason for this is that these models are structured poorly i.e., they employ poor averaging procedures and use poor eddy viscosity representations. In addition faulty verification procedures are used by attempting to predict point to point field data and neglecting the overall stochastic character of the turbulent flow field. In this report the main objective is to develop a mathematical model which, by using relatively coarse grids, is able to predict the correct energy cascade process on the turbulent flow field. In this way more confidence can be placed in the computed values of the averaged quantities. The equations for this model and their numerical representation have been presented in Chapters V and VI. In the remainder of this thesis the application of this model will be demonstrated and the suggested formulations justified.

There are basically six problems which were investigated. The effect on the cascade process of the following four processes was investigated: (a) basin size; (b) wind shear; (c) time step; and (d) non-filtration of the equations. The two additional problems are the effect of the proper turbulent

field on the transport of: a) a passive contaminant; and b) a biochemically active contaminant. To address these problems the following input parameters, as defined in Chapter V, Section F are required: horizontal reference length, b_0 ; vertical reference length, h_0 ; reference velocity, u_0 ; characteristic eddy viscosity, A_H ; and the reference concentration, c_M . Also the Reynolds number, Re ; the Froude number, Fr ; and the Prandtl number, Pr ; have to be calculated. After these parameters are defined the following quantities will have to be specified: grid sizes ($\Delta x, \Delta y, \Delta z$); filter lengths ($\Delta_1, \Delta_2, \Delta_3$); the value of the filter constant, γ ; the residual field coefficient, c ; the size of the time step, Δt ; and the surface wind shear.

In the remainder of this chapter four sections are presented which describe the model input and output procedures: (a) basin selection and input parameters; (b) surface wind shear specification; (c) the statistical preparation of the results; and (d) a summary of the computer runs.

A. Basin Selection and Input Parameters

Three basins are used to examine and verify the developed model, all are rectangular and without any sharp boundaries. The reason for the selection of these simple basins is that more research is required for the correct representation of irregular solid boundaries. Therefore for this stage simple basins were chosen. It is desired for the grid cells to be included in the inertial subrange so that the eddy viscosities can be computed as in Chapter V, Section D. As the field data show (Chapter III, Section A.7) scales of 100 m

were found in the inertial subrange. Therefore, it was decided to limit the horizontal grid size around 100 m. Table 7.1 shows the dimensions and the input parameters of the three basins.

Table 7.1 Basins and Input Parameters

| BASIN 1 |
|---|
| <p>Length = 1700 m, Width = 900 m, Depth = 16 m</p> <p>$b_0 = 1700 \text{ m}$, $h_0 = 16 \text{ m}$, $u_0 = 0.1 \text{ m/sec}$.</p> <p>$A_H = 0.1 \text{ m}^2/\text{sec}$, $Re = 1700$, $Fr = 799 \cdot 10^{-5}$</p> <p>$Dx = 100 \text{ m}$, $Dy = 100 \text{ m}$, $Dz = 2 \text{ m}$</p> |
| BASIN 2 |
| <p>Length = 1360 m, Width = 900 m, Depth = 16 m</p> <p>$b_0 = 1360 \text{ m}$, $h_0 = 16 \text{ m}$, $u_0 = 0.1 \text{ m/sec}$</p> <p>$A_H = 0.1 \text{ m}^2/\text{sec}$, $Re = 1700$, $Fr = 799 \cdot 10^{-5}$</p> <p>$Dx = 80 \text{ m}$, $Dy = 80 \text{ m}$, $Dz = 2 \text{ m}$</p> |
| BASIN 3 |
| <p>Length = 2040 m, Width = 1080, Depth = 16 m</p> <p>$b_0 = 2040 \text{ m}$, $h_0 = 16 \text{ m}$, $u_0 = 0.1 \text{ m/sec}$</p> <p>$A_H = 0.1 \text{ m}^2/\text{sec}$, $Re = 2040$, $Fr = 799 \cdot 10^{-5}$</p> <p>$Dx = 120 \text{ m}$, $Dy = 120 \text{ m}$, $Dz = 2 \text{ m}$</p> |

The transport equation was solved by assuming uniform initial conditions of the contaminants throughout the basin. The quantity C_M in this equation takes the following values depending on the species it represents (phytoplankton, zooplankton, oxygen and nutrients) (Smarek, 1978).

Phytoplankton: $C_M = 1 \text{ gr/m}^3$

Zooplankton: $C_M = 0.4 \text{ gr/m}^3$

Oxygen: $C_M = 13.1 \text{ gr/m}^3$

Nutrients: $C_M = 0.013 \text{ gr/m}^3$

The values of the filter lengths, $\Delta_1, \Delta_2, \Delta_3$, are specified in Chapter IV, Section D as:

$$\Delta_1 = 2\Delta x \quad , \quad \Delta_2 = 2\Delta y \quad , \quad \Delta_3 = 2\Delta z.$$

The value of the coefficient, γ , is specified by Kwak, et al., (1975) as $\gamma = 6$

It was found that a time step greater than 2 minutes causes a numerical instability in the model predictions, therefore $DT = 2$ minutes was chosen for most of the runs (Table 7.2).

B. Surface Wind Shear Specification

To check the ability of the mathematical model to predict the correct energy cascade process, turbulence has to be generated in the flow field. Kwak, et al. (1975), Shaanan, et al. (1975), Mansour, et al. (1977) and Ferziger, et al. (1977) mathematically created a spectrally correct initial field and studied how the mathematical model predicted its decay in time. In this report it is desired to check if the model is able not only to maintain but

to predict the correct cascade process. Therefore, the initial field is set to zero and the turbulence is transferred through the surface boundary by a wind shear. It is recognised that solid boundaries are of equal importance in introducing turbulence into the flow field. However, the correct treatment of rough boundaries is out of the scope of this thesis. It was assumed that the wind field over the lake has a fully developed three-dimensional character. Therefore, according to Kolmogorov's theory its power spectrum should have a slope of $-5/3$. It was also assumed that the power spectrum of the wind shear will present the same $-5/3$ slope as the wind spectrum. This generated the need of creating a wind shear field whose power spectrum would decay as $-5/3$. It was found that under certain conditions a 1-Lag Markov model can be formulated which satisfies the $-5/3$ slope. Therefore, the wind shear is assumed to have the following form:

$$\tau_i = \bar{\tau} + \tau'_i$$

where

$$\tau'_i = \rho_1 \tau'_{i-1} + t_i \sigma \sqrt{1-\rho_1^2} \quad \text{and} \quad (7.1)$$

τ_i = wind shear at time level i ;

$\bar{\tau}$ = mean wind shear;

ρ_1 = 1 - lag correlation coefficient;

σ^2 = variance of τ' ; and

t_i is a random variable given by:

$$t_i = \sqrt{R_3} \cos(2\pi R_2) \quad (7.2)$$

In Equation (7.2)

$$R_3 = -2 \log(R_1) \quad (7.3)$$

and R_1 , R_2 are random numbers. Experimentation showed that when $\theta_1 = 0.5$ and $\sigma^2 = 1$ the power spectrum of τ_i' would have a $-5/3$ slope. This is shown in Figure 7.1 where 140 values were generated using a time step of 2 minutes. The power spectral density is computed as described in the next section using 70 lags.

It was decided to avoid highly complicated nonhomogeneous turbulence, therefore Equation 7.1 was applied at all surface nodal points independently at each direction. In this way a homogeneous field was generated at the surface. Additionally, it is understood that it is not possible for homogeneous conditions to exist in a closed basin, especially near the boundaries. This was resolved as it is in the field by selecting the sites for data acquisition at the center of the basin and assuming local isotropy. However, it should be mentioned that even at the center of the basin homogeneity is a rather big assumption. It is used only because of its relative simplicity, and its analogous use in the acquisition of data to be used for comparison purposes.

C. Statistical Preparation of the Results

The model was run for about 120 to 140 time steps (Table 7.2) after the value of the mean velocity reached a more or less steady state. Time traces of the velocities and concentrations at the center of the basin and at several

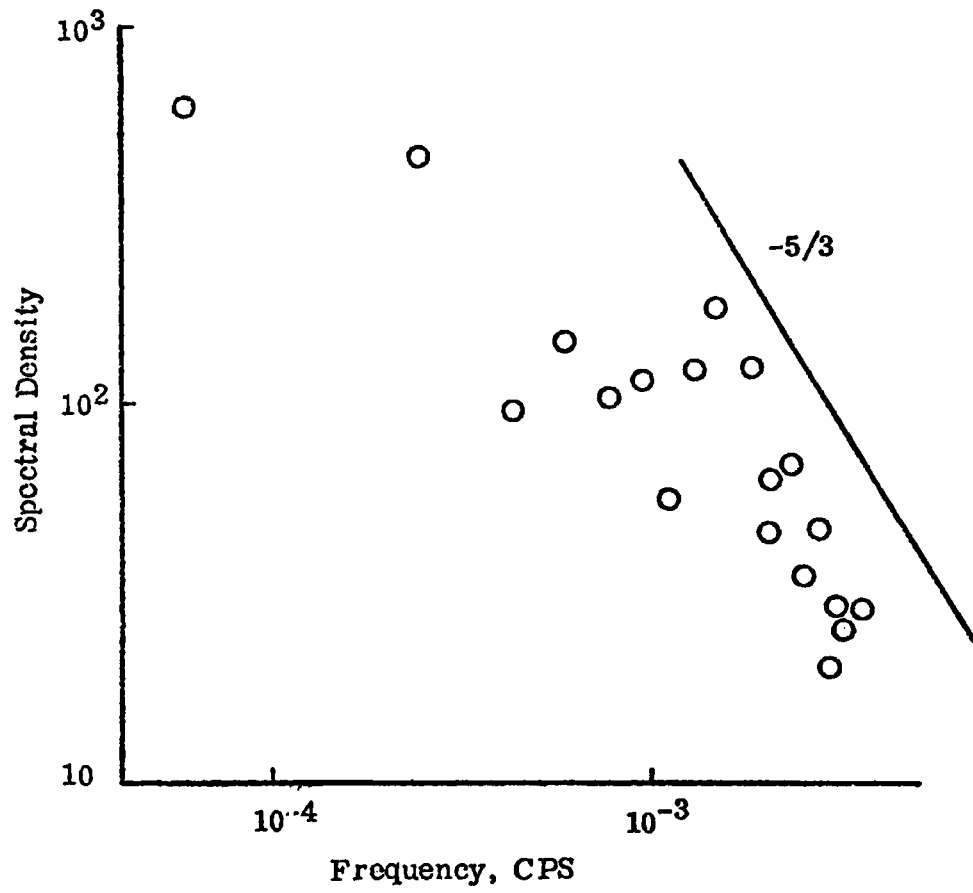


Figure 7 1 1-Lag Markov Model

different depth levels were stored. These traces were detrended and the power spectral density was computed by using the subroutine BMD02T of the BMD computed package (Dixon, 1974). This subroutine was modified to compute the Fourier transform of the autocorrelation instead of the Fourier transform of the autocovariance as it was originally written. The number of lags used for the computation of the autocorrelation coefficient was one half or smaller of the number of points in each trace. (Table 7.2). It was considered that this would give a correct value of the autocorrelation coefficient even for large lag times. The computed time spectra were converted to wave number spectra by using Taylor's frozen turbulence hypothesis which is permitted since $u'_i/u_i \ll 1$. Using this technique three one-dimensional wave number spectra were computed at each of the observed nodal points. The three-dimensional wave number spectra were computed as in Tennekes and Lumley (1972, p.250) by adding the three one-dimensional energy spectra. In order to smooth the spectrum the power spectral density at wave number, k , was integrated over the points between the cells of radius $(k + 2 k_1)$ and $(k - 2 k_1)$, where k_1 is the wave number in x-direction. The concentration spectra were similarly computed.

D. Summary of Runs

All the computer runs made are summarized in Table 7.2 where the following information is included:

- Column 1. Number of computer run
- Column 2, Column 3. Indicate if filtered or unfiltered model is used.
- Column 4, Column 5. Indicates if this run is a circulation or transport run.
- Column 6. Number of Basin as in Table 7.1
- Column 7. Size of time step
- Column 8, Column 9, Column 10. Indicate the mean shear stress applied in x and y direction and the corresponding wind speed.
- Column 11, Column 12, Column 13. Indicate if the transport run is for a passive contaminant or for the complete biological model and the Prandtl number (Pr) used.
- Column 14. Indicates how many steps were used for the computation of the spectra.
- Column 15. Indicates the number of the lags used for the computation of the spectra.

It must be also noted that in Run 7 the wind field was set to zero after the 25 time step. Before this step the wind field of Run 1 was used. Also in Run 12 the deterministic part in Equation (7.1) was set to zero.

Table 7.2 Summary of Computer Runa

| Run # | Filtered | Unfiltered | Circulation | Transport | Basin # | Time Step (sec) | τ_x (dimensionless) | τ_y (dimensionless) | Wind (mph) | Passive Contamin. | Active Contamin. | Pr | Spectra | Lags |
|-------|----------|------------|-------------|-----------|---------|-----------------|--------------------------|--------------------------|------------|-------------------|------------------|-----|---------|------|
| 1 | X | | X | | 1 | 120 | 4 | 4 | 6.1 | | | | 120 | 50 |
| 2 | X | | X | | 2 | 45 | 4 | 4 | 6.1 | | | | 120 | 60 |
| 3 | X | | X | | 3 | 120 | 4 | 4 | 6.1 | | | | 140 | 60 |
| 4 | | X | | | 1 | 120 | 4 | 4 | 6.1 | | | | 120 | 50 |
| 5 | X | | X | | 1 | 90 | 11 | 11 | 10.1 | | | | 150 | 75 |
| 6 | X | | X | | 1 | 30 | 4 | 4 | 6.1 | | | | 480 | 190 |
| 7 | X | | X | | 1 | 120 | 0 | 0 | 0 | | | | 40 | 25 |
| 8 | X | | | X | 1 | 120 | 4 | 4 | 6.1 | X | | 1.0 | 120 | 50 |
| 9 | X | | | X | 1 | 120 | 4 | 4 | 6.1 | X | | 1.5 | 120 | 50 |
| 10 | X | | | X | 1 | 120 | 4 | 4 | 6.1 | X | | 2.0 | 120 | 50 |
| 11 | X | | | X | 1 | 120 | 4 | 4 | 6.1 | | X | 1.0 | 120 | 50 |
| 12 | X | | X | | 1 | 90 | 4 | 4 | 6.1 | | | | 140 | 70 |

CHAPTER VIII

RESULTS

In the previous chapter the basins, the input information, and the method of spectra computation were presented. In this chapter the results obtained will be shown. The chapter is divided into 5 parts. First, the optimization of the residual field coefficient c is presented. Second, computational performance details of the model are presented. The third and fourth parts display results for the averaged quantities and also the computed velocity and concentration spectra. Finally preliminary observations of the results are presented.

A. Optimization of the Residual Field Coefficient, c

The residual field model (5.26) requires that the coefficient, c , be determined. This coefficient controls the size of the eddy viscosity, K and through that the size of the residual stresses. As mentioned in Chapter V, Section C, the residual stresses in addition to the Leonard Stresses control the energy cascade process. Even though the residual stresses play a secondary role in this process their size (through the coefficient, c) has to be determined carefully. Large values for the coefficient, c , will overestimate

the role of the residual stresses while small values will underestimate them. In either case the subgrid scale continuous cascade features are destroyed.

One method of determining the value of the coefficient, c , is that followed by Kwak, et al., (1975). According to this method the value of c is decided by the slope of the energy decay curve. However, the slope of this curve is the primary way of deciding on the worth of our circulation model. Therefore, it was decided to compute the size of the coefficient, c , independently of the slope of the cascade process.

The method of Spraggs and Street (1975) was used for the determination of c . According to this method the coefficient is determined once and this value is used in all subsequent computer runs without any new adjustment. Accordingly the circulation model was run in Basin 1 for a sufficient number of time steps and the maximum eddy viscosity was plotted as a function of time step. The results are shown in Figure 8.1. It was found that the value $c=0.001$ was very small. The maximum eddy viscosity kept increasing until the 49th time step when the solution turned unstable and the program was interrupted. On the other hand the value of $c=0.05$ was very large because the solution turns unstable at the 5th time step. The results for $c=0.01$, $c=0.008$ and $c=0.005$ are shown in Figure 8.1. The values of $c=0.01$ and $c=0.008$ were considered large because of the erratic initial behavior of the corresponding curves. The value of $c=0.005$ was chosen because of the smooth transition of the maximum eddy viscosity coefficient to a relatively stable value. This value was used in all the computer runs made. The obtained results follow.

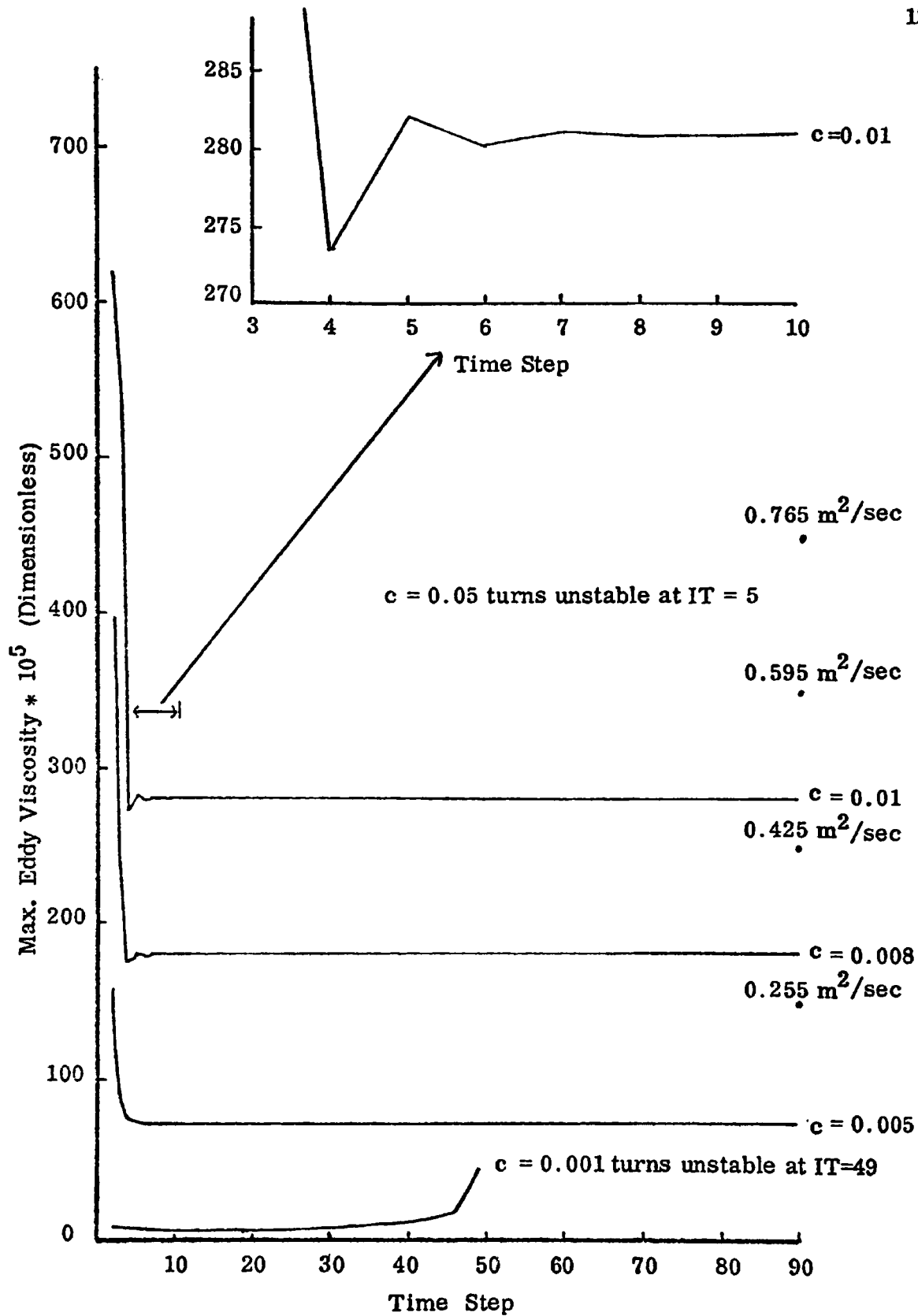


Figure 8.1 Optimization of Subgrid Coefficient "c"

B. Program Performance Results

All the computer runs were made on the IBM 360/178 computer of The Ohio State University. It must be noted that in this computer the specified storage does not affect the cost of the program. The cost depends directly on the execution time which is a function of the number of computations. Therefore, not too much care was taken to reduce the storage of the programs. The computational details are summarized below for a 9x10x18 grid.

Storage

Circulation Program: 760 K

Transport Program: 720 K

CPU Time Per Computational Step (approximately)

Circulation: 1.7 sec.

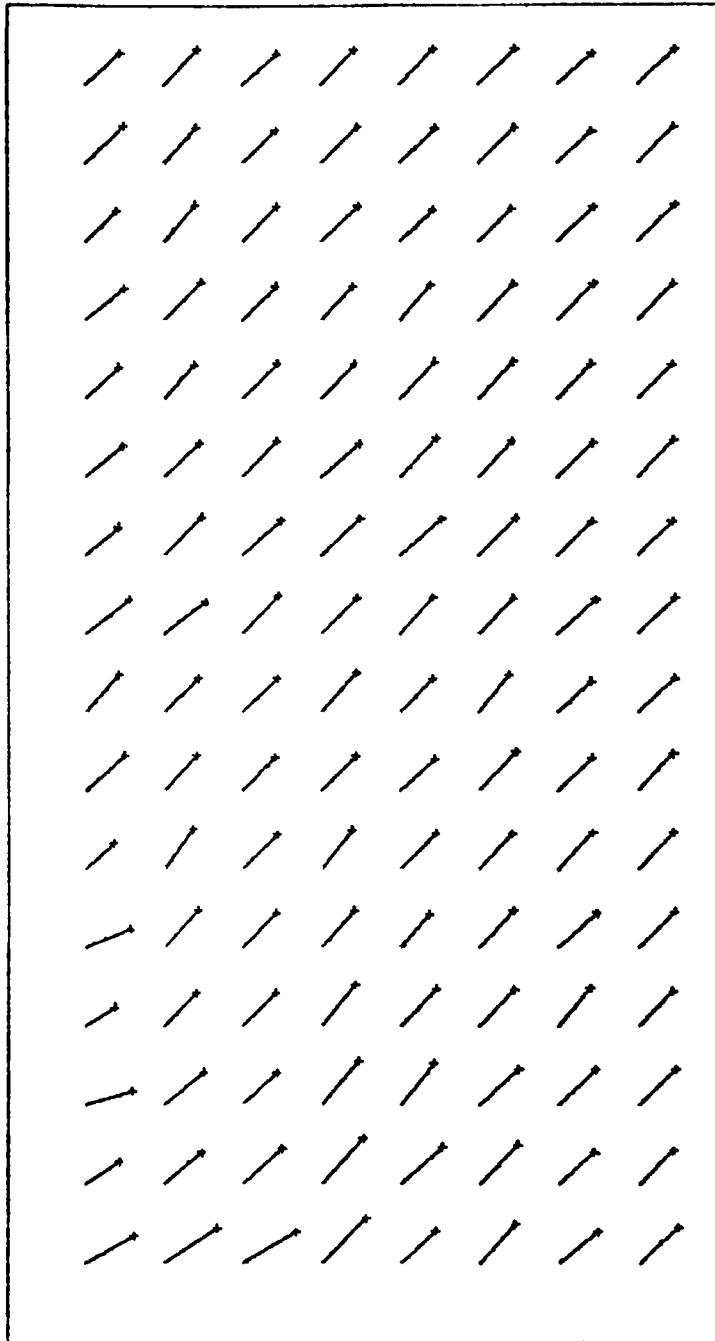
Transport (passive contaminant, one equation): 1.5 sec.

Transport (complete biological model, four equations): 5.4 sec.

The total real time of calculations varied from approximately 2 to 5 hours.

C. Predicted Results-Averaged Quantities

In this section typical results for the averaged quantities are presented. They consist of the output of Run 1 (Table 7. 2). Figures 8.2, 8.3, 8.4, 8.5 and 8.6 show typical velocity fields for five different layers at the 80th time step. U and V vertical profiles are shown in Figures 8.7 and 8.8. Also the vertical velocities at an zy plane at the center of Basin 1 are presented in Figure 8.9. All these results are indicative of the circulation pattern in the lake as depicted by Liggett (1970) and Lick (1976).



VELOCITY FIELD AT DEPTH=0.000
FILTERED, TIME STEP=80


WIND

SCALE:



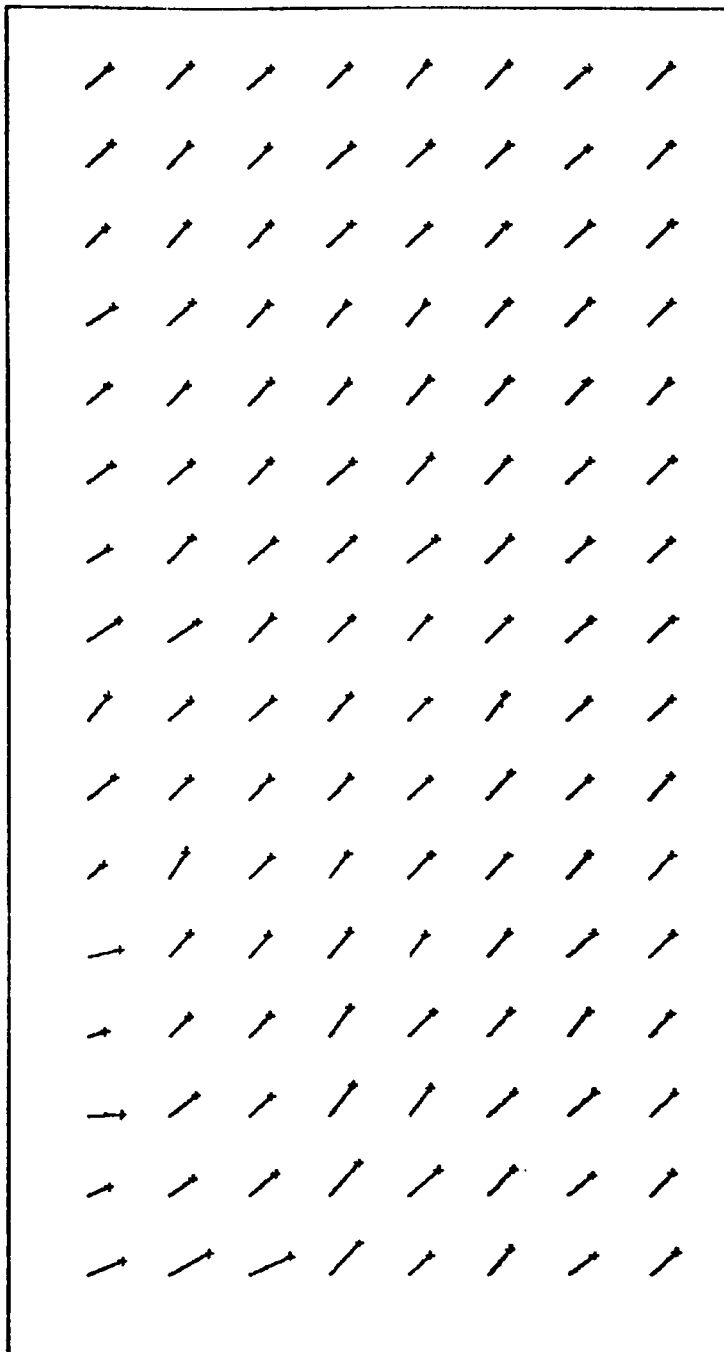


 100 M  30 CM/SEC

Figure 8.2



VELOCITY FIELD AT DEPTH=0.125
 FILTERED, TIME STEP=80


 WIND
 SCALE:


 100 M


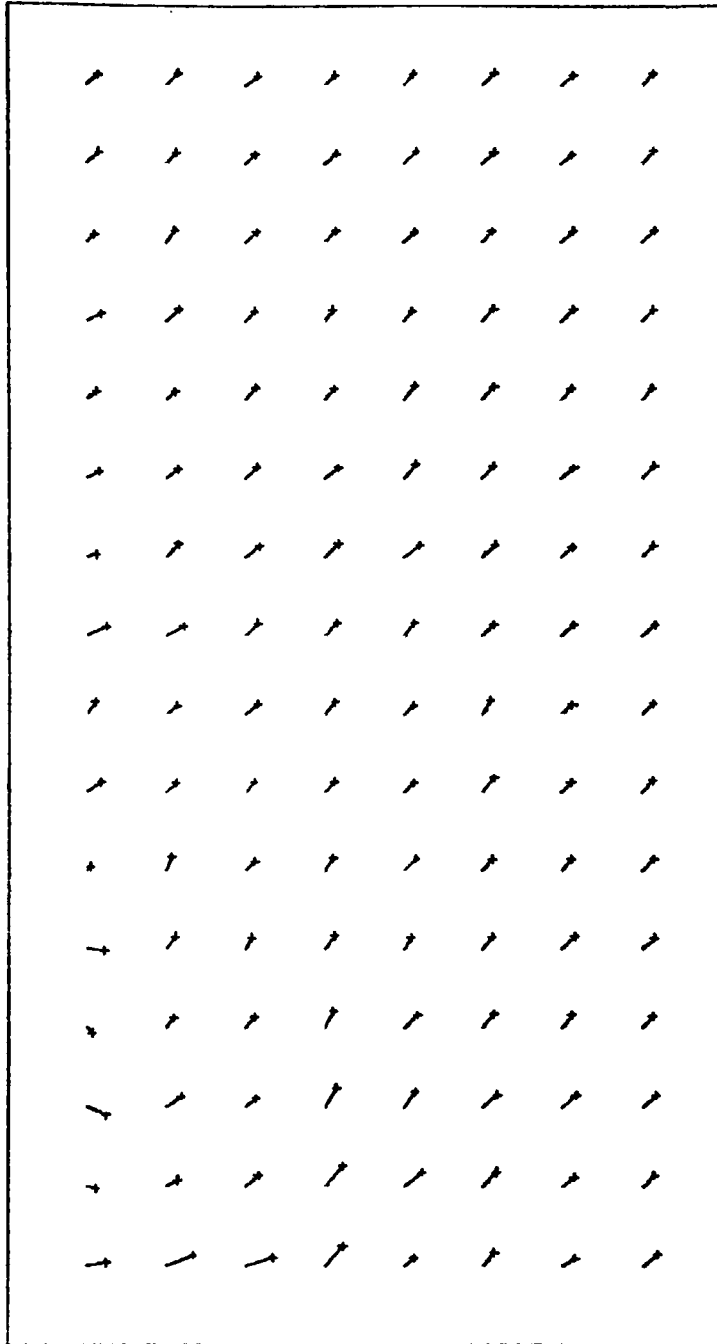

 30 CM/SEC

Figure 8.3



VELOCITY FIELD AT DEPTH=0.250
 FILTERED, TIME STEP=80


 WIND

SCALE:



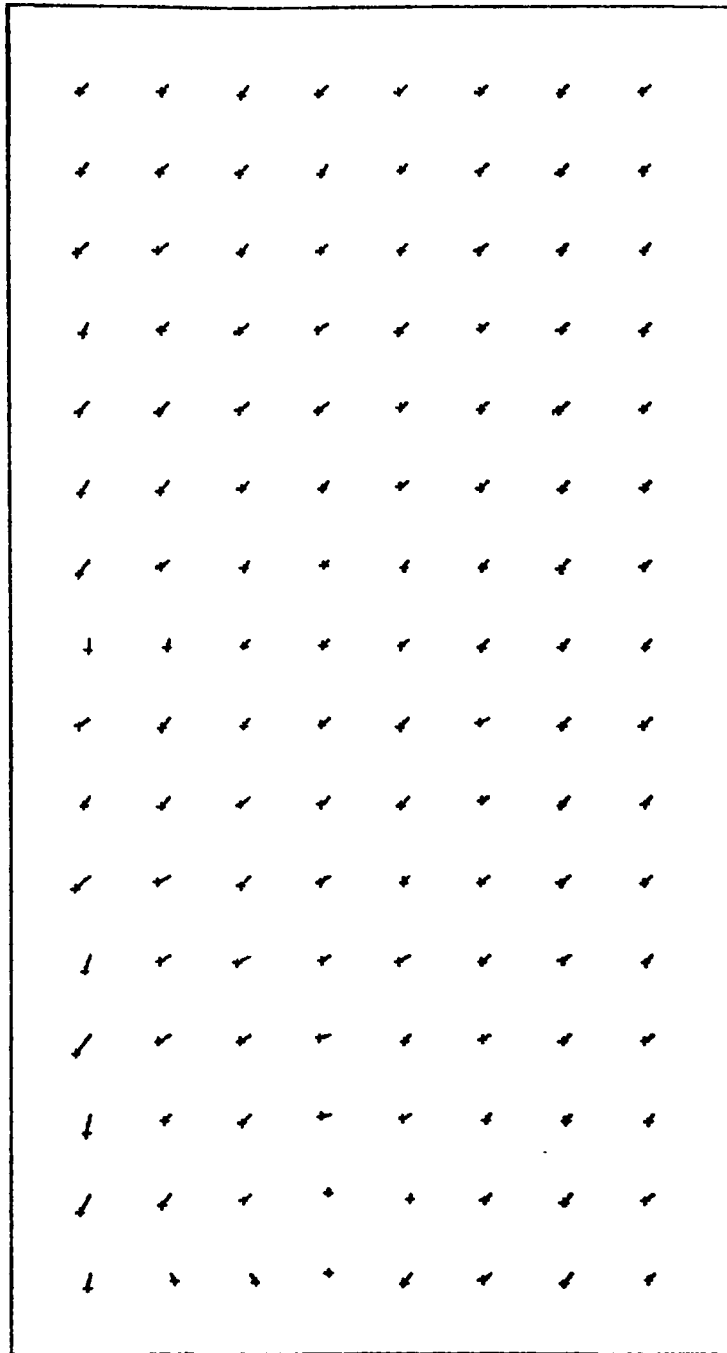


 100 M 30 CM/SEC

Figure 8.4



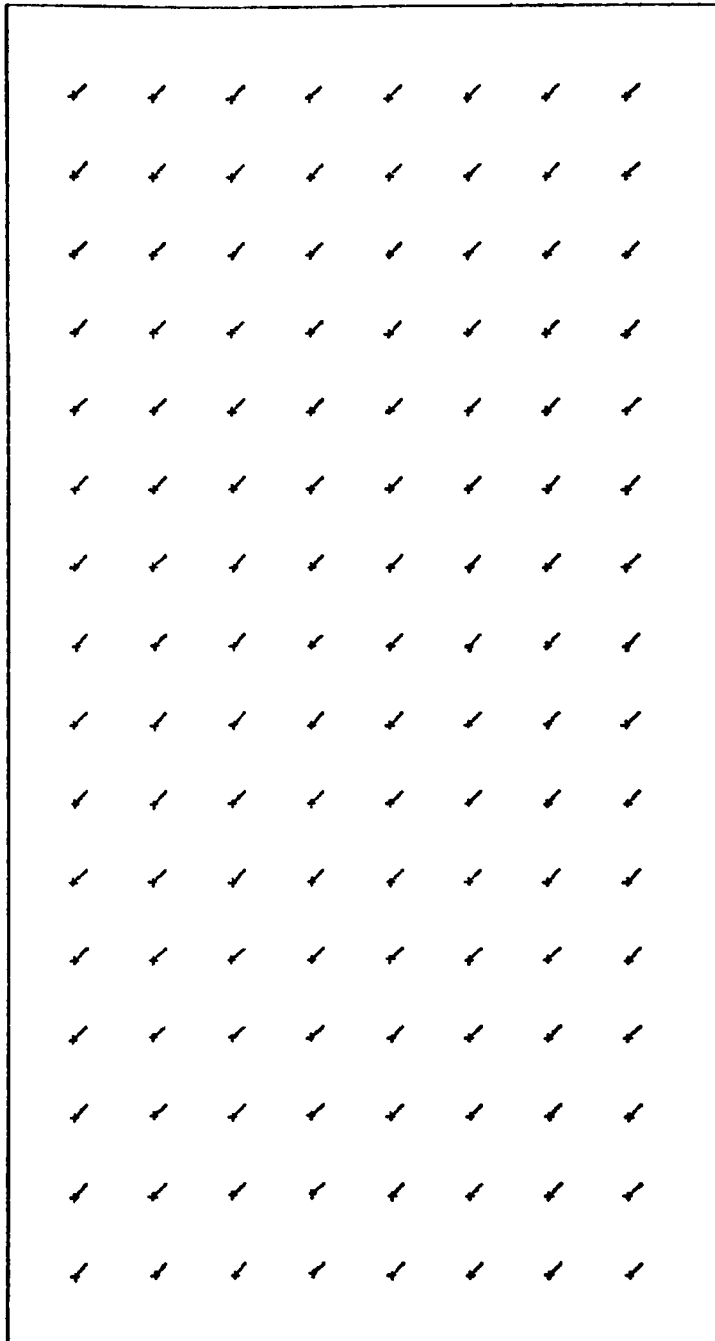
VELOCITY FIELD AT DEPTH=0.500
 FILTERED, TIME STEP=80


 WIND

SCALE:

 100 M
  30 CM/SEC

Figure 8.5



VELOCITY FIELD AT DEPTH=0.875
 FILTERED, TIME STEP=80


 WIND



SCALE:
 100 M  30 CM/SEC

Figure 8.6

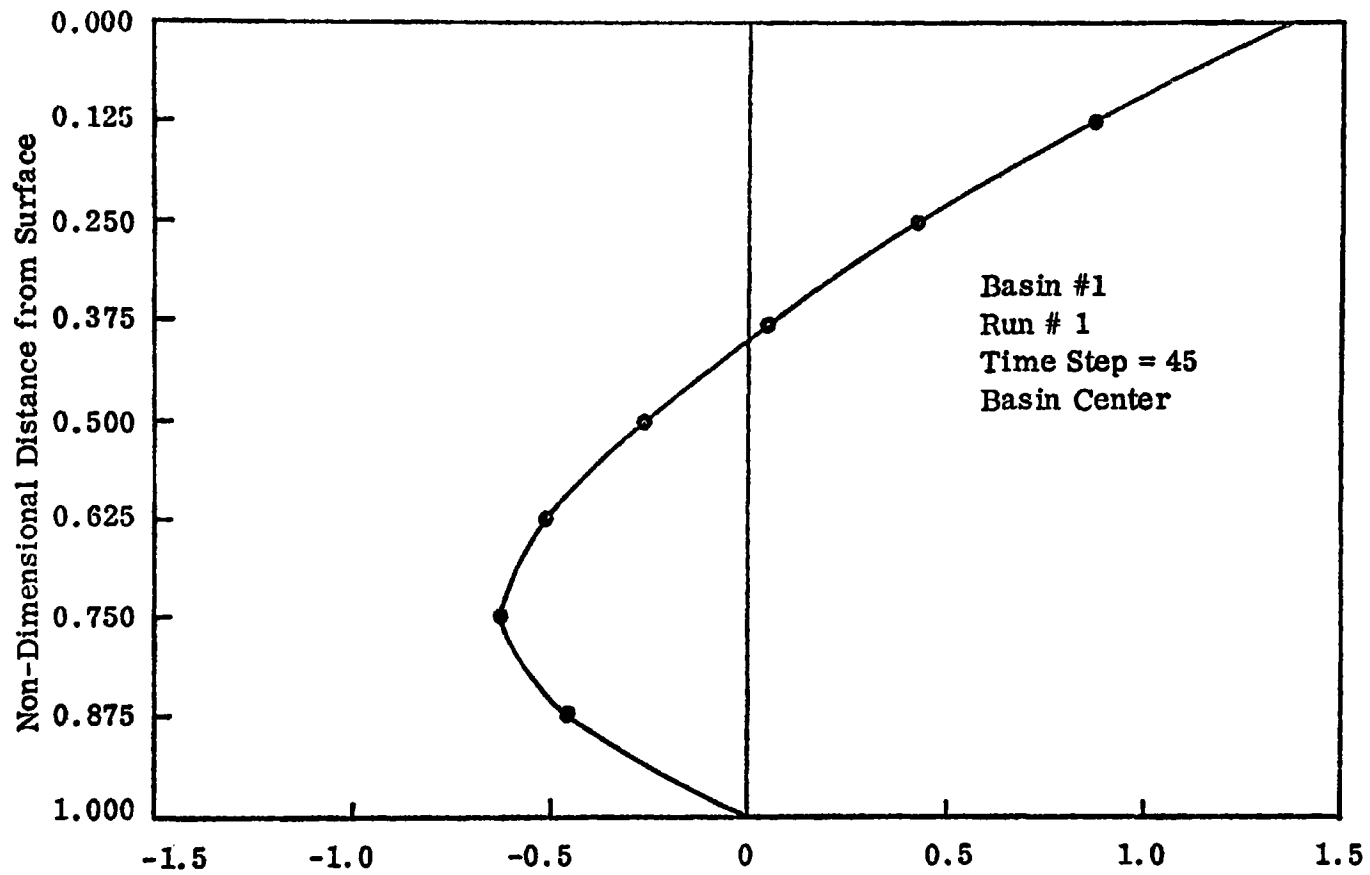


Figure 8.7 Non-Dimensional U-Velocity Profile

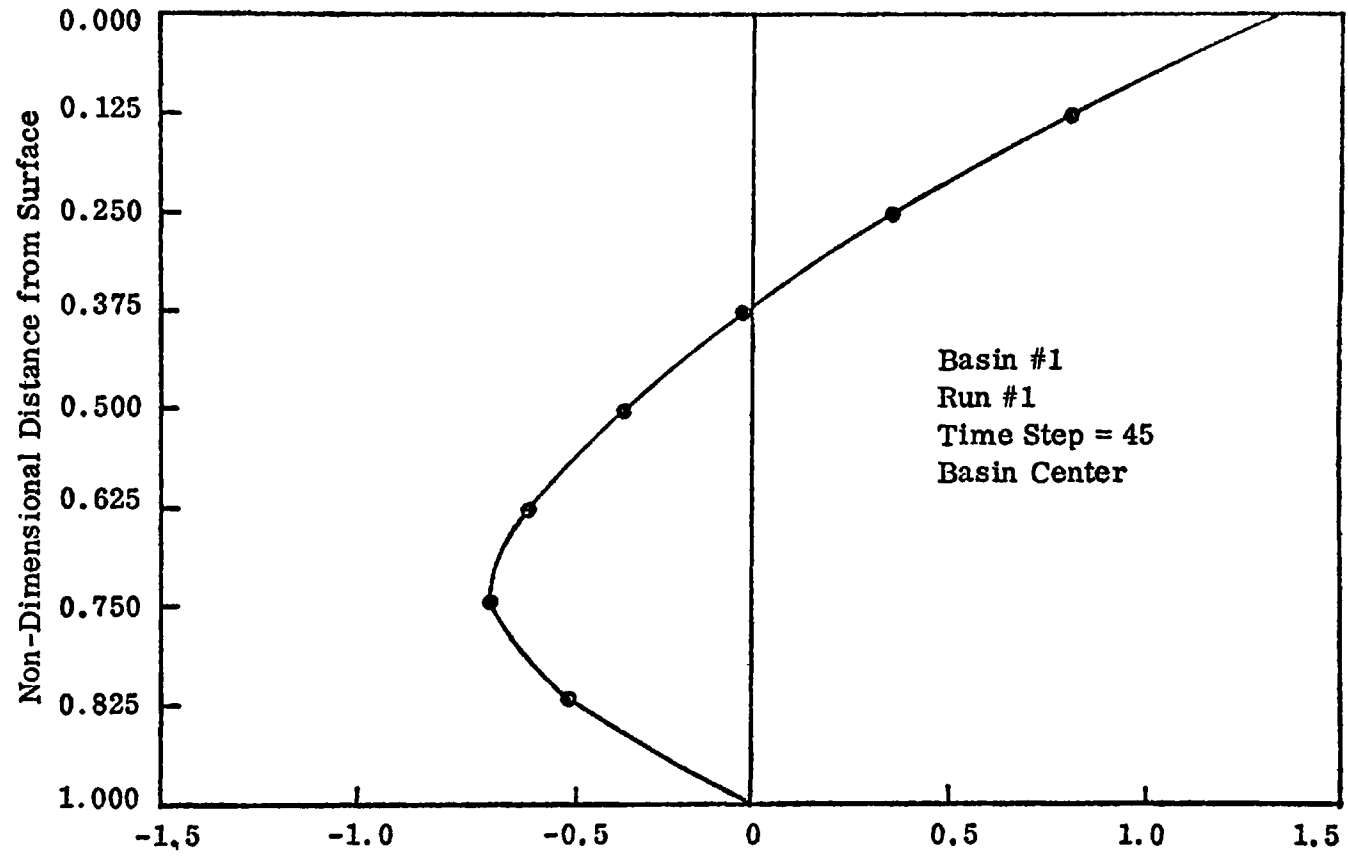


Figure 8.8 Non-Dimensional V-Velocity Profile

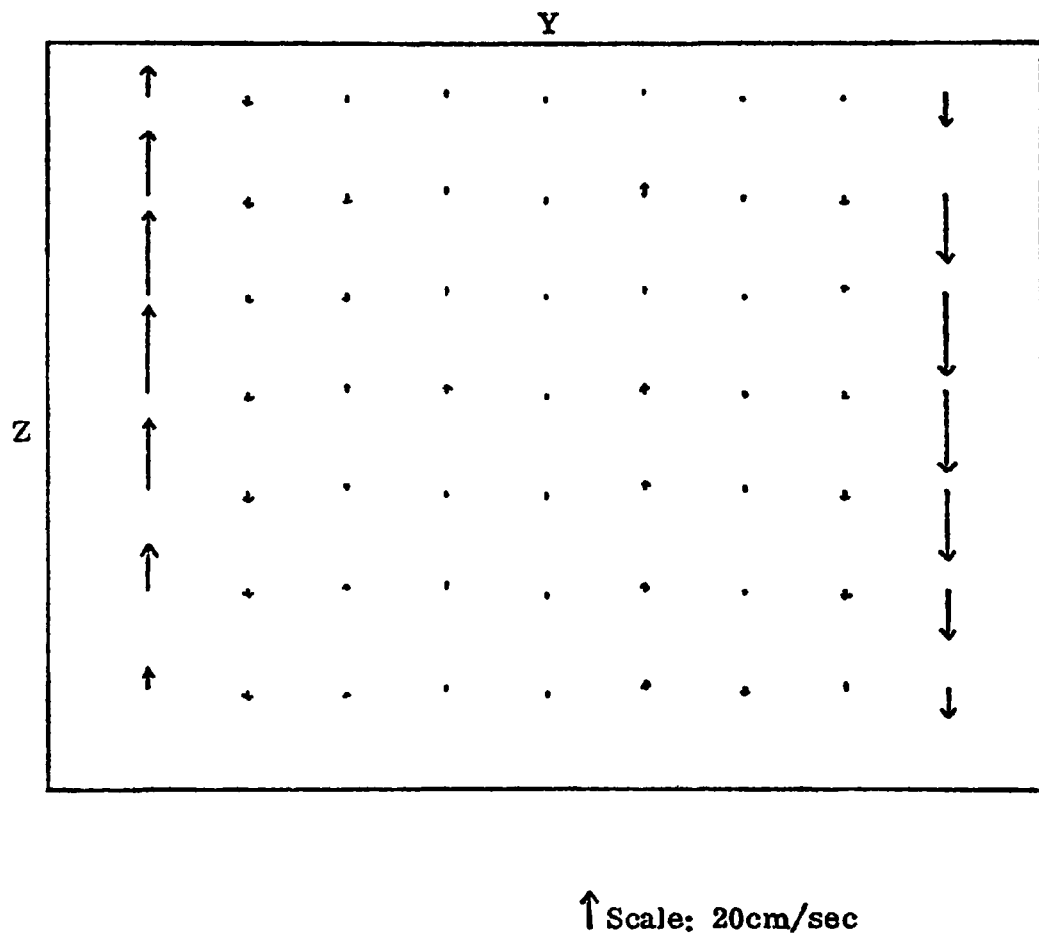


Figure 8.9 Vertical Velocities at Basin Center for Basin 1, Run 1 and Time Step=45

D. Predicted Results - Turbulence Spectra

In this section the velocity spectra, the passive contaminant spectra, and the biochemically active contaminant spectra are presented. In the next section preliminary interpretation of the results will be made. The discussion of the results will follow this chapter.

1) Velocity Spectra

a) Spectra at Different Depths

Here the spectra obtained from Run 1 are presented. The objective of this run is to examine the energy spectra and its variation with depth. They are shown in Figures 8.10, 8.11 and 8.12.

b) Spectra with Different Basins

The results from Runs 2 and 3 are presented in Figures 8.13 through 8.18 and display the spectrum from basins of different size.

c) Spectra with Different Shears

Here the results of Runs 5 and 7 are presented. The objectives of these runs were: (1) to see how a high shear affects the velocity spectra, and (2) to examine how a die-away wind field affects the spectra. Figures 8.19 through 8.24 detail these results.

d) Spectra with Different Time Step

The spectra obtained from Run 6 are shown in Figures 8.25 through 8.27. The objective of this run was to determine the influence of time step size on the velocity spectra.

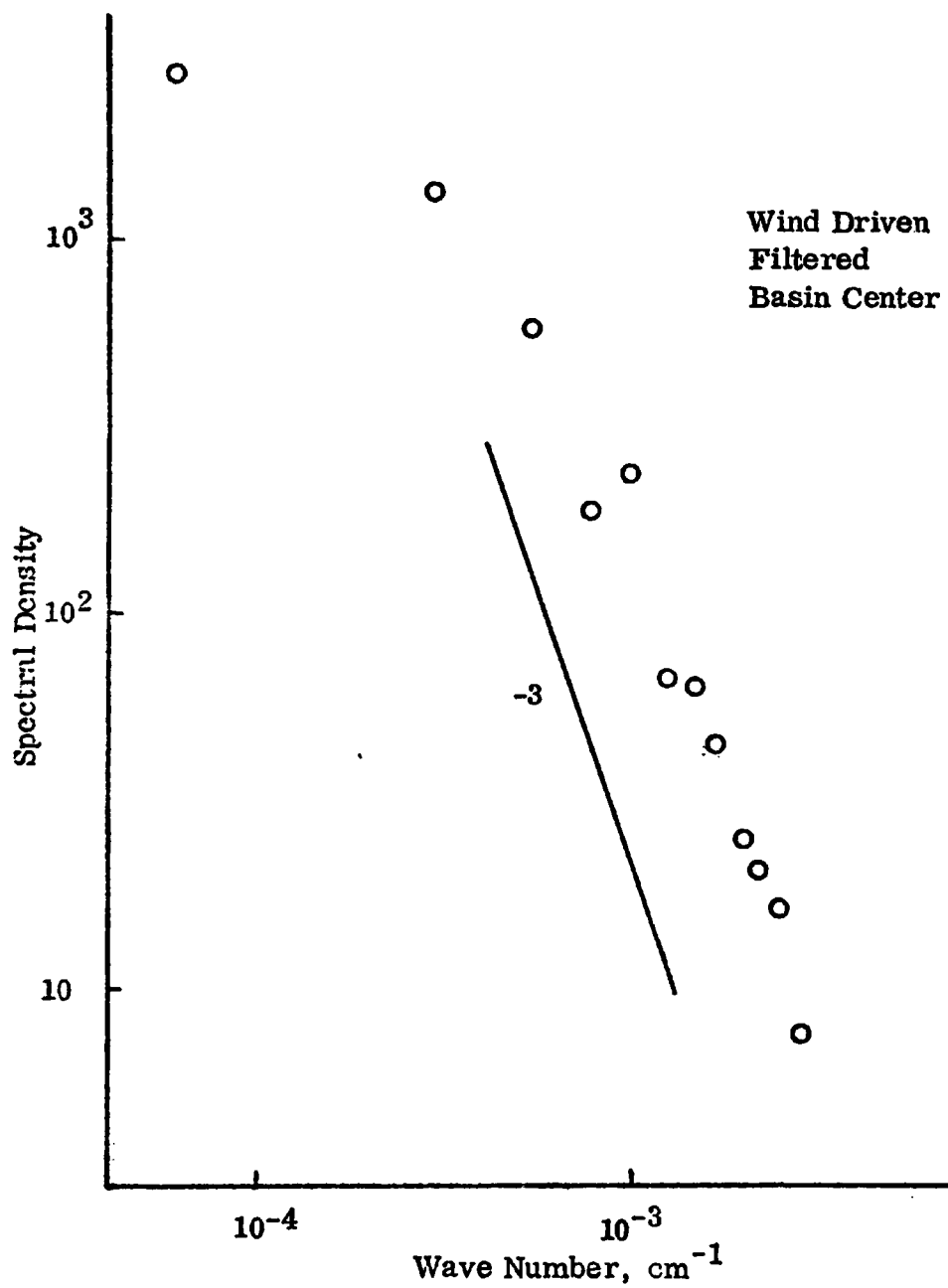


Figure 8.10 Energy Spectrum; Depth=0.125; Run 1

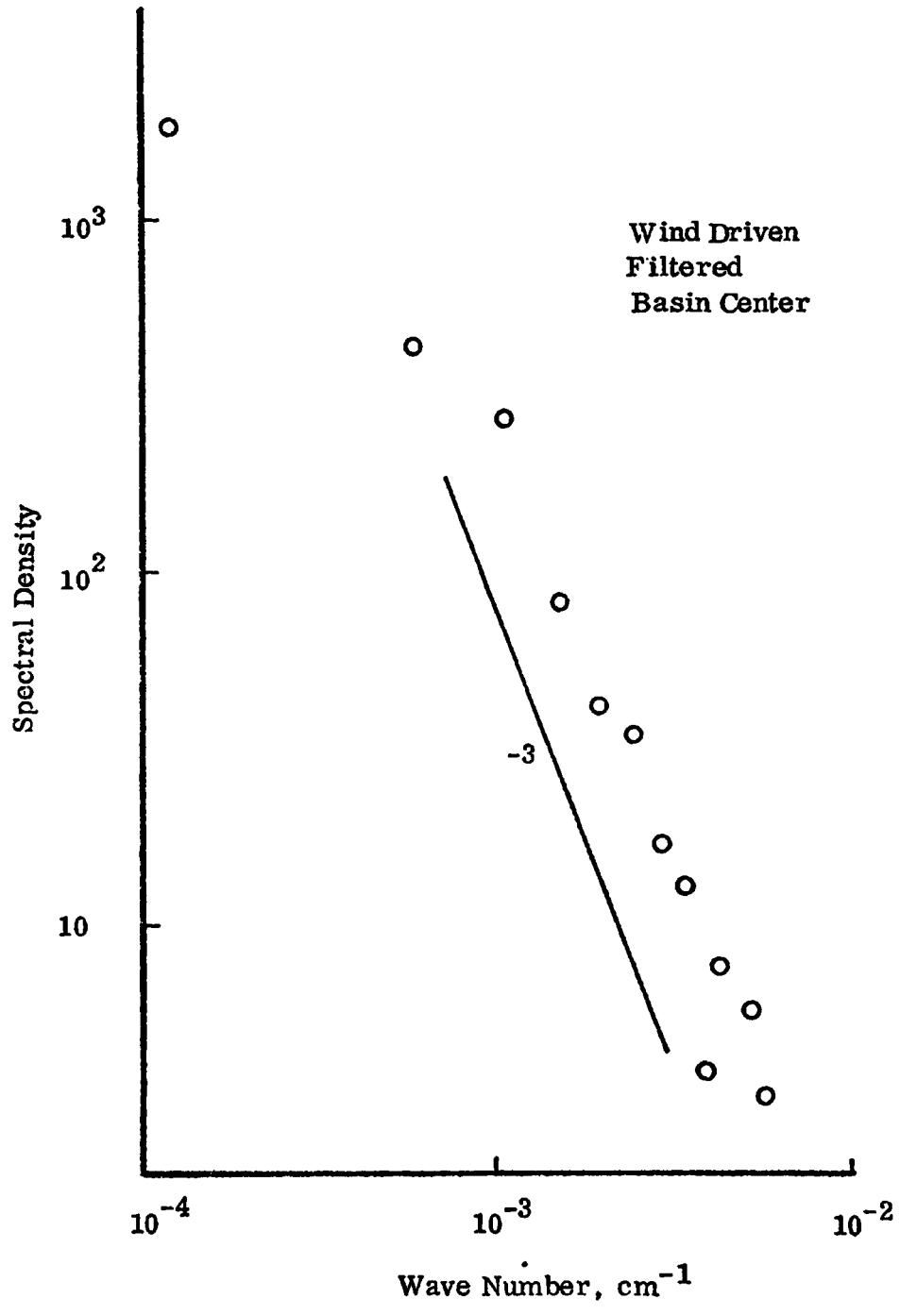


Figure 8.11 Energy Spectrum; Depth=0.25; Run 1

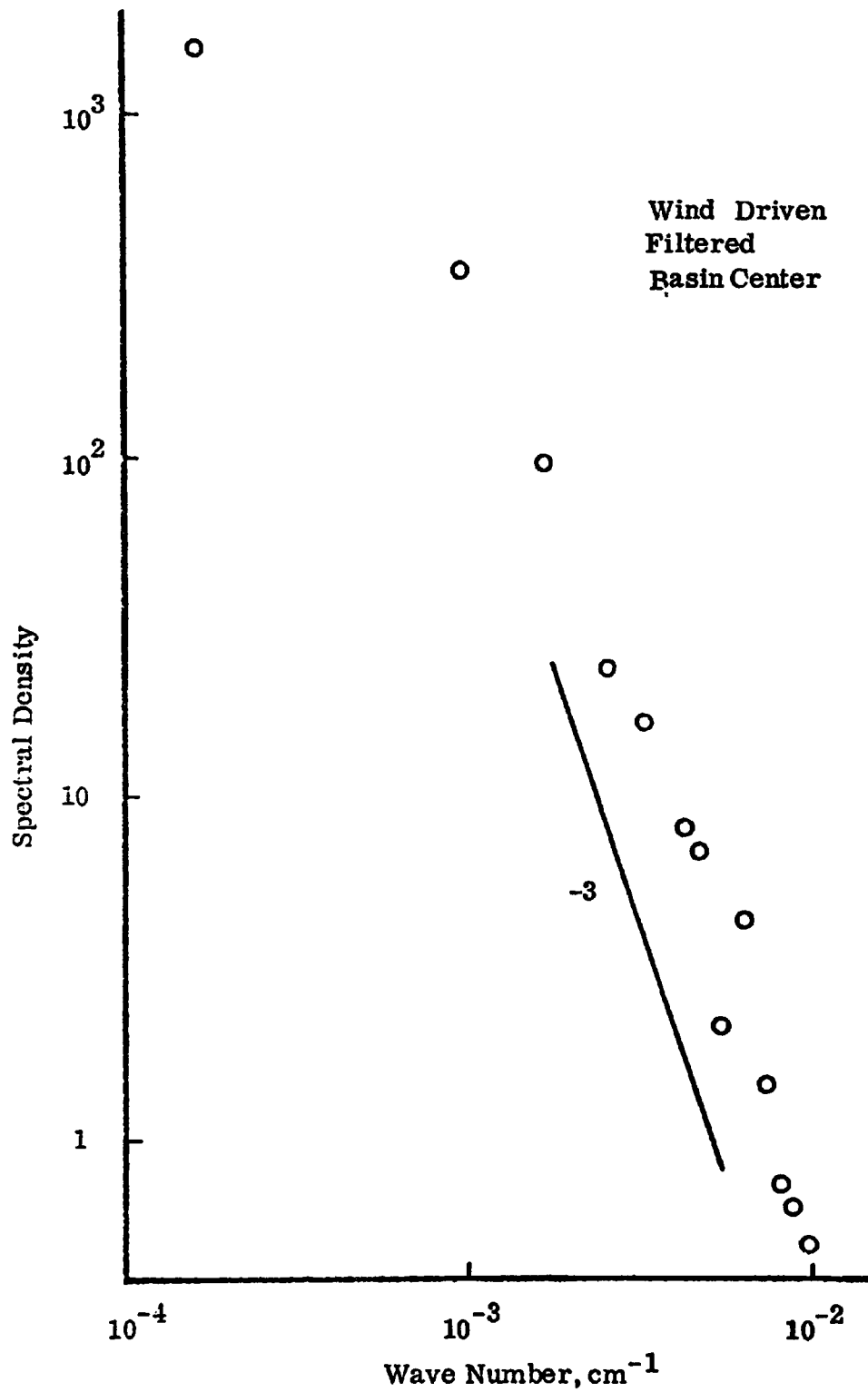


Figure 8.12 Energy Spectrum; Depth=0.5; Run 1

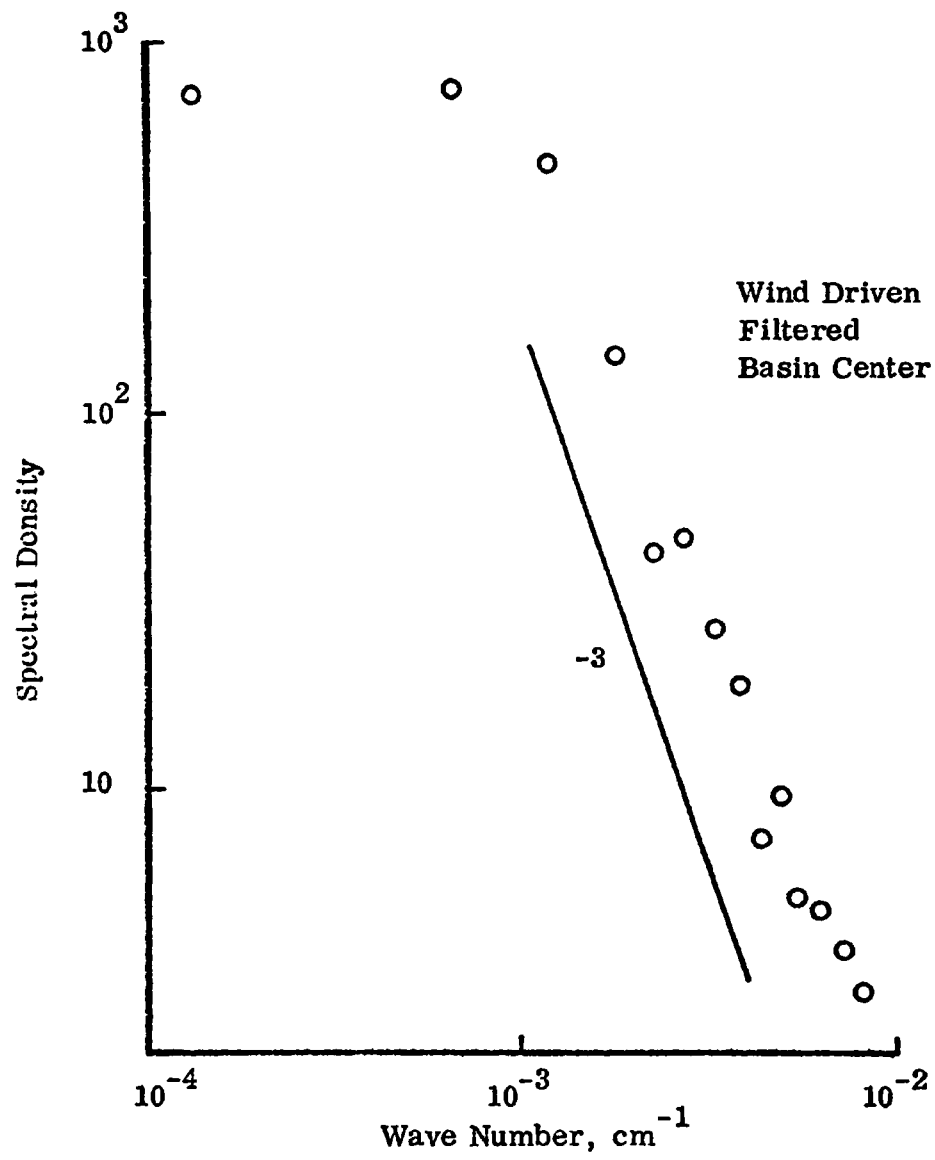


Figure 8.13 Energy Spectrum; Depth = 0.125; Run 2

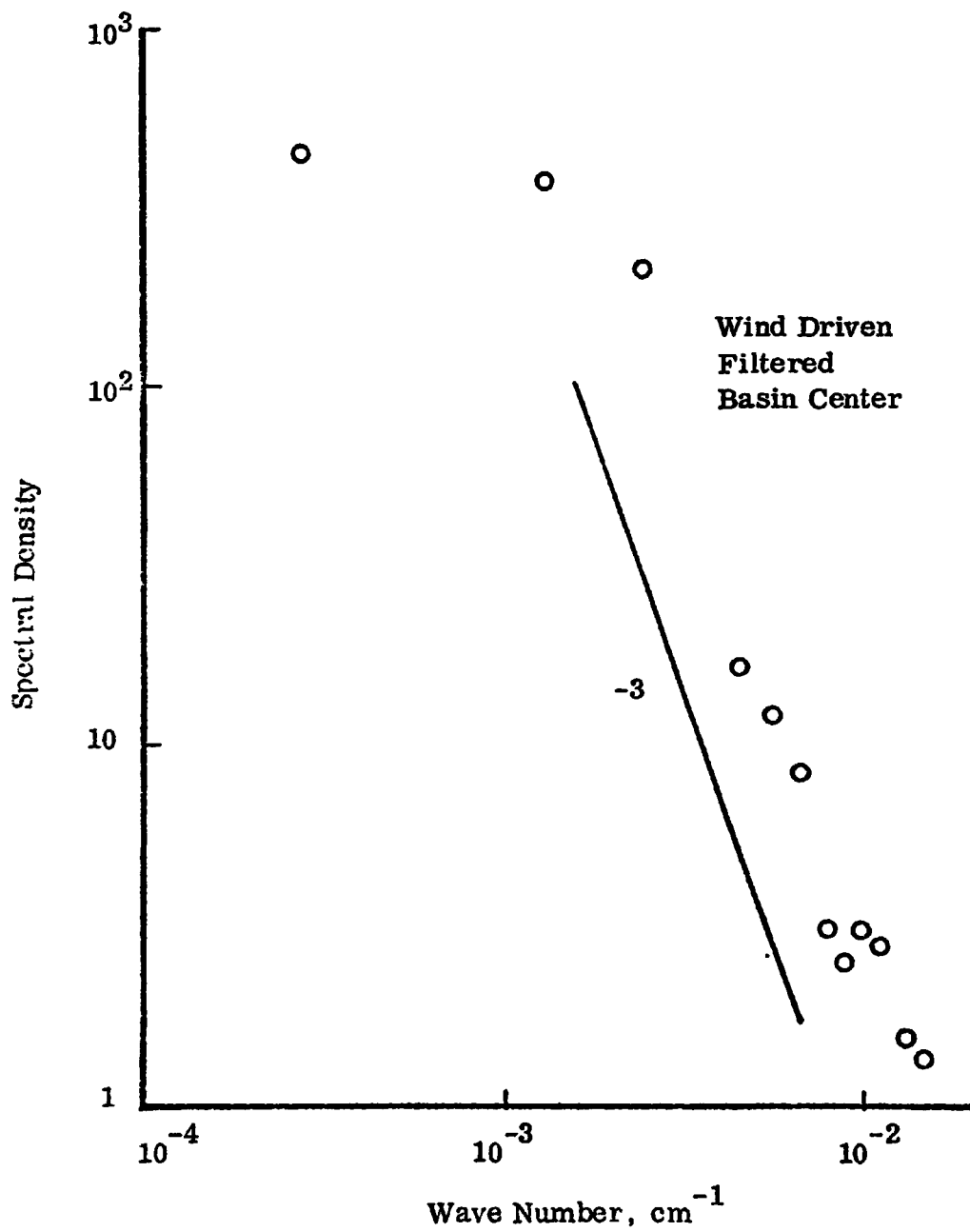


Figure 8.14 Energy Spectrum; Depth = 0.250; Run 2

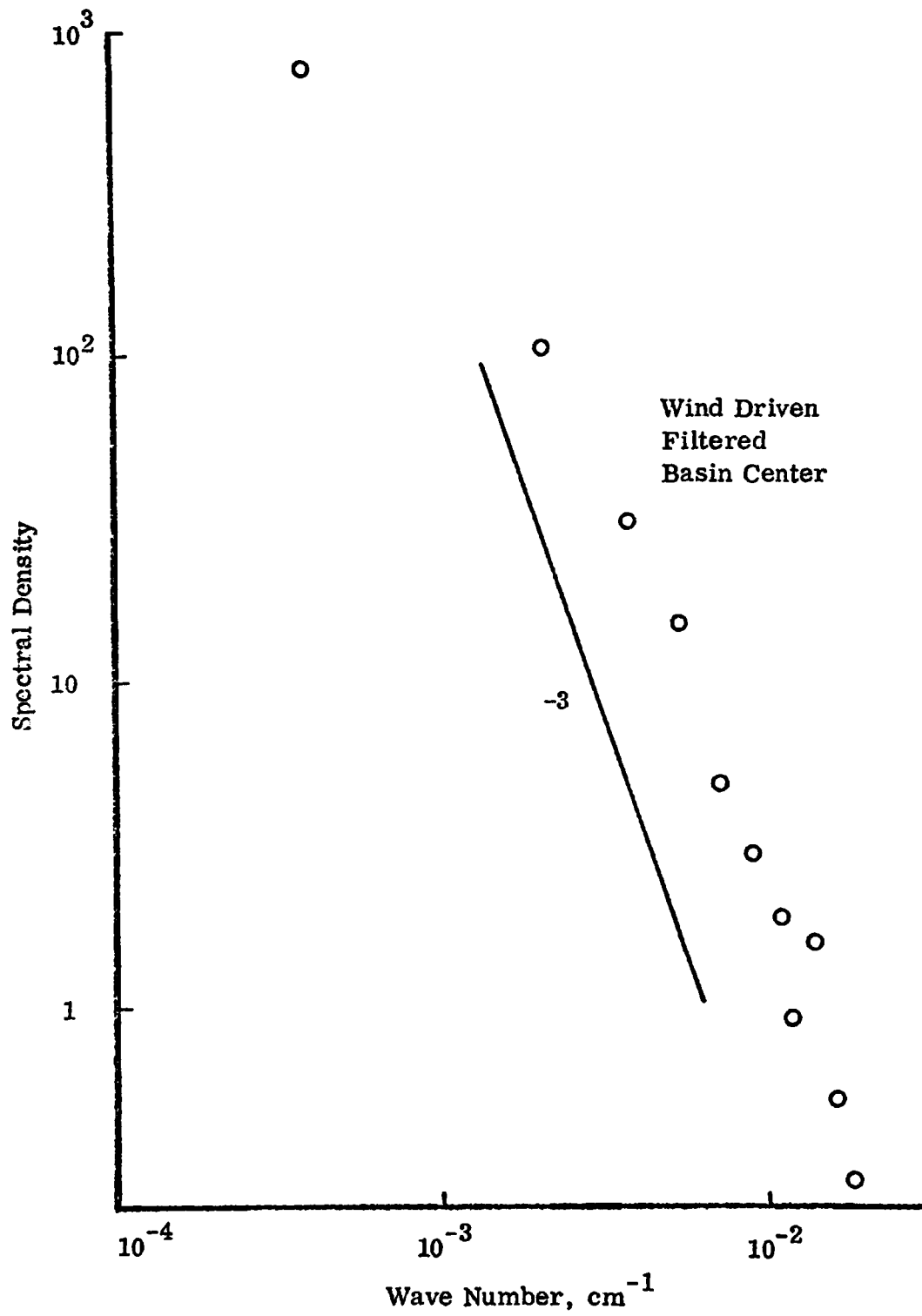


Figure 8.15 Energy Spectrum; Depth = 0.5; Run 2

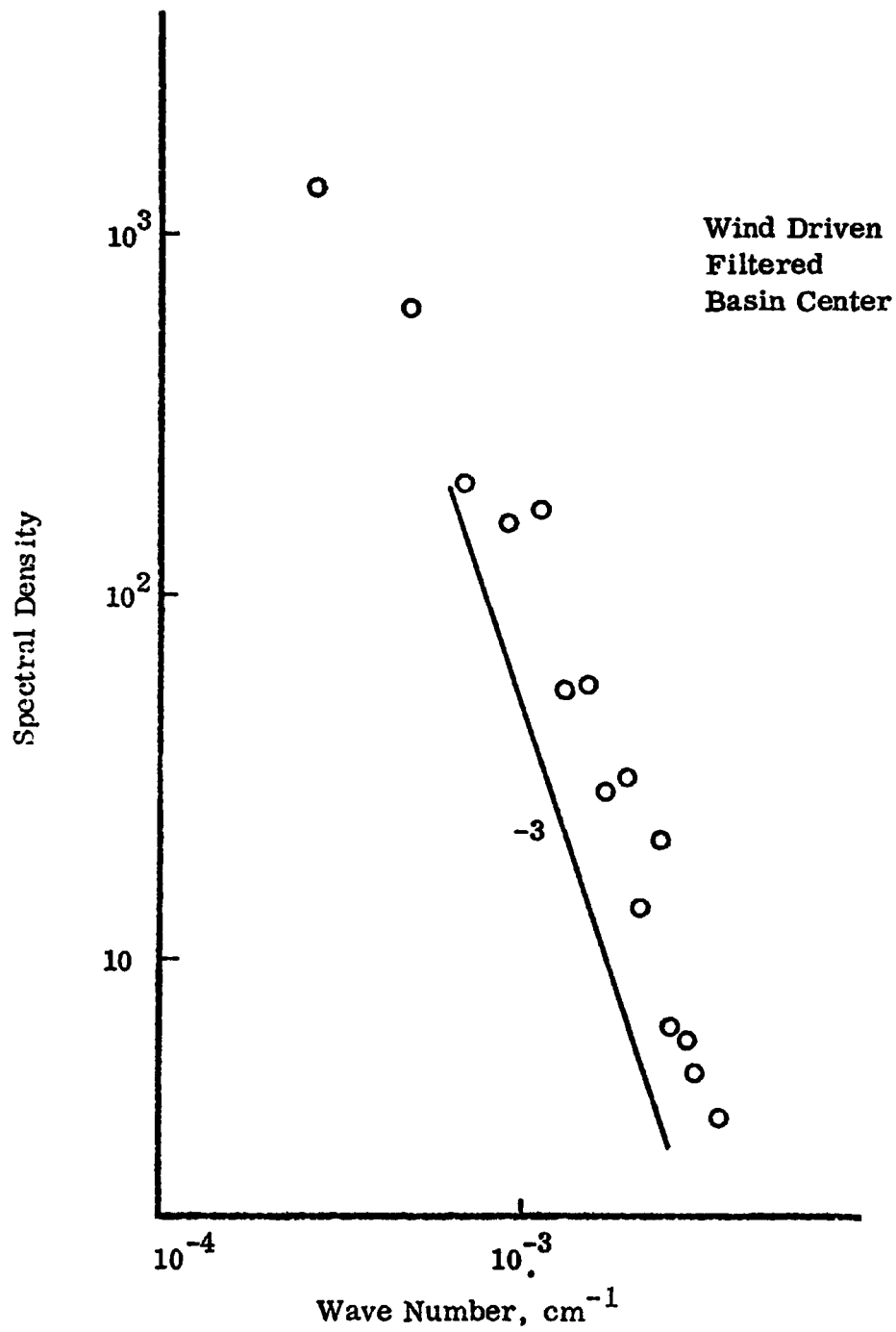


Figure 8.16 Energy Spectrum; Depth = 0.125; Run 3

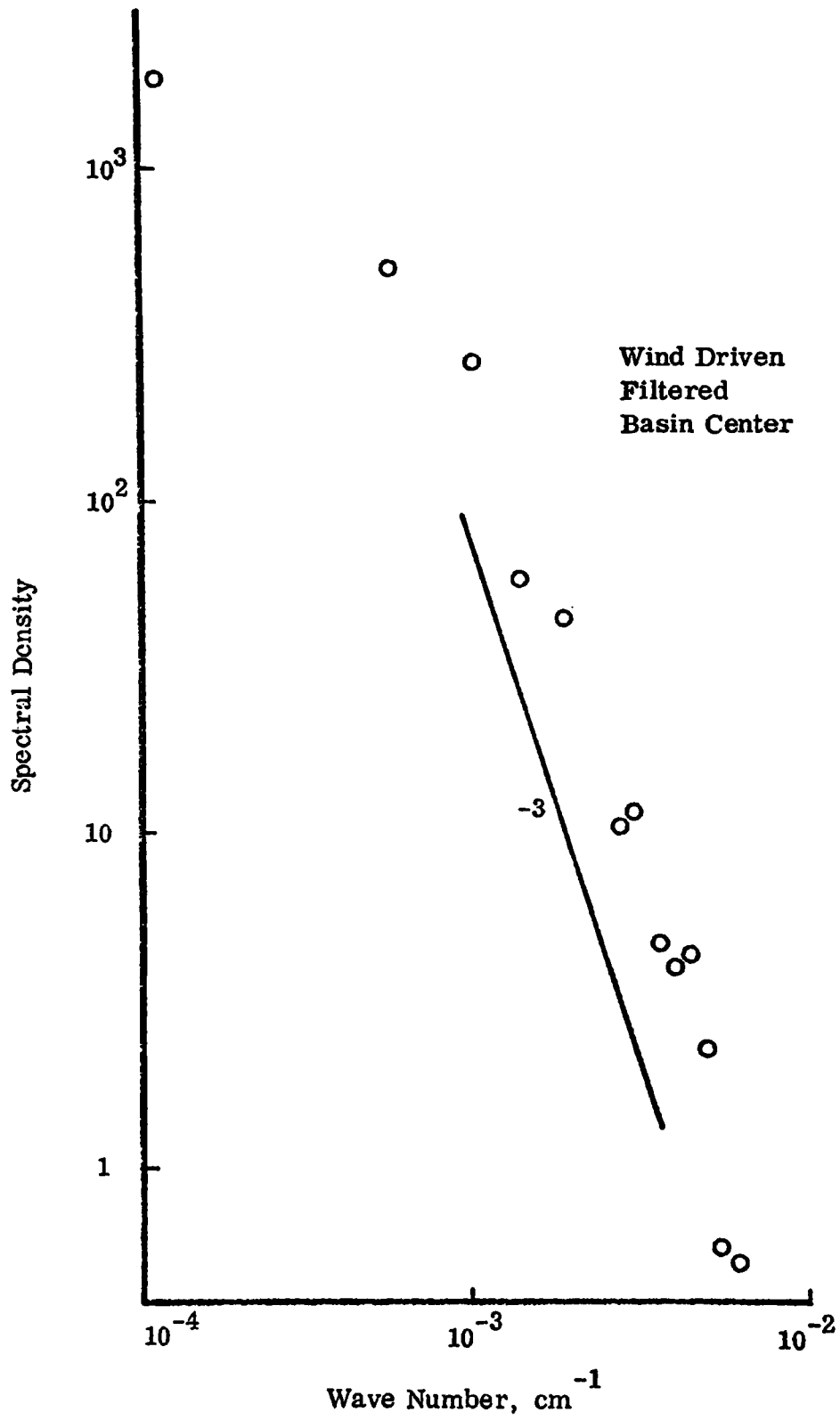


Figure 8.17 Energy Spectrum; Depth = 0.250; Run 3

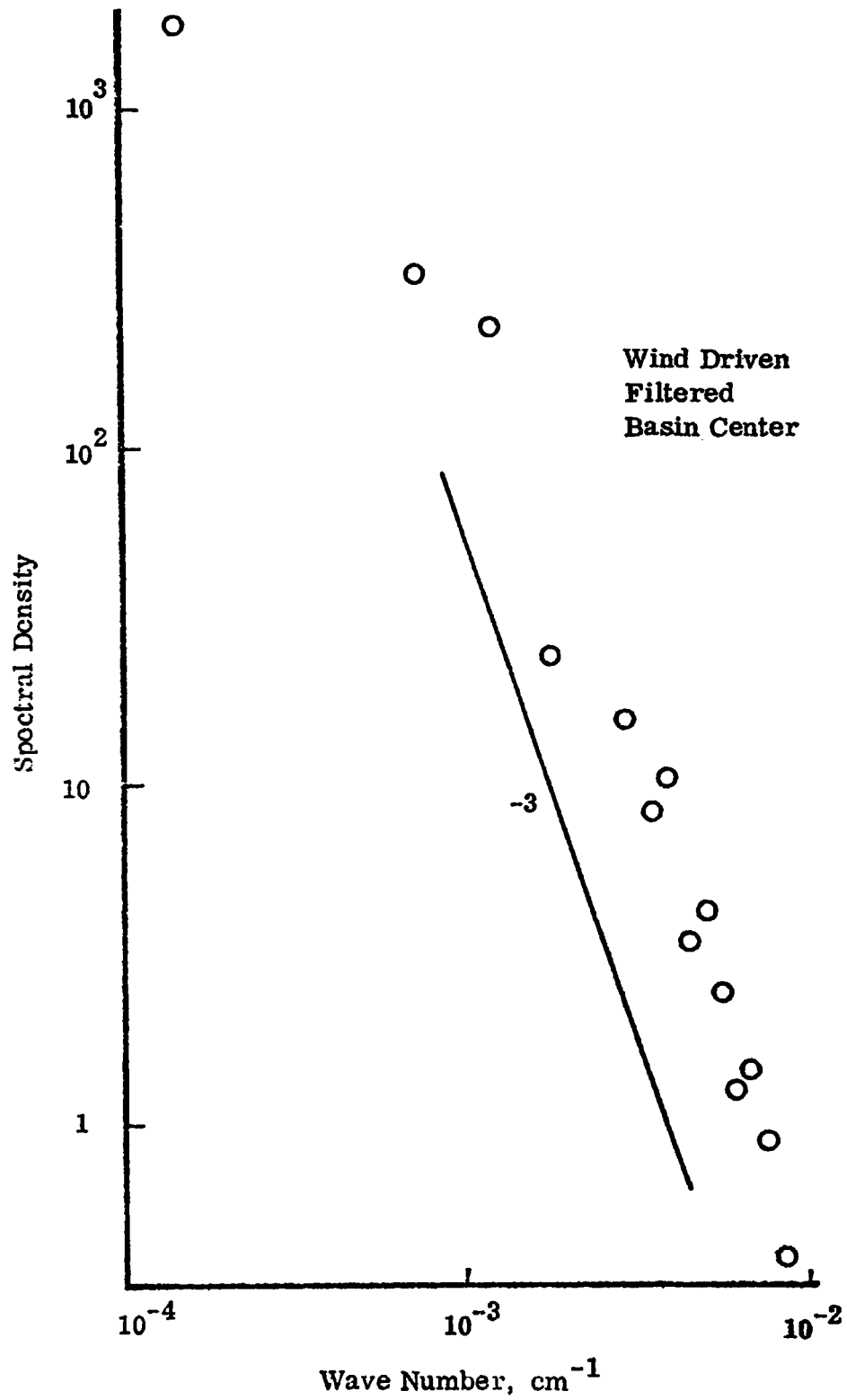


Figure 8.18 Energy Spectrum; Depth = 0.5; Run 3

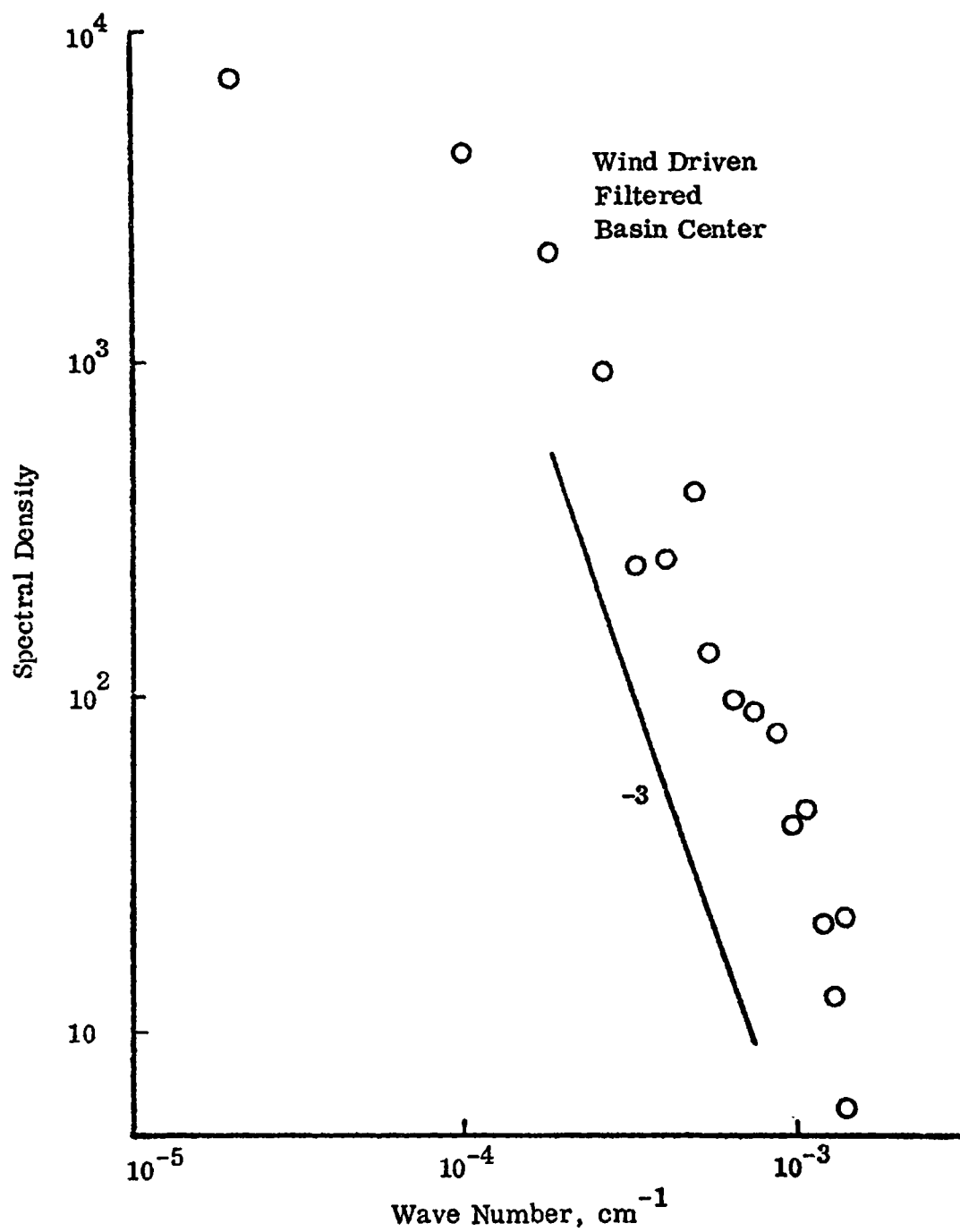


Figure 8.19 Energy Spectrum; Depth = 0.125; Run 5

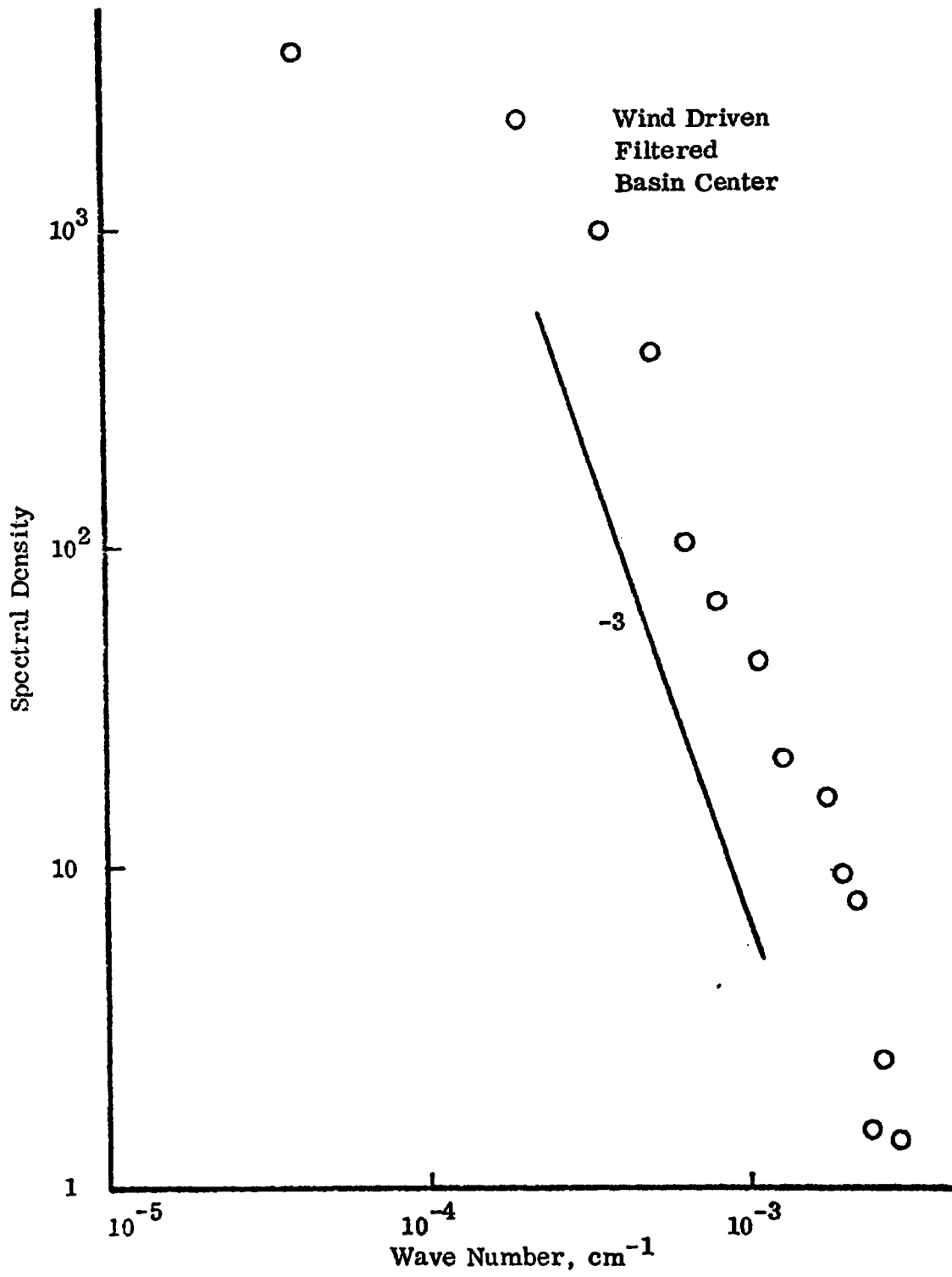


Figure 8.20 Energy Spectrum; Depth = 0.250; Run 5

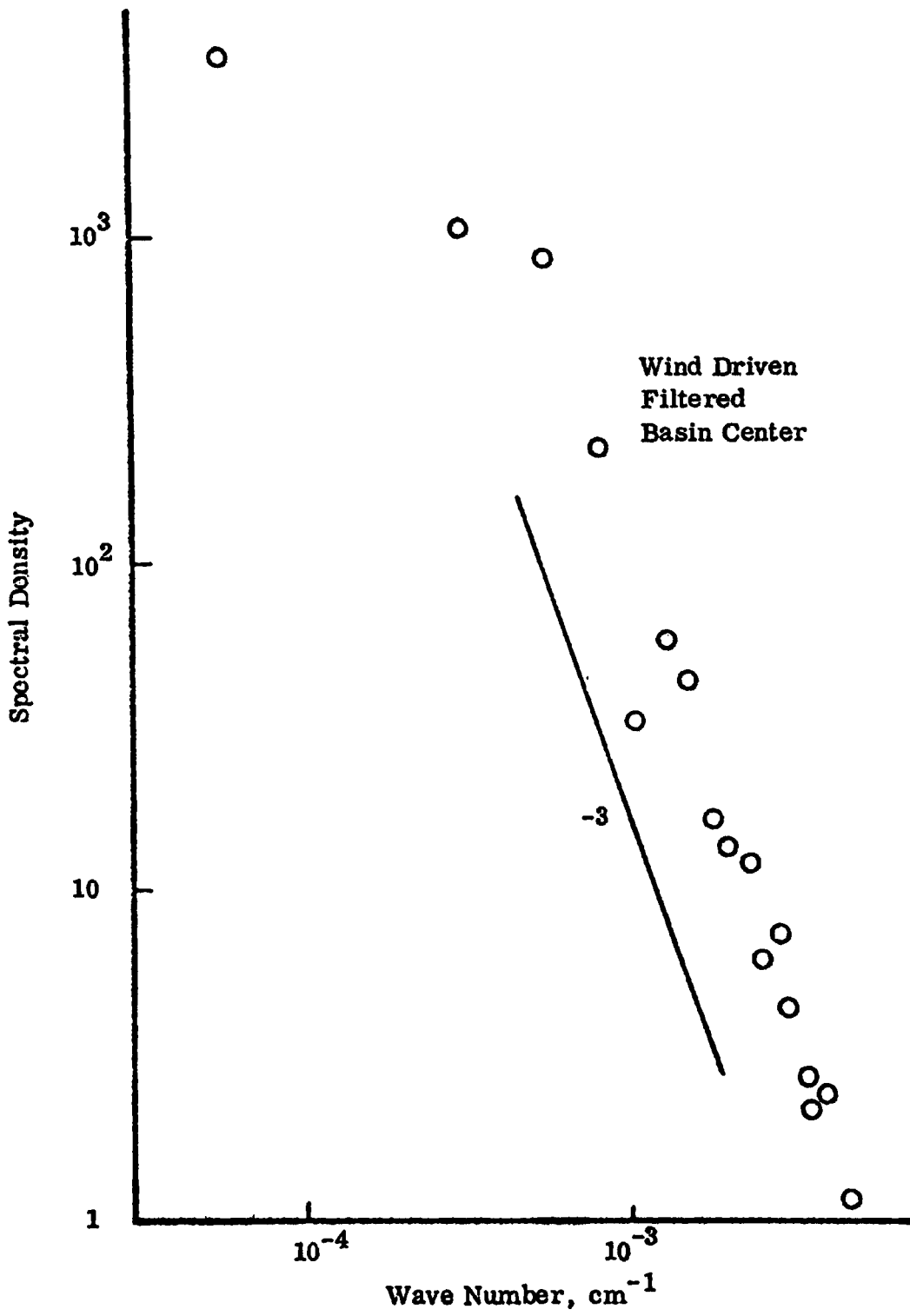


Figure 8.21 Energy Spectrum; Depth = 0.5; Run 5

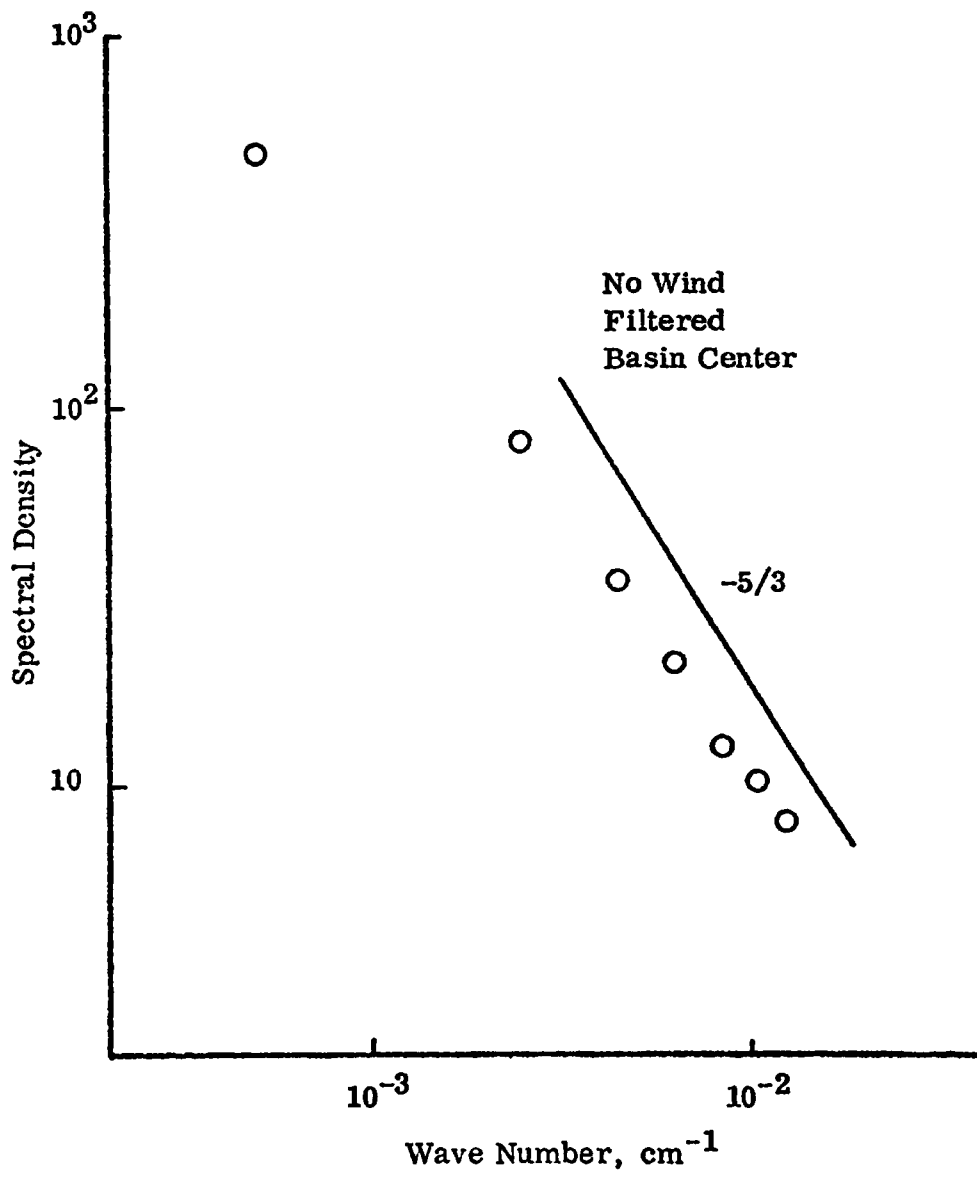


Figure 8.22 Energy Spectrum; Depth=0.125; Run 7

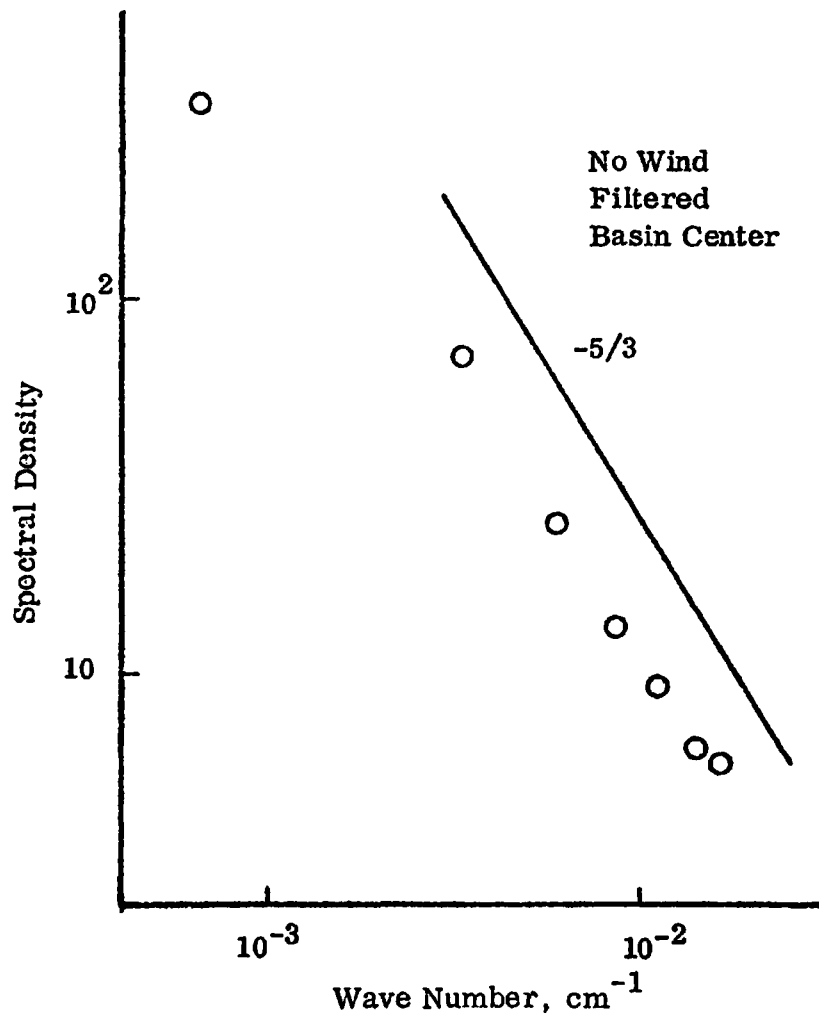


Figure 8.23 Energy Spectrum; Depth=0.25 ; Run 7

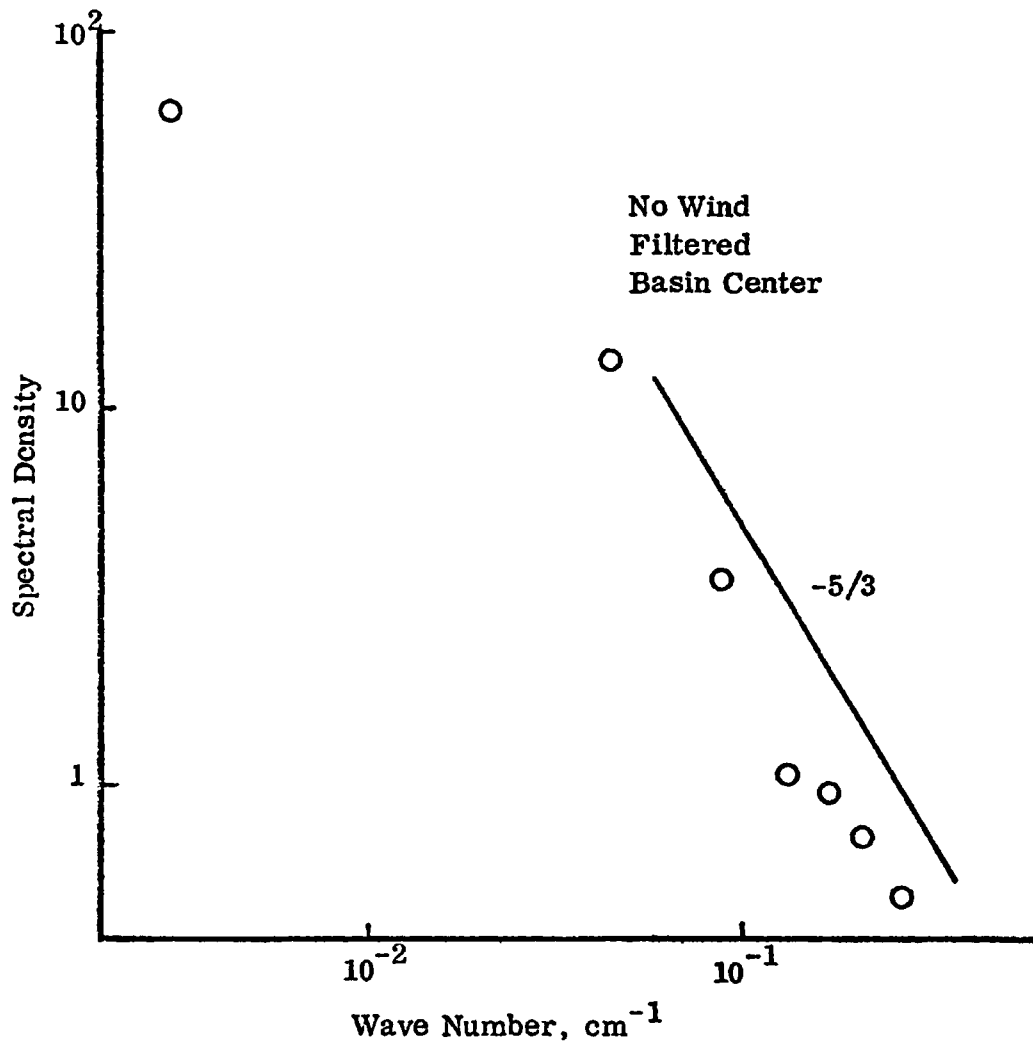


Figure 8.24 Energy Spectrum; Depth=0.5; Run 7

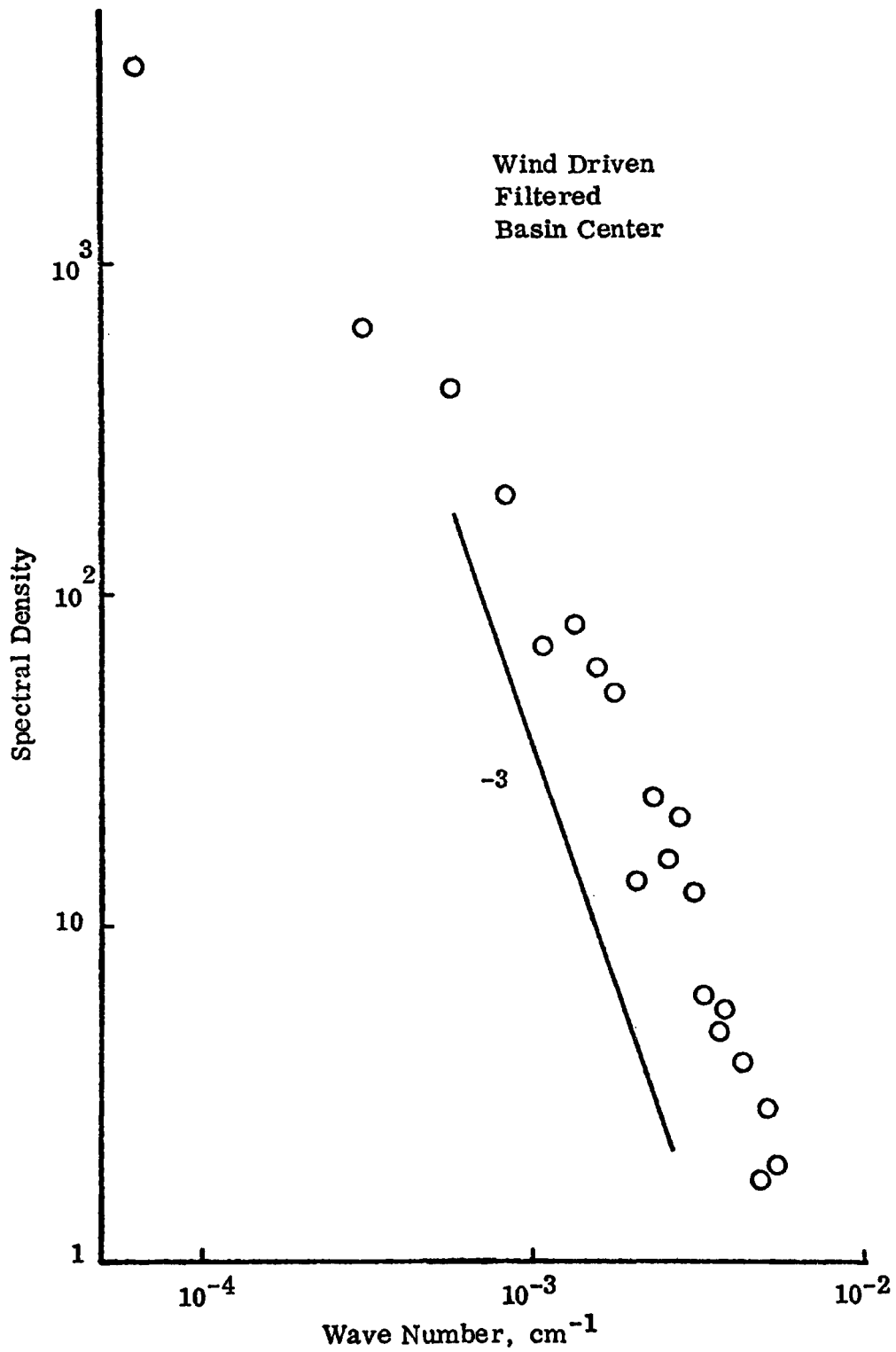


Figure 8.25 Energy Spectrum; Depth=0.125; Run 6

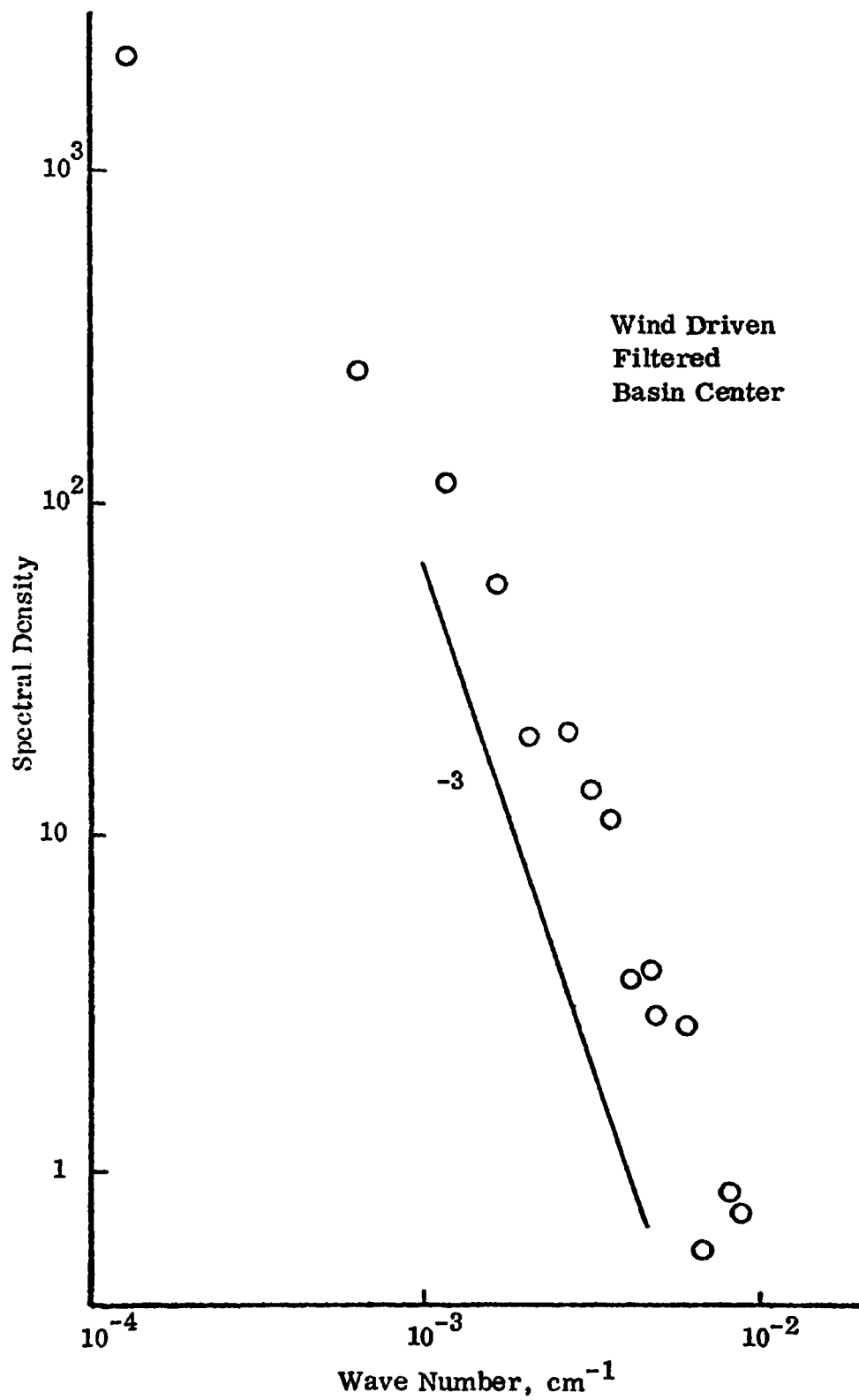


Figure 8.26 Energy Spectrum; Depth=0.250; Run 6

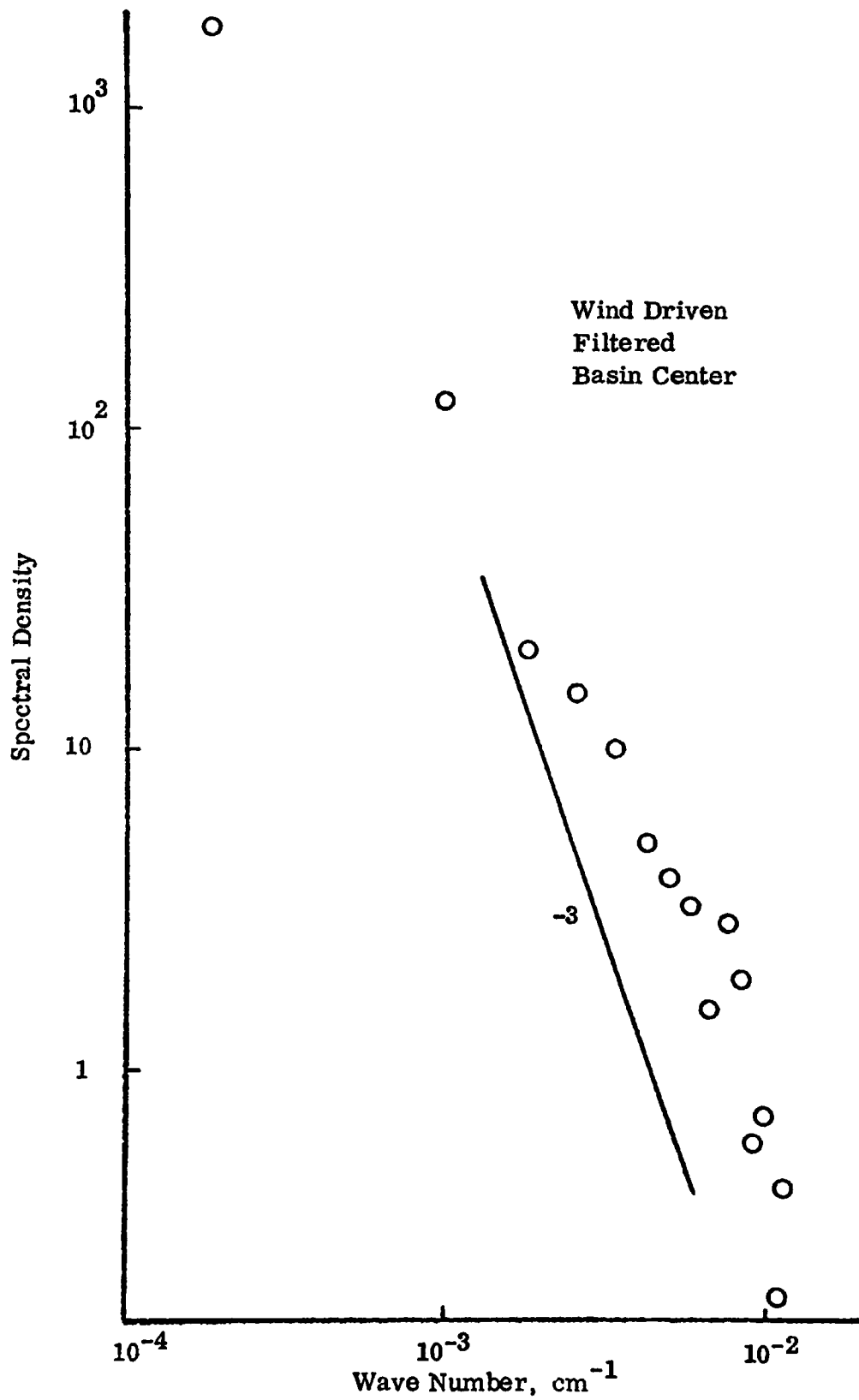


Figure 8.27 Energy Spectrum; Depth=0.5; Run 6

e) Spectra with no Deterministic Structure in the Surface
Boundary Condition

The results of Run 12, where the deterministic part of Equation (7.1) was set to zero, are presented in Figures 8.28, 8.29 and 8.30. The objective of this run was to examine how the velocity spectra are influenced by a wind shear whose spectral density curve does not decay as $-5/3$ (Figure 7.1).

f) Spectra with no Filtration

The objective of this run was to see if just the fourth order differencing scheme was responsible for the improved prediction. Filters were made inoperable by setting the filter lengths to zero resulting in a model similar to Bedford and Shah's (1977) but in fourth order differences. The results of this run are shown in Figures 8.31 and 8.32.

2) Passive Containment Spectra

a) Spectra at Different Depths

The concentration spectra of Run 8 are presented in Figures 8.33 through 8.35.

b) Spectra with Different Prandtl Number

The spectra of Runs 9 and 10 are shown in Figures 8.36 through 8.41. With the results of Run 8 they demonstrate the effect of Prandtl number on the computed spectra.

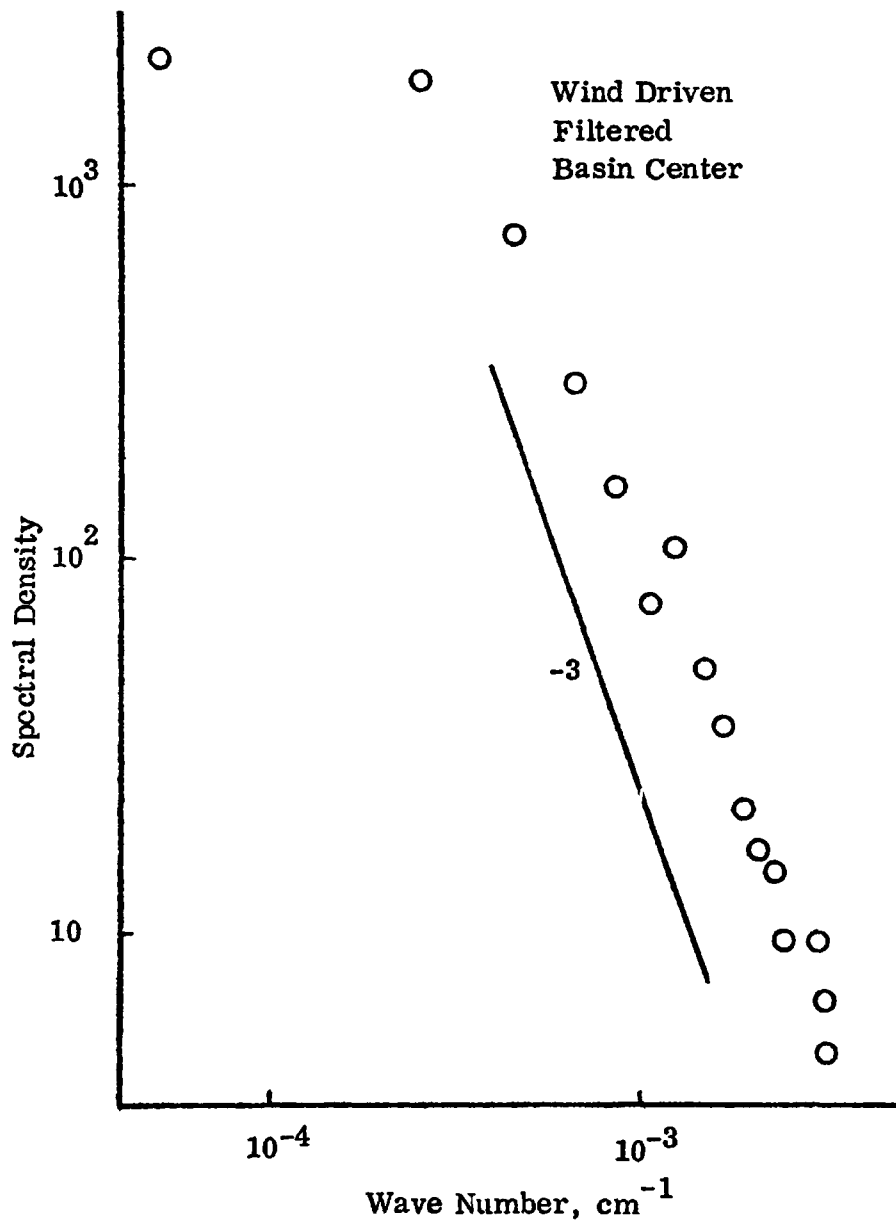


Figure 8.28 Energy Spectrum; Depth=0.125; Run 12

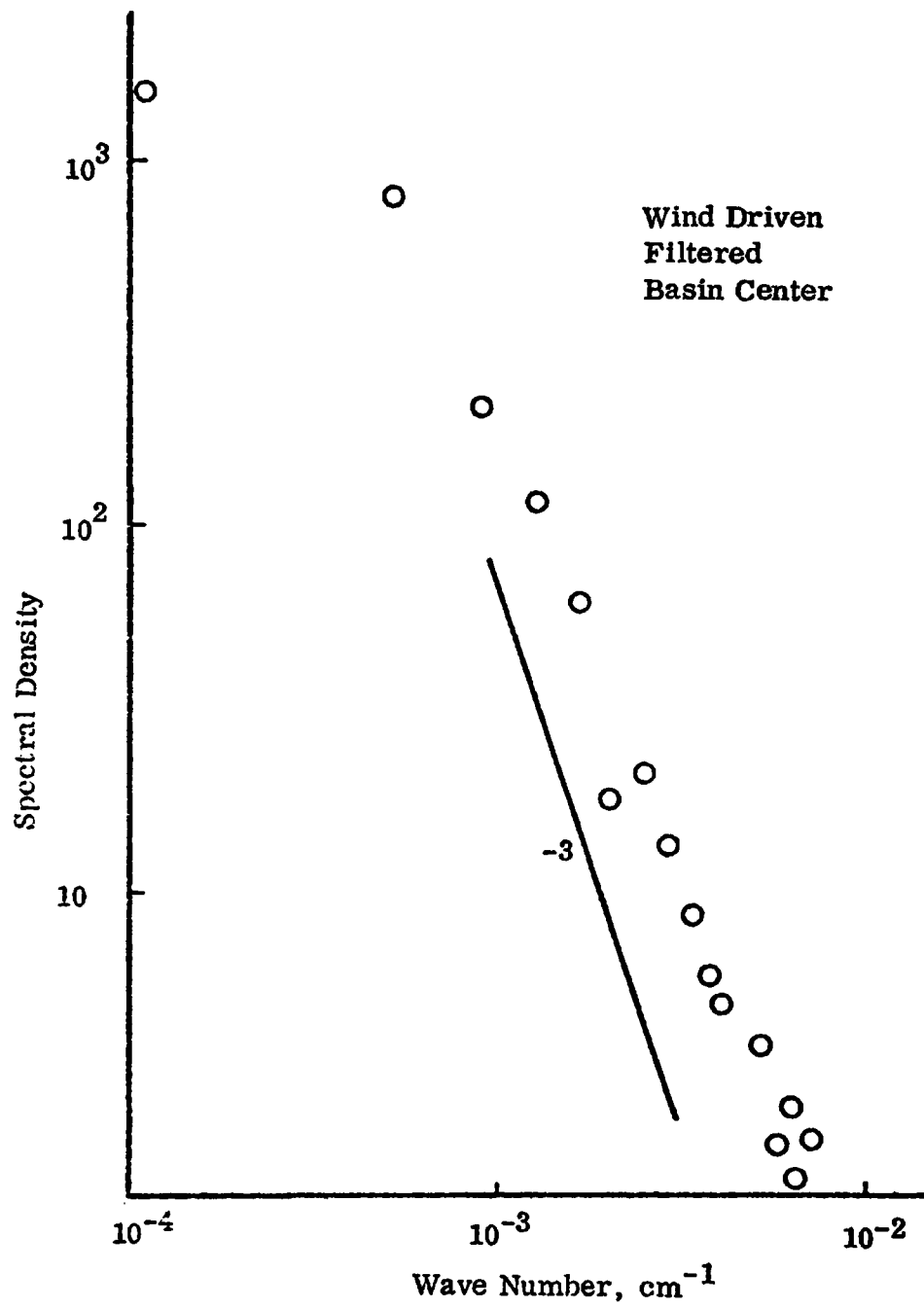


Figure 8.29 Energy Spectrum; Depth=0.250; Run 12

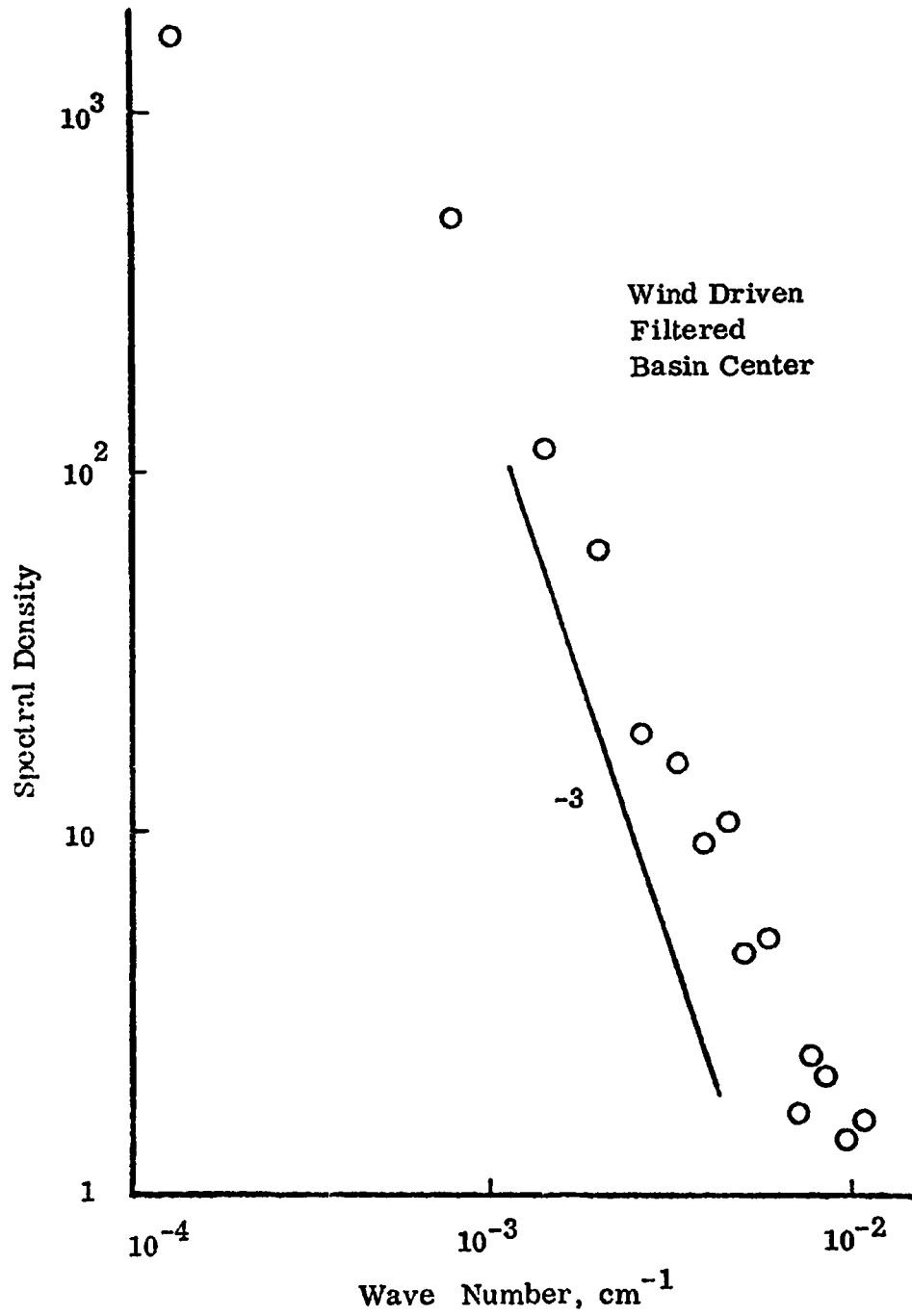


Figure 8.30 Energy Spectrum; Depth=0.5; Run 12

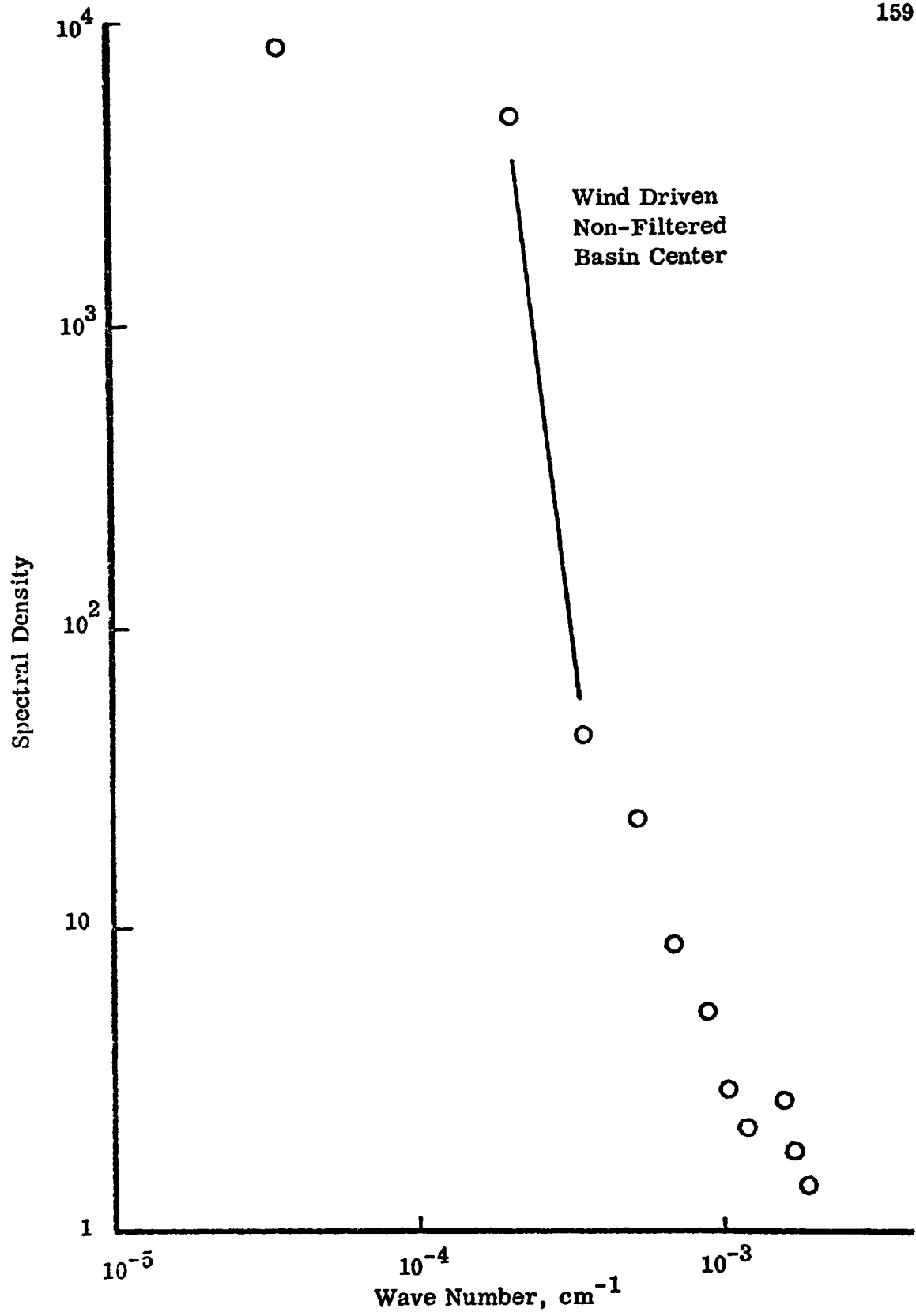


Figure 8.31 Energy Spectrum; Depth=0.0; Run 4

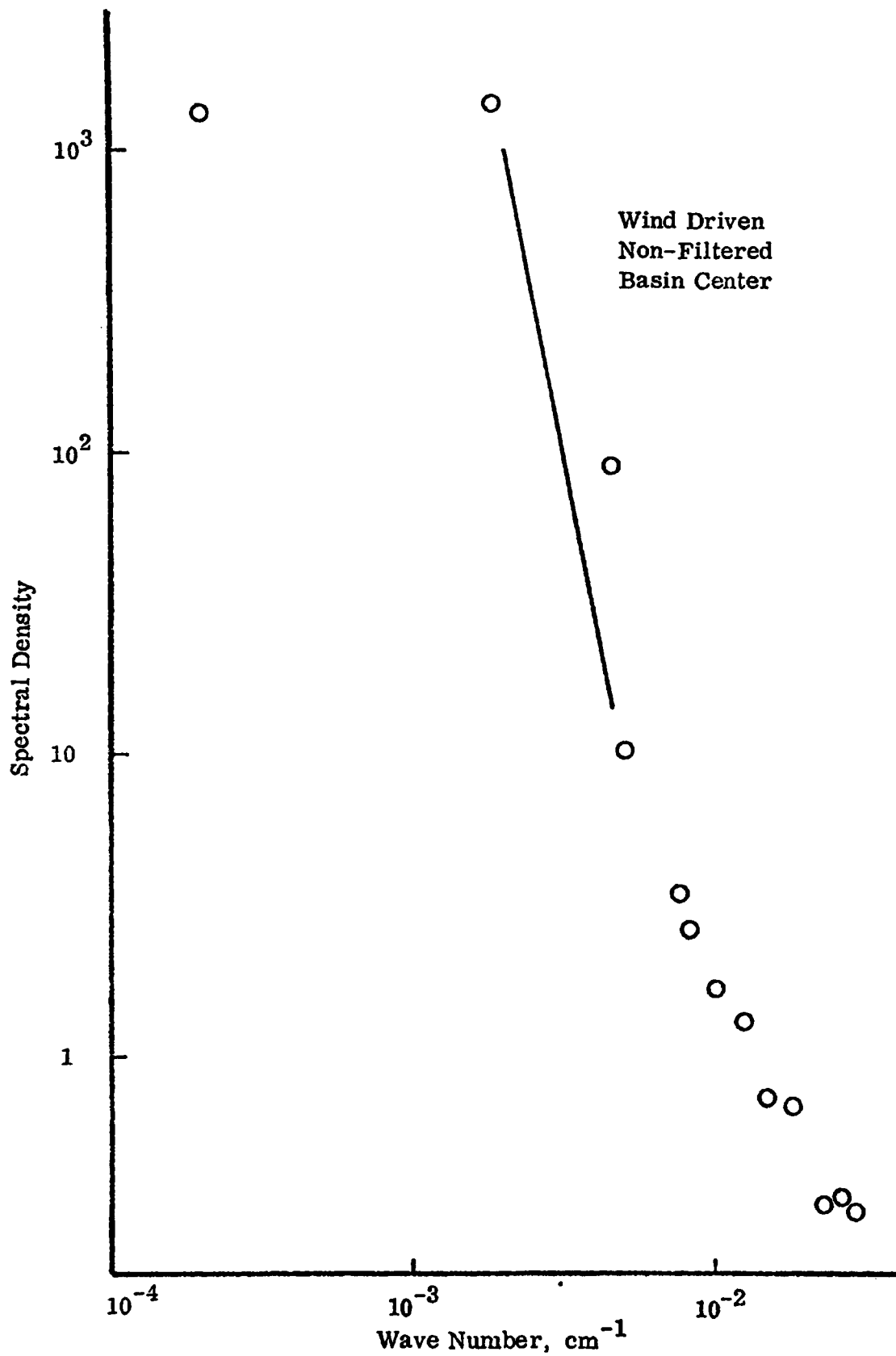


Figure 8.32 Energy Spectrum; Depth = 0.5; Run 4

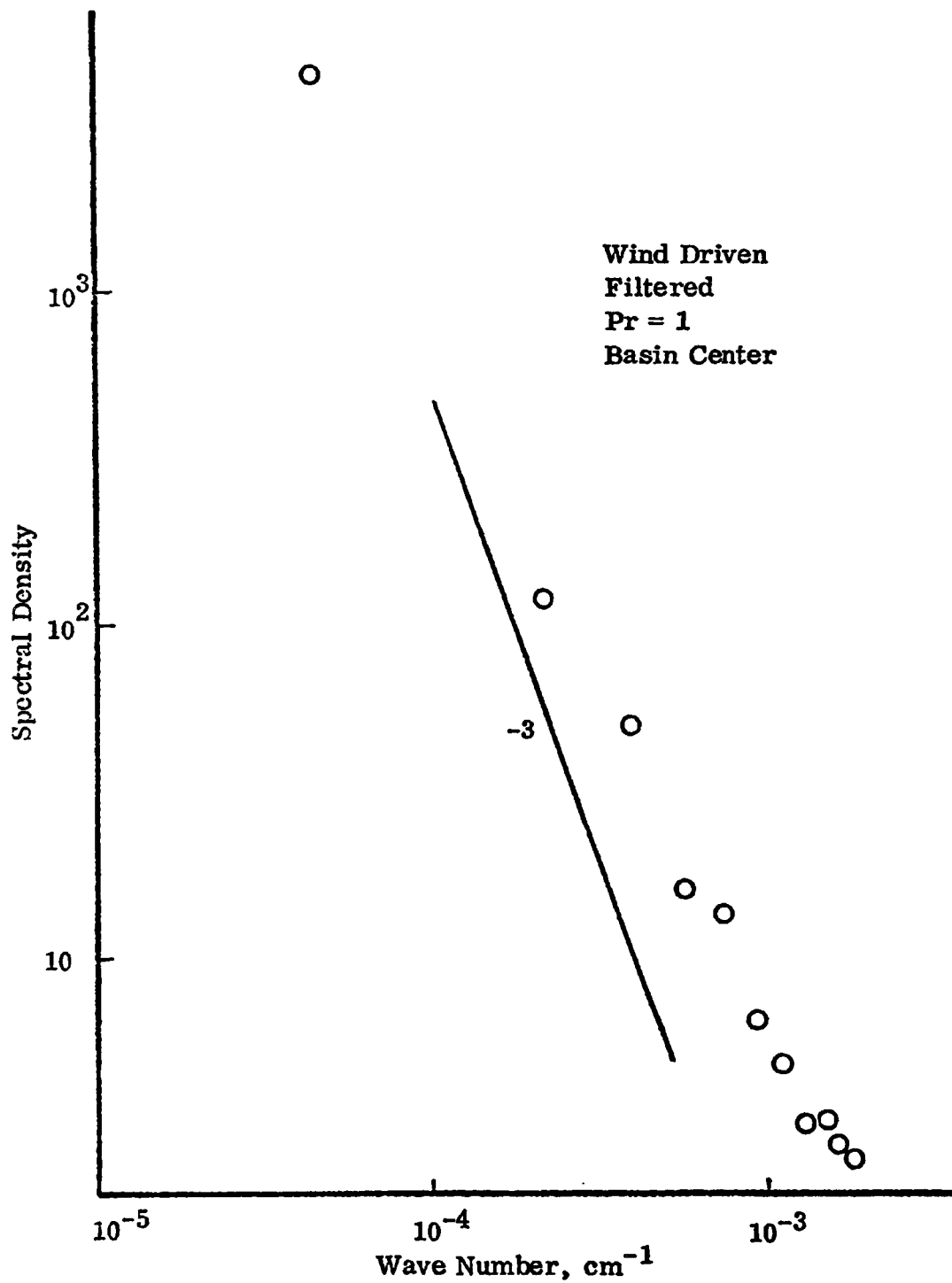


Figure 8.33 Concentration Spectrum; Depth=0.125; Run 8

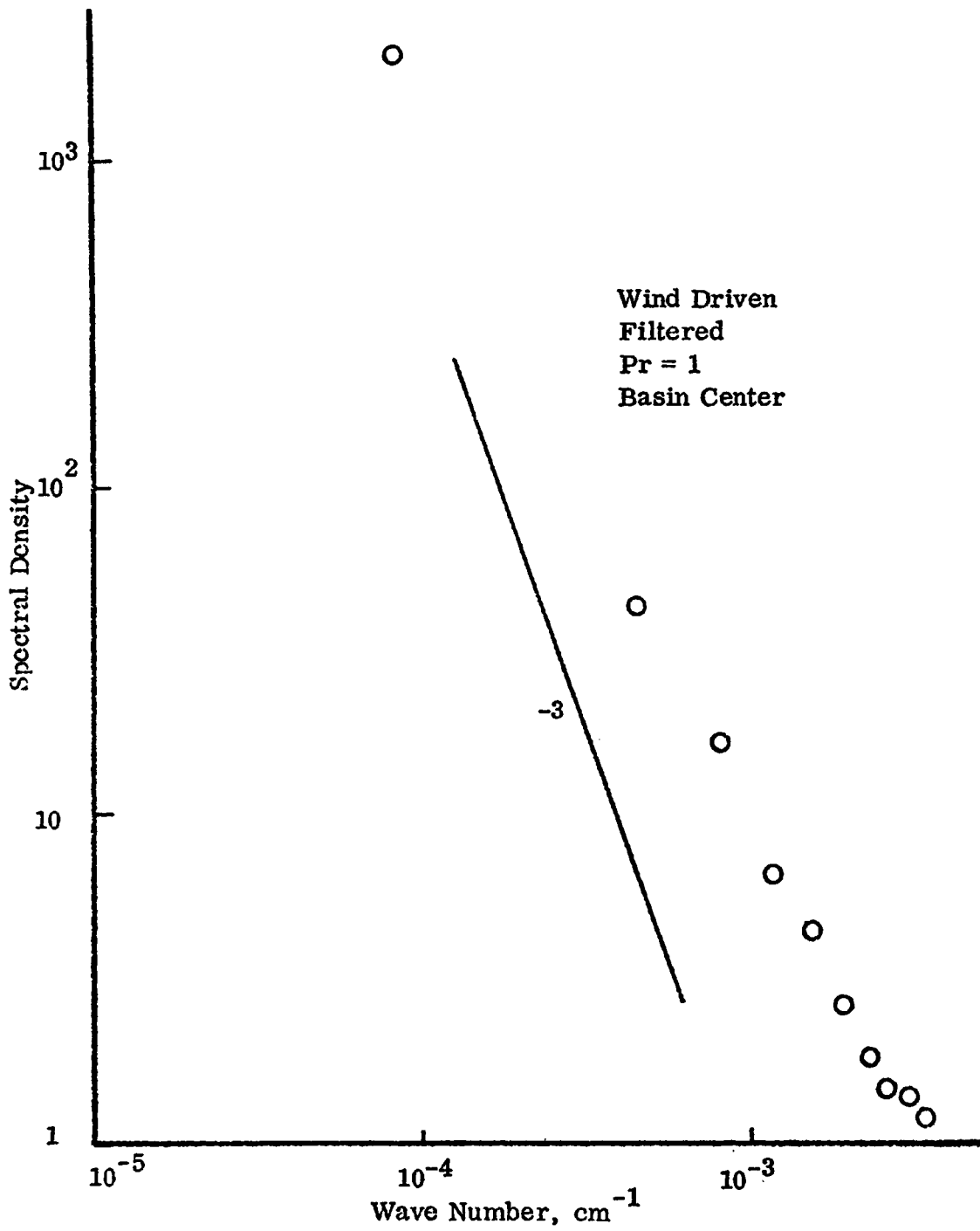


Figure 8.34 Concentration Spectrum, Depth=0.250; Run 8

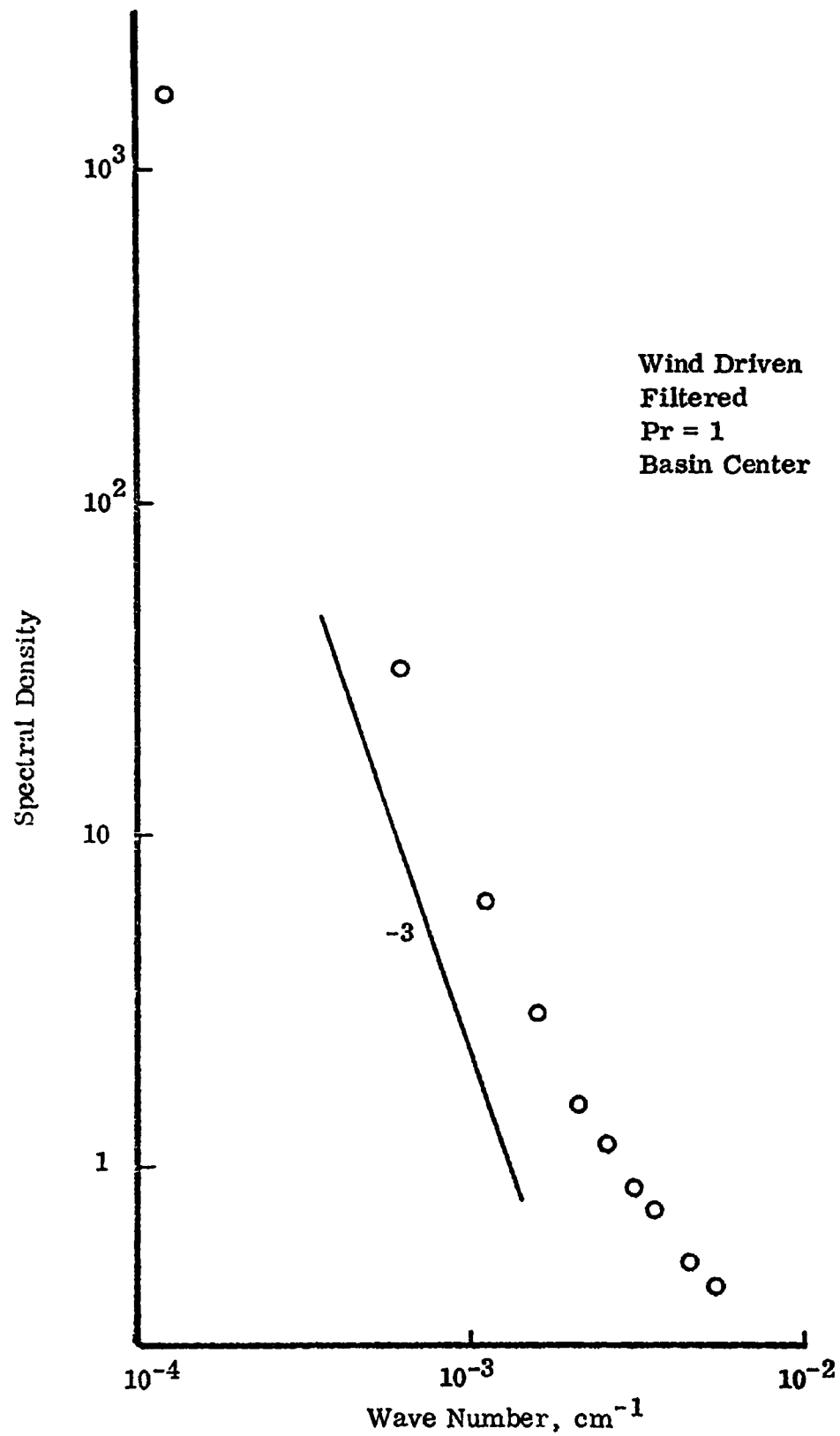


Figure 8.35 Concentration Spectrum; Depth = 0.5; Run 8

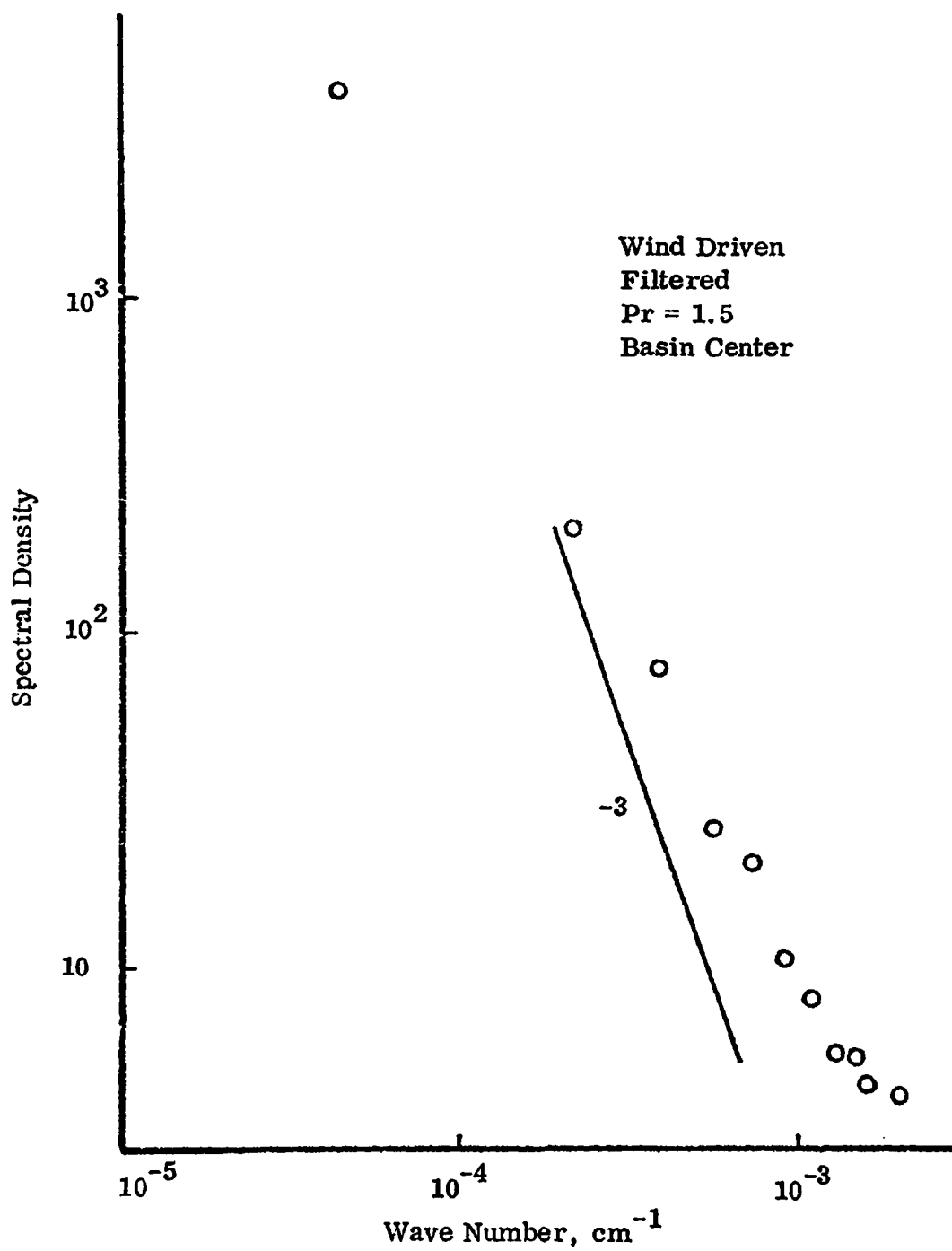


Figure 8.36 Concentration Spectrum; Depth = 0.125; Run 9

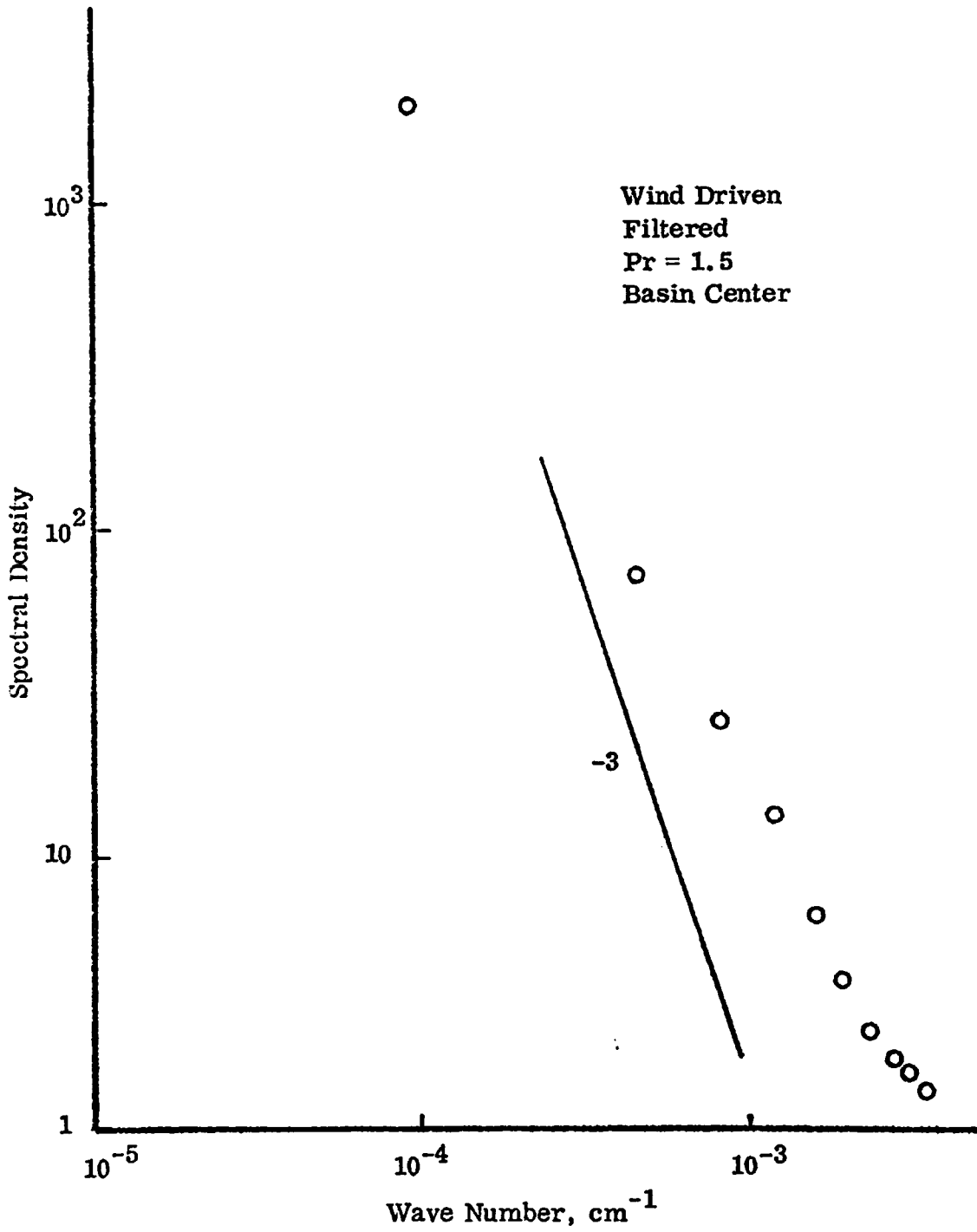


Figure 8.37 Concentration Spectrum; Depth=0.250; Run 9

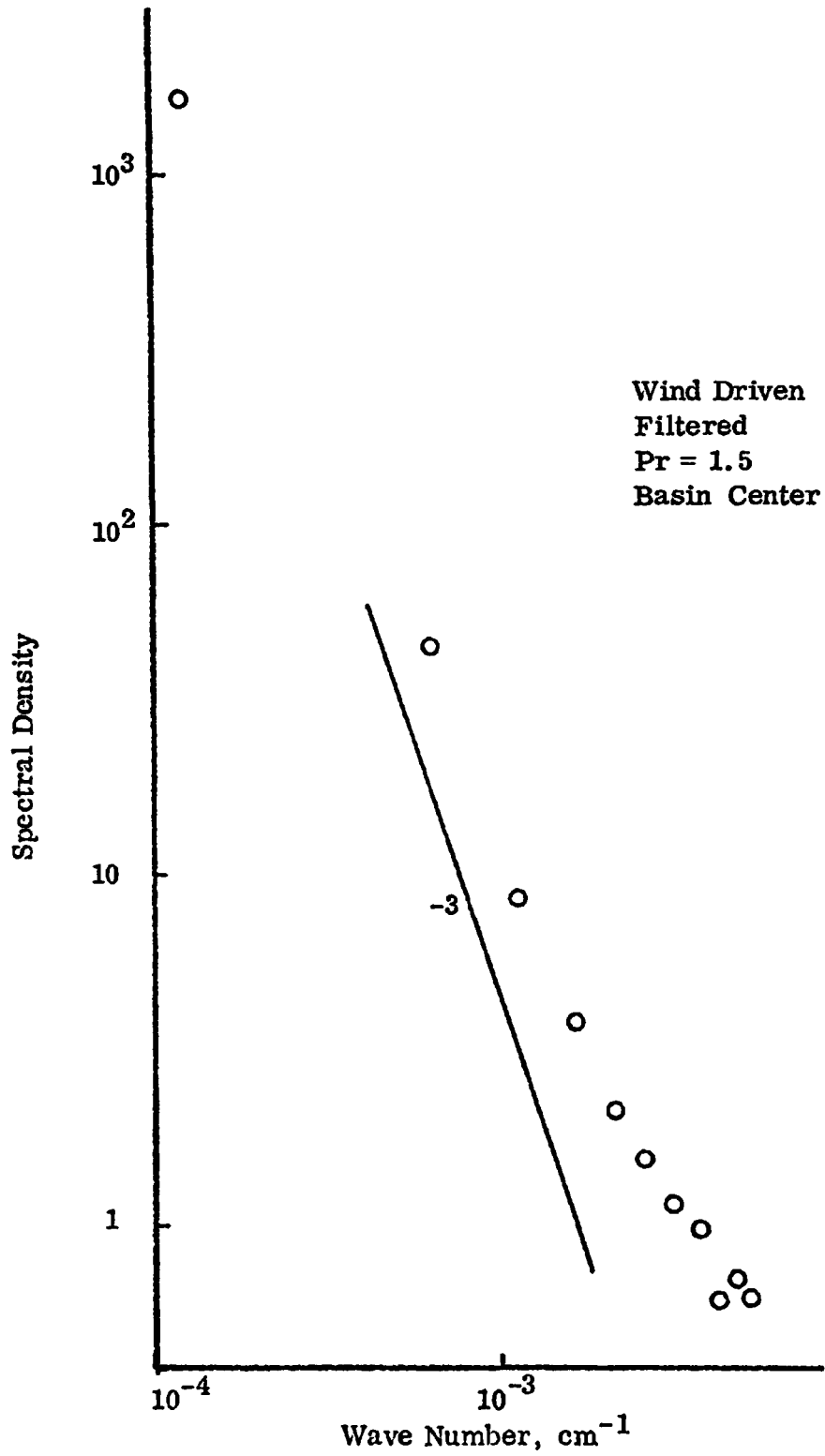


Figure 8.38 Concentration Spectrum; Depth=0.5; Run 9

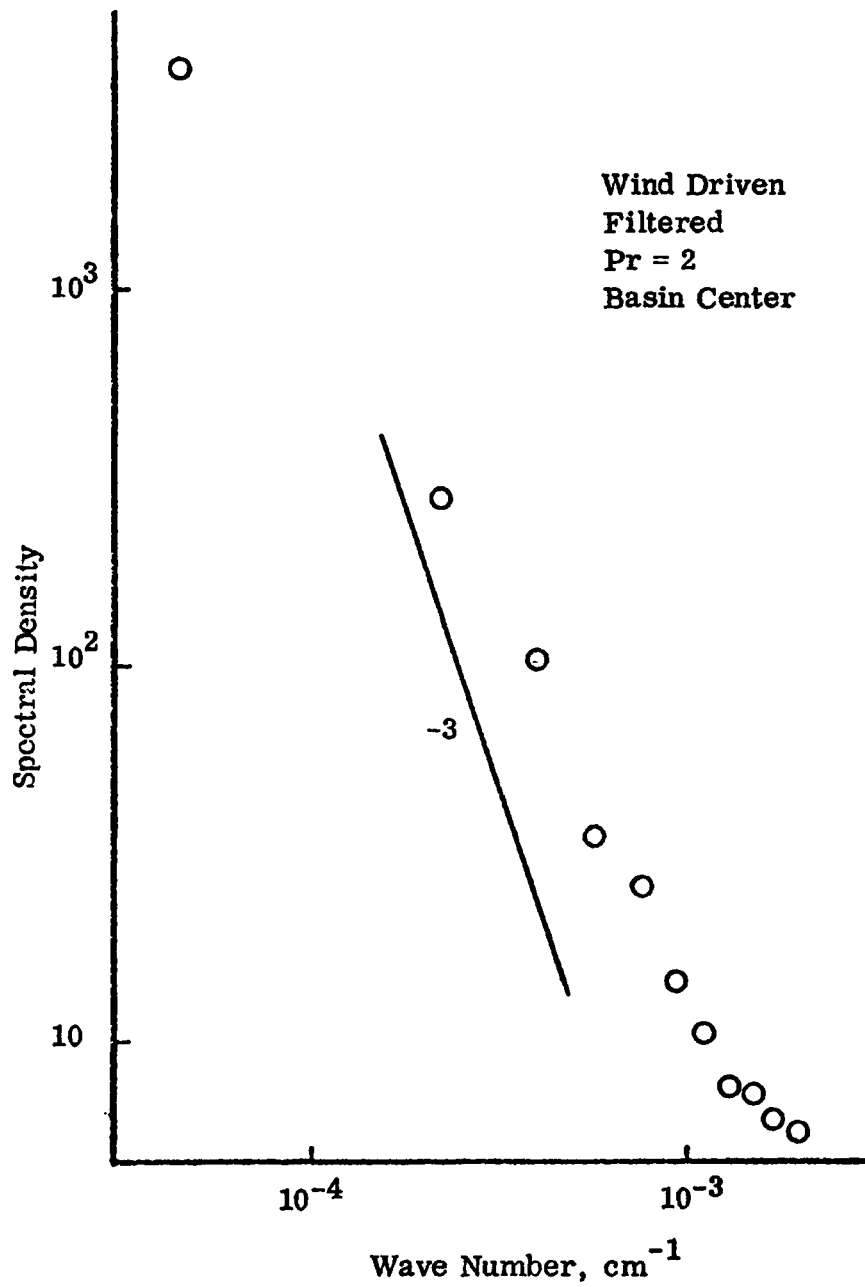


Figure 8.39 Concentration Spectrum; Depth=0.125; Run 10

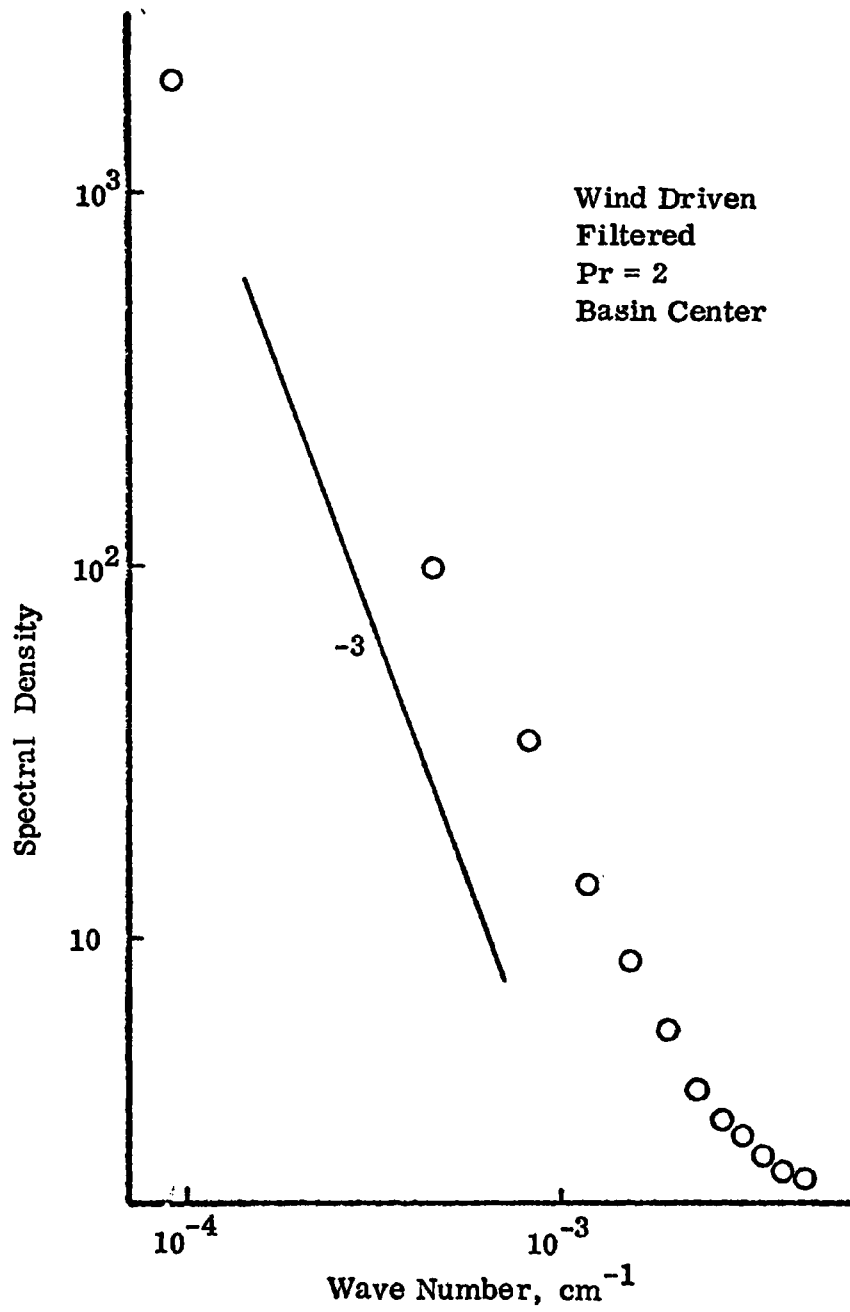


Figure 8.40 Concentration Spectrum; Depth=0.25; Run 10

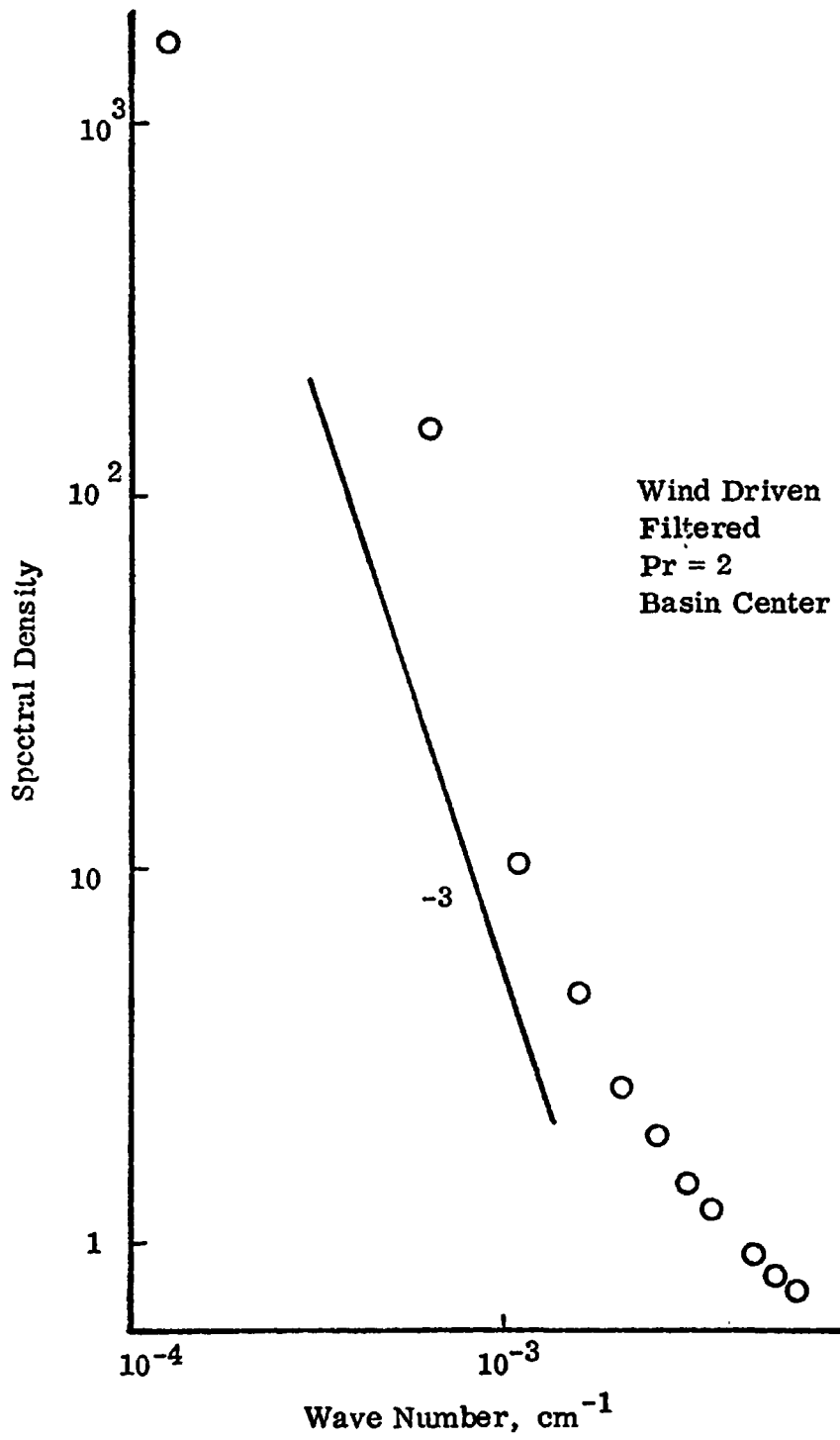


Figure 8.41 Concentration Spectrum; Depth=0.5; Run 10

3) Biochemically Active Contaminant Spectra

The concentration Spectra of the complete biological model are shown in Figures 8.42, 8.43 and 8.44.

E. Preliminary Observations of the Results

1) Velocity Spectra

The following are observed in Figures 8.10 through 8.32.

1. Common characteristic of all circulation runs except Run 4 (no filtration) and Run 7 (no wind) is the -3 slope of the spectrum.

ii. The maximum length scales where the -3 slope is observed vary from run to run and they also depend on the depth where the spectra are obtained. These scales are summarized in Table 8.1. It can be seen that there is a general decrease of the maximum scale with depth.

iii. There is generally an increase in the size of scales where a -3 slope exists when going from smaller to larger Reynolds number (smaller to larger basin). This is shown in Figure 8.10 through 8.18 and also in Table 8.1.

iv. There is a shift of the spectral density curve to the smaller wave numbers going from a weak to a strong wind. This is shown from comparison of Figures 8.19 through 8.21 (Run 5) with Figures 8.10 through 8.12 (Run 1) and also Table 8.1.

v. Comparison of the same runs as in 4 indicate that there is an upward movement of the curves to higher levels of energy going from a weak to a strong wind.

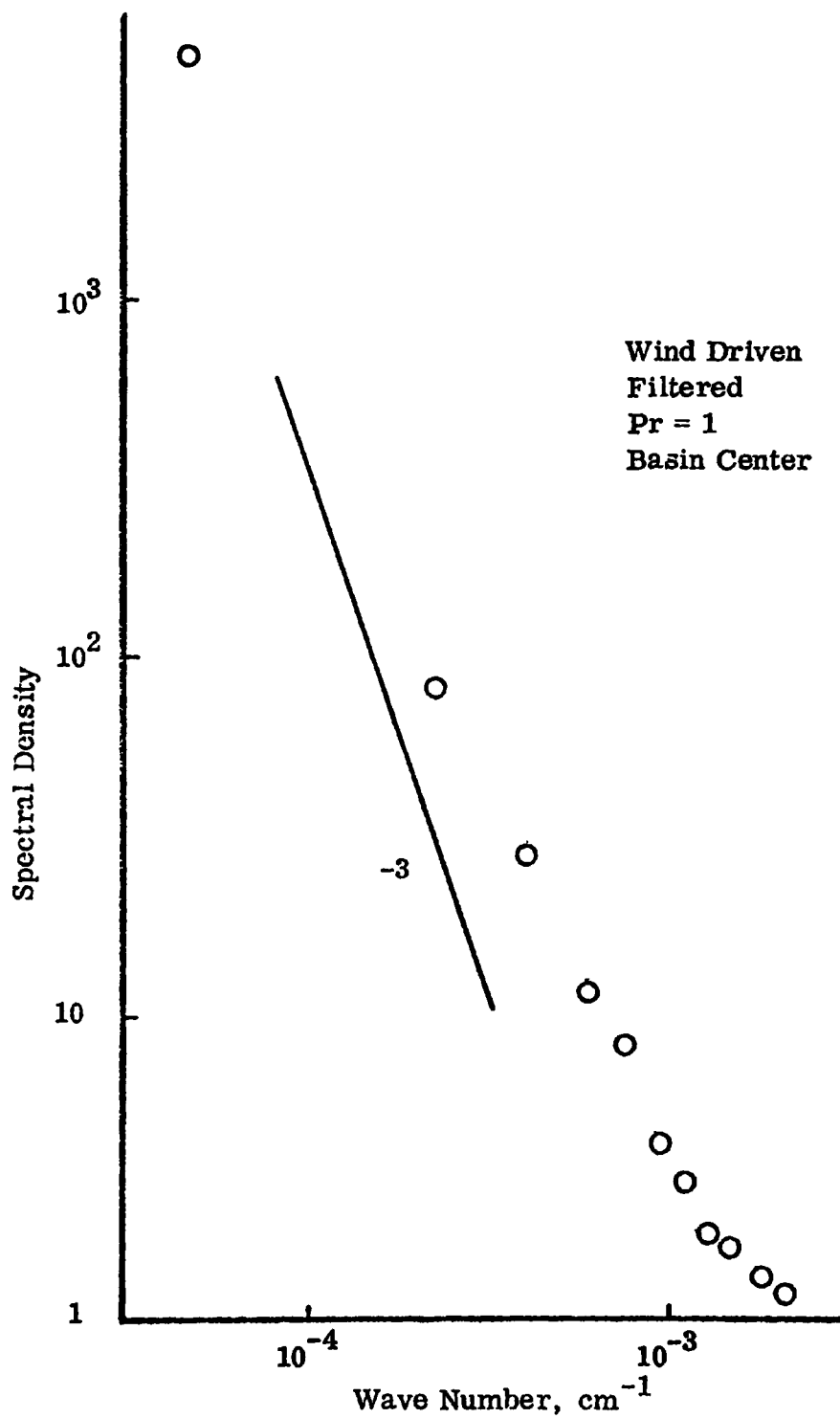


Figure 8.42 Concentration Spectrum; Biochemically Active Contaminant;
Depth=0.125; Run 11

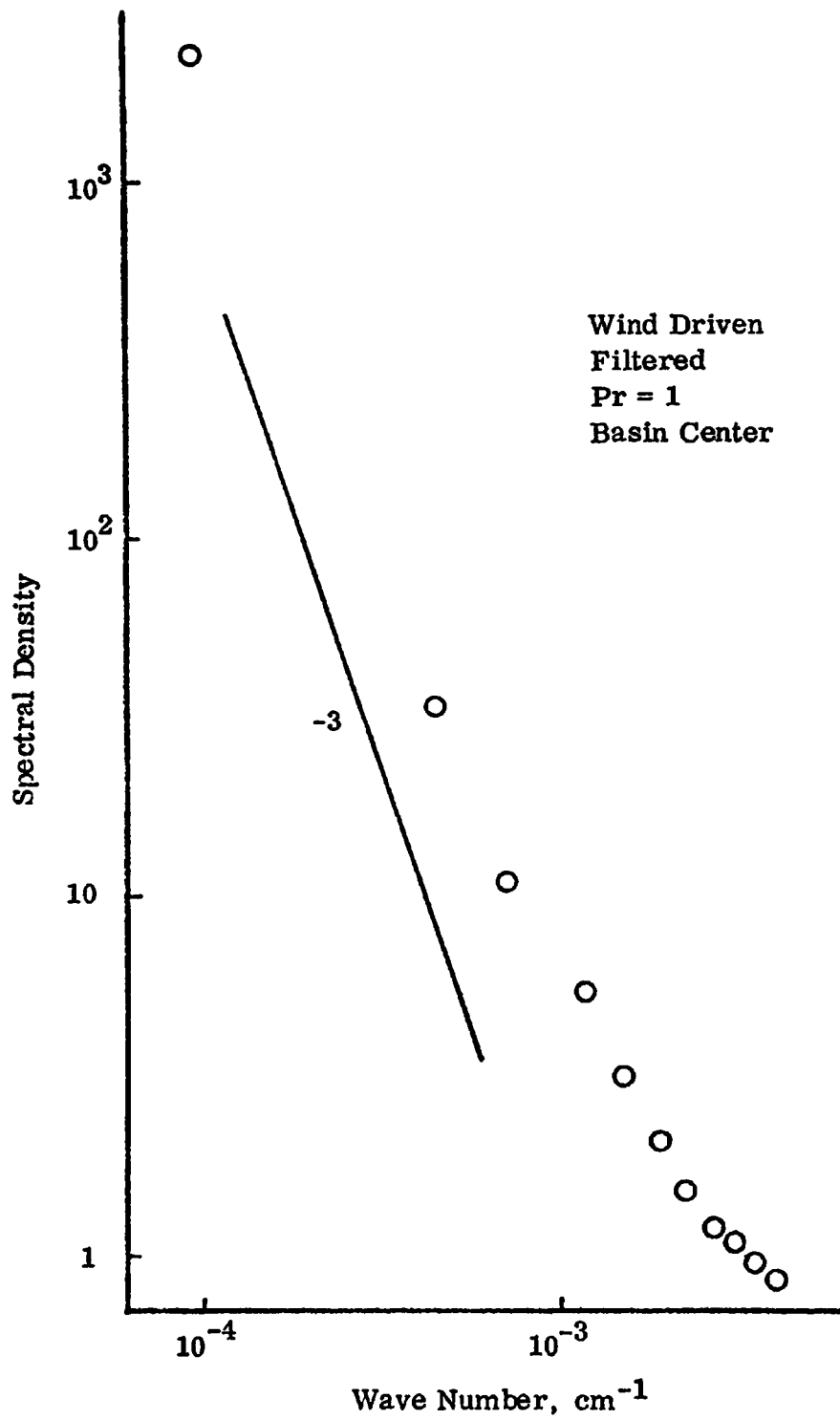


Figure 8.43 Concentration Spectrum; Biochemically Active Contaminant;
Depth=0.250; Run 11

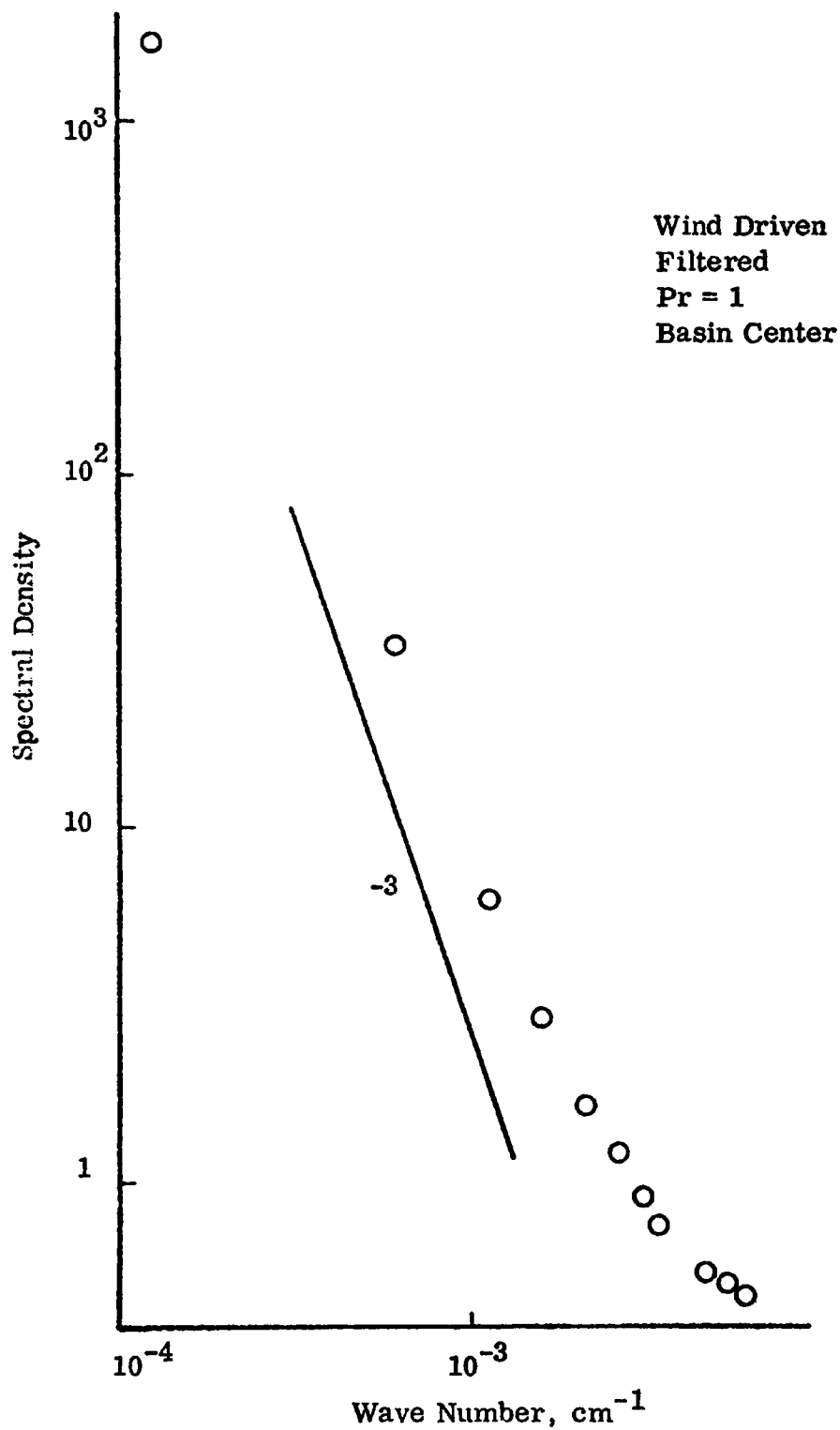


Figure 8.44 Concentration Spectrum; Biochemically Active Contaminant;
Depth=0.5; Run 11

Table 8.1 Maximum Length Scales (m) where a -3 Slope is Observed. Concentration Runs Include also the Maximum Scale where the Tail End Changes Slope.

| Node | Run #1 | Run #2 | Run #3 | Run #5 | Run #6 | Run #7 Tail | Run #8 Tail | Run #10 Tail | Run #11 Tail |
|------|--------|--------|--------|--------|--------|----------------|----------------|-----------------|-----------------|
| 2 | 120 | 52 | 126 | 419 | 63 | 120 57 | 120 57 | 120 57 | 120 57 |
| 3 | 63 | 31 | 63 | 179 | 31 | 63 30 | 63 30 | 63 30 | 63 30 |
| 5 | 37 | 21 | 52 | 125 | 18 | 37 25 | 37 21 | 37 21 | 37 21 |

vi. Figures 8.22 — 8.24 demonstrate that when the wind field dies away the slope of the spectral density curve approaches $-5/3$.

vii. There is no effect on the slope of the spectra when a small time step is used (Run 6, Figures 8.25 — 8.27, Table 8.1). However, a comparison of Run 6 with Run 1 (mild wind) shows that the -3 slope starts at a smaller scale in Run 6 than in Run 1.

viii. Figures 8.28 to 8.30 show that it is not required for the wind shear spectral density curve to have the form shown in Figure 7.1, in order for the velocity spectra to show a -3 slope. No matter what the form of the energy input is the flow field adjusts itself to a two-dimensional character.

ix. Figures 8.31 and 8.32 indicate that when an unfiltered model is used the cascade process is not represented correctly. At a length scale of about twice the grid size the energy drain to smaller scales becomes erratic and incomplete.

2) Concentration Spectra

i. Comparison of Figures 8.10 — 8.12 (Run 1) with Figures 8.33 to 8.44 (concentration spectra) and also Table 8.1 indicate that there is a range of scales where both the velocity and concentration spectra follow more or less the same -3 slope.

ii. All the concentration spectra separate from the corresponding velocity spectra at small length scales (Table 8.1) showing a very characteristic end tail.

iii. Comparison of runs with different Prandtl numbers indicate that this end tail is more well defined at larger Prandtl numbers.

iv. Comparison of Figures 8.42 to 8.44 (Biologically active contaminant) with Figures 8.33 to 8.35 (passive contaminant) indicate that there is no significant difference at the shape of the corresponding spectra.

v. Comparison of the same runs as in 4 indicate that the variance in the second and third nodes is lower for the phytoplankton than for the passive contaminant.

The interpretation of these observations and the discussion of the results are presented in the next chapter.

CHAPTER IX

INTERPRETATION AND DISCUSSION

In the previous chapter some preliminary observations were made about the results. This chapter is devoted to interpreting and discussing these results and is therefore divided into two parts. In the first part interpretations will be made and supported by available field data. In the second part some of the more characteristic features of the model will be discussed. Also an answer to a problem called "paradox of plankton" which is often encountered in limnology will be suggested.

A. Interpretation

One of the first observations from the circulation runs (except the ones with no wind and filtration) is that there is a range of scales where the spectrum follows a -3 slope. As in Chapter III, Section A.8 this is a characteristic of 2-D turbulence or non-equilibrium flows. Mathematically, two-dimensionality can be expected in all of the basins where the model was tested since in all of them the ratio of the vertical to horizontal length is very small. Two-dimensionality is observed in shallow regions of lakes and also in atmospheric turbulence. Typical lake two-dimensional turbulence is shown in Figure 9.1 as reproduced

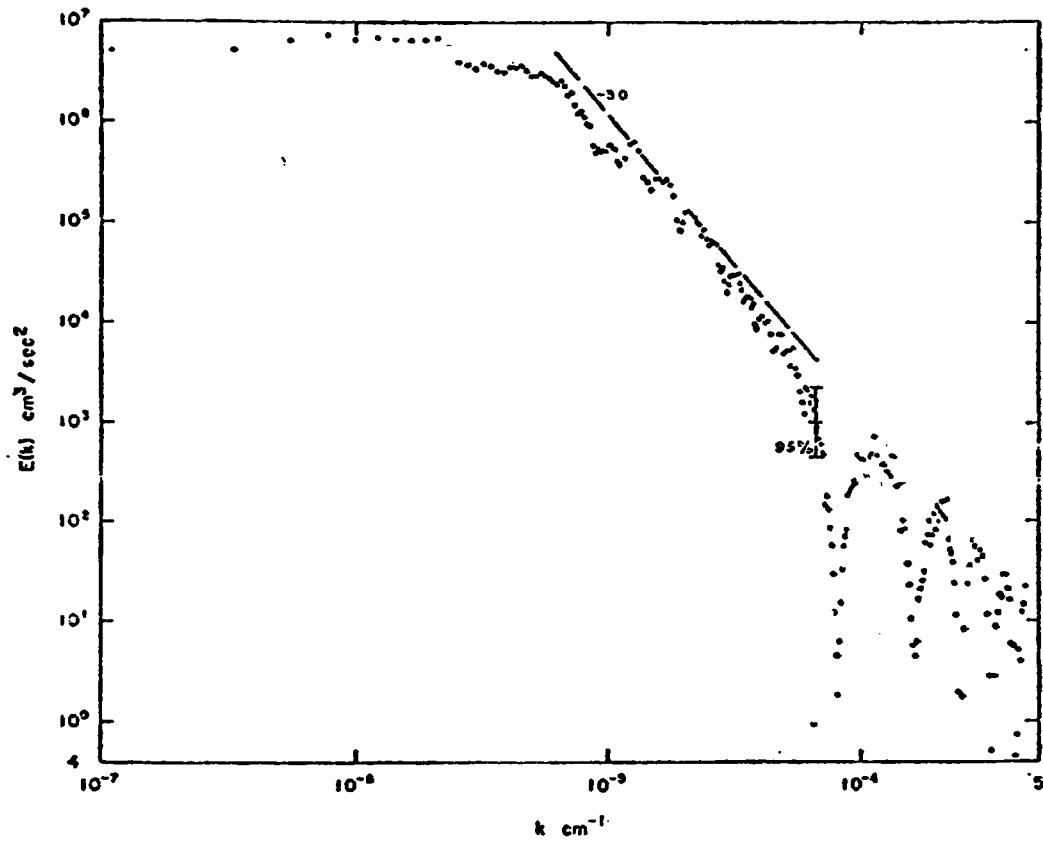


Figure 9.1 Kinetic Energy Spectrum Indicating Two-Dimensional Turbulence (after Palmer, 1973).

from Palmer (1973). It indicates the energy spectrum at 5.3 m below the surface in 9 m of water. Figure 9.2 is indicative of large scale atmospheric kinetic energy spectral distribution. In both of these figures the range of scales with the -3 slope is very characteristic.

It was observed that the maximum length scales where a -3 slope exists varies according to the depth where the spectrum is obtained and also according to the size of the basin. There is generally a size decrease with depth of the scales where a -3 slope is observed and also a decrease of the scales going from a large to a small basin. They are both expected. The decay of the mean velocity with depth involves turbulent components of smaller scales. These in turn result in a shift of the enstrophy subrange to the smaller scales. On the other hand larger basins involve larger eddies. Therefore, the scales where a -3 slope is observed are generally larger in the large basins.

It was observed that a strong wind has two effects on the spectral density curves. The first is that there is a shift of the curves to larger length scales and secondly an upward movement to higher levels of energy. The shift of the curves to larger length scales has been observed by Lemmin, et al., (1974). Figure 9.3 details five spectra for a period of time during which the wind was blowing for the first three spectra and then not for the last two. The movement of the curves to the larger scales during increasing wind is characteristic and supports the results obtained in the thesis.

Lemmin also observed another interesting phenomenon in the same paper. Figure 9.4 indicates a sequence of four curves obtained during a

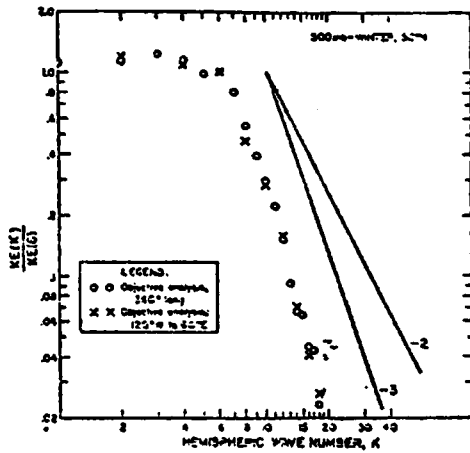


FIG. 1. Kinetic energy spectra, 300 mb, 20N, for the winter season (data sets Iw and IIw, Table I) plotted on a full logarithmic scale. Shown are the spectral estimates using data from all longitudes and for a 180° segment from 120W to 60E. For purposes of comparison all estimates have been standardized by division by the estimate for wavenumber 6.

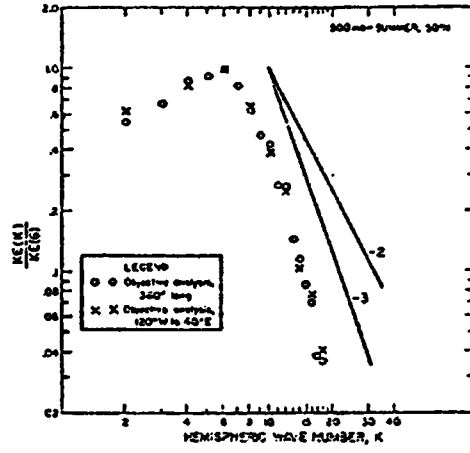


FIG. 2. Same as for Fig. 1, but for summer season (data sets Is and IIa, Table I).

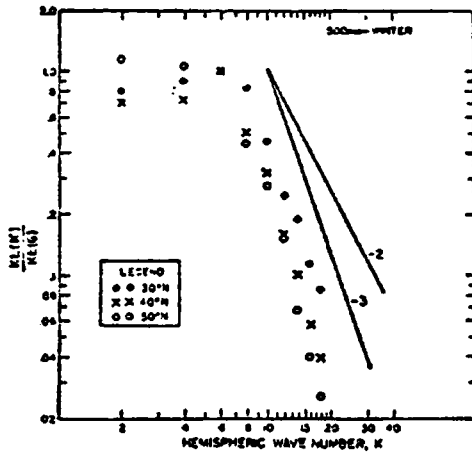


FIG. 5. Kinetic energy spectra, 500 mb, for the winter season plotted on a full logarithmic scale. Spectra for latitudes 30, 40 and 50N are shown. Standardization as in previous figures.

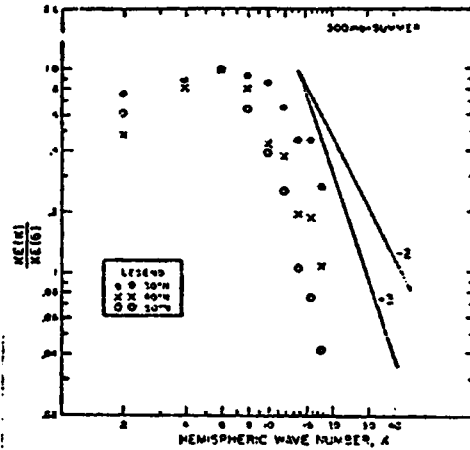


FIG. 6. Same as Fig. 5, but for summer season.

Figure 9.2 Kinetic Energy Spectra Indicating Two-Dimensional Atmospheric Turbulence (after Julian, et al., 1970).

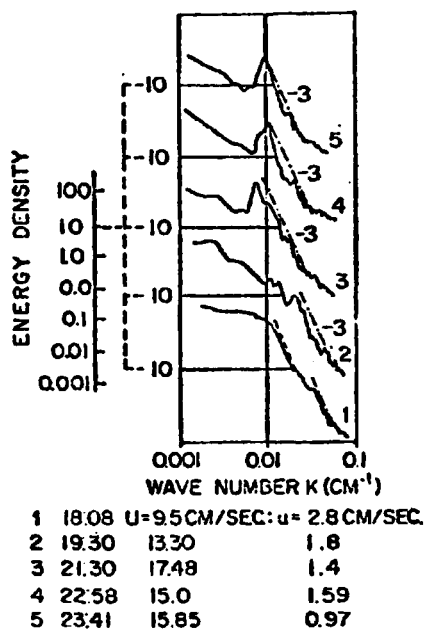


Figure 9.3 Energy Spectra Subject to an increasing and subsiding Wind Field (after Lemmin, et al., 1974)

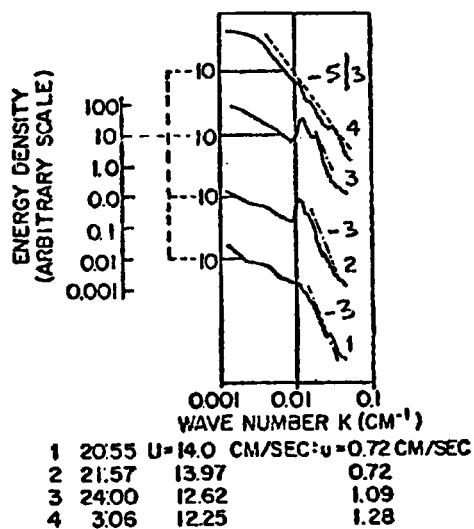


Figure 9.4 Energy Spectra Subject to a diminishing Wind Field (after Lemmin, et al., 1974)

diminishing wind field. It is seen that a -3 slope turns to a $-5/3$ (two-dimensionality to three-dimensionality) at the end of the wind shearing process.

This phenomenon as determined in the calculation is observed in Figures 8.22 through 8.24. This interpretation is compromised by the structure of the model and the statistical procedure used to obtain the spectra. Only 40 values were used for the computation of the spectra. In the rest of the runs at least 120 values were used. The low number of data points was required because of the rapid instantaneous response of the model to the change in boundary condition. It is apparent that the resulting transition to the $-5/3$ slope was very fast (80 minutes only). This can be explained by the rigid lid assumption which is used in this model. According to this assumption any surface boundary condition change is transmitted instantaneously to the whole flow field. This is discussed further in the next section.

The results of Run 12 suggest that the spectral density of the wind shear does not have to follow a $-5/3$ slope in order for the model to predict a -3 velocity field. The velocity spectra obtained are independent of the shape of the surface boundary condition. In any surface disturbance the basin, as it should, adjusts itself to a two-dimensional flow field. This should become an item of further study. It was observed that when an unfiltered model (Figure 8.31, 8.32) was used the cascade process had an erratic character. Comparison with the filtered model indicates that the energy does not drain smoothly to the smaller scales. Actually it accumulates at the large scales until a point where the spectral density curve abruptly drops to small levels of energy. This is

a deficiency of the unfiltered model which makes questionable the whole transport process predicted by it. It should be mentioned here that to date all existing transport models are unfiltered models. The results obtained here indicate that these models need to be revised.

There are many field data indicating that concentration spectra are similar to velocity spectra. Figures 9.5 and 9.6 borrowed from Leigh-Abbott and Coil (1978) are indicative of typical chlorophyll spectra in Lake Tahoe. Figure 9.7 indicates the temperature and chlorophyll a spectra in North Atlantic taken by Fasham and Pugh (1976). Figure 9.8 is borrowed by Powell, et al. (1975) and it shows the chlorophyll and the current spectrum in Lake Tahoe. According to the authors there is a range of scales where turbulence directly governs the distribution of organisms. For length scales of about 100m or larger the diverging shape of the two spectra indicates that biological processes are the dominant factor contributing to the observed chlorophyll variance. Finally Figure 9.9 is a theoretical chlorophyll spectrum obtained by Denman, et al. (1977). It indicates that for wave numbers greater than k_c (wave number depending on the dissipation rate and phytoplankton growth rate) the chlorophyll spectrum follows the velocity spectrum. Figures 8.10 through 8.12 (velocity spectra), Figures 8.33 — 8.44 (concentration spectra) and Table 8.1 indicate that generally the concentration spectra are consistent with the field data observations in the slopes of the spectra and also the length scales. The $-5/3$ slope of Figures 9.8 and 9.9 does not indicate any difference because these figures represent fully three-dimensional conditions while the predicted

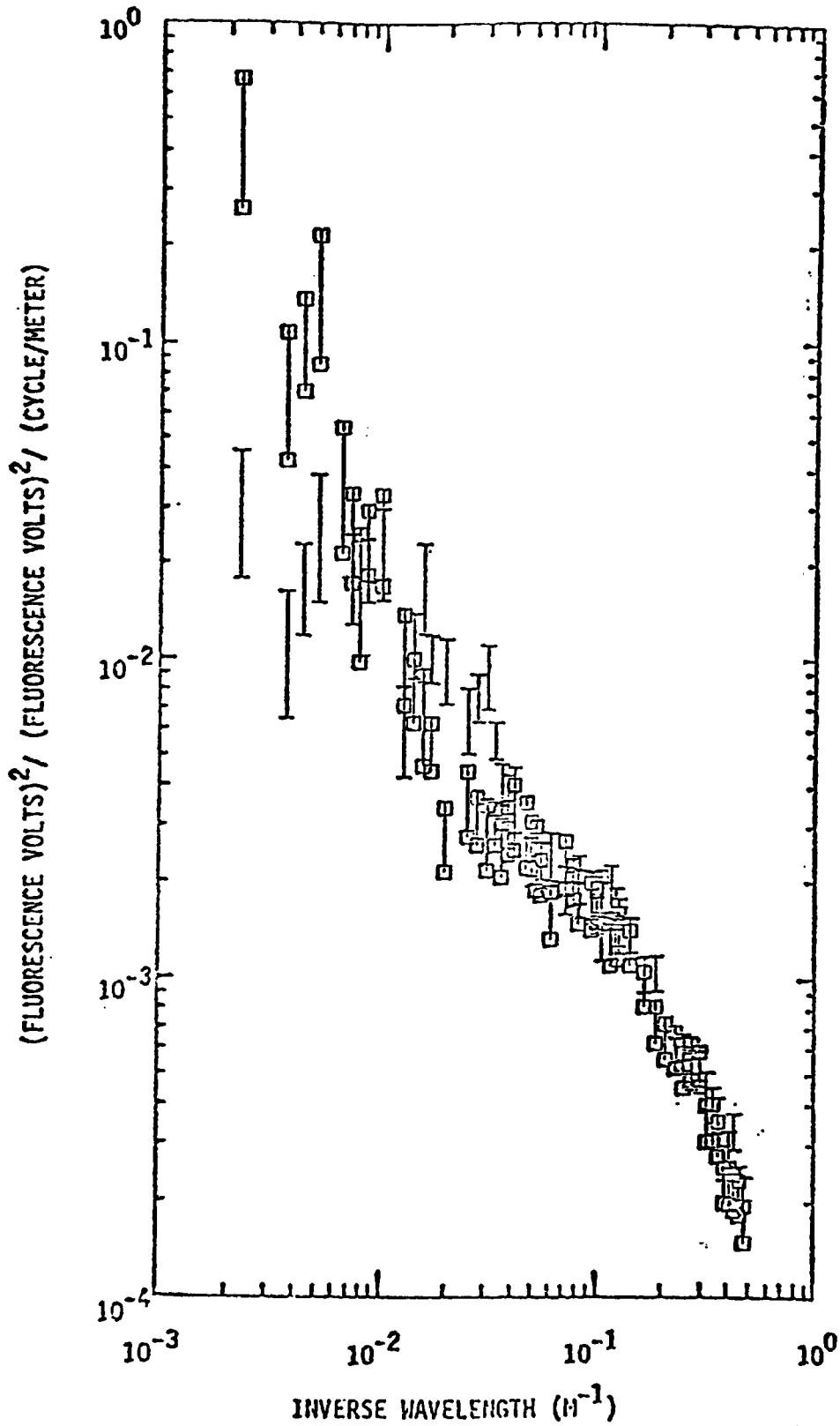


Figure 9.5 Chlorophyll Spectrum (after Leigh-Abbot, et al., 1978)

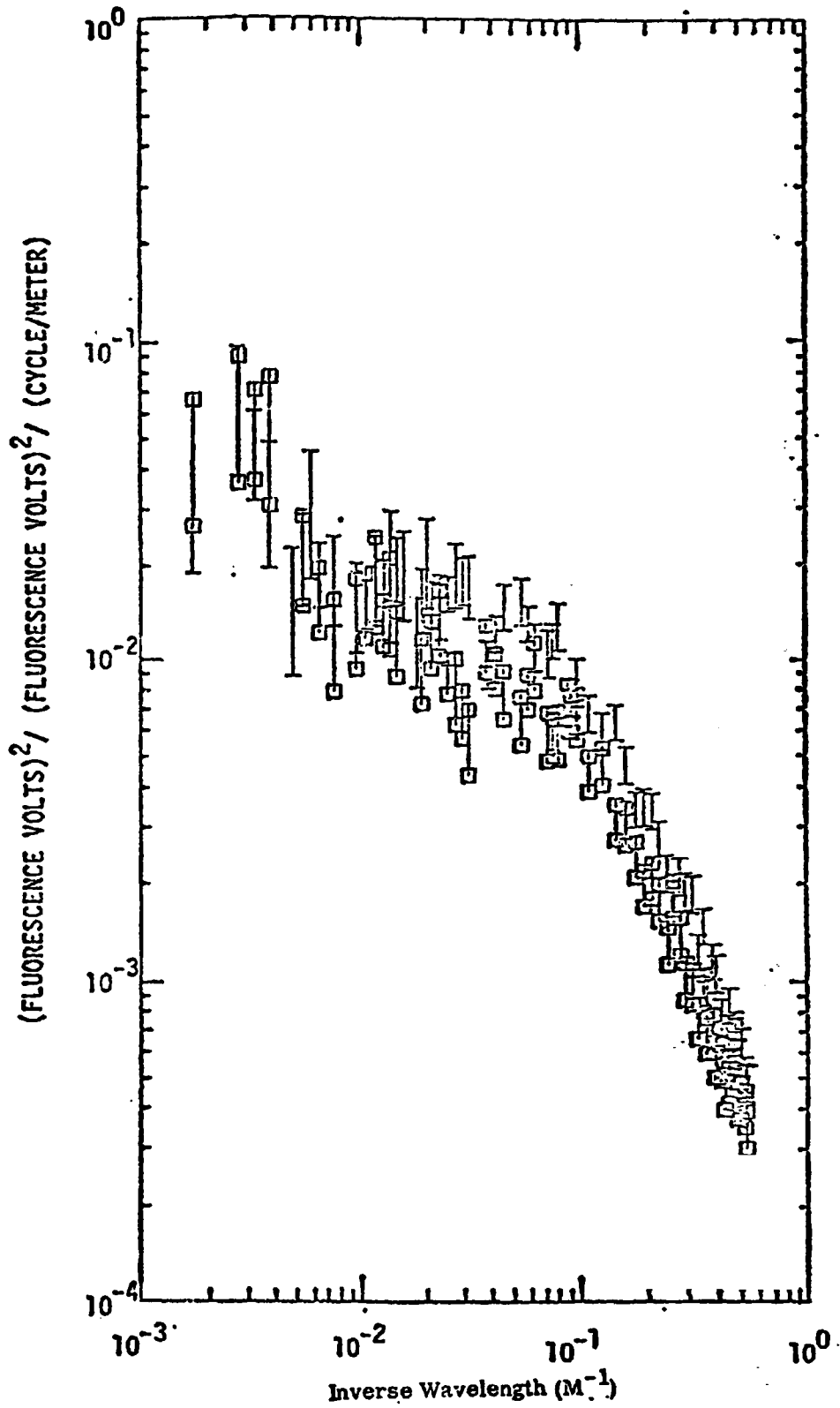


Figure 9.6 Chlorophyll Spectrum (after Leigh-Abbot, et al., 1978)

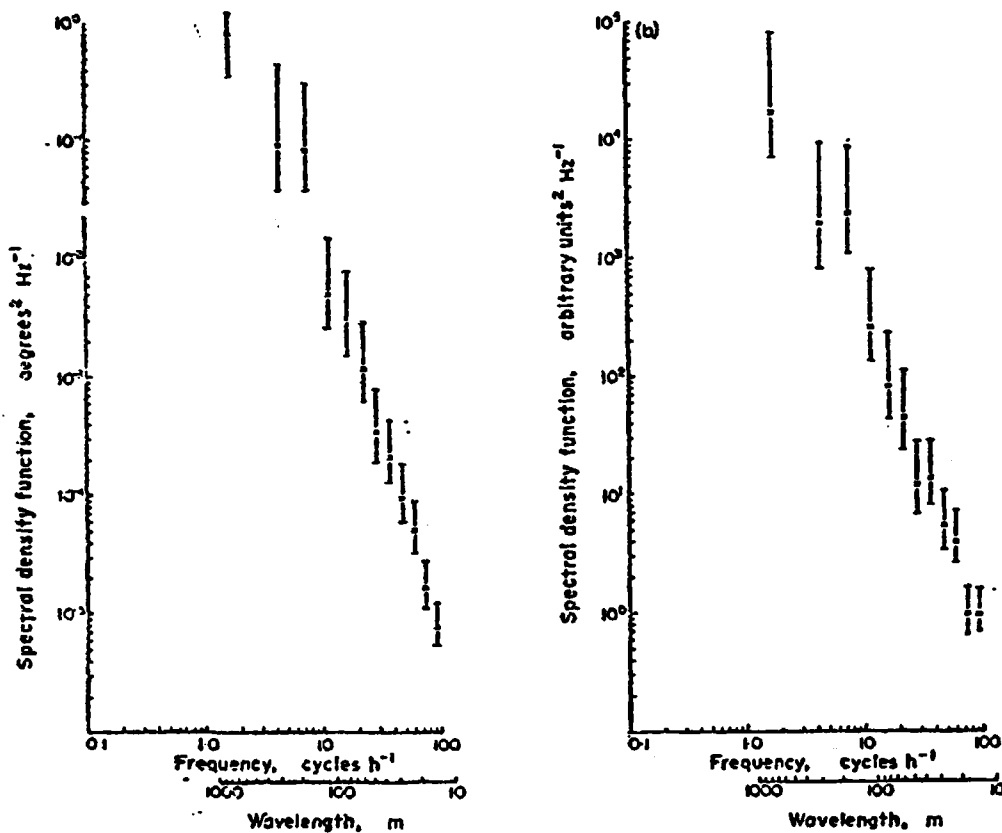


Figure 9.7 Temperature and Chlorophyll a Spectra (after Fasham and Pugh, 1976)

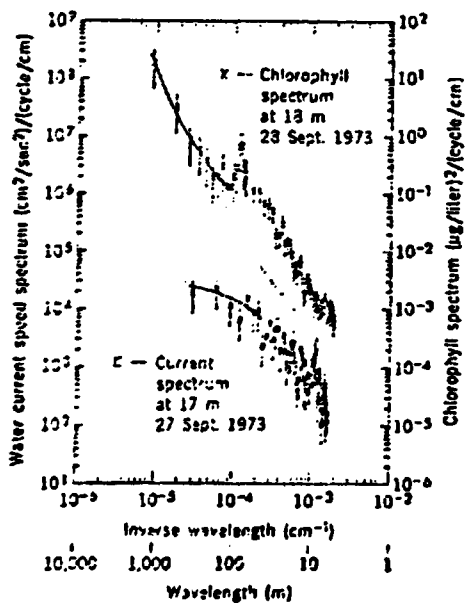


Figure 9.8 Energy and Chlorophyll a Spectra (after Powell, et al., 1975)

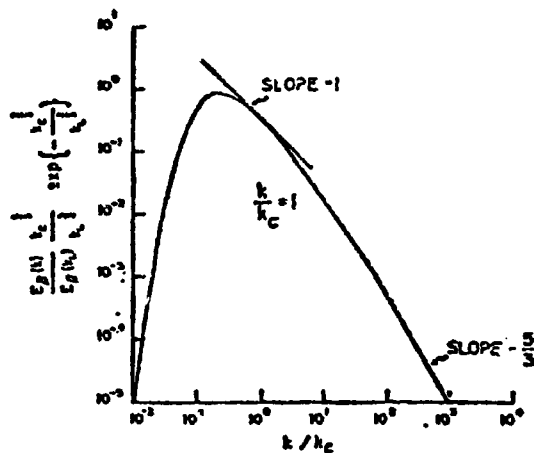


Figure 9.9 Theoretical Chlorophyll Spectrum (after Denmon, et al., 1977)

spectra are two-dimensional. The characteristic feature of the concentration spectra, is the end tail separation (Table 8.1). This becomes more noticeable with increasing Prandtl numbers. Figure 9.10 indicates chlorophyll a spectra observed by Fasham and Pugh (1976) in North Atlantic indicating this end tail shift. Figure 9.11 also shows theoretical velocity and temperature spectra for $Pr \geq 1$ obtained by Monin and Yaglom (1975). It is seen that at small scales there is a characteristic slope change of the temperature spectrum. As Monin and Yaglom explain this change in slope is due to the fact that at these scales molecular viscosity plays an appreciable role while thermal diffusivity still has no effect on the temperature spectrum.

It was observed that the biologically active contaminant spectra (Figures 8.42 — 8.44) and the passive contaminant spectra (Figures 8.33 through 8.35) do not show any significant difference in their shape as expected. This is attributed to the fact that the time of comparison did not exceed four hours. Total times of at least a few days would be required for differences to be shown. However, that long total times were out of the scope of this thesis. The major reason is that times of four hours were sufficient for a study of the influence of the velocity spectra which was where most of the effort was expanded. However, there is a difference between the passive and the active contaminant spectra. The variance level for the active case at the second and third nodes is reduced in comparison to the passive case. It seems that a biologically active contaminant has a special property not present in a passive contaminant, which suppresses the variance in lower levels.

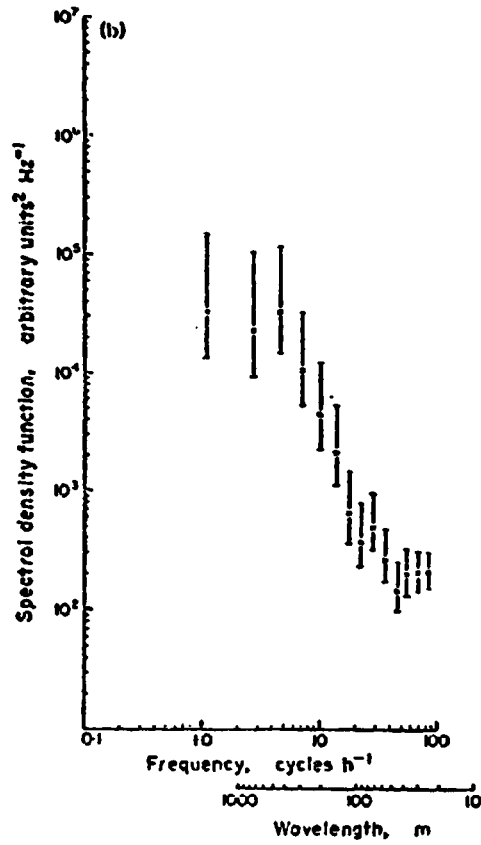


Figure 9.10 Chlorophyll a Spectrum (after Fasham and Pugh, 1976)

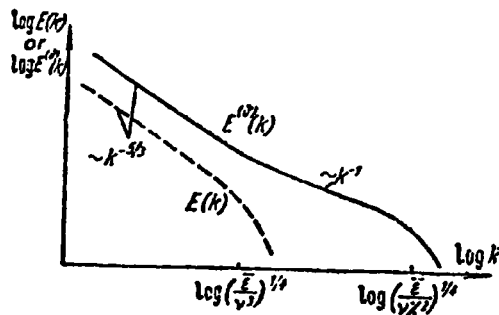


Figure 9.11 Schematic Space of the Velocity and Temperature Spectra for $Pr \geq 1$ (after Monin and Yaglom, 1975)

The last section is devoted to extending these results and pointing out the implications these results have for numerical analysis.

B. Discussion

In this section some of the results will be critically reviewed, some of the assumptions used in the construction of the three-dimensional model will be questioned, some characteristics of the model will be pointed out. Finally an explanation to the observed phytoplankton problem called the "paradox of the plankton," will be suggested.

It was mentioned in the previous section that all the spectra obtained in this thesis follow a -3 slope indicating two-dimensionality or sheared flows. It was justified by the fact that the ratio of the vertical to horizontal scale is very small and that a shear is present. This can indeed be true but the depth of the basin itself (16m) suggests that a three-dimensional field could and should exist. Actually Palmer (1973) has shown that the velocity spectrum at 5.8m of 22m depth of water shows a characteristic $-5/3$ slope. One of the possible explanations why a -3 slope is consistently obtained here is that the shallow water assumption (Chapter V, Section B) is used in the derivation of the filtered transport equations. According to this assumption the vertical velocity component is diminished in comparison to the horizontal velocity components. Therefore, it is not reasonable to expect the shallow water equations to produce a fully three-dimensional character under shear. However, these equations are very commonly (Table 2.1) used even in deep basins. The results obtained here suggest

that one must be very careful in using these equations especially if the objective is to obtain a statistically correct, three-dimensional velocity field.

Another assumption used in the derivation of the transport equations is the rigid lid assumption. According to this assumption any surface pressure change is transmitted instantaneously to the whole velocity field. This is reflected in the surprisingly fast change of the spectrum to a $-5/3$ slope when the wind is exhausted. This suggests that the rigid lid assumption can cause an erratic response of the flow field to any external condition. However, this requires more research since as was mentioned in the previous section the number of points used in the computation of the spectra is rather small. This in turn might affect the slope of the computed spectrum.

In all of the computer runs here, spectra were computed away from solid boundaries. There are basically two reasons for this. The first is that Taylor's frozen turbulence hypothesis would not apply close to the boundaries (Chapter III, Section A.5). Therefore all the computations, based on this assumption, would be wrong. The second reason is that the boundary conditions used are not correct, in the sense that they do not consider the boundary layer formation. Future research in the determination of boundary conditions could possibly allow the examination of spectra closer to walls provided that different method will be found for their computation.

Table 8. 1 shows that the maximum scales where a -3 slope was observed range from 419m in Run 5 to 18m in Run 6. This indicates that perhaps smaller grids should be used in order for the cells to be included in this range of

scales. However, the relatively coarse grid of 100m allowed a very reasonable representation of the cascade process which did not violate either the shape or slope of the theoretically expected spectra. Therefore, a smaller grid is not recommended. Although mesh refinement would undoubtedly improve the behavior of the model, it would increase the cost a great deal. Consequently it would be very uneconomical to use the model in larger basins.

Two characteristics of the model should be mentioned here as improvements to be considered in future modeling efforts. These are: (1) The computation of the eddy viscosity as a function of grid size; and (2) Model verification by statistical methods. As it was mentioned in Chapter II, the great majority of transport models use arbitrarily defined and tuned eddy viscosities. In this thesis they are computed based on the volume of the cell and on theoretical energy conservation considerations of the inertial subrange (Chapter V, Section D). The use of these coefficients requires the determination of one scalar coefficient. This coefficient is computed just once, and this value is used in all the computer runs made. This has enormous implications for modelers who now must tune, adjust and recalculate to achieve proper answers.

The second characteristic lies in the concept of model verification. As mentioned in Chapter II, all the existing transport models use faulty verification procedures by trying to predict the field data of a predominantly random process. In this thesis a statistical verification procedure is suggested as an alternative. This is a more reliable approach and it is much easier to collect

data, as it requires no more than velocity histories at certain points in the lake for preliminary model verification. Once known the statistics can be used to generate monitoring sites for long term data collection.

The results obtained here suggest an answer to a limnological problem that Hutchinson (1961) calls "the paradox of plankton". For details on this phenomenon the reader is referred to Richerson, et al., (1970), Platt, et al. (1970), Platt (1972), Platt and Filion (1973), Steele (1974), Denman (1976), and Denman and Platt (1976). The "Paradox of Plankton" relates to the fact that the examination of a small volume of water yields some tens of phytoplankton species while according to the competitive exclusion principle (Hutchinson, 1961) there should be only one species. One of the assumptions of the competitive exclusion principle is that the competing species are at equilibrium and that conditions do not change very rapidly. Therefore, there is enough time for the superior competitor to cause the extinction of the others. However, as it was pointed by Hutchinson (1961) and it is also concluded from the comparison of the velocity and concentration spectra this is not the case. Turbulence is very important in any biological process. Even though the total time the complete biological model run was not long enough it can be speculated from Figures 8.42 — 8.44 that plankton is not allowed in one place for a long time. Turbulence causes a rapid succession of conditions at each place. No organism is allowed to stay in one place a long time in order to cause the extinction of the others. Therefore, the assumption of equilibrium might not hold.

In the next chapter the major conclusions of this report are summarized.

CHAPTER X

CONCLUSIONS

The major conclusions of this report are the following:

- (1) The computation of detailed turbulent lake transport processes requires that the equations be filtered. Unfiltered equations, the normal model structure, predict an erratic cascade process which makes the predicted flow field questionable.
- (2) Very small computational cells are not required for the prediction of the correct energy cascade process in a turbulent flow field. A cell size of 100m has been shown to be very sufficient.
- (3) The relatively coarse grid of 100m is very effective in preserving the correct statistical characteristics of the turbulent flow field.
- (4) The shallow water equations must be used with caution. The predicted energy cascade process always has a -3 slope which may suggest accelerated non-equilibrium conditions or the presence of 2-D turbulence. Two-dimensional conditions may be appropriate for very shallow basins, but for basins even as deep as 16m such an assumption is unrealistic. This suggests that in these basins the full 3-D Navier-Stokes equations must be used.

- (5) The rigid lid assumption results on instantaneous response of the flow field to any external condition. The instantaneous response is unrealistic in its representation of the collapse of a 2-D wind sheared velocity field to a 3-D unstressed situation and therefore this formulation will not permit sound calculation of this type of process.
- (6) The eddy viscosities must be computed considering the volume of the computational cell and the theoretical consideration of the inertial subrange. Arbitrarily defined eddy viscosities will lead to erratic results and are no longer necessary. This results in a much reduced need for tuning in model calculations.
- (7) The verification procedure of a transport model by predicting field data must be augmented by additional and fundamental verification of the statistics. Turbulence is a predominantly random process. Therefore, only statistical verification procedures should be used. Only after this verification, can field data be properly taken and prepared for model verification.
- (8) There is a range of scales (Table 8.1) where the concentration spectra follow the corresponding velocity spectra. At small scales (Table 8.1) the concentration spectra show a characteristic separation tail which is more intense the larger the Prandtl number.
- (9) For the time periods the model was tested the passive contaminant and the active contaminant spectra did not show any significant difference in their shapes. The only difference is that the variance level for the active contaminant at the second and third nodes is lower than the variance of the passive contaminant.

APPENDIX A

FOURIER TRANSFORMS

Two cases of the Fourier transform will be considered. The first one is when the data are given in a continuous form with respect to the independent variable, θ (θ = time or space variable) and the second when the data are given at discrete points. The interest in turbulence computations lies primarily in the discrete case. However, since the discrete Fourier transform is an extension of the continuous case both are presented here. For details on the derivations the reader is referred to Jenkins and Watts (1968), Stanley (1975) and Bloomfield (1976).

a) **The Continuous Fourier Transform**

Let a function $f(\theta)$ have a period or wavelength of θ and be defined in the interval $-\theta/2$ to $\theta/2$. The complex (or exponential) Fourier series expansion for this function is given as:

$$f(\theta) = \sum_{m=-\infty}^{\infty} F(m) e^{j\frac{2\pi}{\theta} m \theta} \quad , \quad (\text{A.1})$$

where;

$$F(m) = \frac{1}{\theta} \int_{-\theta/2}^{\theta/2} f(\theta) e^{-j\frac{2\pi}{\theta} m \theta} d\theta \quad . \quad (\text{A.2})$$

Additionally the following terms are defined:

$\frac{2\pi}{\theta}$ is the fundamental radian frequency (θ = time variable) or wave number (θ = space variable).

m is an integer defining the order of the harmonic.

Expansions (A.1) and (A.2) are valid if the following Dirichlet conditions hold (Miller, p.83):

- a. $f(\theta)$ never becomes infinite;
- b. $f(\theta)$ has at most a finite number of maxima and minima; and
- c. $f(\theta)$ has at most a finite number of discontinuities.

The set of coefficients $F(m)$ is often called the Fourier spectrum or spectrum of $f(\theta)$

The Fourier transform is a special case of the Fourier series expansion (A.1) and (A.2). It applies when the spectrum of a non-periodic signal is desired. This non-periodic signal may be thought as arising from a periodic signal in which the period of wavelength θ is allowed to increase without limit. In this case the fundamental frequency or wave number $2\pi/\theta$ approaches zero and therefore the spectrum $F(m)$ is a continuous function of frequency or wave number. Equations (A.1) and (A.2) are now written as:

$$f(\theta) = \int_{-\infty}^{\infty} F(\omega) e^{j\omega\theta} d\omega \quad (\text{A.3})$$

where;

$$F(\omega) = \int_{-\infty}^{\infty} f(\theta) e^{-j\omega\theta} d\theta \quad , \quad (\text{A.4})$$

and ω is the continuous radian frequency or wave number. $F(\omega)$ is defined as the Fourier transform of $f(\theta)$, and $f(\theta)$ is the inverse Fourier transform of $F(\omega)$. Physically the Fourier transform represents the distribution of signal strength with frequency or wave number, ω

b) **The Discrete Fourier Transform**

Consider that the function $f(\theta)$ is not continuous in θ but is defined at N discrete intervals of length Λ . Consider also that the frequency, ω , is defined at discrete intervals, Ω . Then Equations (A.3) and (A.4) are written as:

$$f(n\Lambda) = \frac{1}{N} \sum_m F(m\Omega) e^{j2\pi mn\Omega\Lambda} \quad ; \text{ and} \quad (\text{A.5})$$

$$F(m\Omega) = \sum_n f(n\Lambda) e^{-j2\pi mn\Omega\Lambda} \quad . \quad (\text{A.6})$$

Equations (A.5) and (A.6) are called a discrete Fourier transform pair

APPENDIX B

AUTOCORRELATION FUNCTIONS

The power spectrum, as it is discussed in Chapter III is the Fourier transform of the autocorrelation function. Therefore, an understanding of the autocorrelation function is very important in the study of turbulence.

Consider a signal $f(\theta)$, generated by a random process. The covariance of this series is defined as:

$$\text{Cov} = E \left\{ (f(\theta_i) - \bar{f}) (f(\theta_j) - \bar{f}) \right\} \quad ; \quad (\text{B.1})$$

where, E denotes expected value and \bar{f} is the ensemble mean. Assuming that \bar{f} is zero, (B.1) is written as:

$$\text{Cov} = E \left\{ f(\theta_i) f(\theta_j) \right\} \quad . \quad (\text{B.2})$$

In a stationary (if θ is time variable) or a homogeneous (if θ is space variable) random process the covariance will depend only on the time or distance of separation, r . Equation (B.2) is then written as:

$$\text{Cov}(r) = E \left\{ f(\theta) f(\theta + r) \right\} \quad (\text{B.3})$$

or

$$\text{Cov}(r) = \lim_{\theta \rightarrow \infty} \frac{1}{\theta} \int_{-\theta/2}^{\theta/2} f(\theta) f(\theta + r) d\theta \quad . \quad (\text{B.4})$$

For the discrete case of $f(\theta)$ given at n discrete intervals (B.4) is written as:

$$\text{Cov}(\tau) = \frac{1}{n-\tau} \sum_{\theta=1}^{n-\tau} f(\theta) f(\theta + \tau) \quad \tau = 0, 1, 2, \dots \quad (\text{B.5})$$

where τ denotes the number of lags. Equation (B.5) is the computational form of (B.4). By definition, $\text{Cov}(0)$ is the variance of the random process. The ratio of $\text{Cov}(\tau)/\text{Cov}(0)$ is called the autocorrelation function. It describes the general dependence of the data at one time or region in space upon the data at another time or region in space. Deterministic data will have a persistent autocorrelation function over all lags in contrast to random data where the autocorrelation function approaches zero for a large number of lags. Therefore, autocorrelation analysis is used to detect a random from a deterministic process. Figure B.1 borrowed from Bendat and Piersol (1966) shows this property of the autocorrelation function. In this figure $R_x(T)$ denotes the autocorrelation function and T is the time displacement or lag. Figure B.1a is a deterministic wave, Figure B.1b is a deterministic wave plus a random noise, Figure B.1c is a narrow-band random noise and Figure B.1d is a completely random process.

For more details on the autocorrelation function the reader is referred to Jenkins and Watts (1968) and Bendat and Piersol (1966).

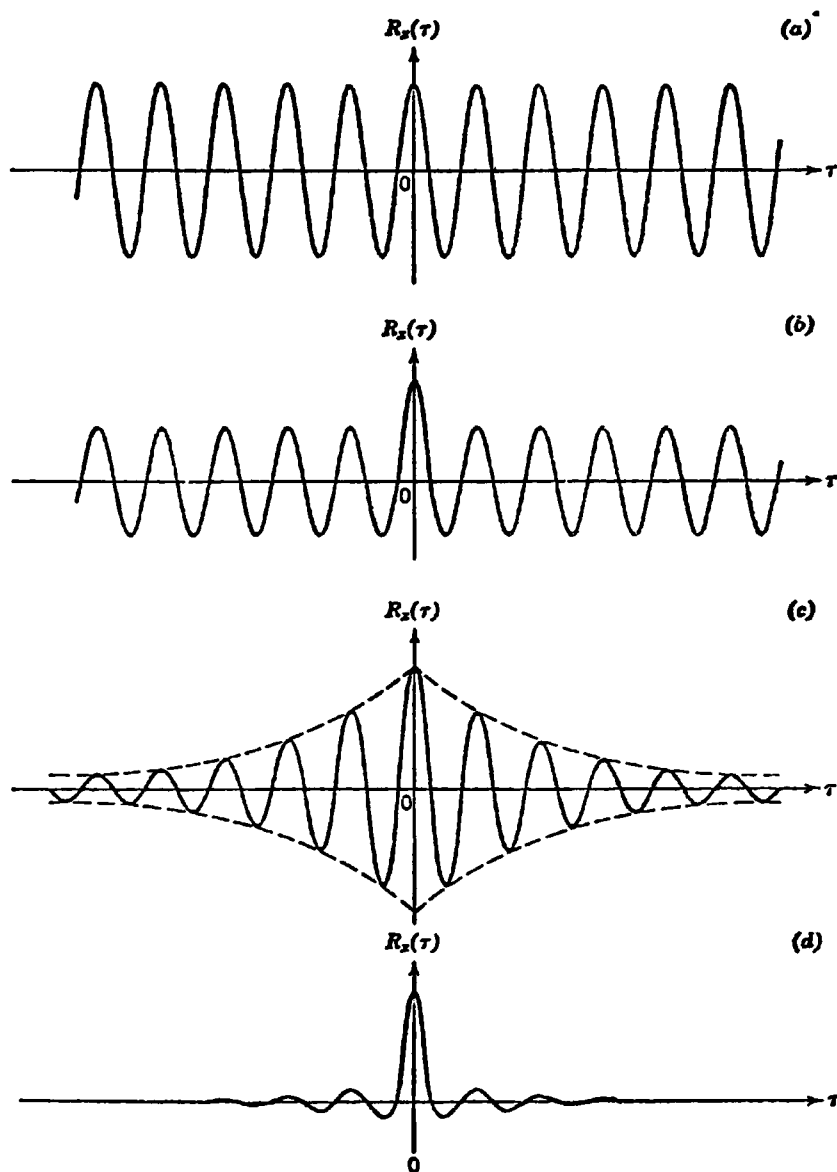


Figure B. 1 Autocorrelation function plots (autocorrelograms). (a) Sine wave. (b) Sine wave plus random noise. (c) Narrow-band random noise. (d) Wide-band random noise. (after Bendat and Piersol, 1966)

APPENDIX C

DEFINITION OF STATIONARITY AND ERGODICITY

Stationarity and ergodicity are two concepts used very widely in the discussion of turbulent flows and their comprehension is necessary in the understanding of turbulence.

Consider an experiment which is performed under identical conditions N times and recorded as a function of time, t . Let the k^{th} experiment be denoted as: $f_k(t)$ where $k=1, N$. If the value of the experiment is recorded at a time t then the arithmetic mean over all experiments is computed as:

$$\mu(t) = \frac{1}{N} \sum_{k=1}^N f_k(t) \quad . \quad (\text{C.1})$$

After a sufficiently large number of experiments, N , the mean, $\mu(t)$, will start oscillating around a constant value, $\overline{\mu(t)}$. This dynamic stability of the mean indicates that the collection of identical experiments constitutes a statistical ensemble. The value over which the arithmetic mean oscillates ($\overline{\mu(t)}$) is called the probability mean. Consider now that the autocorrelation function is defined over the same number of experiments, N , that the probability mean was defined, i.e.

$$R(t, t+\tau) = \frac{1}{N} \sum_{k=1}^N f_k(t) f_k(t+\tau) \quad . \quad (\text{C.2})$$

Then if the value of $\overline{\mu(t)}$ and $R(t, t+\tau)$ vary as t varies the process is called nonstationary. If the value of $\overline{\mu(t)}$ and $R(t, t+\tau)$ do not vary as the time, t , varies then the process is called weakly stationary or stationary. When all the higher order moments and joint moments are time invariant, as well, then the

process is called strongly stationary. Usually when a process is weakly stationary it is considered as strongly stationary (Bendat and Piersol, 1966, p.11).

Ergodicity is also a very important concept in the description of any set of random data. The need for this concept arises from the inability to repeat the same experiment more than once. In this case the probability mean and the autocorrelation function as defined above cannot be obtained. Instead the mean and the autocorrelation have to be obtained over the one experiment as:

$$\mu_k = \lim_{n \rightarrow \infty} \frac{1}{n} \sum_{i=1}^n f_i \quad , \quad \text{and} \quad (\text{C.3})$$

$$R_k(\tau) = \lim_{n \rightarrow \infty} \frac{1}{n-\tau} \sum_{t=1}^{n-\tau} f(t) f(t+\tau) \quad . \quad \tau = 0, 1, 2, \dots \quad (\text{C.4})$$

If the process is ergodic then the mean and autocorrelation defined by Equations (C.3) and (C.4) equal the probability mean, $\overline{\mu(t)}$, and the autocorrelation function defined defined by Equation (C.3). Therefore, ergodicity if it exists allows the results of one experiment to replace the ensemble results. This is very important in geophysical flows where the lack of repetition makes the use of probability averaging impossible.

APPENDIX D
COMPUTER PROGRAMS

The computer programs used in this research were initiated for analytical purposes and in themselves are not the end products of this research. Therefore, the program listings and brief operating notes are available to the serious reader upon written request and at a cost necessary to cover only reproduction and mailing charges. Address inquiries to:

Dr. K. W. Bedford
Department of Civil Engineering
The Ohio State University
2070 Neil Avenue
Columbus, Ohio 43210

REFERENCES

1. Allender, J.H., M.J. Berger and K.D. Saunders, "Preliminary Verification of Numerical Circulation Models for Lake Michigan," Symposium on Modeling of Transport Mechanisms in Oceans and Lakes, Burlington, Ontario, 6-8 October, 1975.
2. Allender, J.H., and K.D. Saunders, "Intercomparison of Results from Numerical Circulation Models for Lake Michigan," 19th Conference on Great Lakes Research Programme, Guelph, Ontario, May 4-6, 1976.
3. Ames, W.F., "Nonlinear Partial Differential Equations in Engineering," Academic Press, New York, 1965.
4. Baca, R.G., and R.C. Arnett, "A Limnological Model for Lakes and Impoundments," USEPA Conference on Environmental Modeling and Simulation, Cincinnati, 1976.
5. Ball, F.K., "Second-Class Motions of a Shallow Liquid," J. Fluid Mech., 23(3), 545-561, 1965.
6. Bedford, K.W. and I.S. Rai, "Efficient Pressure Solutions for Circulation Prediction," J. of the Hydraulics Division, ASCE, Hy 6, 104, 1978.

7. Bedford, K.W., and B. Shah, Maumee Bay Sediment Transport Mechanisms During Spring Flood, " EPA/IJC Project Completion Report, PLUARG, 1977.
8. Bendat, J.S. and A.G. Piersol, "Measurement and Analysis of Random Data," Wiley, New York, 1958.
9. Bennet, J.R., "On the Dynamics of Wind-Driven Lake Currents," J. of Physical Oceanography, 4(3), 400-414, 1974.
10. Benton, G.S. and A.B. Arthur, "Spectra of Large-Scale Atmospheric Flow at 300 Millibars," J. Meteor., 15, 404-410, 1958.
11. Bierman, V.J., "Mathematical Model of the Selective Enhancement of Blue-Green Algae by Nutrient Enrichment," A paper in Modeling Biochemical Processes in Aquatic Ecosystems, R. P. Canale (Ed.), Ann Arbor Science, 1976.
12. Blackman, R.B., and J.W. Tukey, "The Measurement of Power Spectra," Dover, New York, 1958.
13. Bloomfield, P., "Fourier Analysis of Time Series: An Introduction," Wiley, New York, 1976.

14. Boyce, F.M., "Some Aspects of Great Lakes Physics of Importance to Biological and Chemical Processes," J. Fisheries Research Board of Canada, 31(5), 689-730, 1974.
15. Bradshaw, P., "The Understanding and Prediction of Turbulent Flow," Aeronautical Journal, 403-419, 1972.
16. Brigham, E.O., "The Fast Fourier Transform," Prentice-Hall, Englewood Cliffs, New Jersey, 1974.
17. Bryan, K., "A Numerical Model for the Study of the Circulation of the World Ocean," J. Comp. Phys. 4: 347-376, 1969.
18. Canale, R.P., D.J. Hineman and H.E. Allen, "A Dynamic Model for Phytoplankton Production in Grand Traverse Bay," Proceeding 16th Conf. Great Lakes Res., Ann Arbor, 1973.
19. Cannon, G.A., "Statistical Characteristics of Velocity Fluctuations at Intermediate Scales in a Coastal Plain Estuary," J. of Geophysical Research, 76 (24), 5852-5858, 1971.
20. Carnahan, B., H.A. Luther, and J.O. Wilkes, "Applied Numerical Methods," Wiley, New York, 1969.
21. Chen, C.W., M. Lorenzen and D.J. Smith, "A Comprehensive Model for Lake Ontario," Great Lakes Environmental Research Laboratory, Ann Arbor, 1975.

22. Cheng, R.T., T.M. Powell, and T.M. Dillon, "Numerical Models of Wind Driven Circulation in Lakes," USGS, Menlo Park, California, 1976.
23. Collatz, L., "The Numerical Treatment of Differential Equations," Springer-Verlag, Berlin, 1960.
24. Cooper, G.R., and C.D. McGillem, "Methods of Signal and System Analysis," Holt, Rinehart and Winston, New York, 1967.
25. Crowley, W.P., "A Global Ocean Model, Part I.," J. Comp. Phys. 3: 111-147, 1968.
26. Daly, B.J., and F.H. Harlow, "Transport Equations in Turbulence," The Physics of Fluids, 13 (11), 2634-2649, 1970.
27. Deardorff, J.W., "A Numerical Study of Three-Dimensional Turbulent Channel Flow at Large Reynolds Numbers," J. Fluid Mechanics, 41(2), 453-480, 1970.
28. Deardorff, J.W., "On the Magnitude of the Subgrid Scale Eddy Coefficient," J. of Computation Physics 7, 120-133, 1971.
29. Deardorff, J.W., "The Use of Subgrid Transport Equations in A Three-Dimensional Model of Atmospheric Turbulence," J. of Fluids Engineering, Transactions of the ASME, 429-438, 1973.

30. Denman, K.L. , "Covariability of Chlorophyll and Temperature in the Sea," *Deep-Sea Research*, 23, 539-550, 1976.
31. Denman, K.L. and T.Platt, "The Variance Spectrum of Phytoplankton in a Turbulent Ocean," *J. of Marine Research*, 34, 593-601, 1976.
32. Denman, K. , A. Okubo and T. Platt, "The Chlorophyll Fluctuation Spectrum in the Sea," *Limnology and Oceanography*, 22(6), 1033-1038, 1977.
33. Dillon, T.M. and T.M. Powell, "Low-Frequency Turbulence Spectra in the Mixed Layer of Lake Tahoe, California-Nevada," *J. of Geophysical Research*, 81 (36), 6421-6427, 1976.
34. Di Toro, D.M. , D.J. O'Connor and R.V. Thomann, "A Dynamic Model of the Phytoplankton Population in the Sacramento San Joaquin Delta," *Nonequilibrium Systems in Natural Waters*, Adv. Chemical Ser. 106, Am. Chemical Soc., Washington, 1971.
35. Dixon, W.J. , "Biomedical Computer Programs," University of California Press, Berkeley, 1974.
36. Dudewicz, E.J. , "Introduction to Statistics and Probability," Holt, Rinehart and Winston, New York, 1976.

37. Durst, F., V.W. Goldschmidt, B.E. Launder, F.W. Schmidt, and J.H. Whitelaw, "Symposium on Turbulent Shear Flows," Volume 1, University Park, Pennsylvania, April 18-20, 1977.
38. Fasham, M.J.R. and P.R. Pugh, "Observations on the Horizontal Coherence of Chlorophyll a and Temperature," *Deep Sea Research*, 23, 527-538, 1976.
39. Favre, A., J. Caviglio and R. Dumas, *Recherche Aeronaut.*, No. 32, p.21, 1953.
40. Ferziger, J.H., U.B. Mehta and W.C. Reynolds, "Large Eddy Simulation of Homogeneous Isotropic Turbulence," *Symposium on Turbulent Shear Flows*, University Park, Pennsylvania, 1977.
41. Fiering, M.B., "Multivariate Technique for Synthetic Hydrology," *J. of the Hydraulics Division, ASCE*, 90, HYS, 43-59, 1964.
42. Fiering, M.B. and B.N. Jackson, "Synthetic Streamflows," *Americal Geophysical Union, Water Resources Monograph 1*, 1971.
43. Fjortoft, R., "On the Changes in the Spectral Distribution of Kinetic Energy for Two-Dimensional, Nondivergent Flow," *Tellus*, 5(3), 225-230, 1953.
44. Gedney, R.T., and W.Lick, "Wind Driven Currents in Lake Erie," *J.G.R.* 77, 2714-2723, 1972.

45. Grant, H. L., A. Moilliet and W.M. Vogel, "Some Observations of the Occurrence of Turbulence in and above the Thermocline," *J. Fluid Mechanics*, 34, 3, 443-448, 1968.
46. Grant, H. L., R.W. Stewart and A. Moilliet, "Turbulence Spectra from a Tidal Channel," *J. Fluid Mechanics*, 12, 241-268, 1962.
47. Hamming, R.W., "Digital Filters," Prentice Hall, 1977.
48. Harlow, F.H. and P.I. Nakayama, "Turbulence Transport Equations," *The Physics of Fluids*, 10(11), 2323-2332, 1967.
49. Haq, A., and W. Lick, "On the Time-Dependent Flow in a Lake," *J. of Geophysical Research*, 80(3), 431-437, 1975.
50. Hinze, J.O., "Turbulence," McGraw-Hill, New York, 1975.
51. Hutchinson, G.E., "The Paradox of Plankton," *The American Naturalist*, XVC(882), 137-145, 1961.
52. Jenkins, G.M., and D.G. Watts, "Spectral Analysis and its Applications," Holden-Day, San Francisco, 1968.
53. Julian, P.R., W.M. Washington, L. Hembree and C. Ridley, "On the Spectral Distribution of Large-Scale Atmospheric Kinetic Energy," *J. of the Atmospheric Sciences*, 27, 376-387, 1970.

54. Karman, T. Von, "Mechanische Ahnlichkeit Und Turbulenz, Nachr. Ges. Wiss. Gottingen, Math.-Phys. Kl., 58-76, 1930.
55. Kolmogorov, A.N., "Energy Dissipation in Locally Isotropic Turbulence," Dokl, Akad. Nauk SSR, 32, No. 1, 19-21, 1941.
- 56.a Kraichnan, R.H., "Inertial Ranges in Two-Dimensional Turbulence," The Physics of Fluids, 10(7), 1417-1423, 1967.
- 56.b Kraichnan, R.H., "Inertial-Range Transfer in Two-and Three-Dimensional Turbulence," J. Fluid Mechanics, 47(3), 525-535, 1971.
57. Kreiss, H. and J. Olinger, "Methods for the Approximate Solution of Time Dependent Problems," GARP Publications Series, No. 10, 1973.
58. Kuo, F.F., "Network Analysis and Synthesis," Wiley, New York, 1962.
59. Kwak, D., W.C. Reynolds, and J.H. Ferziger, "Three-Dimensional Time Dependent Computation of Turbulent Flow," Department of Mechanical Engineering, Stanford University, Report No. TF-S, 1975.
60. Leendertse, J.J., "A Water Quality Simulation Model for Well Mixed Estuaries and Coastal Seas, Vol. 1, Principles of Computation," Rand Corp., 1970.

61. Leigh-Abbott, M. R., and J.A. Coil, "Effects of a Coastal Front on the Distribution of Chlorophyll in Lake Tahoe, California-Nevada," Paper presented at IAGLR Coastal Processes Conference, Sandridge, Ontario, February 21-24, 1978.
62. Leith, C. E., "Numerical Simulation of the Earth Atmosphere," *Methods in Computational Physics*, 4, p.1, 1965.
63. Leith, C. E., "Diffusion Approximation for Two-Dimensional Turbulence," *Phys. Fluids*, 11, 671-673, 1968.
64. Leith, C. E., "Two-Dimensional Eddy Viscosity Coefficients," *Proceedings of the WMO/IUGG Symposium on Numerical Weather Prediction in Tokyo*, pp.I-41 - I-44, 1968.
65. Lemmin, U., J.T. Scott and U.H. Czapski, "The Development from Two-Dimensional to Three-Dimensional Turbulence Generated by Breaking Waves," *J. of Geophysical Research*, 79 (24), 3442-3448, 1974.
66. Leonard, A. "Energy Cascade in Large-Eddy Simulations of Turbulent Fluid Flows," *Advances in Geophysics*, 18A, 237-248, 1974.
67. Lick, W., "Numerical Models of Lake Currents," *U.S. EPA Ecological Research Series*, Dept. EPA-600/3-76-020, 1976.

68. Lick, W., "Numerical Modeling of Lake Currents," *Annual Review of Earth and Planetary Sciences*, 4, 49-74, 1976.
69. Liggett, J.A., "Unsteady Circulation in Shallow Homogeneous Lakes," *J. of the Hydraulics Division ASCE*, 95, HY4, 1273-1288, 1969.
70. Liggett, J.A., "Cell Method for Computing Lake Circulation," *J. of the Hydraulics Division, ASCE*, 96, HY3, 725-742, 1970.
71. Liggett, J.A. and C. Hadjithodorou, "Circulation in a Shallow, Homogeneous Lake," *J. of the Hydraulics Division, ASCE*, 95, HY2, 609-620, 1969.
72. Lilly, D.K., "The Representation of Small-Scale Turbulence in Numerical Simulation Experiments," *Proceedings of the IBM Scientific Computing Symposium on Environmental Sciences*, IBM form No. 320-1951, 195-210, 1967.
73. Lilly, D.K., "Numerical Simulation of Two-Dimensional Turbulence," *High-Speed Computing in Fluid Dynamics, The Physics of Fluids Supplement II*, II-240-II-249, 1969.
74. Lilly, D.K., "Numerical Simulation Studies of Two-Dimensional Turbulence: I Models of Statistically Steady Turbulence," *Geophysical Fluid Dynamics*, 289-319, 1972.

75. Lilly, D.K. , "Numerical Simulation Studies of Two-Dimensional Turbulence: II. Stability and Predictability Studies," *Geophysical Fluid Dynamics*, 4, 1-28, 1972.
76. Love, M.S. , "Techniques for Solving Burgers' Equation on a Coarse Mesh with Examples," Department of Nuclear Engineering, Queen Mary College, London, QMC EP 6023, 1976.
78. Lumley, J.L. , "The Spectrum of Nearly Inertial Turbulence in a Stably Stratified Fluid," *J. of the Atmospheric Sciences*, 21, 99-102, 1964.
79. Mansour, N.N. , P. Moin, W-C. Reynolds and J.H. Ferziger, "Improved Methods for Large-Eddy Simulations of Turbulence," Symposium on Turbulent Shear Flows, University Park, Pennsylvania, 1977.
80. Miller, K.S. , "Partial Differential Equations in Engineering Problems," Prentice-Hall, Englewood Cliffs, N. J.
81. Monin, A.S. , and A.M. Yaglom, "Statistical Fluid Mechanics: Mechanics of Turbulence," Volume 1, The MIT Press, Cambridge, Mass. , 1970.
82. Monin, A.S. , and A.M. Yaglom, "Statistical Fluid Mechanics: Mechanics of Turbulence," Volume 2, The MIT Press, Cambridge, Mass. , 1975.

83. Obukhov, A.M., "Energy Distribution in the Spectrum of a Turbulent Flow," *Izvestiya An SSSR, Ser. Geogr. Geofiz.*, No. 4-5, 453-466, 1941.
84. Obukhov, A.M., "Structure of the Temperature Field in a Turbulent Flow," *Izv. Akad. Nank SSSR, Ser. Geogr. i Geofiz.*, 13(1), 58-69, 1949 a.
85. Obukhov, A.M., "Pressure Fluctuations in a Turbulent Flow," *Dokl. Akad. Nauk SSSR*, 66(1), 17-20, 1949 b.
86. Okubo, A., "Equations Describing the Diffusion of an Introduced Pollutant in a One-Dimensional Estuary," *Studies in Oceanography*, 216-226, 1964.
87. Orszag, S.A., "Analytical Theories of Turbulence," *J. Fluid Mechanics*, 41(2), 363-386, 1970.
88. Orszag, S.A. and M. Israeli, "Numerical Flow Simulation by Spectral Methods," *Numerical Models of Ocean Circulation Proceedings of a Symposium held at Durham, New Hampshire, 1972*, National Academy of Science Publ., 1975.
89. Otnes, R.K. and L. Enchson, "Digital Time Series Analysis," Wiley, New York, 1972.

90. Palmer, M.D., "Some Kinetic Energy Spectra in a Nearshore Region of Lake Ontario," *J. of Geophysical Research*, 28(18), 3585-3595, 1973.
91. Paskausky, D. F., "Winter Circulation in Lake Ontario," *Proc. 14th Conf. Great Lakes Research, IAGLR*, 593-606, 1971.
92. Paul, J. F., and W.J. Lick, "A Numerical Model for a Three-Dimensional Variable-Density Jet," *Proc. 16th Conf. Great Lakes Res.*, 818-830, 1973.
93. Paul, J. F. and W.J. Lick, "Lake Erie International Jetport Model Feasibility Investigation: Application of Three-Dimensional Hydrodynamic Model to Study Effects of Proposed Jetport Island on Thermocline Structure in Lake Erie," *Lake Erie Regional Transportation Authority, Contract Report H-75-1, Report 17-6*, 1976.
94. Platt, T., "Local Phytoplankton Abundance and Turbulence," *Deep Sea Research*, 19, 183-187, 1972.
95. Platt, T., L.M. Dickie and R.W. Trites, "Spatial Heterogeneity of Phytoplankton in a Near-Shore Environment," *J. Fisheries Research Board of Canada*, 27(8), 1453-1473, 1970.

96. Platt, T. and C. Filion, "Spatial Variability of the Productivity: Biomass Ratio for Phytoplankton in a Small Marine Basin," *Limnology and Oceanography*, 18(5), 743-749, 1973.
97. Powell, T.M., P.J. Richerson, T.M. Dillon, B.A. Agee, B.J. Dozier, D.A. Godden and L.O. Myrup, "Spatial Scales of Current Speed and Phytoplankton Biomass Fluctuations in Lake Tahoe," *Science*, 189, 1088-1090, 1975.
98. Prandtl, L., "Bericht Über Untersuchungen Zue Ausgebildeten Turbulenz," *Zs. Angew. Math. Mech.*, 5(2), 136-139, 1925.
99. Reynolds, A.J., "Turbulent Flows in Engineering," Wiley, New York, 1974.
100. Reynolds, O. "On the Dynamical Theory of Incompressible Viscous Fluids and the Determination of the Criterion," *Phil. Trans.*, 123-164, 1894.
101. Reynolds, W.C., "Recent Advances in Computation of Turbulent Flows," *Advances in Chemical Engineering*, 9, 193-246, 1974.
102. Reynolds, W.C., "Computation of Turbulent Flows," *Annual Review of Fluid Mechanics*, 8, 1976.

103. Reynolds, W.C., and T. Cebeci, "Calculation of Turbulent Flows,"
Topics in Applied Physics, Vol. 12, Turbulence, Ed: P. Bradshaw,
Springer-Verlag, Berlin, 1976.
104. Richerson, P., R. Armstrong, and C.R. Goldman, "Contemporaneous
Disequilibrium, a New Hypothesis to Explain the 'Paradox of
Plankton'," Proceedings of the National Academy of Sciences,
67(4), 1710-1714, 1970.
105. Roache, P.V., "Computational Fluid Dynamics," Hermosa, Albuquerque,
N.M., 1976.
106. Saffman, P.G., "Model Equations for Turbulent Shear Flow," Studies
in Applied Mathematics, Vol. LIII(1), 17-34, 1974.
107. Scavia, D., B.J. Eadie and C.A. Robertson, "An Ecological Model for
the Great Lakes," USEPA Conf. Environmental Modeling and
Simulation, Cincinnati, Ohio, 1976.
108. Schlichting, H., "Boundary-Layer Theory," McGraw-Hill, New York,
1968.
109. Schumann, U., "On the Numerical Calculation of Turbulent Flows in
Channels and Anuli Geometries," Ph.D. Dissertation, University
of Karlsruhe, 1973.

110. Shaanan, S., J.H. Ferziger and W.C. Reynolds, "Numerical Simulation of Turbulence in the Presence of Shear," Department of Mechanical Engineering, Stanford University, 1975.
111. Sheng, Y. P., "Lake Erie International Jetport Model Feasibility Investigation; The Wind-Driven Currents and Contaminant Dispersion in the Near-Shore of Large Lakes," Contract Report H-75-1, Report 17-5, Lake Erie Regional Transportation Authority, 1975.
112. Sheng, Y. P., and W. Lick, "The Wind Driven Currents and Contaminant Dispersion in the Near-Shore of Large Lakes," Lake Erie Regional Transportation Authority, Report 17-5, 1975.
113. Simons, T. J., "Development of Numerical Models of Lake Ontario," Proc. 14th Conf. Great Lakes Res., IAGLR, 654-669, 1971.
114. Simons, T. J., "Development of Numerical Models of Lake Ontario: Part 2," Proc. 15th Conf. Great Lakes Res., IAGLR, 655-672,
115. Smagorinsky, J., S. Manabe and J. L. Holloway, Jr., "Numerical Results from a Nine-Level General Circulation Model of the Atmosphere," Monthly Weather Review, 93(12), 1965.
116. Smarkel, K. L., "Comparative Study of the Mathematical Formulations for Primary Productivity in Stratified Lakes," Ph. D. Dissertation, The Ohio State University, 1978.

117. Spiegel, M. R., "Mathematical Handbook of Formulas and Tables,"
Schaum's Outline Series, McGraw-Hill, New York, 1968.
118. Spraggs L.D. and R.L. Street, "Three-Dimensional Simulation of
Thermally-Influenced Hydrodynamic Flows," Stanford University,
Technical Report No. 190, 1975.
119. Stanley, W.D., "Digital Signal Processing," Reston, Reston, Virginia,
1975.
120. Steele, J.H., "Spatial Heterogeneity and Population Stability," Nature,
248, 83, 1974.
121. Stewart, R.W., J.R. Wilson and R.W. Burling, "Some Statistical
Properties of Small Scale Turbulence in an Atmospheric Boundary
Layer," J. Fluid Mechanics, 41, 1, 141-152, 1970
122. Taylor, G.I., "Eddy Motion in the Atmosphere," Phil. Trans. Roy.
Soc., A 215, 1-26, 1915
123. Taylor, G.I., "The Transport of Vorticity and Heat Through Fluids in
Turbulent Motion," Proc. Roy. Soc., A 135, 685-706, 1932.
124. Taylor, G.I., "The Spectrum of Turbulence," Proc. Roy. Soc., A164,
No. 919, 476-490, 1938.

125. Tennekes, H., and J.L. Lumley, "A First Course in Turbulence,"
MIT Press, Cambridge, Mass., 1972.

126. Welch, J.E., F.H. Harlow, J.P. Shannon and B.J. Daly, "The MAC
Method," Los Alamos Scientific Laboratory, Los Alamos,
N.M., 1966.

127. Wiin-Nielsen, A., "On the Annual Variation and Spectral Distribution
of Atmospheric Energy," *Tellus*, 19, 540-559, 1967.